Identification of genetic determinants of ATR inhibitor sensitivity in ARID1A mutant ovarian clear cell carcinoma

James Richard Stewart

Institute of Cancer Research

University of London

A thesis submitted for the degree of

Doctor of Philosophy

September 2022

Declaration

I James Richard Stewart confirm that the work presented in this thesis is my own. Where information has been derived from other sources, I confirm that this has been indicated in the thesis.

Abstract

Ovarian clear cell carcinoma (OCCC) is a gynaecological cancer of unmet need characterized by *ARID1A* and *PPP2R1A* mutations. Prior work identified a synthetic lethality between *ARID1A* tumour suppressor mutations in OCCC and inhibition of the ATR kinase, information that has led to phase II proof-of-concept clinical trials assessing an ATR inhibitor (ATRi) in *ARID1A* mutant cancers. Using a genome-wide CRISPR-Cas9 mutagenesis screen in an *ARID1A* mutant OCCC tumour cell line and subsequent genome-wide CRISPR-Cas9 mutagenesis and CRISPR-dCas9 interference screens, I identify multiple protein phosphatase 2A (PP2A) subunit-coding genes as determinants of ATRi sensitivity. Analysis of a cohort of OCCCs indicated that over approximately one half possessed *ARID1A* mutations as well as mutations in the PP2A scaffolding subunit coding gene, *PPP2R1A*. CRISPR-prime editing of *PPP2R1A* demonstrated that cancer-associated hotspot p.R183 missense mutations cause ATRi sensitivity in OCCC cells, even in the presence of *ARID1A* mutations. The synthetic lethality between *PPP2R1A* p.R183 missense mutation and ATRi operated in both *in vitro* and *in vivo* and was characterized by a decrease in cells in replicating S phase of the cell cycle, an increase in cells entering mitosis with sub-4n genomic content and the accumulation of 53BP1 bodies. Mechanistically, this synthetic lethal effect was dependent upon the kinase WNK1, which itself exhibits increased phosphorylation in *PPP2R1A* mutant OCCC cells. Depletion of WNK1 restored the replicating S phase population normally depleted by ATRi and reversed ATRi sensitivity in *PPP2R1A* p.R183 mutant OCCC cells. TOV21G PPP2R1A

p.R183 mutant cells were also observed to be more sensitive to ATRi than *PPP2R1A* wild-type cells in an *in vivo* model system of OCCC. Together with the data presented here, the co-occurrence of *PPP2R1A* and *ARID1A* mutations in OCCC suggests that in addition to *ARID1A*, *PPP2R1A* status should be assessed as a biomarker of ATRi response in on-going clinical trials.

Acknowledgements

I would like to take this opportunity to thank everyone who has helped me during my research for making my time so productive and enjoyable. I would particularly like to thank my supervisors:

Professor Chris Lord for giving me the opportunity to undertake this PhD, for his guidance in helping me develop as a scientist and for always showing a passion for my project

Dr Stephen Pettit for his almost endless patience, technical expertise and his cool head.

Dr Susana Banerjee for being ever supportive of my ambitions and always showing belief in my abilities.

I am grateful to members of the Gene Function Lab who have provided me with so much help, support and entertainment over the last four years. Particular thanks must go to Rachel Brough, Diana Zatreanu, Joseph Baxter and Drago Krastev, whose expertise and friendship has kept me going, even when things were challenging.

Finally, I would like to mention my family and friends, whose support has been indispensable in giving me belief that I could undertake this project.

Table of Contents

List of figures

List of tables.

Abbreviations

53BP1	p53-binding protein 1
AGE	Age-related
AKT	RAC(Rho family)-alpha serine/threonine-protein kinase
ANOVA	Analysis of variance
APOBEC	Apolipoprotein B mRNA editing enzyme
ARID1A	AT-rich interactive domain-containing protein 1A
ARID1B	AT-rich interactive domain-containing protein 1B
ARID2	AT-rich interactive domain-containing protein 2
ATARI	ATr Inhibitor in Combination with Olaparib in Gynaecological Cancers With ARId1A Loss or no Loss
ATCC	American Type Culture Collection
ATM	Ataxia telangiectasia mutated protein
ATR	Ataxia telangiectasia and Rad3 related
ATRi	ATR inhibitor
ATRIP	ATR interacting protein
AUC	Area under curve
AURKA	Aurora kinase A
AURKAi	Aurora kinase A inhibitor
bp	Base pairs
BRAF	v-Raf murine sarcoma viral oncogene homolog B

BRCA 1	Breast cancer 1, early onset gene
BRCA 2	Breast cancer 2, early onset gene
BrDU	5-bromo-2'-deoxyuridine
BRIP1	BRCA1 interacting helicase 1
BSA	Bovine serum albumin
BSO	Buthionine sulfoximine
CA125	Cancer Antigen 125
cBAF	Canonical brahma-related gene 1/brahma (BRG1/BRM)-associated factor
CCLE	Cancer Cell Line Encyclopaedia
CCNE1	Cyclin 1
CCR	Centre for Cancer Research
CDC25A	M-phase inducer phosphatase 1
CDC25C	M-phase inducer phosphatase 3
CDC45	Cell division cycle 45 protein
CDC7	Cell division cycle 7-related protein kinase
CDK	Cyclin dependent kinase
CDK2	Cyclin dependent kinase 2
cDNA	Copy DNA
cGAS	GMP-AMP synthase
CHK1	Checkpoint kinase 1
CHK2	Checkpoint kinase 2
CI	Confidence interval
CK20	cytokeratin 20
CK7	cytokeratin 7

CMV	Cytomegalovirus
cNA	Cytosolic nucleic acid
CRISPR	Clustered regularly interspaced short palindromic repeats
CRISPRa	CRISPR activation
CRISPRi	CRISPR interference
CRISPRn	CRISPR nuclease
CRUK	Cancer Research UK
dCas9	Dead Cas 9
dCK	Deoxycytidine kinase
DCR	Disease control rate
DDR	DNA damage response
DE	Drug effect
DEPC	Diethyl Pyrocarbonate
DMSO	Dimethyl sulfoxide
DNA	Deoxyribonucleic acid
DNA-PK	DNA-dependent protein kinase
dNTP	Deoxynucleoside triphosphate
DSB	Double-strand DNA break
dsDNA	Double-strand DNA
EGFR	Epidermal growth factor
EOC	Epithelial ovarian cancer
ER	Oestrogen receptor
ERBB2	Receptor tyrosine-protein kinase erbB-2
ES	Embryonic stem cells

EZH2	Enhancer of zeste homolog 2
FACS	fluorescence-activated cell sorting
FANCD2	Fanconi anaemia group D2 protein
FBS	Foetal bovine serum
FFPE	Formalin fixed and paraffin embedded
FIGO	International Federation of Gynaecology and Obstetrics
FLT3	Fms Related Receptor Tyrosine Kinase 3
FOXM1	Forkhead Box M1
GCL	Glutamine-cysteine ligase synthetase
GCLC	Glutamate-cysteine ligase synthetase
GINS	SLD5–PSF1–PSF2–PSF3 complex
GSH	Glutathione
GSS	GSH synthetase
GW	Genome-wide
HDAC6	Histone deacetylase 6
HEAT	Huntington, elongation factor, PP2A, TOR kinase
HGSOC	High grade serous ovarian cancer
HIF-1α	Hypoxia-inducible factor 1-alpha
HNF1-β	Hepatocyte nuclear factor 1-beta
HR	Homologous Recombination
HR	Hazard ratio
HRD	Homologous recombination deficiency
HRP	Horseradish peroxidase
HRT	Hormone replacement therapy

ICB	Immune checkpoint blockade
ICI	Immune checkpoint inhibitor
ICON7	International Collaboration on Ovarian Neoplasms 7
IF	immunofluorescence
IHC	Immunohistochemistry
IL-6	Interleukin 6
IL6ST	Interleukin 6 Cytokine Family Signal Transducer
IP	Immunoprecipitation
KRAB	Krüppel-associated box
KRAS	Kirsten Rat Sarcoma virus
LGSOC	Low grade serous ovarian cancer
LOF	Loss of function
MC	Mucinous ovarian cancer
MCM	Mini-chromosome maintenance complex
miRNA	Micro RNA
MLH1	MutL protein homolog 1
MMR	Mismatch repair
MOPS	3-(N-morpholino)propanesulfonic acid
MRE11	Double strand break repair nuclease
mRNA	Messenger RNA
MSH2	MutS homolog 2
MSH6	MutS homolog 6
mTOR	Mammalian target of rapamycin
ncBAF	Non-canonical brahma-related gene 1/brahma (BRG1/BRM)-associated facto

NF-κB	Nuclear factor kappa B
NGS	Next generation sequencing
NHEJ	Non-homologous end joining
NICE	National Institute for Health and Care Excellence
NRAS	Neuroblastoma RAS viral oncogene homolog
NSCLC	non-small cell lung cancer
OCCC	Ovarian clear cell carcinoma
OR	Odds ratio
ORC	Origin replication complex
OS	Overall survival
OSR1	Oxidative stress responsive kinase 1
PAM	Protospacer adjacent motif
PAOLA-1	Platine, Avastin and OLAparib in 1st Line
PARP	Poly(ADP)-ribose polymerase
PARPi	Poly(ADP)-ribose polymerase inhibitors
pBAF	Polybromo-asscoiatedl brahma-related gene 1/brahma (BRG1/BRM)-associated factor
PBRM1	Protein polybromo-1
PBS	Phosphate buffered saline
PCA	Principle component analysis
PCR	Polymerase chain reaction
PD-1	Programmed cell death protein 1
PD-L1	Programmed death-ligand 1
PD-L2	Programmed death-ligand 2

PDGFR	platelet-derived growth factor receptor
pegRNA	Prime editing guide RNA
PFS	Progression free survival
PI	Propidium iodide
PI3K	Phosphoinositide 3-kinases
PIK3CA	Phosphatidylinositol-4,5-bisphosphate 3-kinase, catalytic subunit alpha
PIK3IP1	PI3K-interacting protein 1 gene
PIKK	Phosphatidylinositol 3 kinase-related kinase
PLK1	Polo-like kinase 1
PMS2	Post meiotic segregation 1
Pol III	DNA polymerase III
PP1	Protein phosphatase 1
PP2A	Protein phosphatase 2
PPP2CA	Protein Phosphatase 2 Catalytic Subunit Alpha
PPP2R1A	Protein Phosphatase 2 Scaffold Subunit Alpha
PPP2R2A	Protein Phosphatase 2 regulatory subunit B alpha
PPP2R2B	Protein Phosphatase 2 regulatory subunit B beta
PR	Progesterone receptor
PRC2	Polycomb repressive complex 2
PTEN	Phosphatase and tensin homolog
RAD51C	RAD51 paralog C
RAD51D	RAD51 paralog D
RFP	Red fluorescent protein

RIF1	Replication timing regulatory factor 1
RISC	RNA silencing complex
RMH	Royal Marsden Hospital
RNA	Ribonucleic acid
RNR	Ribonucleotide reductase
ROS	Reactive oxygen species
RPA	Replication protein A
SEM	Standard error of the mean
SF	Surviving fraction
SF_{50}	50% surviving fraction
sgRNA	Single guide RNA
shRNA	Short hairpin RNA
siRNA	Short interfering RNA
SMAP	Small molecule PP2A activators
SMARCA4	SWI/SNF Related, Matrix Associated, Actin Dependent Regulator Of Chromatin, Subfamily A, Member 4
SMARCB1	SWI/SNF-related matrix-associated actin-dependent regulator of chromatin subfamily B member 1
SMG-1	suppressor of morphogenesis in genitalia
SPRY1	Sprouty RTK Signalling Antagonist 1
ssDNA	Single-strand DNA
SSDR	Single strand DNA repair
STAT3	Signal transducer and activator of transcription 3
STING	Stimulator of interferon genes

SWI/SNF	SWItch/Sucrose Non-Fermentable
TCGA	The Cancer Genome Atlas Project
TGF-β	Transforming growth factor beta
TIDE	Tracking of indels by decomposition
TMT	Tandem mass tag
TOP2A	Topoisomerase 2-ALPHA
TOPB1	DNA topoisomerase binding protein 1
TRRAP	Transformation/transcription domain-associated protein
VEGF	vascular endothelial growth factor
VEGFA	vascular endothelial growth factor A
VEGFR1	Vascular endothelial growth factor receptor 1
VEGFR2	Vascular endothelial growth factor receptor 2
VEGFR3	Vascular endothelial growth factor receptor 3
VPR	VP64-p65-Rta
VTE	Venous thromboembolism
WEE1	Mitosis inhibitor protein kinase Wee1
WHO	World Health Organisation
WNK1	With no lysine kinase 1
WT	Wild-type
WT1	Wilms tumour protein 1
YES1	Proto-oncogene tyrosine-protein kinase Yes

Chapter 1. Introduction

1.1 Ovarian cancer

1.1.1 Overview of Ovarian Cancer

Ovarian cancer does not represent a singular disease, rather the term refers to a group of heterogeneous malignancies with unique histopathological features, differing tissues of origin and molecular aberrations. Broadly, ovarian cancer can be classified as malignant epithelial carcinomas (EOC), accounting for approximately 90% of cases, and non-epithelial ovarian cancer, which accounts for the remaining 10%. There are five major histological subtypes of EOC; high grade serous (HGSOC), low grade serous (LGSOC), mucinous (MC), endometroid (EOC) and clear cell (OCCC) (McCluggage 2011, Banerjee and Kaye 2013). Non-epithelial ovarian cancer refers to a group of malignant germ cell tumours (including dysgerminomas, yolk sac tumours and teratomas) along with potentially malignant sex cord stromal tumours, of which granulosa cell tumours are the most common (Ray-Coquard, Morice et al. 2018). The histological classification together with molecular features associated with each subtype are summarised in Figure 1.1.

Epithelial ovarian cancer (EOC) is the ninth most common cancer in the world and represents the fourth highest cause of cancer death in women (Reid, Permuth et al. 2017, WHO 2020). Despite high initial response rates to treatment with a combination of surgery and chemotherapy, the five-year survival rate for women diagnosed with stage III and IV disease remains 25%

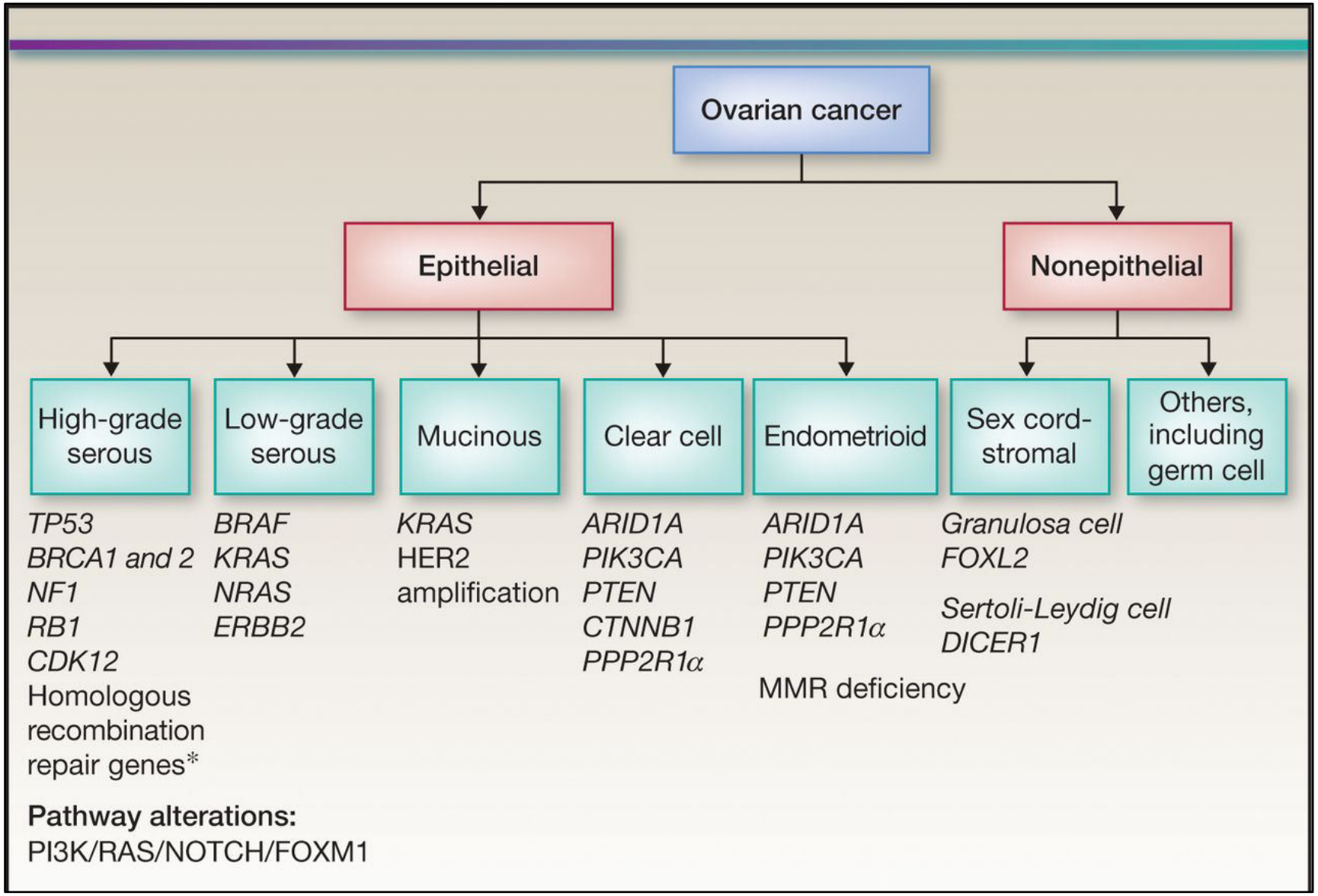

Figure 1.1 Summary of the histological subtypes of ovarian cancer together with their associated driver mutations.

Taken from Banerjee and Kaye (2013)

(Ledermann, Raja et al. 2013). The majority of patients that relapse will go on to receive multiple lines of therapy. Despite these, diminishing treatment-free intervals are common, as is the development of resistant disease

EOC is subdivided into a number of distinct histopathological subtypes, each with its own clinical behaviour and prognosis. High grade serous (HGSOC) is the most common subtype, accounting for approximately 70% of cases (Mackay, Brady et al. 2010, Zhou, Wu et al. 2018). Inherited genetic mutations are responsible for up to 20% of EOC, the majority of which are in the *BRCA1* and *BRCA2* genes, with a lesser contribution from the Lynch syndrome genes (*MLH1*, *MSH2*, *MSH6*, *PMS2*), and other homologous recombination-associated genes such as *BRIP1*, *RAD51C* and *RAD51D* (Stratton, Gayther et al. 1997, Risch, McLaughlin et al. 2001, Kastrinos, Stoffel et al. 2008, Senter, Clendenning et al. 2008, Bonadona, Bonaiti et al. 2011, Loveday, Turnbull et al. 2011, Rafnar, Gudbjartsson et al. 2011, Loveday, Turnbull et al. 2012, Lin-Hurtubise, Yheulon et al. 2013). The prevalence of germline *BRCA1* and *BRCA2* mutations has been estimated to be as high as 17% for serous ovarian cancers, whilst a further 6% of HGSOC harbour a somatic mutation (McCluggage 2011). Other rarer subtypes of EOC include endometroid (9-11%), low grade serous (10%), mucinous (3%) and clear cell carcinoma (5-13%) (Deavers, Gershenson et al. 2002, McCluggage 2011, Banerjee and Kaye 2013).

1.1.2 Ovarian cancer incidence and mortality

Globally there are 313,959 new cases of ovarian cancer diagnosed each year, with a cumulative lifetime risk of 0.73% (WHO 2020). In the UK, there are approximately 7500 cases of ovarian cancer per year, accounting for 4% of new cancer diagnoses in women (CRUK 2018). Ovarian cancer is predominantly a disease of post-menopausal women, with 80% of cases being identified in women over the age of 50 years (Jayson, Kohn et al. 2014) and 25% of new cases in women aged 75-79 years (CRUK 2018).

Overall survival for women diagnosed with ovarian cancer remains poor, with 207,252 deaths globally each year (WHO 2020). In the UK there are approximately 4,000 deaths due to ovarian cancer each year, accounting for 5% of female cancer deaths (CRUK 2018). In the UK, the one, five and ten year survival is 72, 43 and 35% respectively (CRUK 2018), with little improvement observed over the last two decades. The stage at diagnosis heavily impacts survival in women with ovarian cancer, with a 93% five-year survival for women diagnosed with stage I disease compared to 13% for those women diagnosed with stage IV disease (CRUK 2018).

1.1.3 FIGO staging

Accurate staging of newly diagnoses of ovarian cancer is of vital importance in guiding therapy and prognostication. The International Federation of Gynaecology and Obstetrics (FIGO) staging system is the most widely accepted method for ovarian cancer staging. The FIGO staging system was

updated in 2014 (Table 1.1) and stipulates that, where possible, the grade, histological subtype and organ or origin (e.g. ovary, peritoneum, fallopian tube) should be specified (Prat and Oncology 2015).

1.1.4 Molecular and histological classification of ovarian cancer

The various ovarian cancer subtypes can be differentiated by light microscopy (Prat and Oncology 2014) but are also associated with distinct molecular aberrations; the presence of these molecular alterations not only aids subclassification but also offers a divergence in potential therapeutic options. Analyses performed as part of The Cancer Genome Atlas (TCGA) identified the near ubiquitous presence of *TP53* mutations in HGSOC (Cancer Genome Atlas Research 2011) and tumoural loss of TP53 expression has now been incorporated in the diagnostic pathway for this EOC subtype (Kobel, Piskorz et al. 2016). Serous ovarian cancers often display defects in homologous recombination (HR) in part due to the relative high prevalence of both germline and somatic, *BRCA1* (12%) and *BRCA2* (11%) mutations along with other genes involved in HR including *CDK12* and *RAD50* (Cancer Genome Atlas Research 2011). *Cyclin E* (*CCNE1*) amplification is observed in up to 20% of HGSOCs (Kanska, Zakhour et al. 2016). LGSOC is a distinct clinical entity to HGSOC, with a younger age at presentation, more indolent clinical course, and resistance to standard cytotoxic chemotherapy but prolonged overall survival (OS) (Gershenson 2016). Activating mutations in genes involved in the mitogen activated protein kinase network, including *KRAS*, *BRAF* and *NRAS*, together with *ERBB2* amplification, are frequently observed in LGSOC

STAGE I: Tumor confined to ovaries					
OLD			NEW		
IA	Tumor limited to 1 ovary, capsule intact, no tumor on surface, negative washings/ascites.		IA	Tumor limited to 1 ovary, capsule intact, no tumor on surface, negative washings.	
IB	Tumor involves both ovaries otherwise like IA.		IB	Tumor involves both ovaries otherwise like IA.	
IC	Tumor involves 1 or both ovaries with any of the following: capsule rupture, tumor on surface, positive washings/ascites.		*IC Tumor limited to 1 or both ovaries*		
			IC1	*Surgical spill*	
			IC2	*Capsule rupture before surgery or tumor on ovarian surface.*	
			IC3	*Malignant cells in the ascites or peritoneal washings.*	
STAGE II: Tumor involves 1 or both ovaries with pelvic extension (below the pelvic brim) or primary peritoneal cancer					
OLD			NEW		
IIA	Extension and/or implant on uterus and/or Fallopian tubes		IIA	Extension and/or implant on uterus and/or Fallopian tubes	
IIB	Extension to other pelvic intraperitoneal tissues		IIB	Extension to other pelvic intraperitoneal tissues	
IIC	IIA or IIB with positive washings/ascites.				
Old stage IIC has been eliminated					
STAGE III: Tumor involves 1 or both ovaries with cytologically or histologically confirmed spread to the peritoneum outside the pelvis and/or metastasis to the retroperitoneal lymph nodes					
OLD			NEW		
IIIA	Microscopic metastasis beyond the pelvis.		*IIIA (Positive retroperitoneal lymph nodes and /or microscopic metastasis beyond the pelvis)*		
			IIIA1	*Positive retroperitoneal lymph nodes only*	
				IIIA1(i)	*Metastasis ≤ 10 mm*
				IIIA1(ii)	*Metastasis > 10 mm*
			IIIA2	*Microscopic, extrapelvic (above the brim) peritoneal involvement ± positive retroperitoneal lymph nodes*	
IIIB	Macroscopic, extrapelvic, peritoneal metastasis ≤ 2 cm in greatest dimension.		IIIB	*Macroscopic, extrapelvic, peritoneal metastasis ≤ 2 cm ± positive retroperitoneal lymph nodes. Includes extension to capsule of liver/spleen.*	
IIIC	Macroscopic, extrapelvic, peritoneal metastasis > 2 cm in greatest dimension and/or regional lymph node metastasis.		IIIC	*Macroscopic, extrapelvic, peritoneal metastasis > 2 cm ± positive retroperitoneal lymph nodes. Includes extension to capsule of liver/spleen.*	
STAGE IV: Distant metastasis excluding peritoneal metastasis					
OLD			NEW		
IV	Distant metastasis excluding peritoneal metastasis. Includes hepatic parenchymal metastasis.		*IVA*	*Pleural effusion with positive cytology*	
			IVB	Hepatic and/or *splenic parenchymal* metastasis, metastasis to extra-abdominal organs (including inguinal lymph nodes and lymph nodes outside of the abdominal cavity)	

Table 1.1 FIGO ovarian, fallopian tube and peritoneal cancer staging system.

Take from Prat *et al* (2015)

(Jones, Wang et al. 2012, Grisham, Sylvester et al. 2015, Hunter, Anglesio et al. 2015). Activating *KRAS* mutations are also a frequent observation in MC (Mackenzie, Kommoss et al. 2015). Both EOC and OCCC are considered to be endometriosis associated cancers (Pearce, Templeman et al. 2012) and are characterised by distinct genetic changes when compared to other EOC subtypes. Both EOC and OCCC display relatively high rates of *ARID1A* loss-of-function together with alterations in the PI3K-AKT pathway including activating *PIK3CA* mutations and *PTEN* loss mutations (Jones, Wang et al. 2010, Wiegand, Lee et al. 2011). OCCC will be discussed in detail in the following section.

1.2 Ovarian clear cell carcinoma

1.2.1 Overview and diagnostic criteria

OCCC accounts for approximately 5-11% of EOC cases and is characterised by a number of distinct histopathological, molecular and clinical features which distinguish it from other EOC subtypes. With respect to histopathology, OCCC is known to have glycogen-containing cells with abundant clear cytoplasm and hobnail cells (Serov 1973). The presence of scanty cytoplasm with large nuclei that extend into the lumen, lining tubules and cysts, define hobnail cells (Ordi, Romagosa et al. 2003). OCCC can be routinely diagnosed through immunohistochemistry. Unlike. HGSOC, OCCC usually have a wild-type (WT) pattern of p53 staining (Kobel, Piskorz et al. 2016) and stain negative for Wilms Tumours 1 (WT1), oestrogen receptors (ER) and progesterone receptors (PR)

for cytokeratin 20 (CK20) (McCluggage 2011). Hepatocyte nuclear factor 1-β (HNF1-β) overexpression as determined by immunohistochemistry has been suggested in several studies to be highly specific for OCCC (Tsuchiya, Sakamoto et al. 2003, Kobel, Kalloger et al. 2008). However, HNF1-β immunohistochemistry is not routinely performed in the diagnosis of OCCC.

1.2.2 Clinicopathological features of OCCC

The incidence of OCCC varies according to geographic location. In western populations, OCCC is reported to account for 5-11% of EOC cases (Banerjee and Kaye 2013, Oliver, Brady et al. 2017). Higher incidences of OCCC have been reported amongst women from East Asia, with a rate of 10-11.6 % in Korea (Kim, Lim et al. 2016) and up to 30% in Japan (Okamoto, Glasspool et al. 2014). Women diagnosed with OCCC tend to present at earlier age (median age of presentation of 55 years *vs.* 64 years for serous carcinoma) and are more likely to present with early-stage disease (Chan, Teoh et al. 2008, Okamoto, Glasspool et al. 2014).

In contrast to HSCOC and EOC, OCCC is not associated with a positive family history, with the main risk factor being nulliparity and endometriosis (Kurian, Balise et al. 2005). A pooled meta-analysis of 13 case-control studies reported an association between self-reported endometriosis and OCC with an odds ratio (OR) of 3.05 (95% CI 2.43-3.84, $p<0.0001$) (Pearce, Templeman et al. 2012). This is consistent with a more recent study involving the Danish Cancer Register in which an endometriosis diagnosis was associated with an

increased risk of both ovarian cancer and OCCC with ORs of 1.34 (95% CI: 1.16-1.55) and 3.64 (95% CI: 2.36-5.38) respectively (Mogensen, Kjaer et al. 2016). The risk of OCCC is reduced following tubal ligation (OR = 0.35, 95% CI: 0.12 – 1.0) which is thought to be due to reduction in endometriosis arising through retrograde blood flow (Kurian, Balise et al. 2005). The presence of free iron in endometriosis has been proposed as a mechanistic explanation for the association of endometriosis and OCCC through oxidative stress, which can lead to malignant transformation (Yamaguchi, Mandai et al. 2008, Yamada, Shigetomi et al. 2011).

A number of studies have demonstrated an increased risk of venous thromboembolism (VTE) in patients with OCCC. *Duska et al* first reported that patients with a diagnosis of OCCC had a risk of VTE 2.5 times greater than that of patients with other EOC subtypes, despite adequate thromboprophylaxis (Duska, Garrett et al. 2010). These findings were confirmed by a large case-control study performed amongst Japanese patients, which identified that advanced stage (hazard ratio [HR] 3.38, $p < 0.0001$), thrombocytosis (HR 1.42, $p = 0.032$) and elevated IL-6 levels (HR 8.90, $p = 0.046$) were independent predictors of VTE (Matsuo, Hasegawa et al. 2015). Elevated serum IL-6 levels and an upregulation of IL-6 gene expression signatures in tumour cells have previously been observed in OCCC patients and mouse models of the disease (Chandler, Damrauer et al. 2015, Matsuo, Hasegawa et al. 2015).

1.2.3 Genomic landscape of OCCC

Unlike HGSOC, OCCC usually have wild-type (WT) *TP53* and have a much lower frequency of *BRCA1* and *BRCA2* mutations than HGSOC (Kobel, Kalloger et al. 2008, Itamochi, Oishi et al. 2017). Truncating mutations in *ARID1A* are the most commonly observed genetic aberration in OCCC, being observed in 40-57% of cases (Kuo, Mao et al. 2009, Jones, Wang et al. 2010, Wiegand, Lee et al. 2011). Mutations affecting *PIK3CA* (33%), *PPP2R1A* (7-10%) and *KRAS* (5%) are also frequently observed in OCCC, along with *ERBB2* (14%) and *AKT2* (14%) amplifications (Kuo, Mao et al. 2009, Jones, Wang et al. 2010, Shih Ie, Panuganti et al. 2011, Tan, Iravani et al. 2011). The significance of *ARID1A* mutations and *PPP2R1A* mutations will be discussed in detail in subsequent sections.

Within OCCC, two significant subgroups can be identified based on their mutational status. 26% display a mutational signature associated with apolipoprotein B mRNA editing enzyme, catalytic polypeptide-like (APOBEC) mutation signature (Wang, Bashashati et al. 2017). Indeed, APOBEC mediated kataegis has been proposed as a driver event in OCCC (Shibuya, Tokunaga et al. 2018) and overexpression of APOBEC3B has been associated with improved survival and enhanced response to platinum-based chemotherapy in OCCC (Serebrenik, Argyris et al. 2020). 40% of OCCC cases display an age-related (AGE) mutation signature (Wang, Bashashati et al. 2017).

When compared to HGSOC, the total number of copy number alterations (CNA) are lower in OCCC (Kuo, Mao et al. 2010). However, the proportion of CNAs arising as a result of whole-arm chromosomal alterations is significantly higher in OCCC compared to HGSOC (46.9 % vs 21.7 %, p<0.0001) (Uehara, Oda et al. 2015). In OCCC, chr20q13.2, a region which encodes zinc finger protein 217 (*ZNF217),* is frequently subject to copy number gain, being observed in 20-36% of patients (Kuo, Mao et al. 2010, Tan, Iravani et al. 2011, Jones, Wang et al. 2012). Furthermore, *ZNF217* amplification has been associated with deleterious outcomes in terms of both progression free survival (PFS) and overall survival (OS) in OCCC (Rahman, Nakayama et al. 2012)

1.2.4 Prognosis and standard of care treatment for OCCC

OCCC is associated with resistance to standard cytotoxic chemotherapy compared to other EOC subtypes. Patients newly diagnosed with OCCC tend to do so with earlier stage (stage I/II) disease compared to HGSOC (57%–81% vs 19%–22%) (Chan, Teoh et al. 2008, Kobel, Kalloger et al. 2010, Wentzensen, Poole et al. 2016). In a case series involving patients enrolled in twelve prospective randomized Gynecologic Oncology Group (GOG) studies, there was significantly improved PFS (0.69, 95% CI 0.50 to 0.96) and a trend towards an OS (HR 0.76, 95% CI 0.53 to 1.09) benefit for patients diagnosed with stage I/II OCCC compared to HGSOC (Oliver, Brady et al. 2017). This is consistent with a meta-analysis of twelve randomised control trials, which found no statistically significant difference in OS between patients

diagnosed with early stage OCCC and HGSOC (HR 1.17, 95% CI; 1.01–1.36) (Lee, Kim et al. 2011). However, in the advanced setting, outcomes are much worse for women diagnosed with OCCC compared to other EOC subtype. Analysis of patients enrolled in the GOG studies along with the meta-analysis revealed significantly worse OS for patients diagnosed with stage III/IV OCCC compared to HGSOC; HR 1.66 (95% CI 1.43 to 1.91) (Oliver, Brady et al. 2017) and HR 1.71 (95% CI 1.57 to 1.86) (Lee, Kim et al. 2011) respectively. The poor outcomes in patients diagnosed with advanced stage OCCC in part reflects the relatively low response rates to systemic chemotherapy, which have been reported to be as low as 1-8% in the second-line setting (Pather and Quinn 2005, Takano, Sugiyama et al. 2008).

In the majority of patients with newly diagnosed OCCC the aim is to perform major debulking surgery. In a retrospective analysis of 254 patients who underwent surgery for OCCC, the absence of residual disease was associated with improvements in PFS compared to those patients with residual disease measuring both less than 1 cm in diameter ($p = 0.04$) and greater than 1 cm ($p < 0.01$). In this analysis only residual tumour diameter was an independent prognostic factor in predicting PFS in advanced disease ($p = 0.02$) (Takano, Kikuchi et al. 2006). Adjuvant chemotherapy is recommended for all patients diagnosed with stage 1C2 or greater OCCC (Colombo, Sessa et al. 2019). The benefit of adjuvant chemotherapy in earlier stage OCCC has not been established, and if considered should be discussed with patients on an individual basis (Timmers, Zwinderman et al. 2009, Mizuno, Kajiyama et al. 2012, Takada, Iwase et al. 2012, Colombo, Sessa et al. 2019). Carboplatin

in combination with paclitaxel is the recommended adjuvant chemotherapy regime for OCCC as well as other EOC subtypes (du Bois, Quinn et al. 2005, Colombo, Sessa et al. 2019).

Bevacizumab (Avastin®, Genentech) is a humanised monoclonal antibody that targets vascular endothelial growth factor A (VEGFA). It was the first targeted agent to be licensed as a maintenance therapy following first-line chemotherapy in EOC, based on the results of the ICON7 clinical trial (NICE 2013, Oza, Selle et al. 2017, EMA 2022). ICON7 enrolled patients with both early and late stage OCCC. In the subgroup analysis of patients with OCCC no significant benefit was observed with the addition of bevacizumab to carboplatin and paclitaxel chemotherapy. It should be noted that this subgroup analysis was underpowered and therefore the activity of bevacizumab for this indication cannot be excluded (Oza, Selle et al. 2017).

Poly (ADP-ribose) polymerase inhibitors (PARPi) have revolutionised the treatment landscape of ovarian cancer. The synthetic lethal interaction between PARPi and *BRCA1* and *BRCA2* mutations is discussed in detail in a subsequent chapter but it should be highlighted that the activity of PARPi in ovarian cancer is not limited to those tumours with defects in either *BRCA1* or *BRCA2*. As previously discussed, in the context of OCCC, *BRCA1* and *BRCA2* mutations are observed at much lower frequencies than other EOC subtypes. Olaparib (Lynparza®, AstraZeneca) monotherapy is only licenced as a first-line maintenance therapy in women with stage III/IV high grade EOC

associated with a *BRCA1* or *BRCA2* mutation (NICE 2019). Niraparib (Zejula®, GlaxoSmithKline) is a PARPi which is licenced as a first-line maintenance therapy following response to first-line platinum-based chemotherapy in women diagnosed with stage III or IV high grade EOC, irrespective of *BRCA1* or *BRCA2* mutation status (NICE 2021). Based on the results of the PAOLA-1 clinical trial, olaparib in combination with bevacizumab is licensed as a first-line maintenance therapy, again after first-line platinum-based chemotherapy, in women diagnosed with stage III or IV high grade EOC where there is evidence of homologous recombination deficiency (HRD) as determined by Myriad myChoice® test, irrespective of whether the observed HRD is due to a BRCA1 or BRCA2 mutation (NICE 2021). The National Institute for Health and Care Excellence (NICE) authorization statement for both niraparib and olaparib with bevacizumab would in theory encompass OCCC due their high grade. However, it should be highlighted that no patients with clear cell histology were enrolled in either the PRIMA or PAOLO-1, the two randomized phase III trials which led to the authorization of niraparib and olaparib with bevacizumab for this indication respectively (Gonzalez-Martin, Pothuri et al. 2019, Ray-Coquard, Pautier et al. 2019). Therefore, PARPi are not routinely used in the context of OCCC despite their market authorization.

1.2.5 Future treatment strategies for OCCC

Despite the distinct clinicopathological and molecular features of OCCC, patients with this disease subtype have historically been included in clinical trials alongside other subtypes of EOC, perhaps going someway to explaining

the poor outcomes and lack of progress for this patient cohort. There is clearly a great need in OCCC to develop biomarker-driven treatments that will lead to clinically meaningful improvements in patient outcomes.

Experimental treatment strategies for OCCC can be divided in to three broad categories:

1. *ARID1A* synthetic lethal approaches
2. Immune checkpoint blockade (ICB)
3. Anti-angiogenic therapy

The function of ARID1A in normal and cancer cells, along with the synthetic lethal interactions currently being exploited in the context of OCCC, will be discussed in detail in the following chapter.

ICB refers the inhibition of immunoregulatory proteins, routinely using monoclonal antibodies, in order to elicit and anti-tumour immune response. Regulatory T cells and activated cytotoxic T cells express cytotoxic T lymphocyte-associated protein 4 (CTLA4), a CD28 homology with a higher binding affinity for the T-cell activating receptor B7 (Buchbinder and Desai 2016). Immune priming and a reduction in regulatory T-cell mediated suppression of inflammatory responses are two mechanisms through which CTLA4-directed monoclonal antibodies are proposed to promote an anti-tumour immune response (Fife and Bluestone 2008). Programmed cell death protein 1 (PD-1) is a negative co-stimulatory receptor, the expression of which is largely confined to activated T cells (Keir, Butte et al. 2008). Binding of

Programmed death-ligand 1 (PD-L1) or Programmed death-ligand 2 (PD-L2) to PD1 leads to the downregulation of immune responses (Pardoll 2012). Therefore, the disruption of this interaction is the target of several immune checkpoint inhibitors (ICIs). The presence or absence of an anti-tumour immune response is not solely dictated by the activity of immune co-stimulatory receptors, but also immune regulatory pathways operating within cancer cells including the cyclic GMP-AMP synthase (cGAS)-stimulator of interferon genes (STING) pathway. Cytosolic nucleic acids (cNA) a by-product of cancer-associated replication stress and ruptured micronuclei, are detected by cGAS which catalyses the conversion ATP and GTP into 2′,3′-cyclic GMP-AMP (cGAMP) (Ablasser, Goldeck et al. 2013, Sun, Wu et al. 2013). This activates a signalling cascade through STING and involving TANK binding kinase 1 (TBK1) and interferon regulatory factor 3 (IRF3) which culminates in the expression of immune stimulated genes and type 1 interferons, thereby promoting an anti-tumour immune response (Sun, Wu et al. 2013, Liu, Cai et al. 2015, Zhao, Du et al. 2019). Importantly, the therapeutic effect of anti-PD-L1 antibody was abolished in cGAS deficient mice highlighting the importance of this pathway to response to ICB (Wang, Hu et al. 2017). The activation of the cCAS-STING pathway has therefore garnered attention as a potential anti-cancer therapeutic approach.

The arrival of ICB has not brought about the same improvements in patient outcomes in EOC as it has in other tumour types such as melanoma, lung cancer and urothelial cancer. Several clinical studies have suggested increased sensitivity of OCCC to ICB. In the phase II study of nivolumab, a

fully human monoclonal immunoglobulin G4 antibody to PD-1, in platinum resistant ovarian cancer, two of the twenty enrolled patients achieved a complete response (CR), one of which had clear cell histology and achieved a durable complete response (Hamanishi, Mandai et al. 2015). Consistently, among the two OCCC patients treated with avelumab, monoclonal antibody of isotype IgG1 against PD-1, in the phase 1b JAVELIN trial, one had a partial response (PR) and the other one had an immune-related PR (Disis, Taylor et al. 2019). The KEYNOTE-100 in which patients were treated with the pembrolizumab, a humanised monoclonal antibody against PD-L1, study enrolled 376 relapsing EOC, of whom 19 were OCCC. The response rate was 15.8 % (95 % CI 3.4 %–39.6 %) in OCCC, compared to 8.5 % (95 %CI 5.5 %–12.4 %) in HGSOC (Matulonis, Shapira-Frommer et al. 2019). Finally, the randomized phase II NRG GY003 trial compared the combination ipilimumab, a fully human anti-CTLA-4 monoclonal antibody, and nivolumab to nivolumab in relapsing EOC. Patients with OCCC (n = 12) had an approximately five-fold greater odds (OR = 5.21; 95 %CI 1.37–19.77) of response compared with the other subtypes (n = 88) (Zamarin, Burger et al. 2020). Based on these observations, several clinical trials have sought to establish the role for ICB in treatment of OCCC.

In addition to the anecdotal evidence from clinical trials supporting the use of ICB in the treatment, there is a rationale to employ this class of drugs in ARID1A-defective cancers. Loss of ARID1A function has been associated with increased microsatellite instability, tumour mutational burden and response to ICB. ARID1A is proposed to recruit the MutS homolog 2 (MSH2) to chromatin

thereby promoting mismatch repair. The loss of this interaction correlated with a microsatellite instability genomic signature with a predominant C>T mutation pattern and increased mutational load across multiple tumour types (Shen, Ju et al. 2018). Consistent with this data, a bioinformatic analysis of cases of gastric cancer found an association between *ARID1A* mutations and increased immune activity, which was linked to increase tumour mutational burden (Li, Li et al. 2019). Tumour cell-line allografts formed by an Arid1a-deficient ovarian cancer cell line in syngeneic mice displayed increased mutation load, elevated numbers of tumour-infiltrating lymphocytes, and PD-L1 expression. Notably, treatment with anti-PD-L1 antibody reduced tumour burden and prolonged survival of mice bearing ARID1A-deficient but not ARID1A-proficient ovarian tumours (Shen, Ju et al. 2018).

Inhibition of the ataxia-telangiectasia mutated (ATM)-checkpoint kinase 2 (CHK2) axis has been shown to promote cGAS-STING activation and potentiate ICB in ARID1A deficient tumours (Wang, Yang et al. 2020). Whilst a similar effect has not been directly reported with Ataxia telangiectasia and Rad3 related (ATR) inhibition, the rationale for combining ATR inhibitor (ATRi) with immune checkpoint blockade (ICB) is two-fold. Firstly, ATR inhibition results in the proteasome dependent reduction in PD-L1 expression in cancer cells leading to enhanced immune cell infiltration (Sun, Yang et al. 2018). In addition, ATR inhibition attenuates irradiation-induced PD-L1 upregulation and decreases the number of tumour-infiltrating regulatory T cells (T_{regs}) in mouse models (Vendetti, Karukonda et al. 2018, Dillon, Bergerhoff et al. 2019, Sheng, Huang et al. 2020). ATR inhibition is associated with increased replication

stress and aberrant cell cycle checkpoints culminating in chromosome segregation defects and the formation of micro-nuclei, as outlined in detail in a subsequent section. cNA release from these micronuclei has been shown to result in cGAS-STING activation with the consequence of increasing inflammatory cell infiltration as well as PD-L1 expression on cancer cells (Harlin, Meng et al. 2009, Diamond, Kinder et al. 2011, Harding, Benci et al. 2017, Mackenzie, Carroll et al. 2017), with the potential to enhance the response to ICB.

MOCCA/APGOT-OV2/GCGS-OV3 was a randomized phase III trial in which patients with relapsed OCCC were randomized to receive either the programmed cell death ligand 1 (PD-L1) specific monoclonal antibody durvalumab (Infinzmi®, Astrazeneca) or physicians choice chemotherapy. In this randomized trial, no significant difference in terms of overall response (OR), PFS or disease control rate (DCR) was observed between the treatment groups (Tan, Choi et al. 2022). Despite the negative outcome of this trial, the results from several other ongoing trials of ICB in OCCC are eagerly awaited (Table 1.2).

Angiogenesis is one of the original hallmarks of cancer described by Hanahan and Weinberg (Hanahan and Weinberg 2000) and it's targeting has been explored as a potential for OCCC. Mabuchi *et al* observed increased levels of vascular endothelial growth factor (VEGF) by IHC in cases of both early and late OCCC and showed *in vivo* that bevacizumab inhibited the growth of OCCC tumour cell line xenografts (Mabuchi, Kawase et al. 2010). Furthermore,

Trial name	NCT Identifier	Phase	Design	Treatment	Reference
PEACOCC	NCT03425565	II	Single arm	Pembrolizumab 200mg, 3 weekly	(University College 2018)
-	NCT03026062	II	Single arm	Either: Sequential tremelimumab 1500 mg 4 weekly for 4 cycles followed by or durvalumab 1500 mg 4 weekly for 9 cycles Or Tremelimumab 1500 mg and durvalumab 1500 mg 4 weekly for 9 cycles	(Center 2017)
BrUOG 354	NCT03355976	II	Randomized	Nivolumab 240mg every 2 weeks +/- ipilimumab 1mg/kg every 6 weeks	(Brown, Bristol-Myers et al. 2017)

Table 1.2 Summary of ongoing clinical trials or clinical trials waiting to report involving ICB in OCCC.

the interleukin 6 (IL6)/signal transducer and activator of transcription 3 (STAT3)/hypoxia inducible factor pathway, a key mediator of angiogenesis, has been shown to be upregulated in OCCC with increased circulating levels of IL-6 observed in both OCCC patients and in mouse models of the disease (Anglesio, George et al. 2011, Chandler, Damrauer et al. 2015). These findings led to the development of the NICCC/ENGOT-OV36 (NCT02866370), a randomized phase II clinical trial in which patients with relapsed OCCC were treated with either nintedanib or physicians choice chemotherapy (Glasspool, Mcneish et al. 2020). Nintedanib is a multi-target tyrosine kinase inhibitor which blocks platelet-derived growth factor receptor (PDGFR) α and β; fibroblast growth factor receptor (FGFR) 1, 2, and 3; vascular endothelial growth factor receptor (VEGFR) 1, 2, and 3; and FLT3, key components of the angiogenic pathway (Hilberg, Roth et al. 2008). Whilst the trial failed to demonstrate superiority of nintedanib over standard of care chemotherapy, translational work is ongoing, including correlation of responses with soluble VEGF and VEGFR levels to determine if there are subgroups of OCCC patients who could benefit (Glasspool, Mcneish et al. 2020). Additionally, the activity of nintedanib within the trial warrants further exploration as to whether it could be combined with other agents, including ICB, to enhance response rates.

1.3 Synthetic lethality as a therapeutic approach to ovarian clear cell carcinoma

1.3.1 Synthetic lethality and the PARP/BRCA paradigm

The term synthetic lethality refers to the situation in biology wherein defects in a gene or protein is tolerated by a cell but when combined, or "synthesised", with defects in another gene or protein is associated with a reduction in viability, Figure 1.2 (Lord, Tutt et al. 2015). PARPi have transformed the treatment landscape of ovarian cancer, exploiting synthetic lethality to kill cancer cells whilst sparing normal tissue from cytotoxicity. Historically, the PARPi/BRCA synthetic lethal interaction was thought to arise from PARP being an integral component of the single strand DNA repair (SSDR) pathway. PARP1 detects and binds to single strand DNA breaks and PARP inhibition was thought to lead to the accumulation of ssDNA breaks, which, if they persist in the face of DNA replication, can give rise to double strand DNA breaks (DSBs)(McGlynn and Lloyd 2002, Farmer, McCabe et al. 2005). *BRCA1* and *BRCA2* are intimately involved in homologous recombination (HR), a process in which DSBs are repaired. When defects in either gene are present, the DNA damage produced as a consequence of PARP inhibition goes unrepaired, resulting in cell cycle arrest and cell death (Ashworth 2008).

The historical assumption that the cytotoxic effect of PARPi arises through the catalytic inhibition of PARP activity, and the resulting SSBR deficit, was

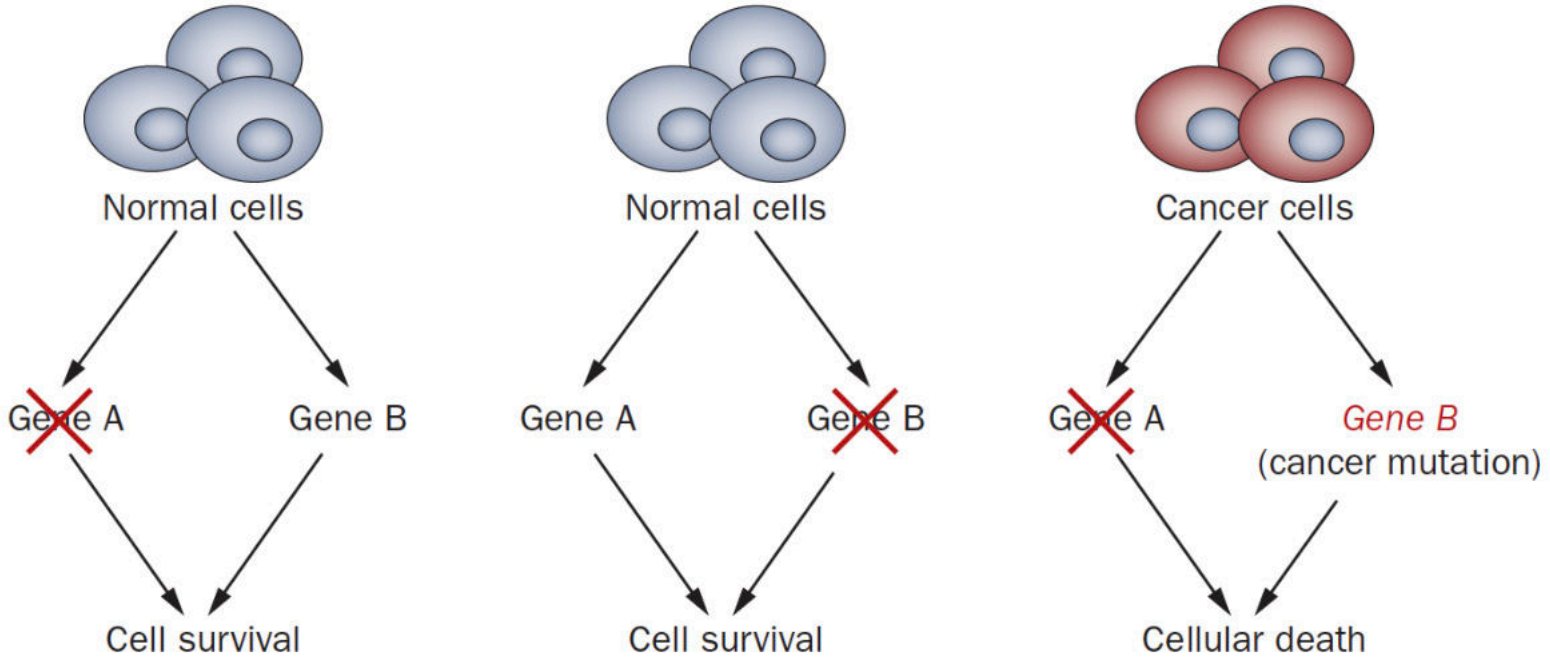

Figure 1.2 Schematic explaining synthetic lethality. Loss of either Gene A or Gene B is tolerated due to the compensating action of the unaltered gene. In cancer cells, a mutation in Gene B leaves cells vulnerable to defects in Gene A. Taken from (Rehman, Lord et al. 2010).

PARP inhibitor	Indication	*BRCA*/HRD status	Treatment Line	Setting	Maintenance/treatment	Reference
Olaparib (Lynparza®, Astrazenca)	Stage III/IV high grade EOC	BRCAmut	1st line	Platinum sensitive	Maintenance	(NICE 2019)
Olaparib with bevacizumab	Stage III/IV high grade EOC	HRD positive	1st line	Platinum sensitive	Maintenance	(NICE 2021)
Niraparib (Zejula®, GlaxoSmithKline)	Relapsed/recurrent HGSOC	*BRCA*wt + *BRCA*mut	2nd line and beyond	Platinum sensitive	Maintenance	(NICE 2022)
Rucaparib (Rubraca®, Clovis	Relapsed/recurrent HGSOC	*BRCA*wt + *BRCA*mut	2nd line and beyond	Platinum sensitive	Maintenance	(NICE 2019)

Table 1.3 Summary of the current NICE appraisals for the three PARPi licenced for the treatment of ovarian cancer.

challenged by the observation that PARPi cytotoxicity is reversed when PARP1 is itself not expressed (Murai, Huang et al. 2012, Pettitt, Rehman et al. 2013, Murai, Huang et al. 2014). Indeed, the observed variability in cytotoxicity between different PARPi *in vitro* despite having the same effect on PARP catalytic activity has been attributed to differential ability to trap PARP on DNA.

Talazoparib displays a 100-fold greater ability to trap PARP than niraparib, which has a greater PARP trapping ability than both olaparib and rucaparib whilst veliparib has very little ability to trap PARP (Hopkins, Ainsworth et al. 2019). Trapping of PARP1 and PARP2 at sites of DNA damage, and the accompanied recruitment of other proteins, results in the formation of a large DNA adduct (Ahel, Horejsi et al. 2009, Gottschalk, Trivedi et al. 2012, Murai, Huang et al. 2012), analogous to the lesion formed by exposure to the topoisomerase II inhibitor etoposide (Pommier, Leo et al. 2010). DNA lesions form a block to replication fork progression leading to their collapse thereby eliciting a DNA damage response. The HR deficiency associated with *BRCA1* and *BRCA2* deficiency impairs a cell's ability to process the DNA lesions caused by trapped PARP, providing a mechanistic basis for the PARP/BRCA synthetic lethal interaction (Lord and Ashworth 2017).

More recently, an additional potential mechanism for the PARP/BRCA synthetic lethal interaction has been proposed. PARP1 has been implicated in the detection and processing of Okazaki fragments (Vaitsiankova, Burdova et al. 2022), short DNA sequences which are produced discontinuously before being ligate to form the lagging strand during DNA replication (Okazaki 2017).

Single strand DNA (ssDNA) gaps are common intermediates encountered on the lagging strand and are more frequently observed in cells with *BRCA1* and *BRCA2* mutations due to a failure to stall replication under conditions of replication stress (Panzarino, Krais et al. 2021). Imposing PARP inhibition in cells with *BRCA1* or *BRCA2* mutations therefore results in the accumulation of ssDNA gaps, which is in itself toxic to cells (Cong, Peng et al. 2021). The cytotoxic effect of PARPi in cells with *BRCA1* mutations was reversed by factors that restrained the accumulation of ssDNA gaps including the loss of p53-binding protein 1 (53BP1) (Cong, Peng et al. 2021), a known cause of PARPi resistance (Jaspers, Kersbergen et al. 2013).

Currently, there are three PARPi licensed for use in the context of ovarian cancer and their NICE appraisal guidance is summarised in Table 1.3. Exploiting the PARPi/BRCA synthetic lethal interaction using PARPi is not unique to ovarian cancer but has been employed in the treatment of prostate (Mateo, Porta et al. 2020), breast (Robson, Goessl et al. 2017, Litton, Hurvitz et al. 2020, Tutt, Garber et al. 2021) and pancreatic (Golan, Hammel et al. 2019) cancers associated with homologous recombination defects. All three of the PARPi licenced for the treatment are inhibitors of PARP1, 2 and 3. Recently, PARPi inhibitor with greater selectivity towards PARP1 *vs.* PARP2 (AZD3505) which also traps PARP1 has been described and its use was associated with lower levels of haematological toxicity in animal models (Illuzzi, Staniszewska et al. 2022). Indeed, in the phase 1 study of AZD3505, dose modifications were required in 3% of patients enrolled, compared to 53%

observed in the phase I studies for first generation PARPi such as olaparib (Yap, Im et al. 2022).

1.3.2 The SWI/SNF complex

In eukaryotic cells over 2 m of DNA is tightly condensed into chromatin within a nucleus measuring less than 5 µm. Accessing this highly compact structure poses a significant challenge. Nucleosomes comprise the basic unit of chromatin, consisting of approximately 147 DNA base pairs wrapped around a histone octamer (Allis and Jenuwein 2016). Chromatin remodelers enable dynamic access to this highly compact structure by transcriptional regulators and DNA repair proteins. SWI/SNF (SWItch/Sucrose Non-Fermentable) complexes are a sub-family of chromatin remodelers which catalyse ATP to mediate nucleosome sliding or ejection (Bao and Shen 2007). Three mature SWI/SNF complexes have been described to date; the canonical brahma-related gene 1/brahma (BRG1/BRM)-associated factor (cBAF) complex, the polybromo-associated BAF (PBAF) complex, and the newly defined non-canonical BAF (ncBAF) complex (Figure 1.3) (Mashtalir, D'Avino et al. 2018, Michel, D'Avino et al. 2018, Chabanon, Morel et al. 2020).

Mutations in the genes encoding the SWI/SNF components are among the most frequently observed in cancer, being found in 20-25% of all cases (Kadoch, Hargreaves et al. 2013, Shain and Pollack 2013). The vast majority of these mutations result in loss of function phenotypes, suggesting they function as tumour suppressor genes in normal cells. Indeed, genetically

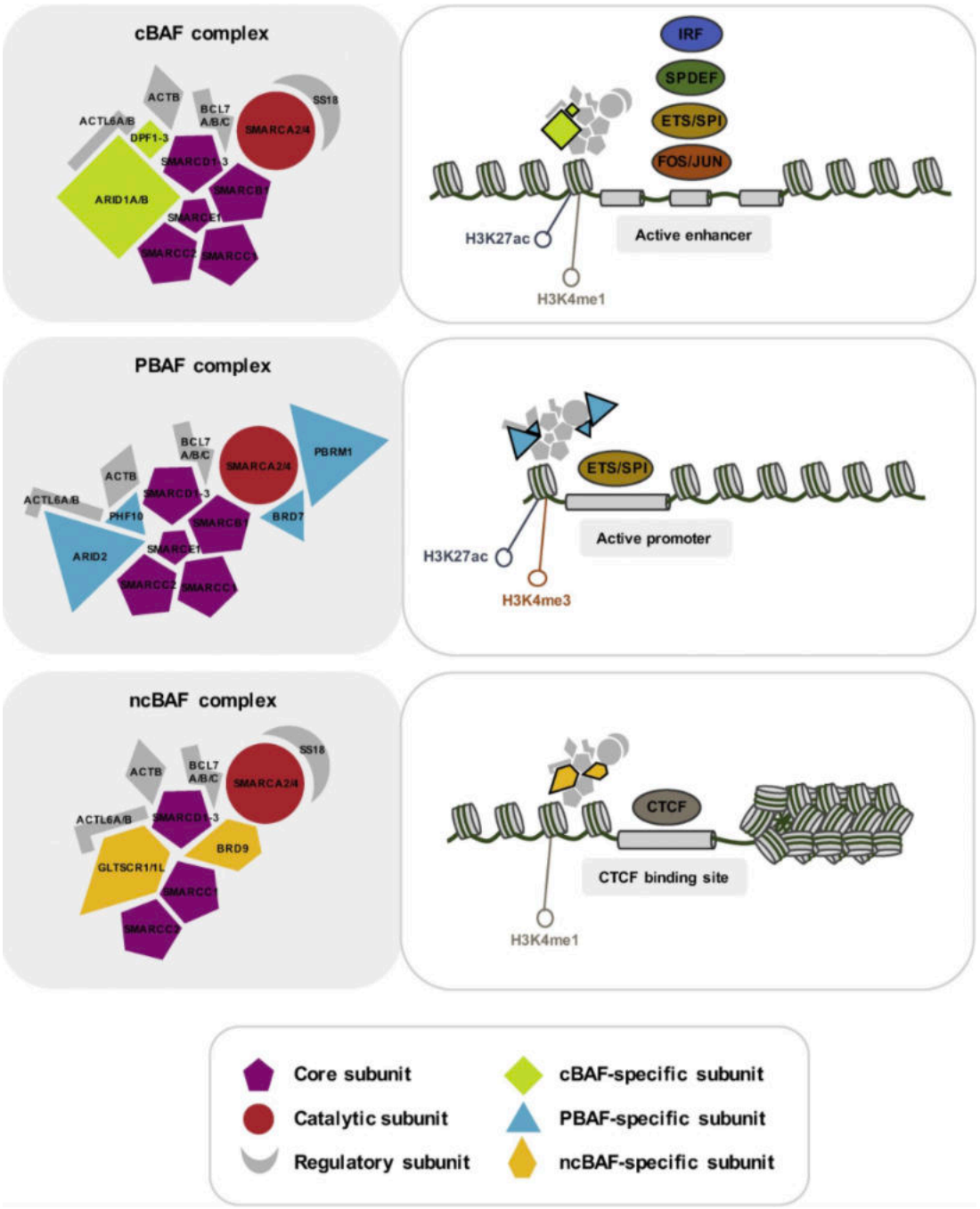

Figure 1.3 Structure and genomic targeting of the cBAF, PBAF and ncBAF complexes. Each complex is composed of three or five core subunits (SMARCC1, SMARCC2, SMARCD1-3, SMARCB1 and SMARCE1), one ATPase subunit (SMARCA2 or SMARCA4), multiple complex-specific subunits and several additional regulatory subunits. Subunit composition determines substrate specificity. cBAF predominantly localise at active enhancers associated with IRF, SPDEF, ETS/SPI or FOS/JUN transcription factors. PBAF complexes predominantly localise at active enhancers associated with the ETS/SPI transcription factor. cBAF complexes are predominantly enriched at CTCF-binding sites. Adapted from *Chabanon et al* (Semin Cancer Biol, 2020).

engineered mouse models of loss of function mutations affecting *Smarcb1, Arid1a, Smarca4* or *Pbrm1* leads to tumour development (Bultman, Herschkowitz et al. 2008, Chandler, Damrauer et al. 2015, Gu, Cohn et al. 2017, Mathur, Alver et al. 2017). The exact mechanism through which these highly prevalent mutations promote tumorigenesis, whether dysregulated transcription or impaired DNA damage response, remains a matter of debate but is likely to be context specific.

1.3.3 ARID1A in normal tissue and cancer

ARID1A (AT-rich interactive domain-containing protein 1A) along with its paralog ARID1B are components of the cBAF complex (Mashtalir, D'Avino et al. 2018) and are responsible for DNA binding (Chandler, Brennan et al. 2013). Loss of *Arid1a* in mice is associated with embryonic lethality due to defects cell self-renewal, differentiation, and cell lineage decisions (Gao, Tate et al. 2008), highlighting its role in development. Loss of ARID1A has been shown to result in aberrant cell cycle control (Nagl, Patsialou et al. 2005). ARID1A also plays a role in HR, which functions as the predominant DSB repair pathway in dividing cells (Watanabe, Ui et al. 2014, Shen, Peng et al. 2015).

ARID1A mutations resulting in loss of ARID1A function are observed in approximately 6% of all cancers (Helming, Wang et al. 2014). Relatively high frequencies of *ARID1A* mutations have been detected in OCCC (35-75%) (Jones, Wang et al. 2010, Maeda, Mao et al. 2010, Wiegand, Shah et al. 2010, Khalique, Naidoo et al. 2018), endometrial cancer (40-55%) (Guan, Mao et al.

2011, Liang, Cheung et al. 2012, Cancer Genome Atlas Research, Kandoth et al. 2013), gastric cancer (20-30%) (Wu and Roberts 2013), bladder cancer (20%)(Wu and Roberts 2013), pancreatic cancer (13%) (Zhang, Mao et al. 2022) and colorectal cancer (12%) (Tokunaga et al., 2020) amongst others.

Heterozygous *ARID1A* mutations are associated with loss, or at least a significant reduction, in ARID1A protein expression (Wiegand, Shah et al. 2010, Miller, Brough et al. 2016). Khalique *et al* assessed the concordance of ARID1A expression as assessed by IHC in a range of gynaecological cancers, finding 100% concordance with mutational status with one of three commercially antibodies tested (Khalique, Naidoo et al. 2018) although this has not been born out in other studies (Table 1.4). As previously discussed, *ARID1A* is the most frequently mutated gene in OCCC (35-75%) (Jones, Wang et al. 2010, Maeda, Mao et al. 2010, Wiegand, Shah et al. 2010, Khalique, Naidoo et al. 2018) and is associated with loss of protein expression (Lowery, Schildkraut et al. 2012, Yamamoto, Tsuda et al. 2012). The presence of *ARID1A* mutations with the associated loss of protein is observed across a range of gynaecological malignancies, which are summarised in Table 1.4.

1.3.4 *ARID1A* synthetic lethal interactions

Due to the relatively high incidence of *ARID1A* loss of function (LOF) mutations across cancer types there has been a focus on the identification of synthetic

	ARID1A gene mutation	Ref	ARID1A loss of expression	Ref
Ovarian clear cell carcinoma	35-75% (median 52%)	(Jones, Wang et al. 2010, Maeda, Mao et al. 2010, Wiegand, Shah et al. 2010, Khalique, Naidoo et al. 2018)	15 - 75%	(Ayhan et al., 2012; Katagiri, Nakayama, Rahman, Rahman, Katagiri, Nakayama, et al., 2012; Lowery et al., 2012; Maeda et al., 2010; Samartzis et al., 2012; Wiegand et al., 2010; Xiao, Awadallah, & Xin, 2012; Yamamoto et al., 2012a; Yamamoto, Tsuda, Takano, Tamai, & Matsubara, 2012)
Ovarian endometroid carcinoma	30-63% (median 47%)	(Khalique et al., 2018; Wiegand et al., 2010)	31 - 55% (median 45%)	(Wiegand, Shah et al. 2010, Ayhan, Mao et al. 2012, Khalique, Naidoo et al. 2018)
Endometrial clear cell carcinoma	17%	(Cerami, Gao et al. 2012, Gao, Aksoy et al. 2013)	20-26% (median 21%)	(Wiegand, Lee et al. 2011, Fadare, Renshaw et al. 2012, Fadare, Gwin et al. 2013, Werner, Berg et al. 2013)
Endometrial endometroid carcinoma	40-55% (median 46%)	(Guan, Mao et al. 2011, Liang, Cheung et al. 2012, Cancer Genome Atlas Research, Kandoth et al. 2013)	19-34% (median 26%)	(Guan, Mao et al. 2011, Wiegand, Lee et al. 2011, Rahman, Nakayama et al. 2013, Werner, Berg et al. 2013)
Cervical adenocarcinoma carcinoma	17%	(Cerami, Gao et al. 2012, Gao, Aksoy et al. 2013)	9-31% (median 28%)	(Guan, Mao et al. 2011, Katagiri, Nakayama et al. 2012, Cho, Kim et al. 2013)
Cervical squamous cell carcinoma	7%	(Cerami, Gao et al. 2012, Gao, Aksoy et al. 2013)	7-16% (median 12%)	(Katagiri, Nakayama et al. 2012, Cho, Kim et al. 2013)
Endometrial carcinosarcoma	20%	(Cerami, Gao et al. 2012, Gao, Aksoy et al. 2013)	-	
Ovarian carcinosarcoma	80%	(Cerami, Gao et al. 2012, Gao, Aksoy et al. 2013)	-	

Table 1.4 Summary of ARID1A mutation and loss of expression frequency in gynaecological cancers.

lethal partners which could be targeted in order to treat ARID1A-deficient cancers, including OCCC. The synthetic lethal interaction between *ARID1A* and Ataxia telangiectasia mutated and Rad3 Related protein kinase (ATR) is the most pertinent to the work contained within this thesis and will be discussed in detail in the subsequent sections.

ARID1A has been proposed to be recruited to double-strand DNA breaks (DSBs) via an interaction with ATR (Shen, Peng et al. 2015). Recruitment of ARID1A to DSBs facilitates efficient processing of DNA ends, producing single stranded DNA which becomes coated in replication protein A (RPA) thereby sustaining the DNA damage signal and promoting cycle arrest. Cells lacking ARID1A display an impaired G_2/M phase DNA damage response and a subsequent sensitivity to the PARPi talazoparib. Buffering between overlapping or partially overlapping functions of paralog pairs that control essential functions, such as *ARID1A* and *ARID1B*, is one way in which cancer cells can tolerate LOF mutations (De Kegel and Ryan 2019). Therefore, targeting paralogs is one way of exploiting synthetic lethality to treat cancer. Project Achilles exploited a short-hairpin RNA (shRNA) screening approach in a range of cancer cell lines to identify context-specific dependencies (Cheung, Cowley et al. 2011, Cowley, Weir et al. 2014). Using data from Project Achilles, *ARID1B* was identified as the number one gene preferentially required for viability in *ARID1A* cells. Cancer cells with ARID1A mutations usually retain at least one functional *ARID1B* allele*. ARID1B g*ene silencing in cell lines with a pre-existing *ARID1A* mutation resulted in destabilization of the SWI/SNF complex and impaired cell growth (Helming, Wang et al. 2014). More recently,

the same group which led Project Achilles expanded their analysis to include 501 cell lines (Tsherniak, Vazquez et al. 2017). This study identified genes encoding several SWI/SNF complex subunits, including *SMARCA4*, *SMARCB1* and *SMARCE1,* as *ARID1A* specific dependencies (Tsherniak, Vazquez et al. 2017)

Enhancer of zeste homolog 2 (EZH2) is a component of the polycomb repressive complex 2 (PRC2), which functions to repress gene expression via histone H3 trimethylation. Two separate groups identified EZH2 as a synthetic lethal partner of *ARID1A* using orthogonal approaches (Bitler, Aird et al. 2015, Kim, Kim et al. 2015). Pharmacological inhibition of EZH2 with the small molecule GSK126 resulted in apoptosis in *ARID1A* mutant cancer cell lines and induced tumour regression of ARID1A-deficient tumour cell line xenografts. Mechanistically, the synthetic lethal interaction was attributed to increased expression of the PRC2 target gene PI3K-interacting protein 1 gene (*PIK3IP1*), an endogenous inhibitor of the PI3K-AKT pathway (Bitler, Aird et al. 2015). *EZH2* gene silencing reduced viability in a range of *ARID1A* mutant tumour cell lines, including several OCCC cell lines (Kim, Kim et al. 2015). Patients with ARID1A-deficient cancers are currently being enrolled in phase II basket study of the EZH2 inhibitor tazemetostat (Prisma and Epizyme 2021). A further study exploring the use of tazemetostat specifically in *ARID1A* mutant relapsed OCCC is currently active, although recruitment has been halted (National Cancer and Oncology 2017).

Subsequent work by Bitler *et al* demonstrated that ARID1A mutant ovarian cancers are dependent on the activity of histone deacetylase 6 (HDAC6). Mechanistically, ARID1A represses HDA6 transcription. Thus, in the absence of functional ARID1A, HDAC6 transcription is increased and leads to the inhibition of the apoptotic function of p53 via acetylation of lysine 120. Pharmacological inhibition of HDAC6 resulted in improved survival in mouse models with OCCC tumour cell line xenografts (Bitler, Wu et al. 2017).

In the context of OCCC, LOF *ARID1A* mutations frequently co-occur with activating hotspot mutations in *PIK3CA (Kuo, Mao et al. 2009)*. *ARID1A* gene silencing in the breast epithelial cell line MCF7 resulted in increased sensitivity to AKT-inhibitors MK-2206 and perifosine along with the PI3K-inhibitor buparlisib, a phenotype that which was also observed in OCCC cell lines with naturally occurring *ARID1A* mutations (Samartzis, Gutsche et al. 2014). This was supported in preclinical models of gastric cancer, in which ARID1A was shown to suppress PIK3CA transcription. In the absence of ARID1A, increased transcription of PIK3CA results in sustained PI3K-AKT signalling culminating to an addiction to the pathway in a process coined oncogene addiction (Weinstein and Joe 2006, Zhang, Yan et al. 2016). The ensuing dependence on PI3K-AKT signalling and sensitivity to small molecule inhibitors of the pathway (Zhang, Yan et al. 2016).

Dasatinib, a multi-drug kinase inhibitor, was identified via a high throughput drug screen performed in twelve OCCC cell lines (Miller, Brough et al. 2016). Dasatinib sensitivity was observed *in vitro* with OCCC cell lines harbouring

naturally occurring *ARDI1A* mutations and in ARID1A-deficient tumour cell line xenografts. The dasatinib response in these models was characterised by arrest in cell cycle phase G1 and increased apoptosis. Using sepharose-linked dasatinib beads and subsequent proteomic assessment, the dasatinib target Proto-oncogene tyrosine-protein kinase Yes (YES1) was found to be activated in *ARID1A* mutant cells. YES1 gene silencing rescued dasatinib sensitivity in *ARID1A* mutant OCCC cell lines (Miller, Brough et al. 2016). The efficacy of dasatinib in recurrent ovarian and endometrial clear cell carcinoma associated with an *ARID1A* mutation was assessed in a single arm phase II study. However, the response rate in this study was 3.8% (1/28) and mean PFS was 2.14 months (95% CI; 1.58 – 7.29 months) (National Cancer and Oncology 2016) suggesting that other clinical approaches to targeting ARID1A defects are still required.

More recently, another high throughput drug screen performed in an *ARID1A* isogenic model of colorectal cancer identified aurora kinase A (*AURKA*) as a synthetic lethal partner to ARID1A. In a similar theme to *ARID1A* and *PIK3CA* interaction, ARID1A represses *AURKA* transcription (Wu, Lyu et al. 2018). ARID1A dysfunction leads to persistent Aurora A activation together with its downstream effector M-phase inducer phosphatase 3 (CDC25C), culminating in an addiction to the pathway (Weinstein and Joe 2006, Wu, Lyu et al. 2018). Exposure to Aurora A inhibitors (AURKAi) was associated with reduced viability of ARID1A mutant cancer cells both *in vivo* and *in vitro* (Wu, Lyu et al. 2018). ENMD-2076 is an orally active AURKAi, which also targets VEGFR, which was trialled in a phase II study enrolling women with relapsed OCCC

(Lheureux, Tinker et al. 2018). Although the trial did not meet its pre-defined primary end-point (6 month PFS rate 22%), loss of ARID1A expression, as determined by IHC, was associated with improved 6 month PFS compared with those cases which demonstrated ARID1A expression (33% vs 12%; p = 0.023) (Lheureux, Tinker et al. 2018).

The final *ARID1A* synthetic lethal interaction that has been described to date is that with gluatathione metabolism. Cell survival relies on intracellular reactive oxygen (ROS) species homeostasis (Gorrini, Harris et al. 2013). Glutathione (GSH) is an important anti-oxidant in cells, which reduces intracellular ROS, and is generated from cysteine, glutamate and glycine by glutamine-cysteine ligase synthetase (GCL) and GSH synthetase (GSS). GCL is comprised of two subunits, glutamate-cysteine ligase catalytic subunit (GCLC) and the glutamate-cysteine ligase modifier subunit (Bin, Huang et al. 2017). Cysteine is the rate-limiting precursor substrate for GSH synthesis. Intracellular cysteine levels are controlled by *SLC7A11*, which encodes the cystine/glutamate transporter XCT (Sasaki, Sato et al. 2002). Reduced expression of *SLC7A11* in *ARID1A* mutant cells results in reduced intracellular cysteine levels and an increased reliance on GCL for the generation of glutathione. Using a high throughput drug screen in an *ARID1A* isogenic model of colorectal cancer, Ogiwara *et al* identified several inhibitors of GCL, namely APR246 and PRIMA-1, which selectively led to the accumulation of ROS and ultimately cell death *in ARID1A* mutant cells. Consistent with this, compounds which either inhibited other components of the glutathione synthesis pathway, such as buthionine sulfoximine (BSO) which blocks GCLC,

or further reduced cysteine levels, such a sulfasalazine, which inhibits SLC7A11, also reduced the viability of *ARID1A* mutant cells (Ogiwara, Takahashi et al. 2019). Taken together, these observations support a synthetic lethal interaction between ARID1A and multiple components of the glutathione metabolism pathway.

Active clinical trials recruiting patients using either *ARID1A* gene expression or ARID1A protein expression as an inclusion criterion are summarised in Table 1.5.

1.3.5 The ARID1A-ATR synthetic lethal interaction

The DNA damage response (DDR) is a complex interconnected network of DNA damage sensors and effectors which is critical in the maintenance of genomic integrity in the face of both exogenous and endogenous DNA damage. ATR is a member of the phosphatidylinositol 3 kinase-related kinase (PIKK) family of serine/threonine protein kinases (Cimprich and Cortez 2008). ATM (Ataxia telangiectasia mutated protein), DNA-dependent protein kinase (DNA-PK), mammalian target of rapamycin (mTOR), suppressor of morphogenesis in genitalia (SMG1) and transformation/transcription domain-associated protein (TRRAP) are other PIKK family members (Lempiainen and Halazonetis 2009). ATR and ATM are two apical regulators of a coordinated DDR. Single stranded DNA (ssDNA), resulting from DNA damage or stressed replication forks (Sancar, Lindsey-Boltz et al. 2004), becomes coated in replications protein A (RPA) which in recruit ATRs and its binding partner,

Target	*NCT Identifier*	*Phase*	*Agent*	*Tumour type*	*Treatment regimen*	*Reference*
EZH2	NCT05023655	II	Tazemetostat	Advanced or metastatic solid tumour harbouring **ARID1A mutation** (except epithelioid sarcoma)	Tazemetostat 800mg bd continuous	(Prisma and Epizyme 2021)
ATR	NCT04065269	II	Ceralasertib (AZD6738)	Women with relapsed ovarian (fallopian tube / primary peritoneal) and endometrial (uterus) clear cell carcinomas with **loss of ARID1A expression**	Ceralasertib 160mg bd days 1-14 of 28 day cycle	(Banerjee, Stewart et al. 2021)
HDAC	NCT05154994	I	Belinostat	Advanced or metastatic urothelial carcinoma harbouring an **ARID1A mutation**	Tremilimumab 1500mg day 1, duravalumab 1500mg day 1, belionostat 1000 mg/m ^{2} days 1-5 of 28 day cycle	(University of and National Cancer 2021)
PARP	NCT04042831	II	Olaparib	Metastatic Biliary Tract Cancer with Aberrant DDR Defects including ***ARID1A* mutation**	Olaparib 400 mg bd continuous	(Academic, Community Cancer Research et al. 2022)

Table 1.5 Summary of clinical trials, which are actively recruiting, stipulating ARID1A mutation or ARID1A protein expression as inclusion criterion or stratification criterion.

ATR interacting protein (ATRIP), thereby activating the DDR (Zou and Elledge 2003, Zeman and Cimprich 2014). RPA coated ssDNA also plays an important role in recruiting the ATR activator DNA topoisomerase binding protein 1 (TOPBP1) (Kumagai, Lee et al. 2006). Activated ATR phosphorylates checkpoint kinase 1 (CHK1) on residues S317 and S345, which in turn phosphorylates and inhibits CDC25A dual phosphatase during cell cycle S phase (Busino, Chiesa et al. 2004). This culminates in the increased phosphorylation of cyclin dependent kinase 2 (CDK2), targeting it for proteosomal degradation. The outcome of this signalling cascade is the activation of both the intra-S phase and G_2/M phase cell cycle checkpoints (Bahassi, Ovesen et al. 2008, Dai and Grant 2010, Ma, Janetka et al. 2011) (Figure 1.4).

Using a short interfering RNA (siRNA) screening approach, Williamson *et al* demonstrated a synthetic lethal interaction between ARID1A and ATR. This novel synthetic lethal effect was evident in OCCC cell lines with naturally occurring *ARID1A* mutations, tumour cell line xenografts and tumour cell line xenografts derived from *ARID1A* mutant endometrial cancer (Williamson, Miller et al. 2016). One mechanistic hypothesis proposes that the topoisomerase enzyme, TOP2A, is localised to DNA in an ARID1A-dependent manner. Therefore, in the absence of ARID1A function, complex chromosomal structures which form during DNA replication and are normally resolved by TOP2A, fail to be processed prior to mitosis (Dykhuizen, Hargreaves et al. 2013). ATR inhibition in ARID1A-defective cells activated DNA damage

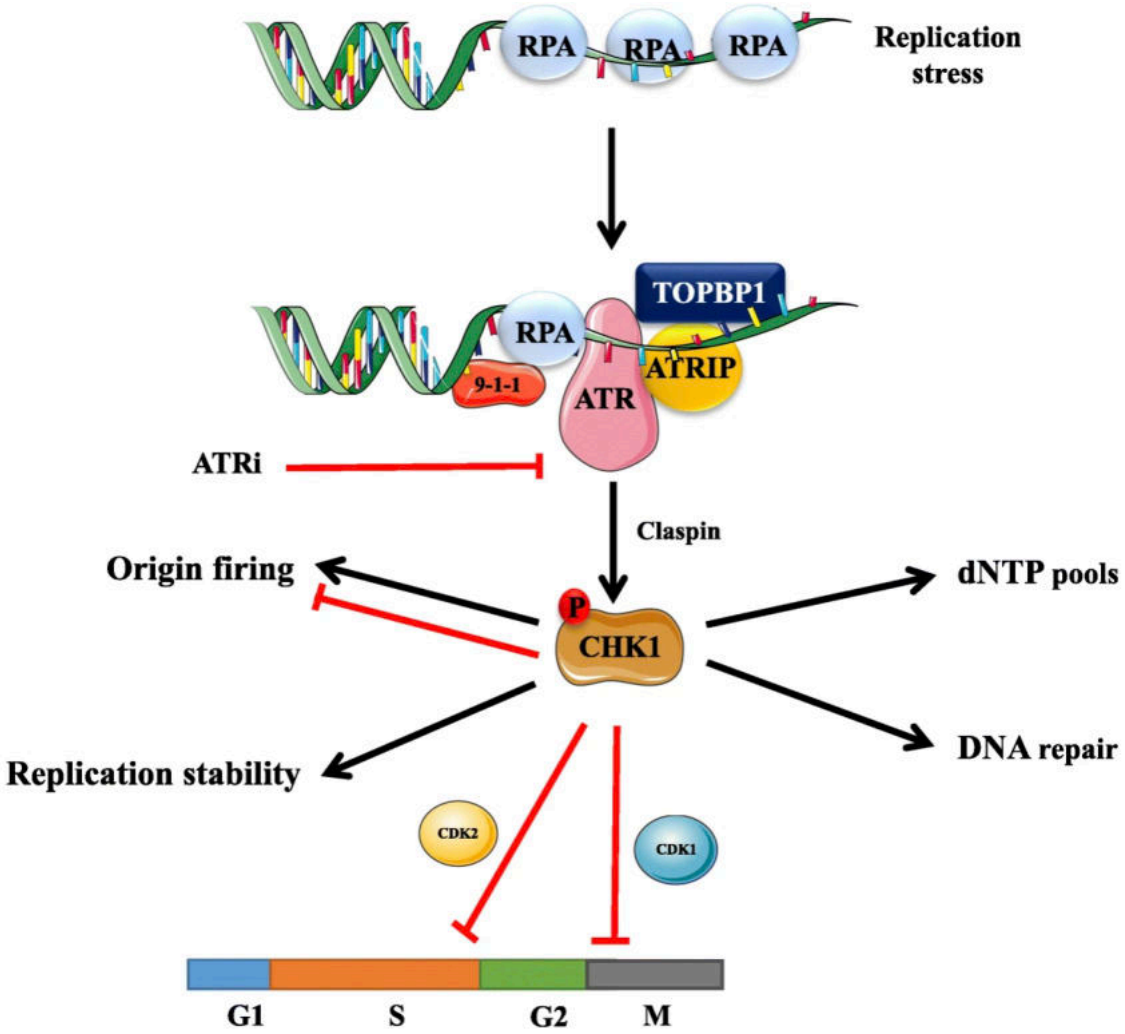

Figure 1.4 Replication stress induced ATR signalling cascade. RPA coated ssDNA, which arises at sites of stalled replication forks or resected DSBs. ATR and its partner ATRIP are recruited and subsequently incorporate Rad9-Rad1-hus1 (9-1-1) and TOPB1, resulting in ATR activation. The ATR adaptor protein clapsin enables CHK1 phosphorylation. Activated CHK1 ensures genomic stability through a variety of mechanisms including activation of S phase and G_2/M phase checkpoints, stabilizing the replications fork, promoting DNA repair and ensuring adequate deoxynucleotides. Adapted from (Mei, Zhang et al. 2019)

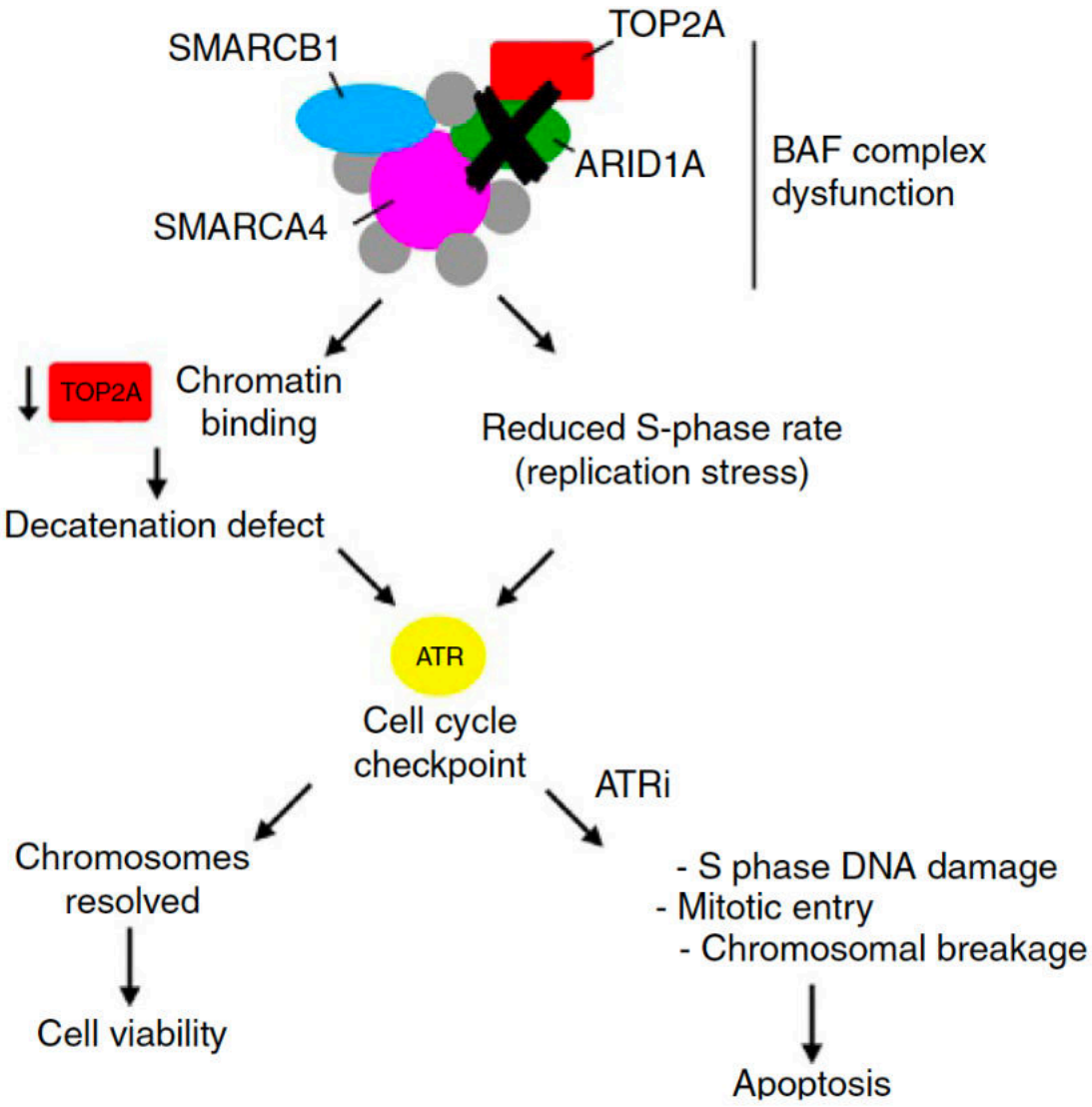

Figure 1.5 A model for the proposed mechanism driving the sensitivity of ARID1A-deficient cells to ATRi. Loss of ARID1A function results in: (i) a defect in the ability of cells to recruit TOP2A to chromatin; and (ii) cell cycle progression defects in both S and G2/M phases of the cell cycle. These factors combined or in isolation might render tumour cells sensitive to small molecule ATRi as these agents impair the ability of cells to mount adequate DDRs, while at the same time accelerating mitotic entry. Taken from (Williamson, Miller et al. 2016).

pathways, increased complex chromosomal structures including anaphase bridges, and impacted cell viability (Williamson, Miller et al. 2016) (Figure 1.5). The work presented by Williamson *et al* was pivotal in identifying the ARIDA-ATR synthetic lethal interaction (Williamson, Miller et al. 2016). However, it did not specify what additional genetic biomarkers, both specific to *ARID1A* mutant OCCC and in general, may be required to elicit clinically meaningful response to ATRi. Additionally, resistance to ATRi, irrespective to the outcome of ATARI, is likely to represent a significant challenge to the future use of this class of anti-cancer therapy. This too was not covered by the work described above.

1.3.6 ATARI clinical trial

Building on the identification of a novel synthetic lethal interaction between ARID1A and ATR (Williamson, Miller et al. 2016), the proof-of-concept ATr Inhibitor in Combination with Olaparib in Gynaecological Cancers With ARId1A Loss or no Loss (ATARI, NCT04065269) was designed. ATARI is an international, academic sponsored phase II clinical trial in which patients with ovarian and endometrial clear cell carcinoma, along with other rare gynaecological tumours, are treated with the ATR inhibitor, AZD6738 (ceralasertib, AstraZeneca), with or without the PARPi olaparib (Banerjee, Stewart et al. 2021).

Cohort 1A of ATARI will recruit patients with ovarian, endometrial, or endometriosis-related carcinomas with clear cell histology and loss of ARD1A

expression as determined by IHC. Patients in cohort 1A will be treated with ceralasertib (AZD6738) monotherapy (160mg tablets twice daily on days 1–14 in a 28 day cycle). If this cohort does not meet its predefined efficacy threshold cohort 1B will open, enrolling the same patient group, who will receive treatment of ceralasertib with olaparib (160 mg ceralasertib tablets once daily on days 1–7 and 300 mg olaparib tablets twice daily continuously in a 28-day cycle). Cohort 2 will enrol patients with ovarian, endometrial, or endometriosis-related carcinomas with clear cell histology an no loss of ARID1A by IHC. Cohort 3 will consist of patients with relapsed gynaecological malignancies irrespective of ARID1A expression status although this will be assessed prior to enrolment. Both cohorts 2 and 3 will receive of ceralasertib with olaparib using the same regiment outlined for cohort 1B (Figure 1.6) (Banerjee, Stewart et al. 2021).

There are several rationales for including ARID1A proficient clear cell carcinomas in ATARI. Firstly, due to the pleiotropic molecular functions that ARID1A performs within a cell, it is possible that the functional outcome of other genomic changes results in an ARID1A-deficient-like phenotype which would aid clear cell tumorigenesis but also impart some sensitivity to ATR inhibition. This is akin to the “BRCAness” phenotype which describes cells collection of phenotypic features which accompany *BRCA1* and *BRCA2* mutations despite no mutation being present in either gene, accounting in part for some of the PARPi responses amongst patients with HGSOC outside the *BRCA* mutant population (Lord and Ashworth 2016). There is also evidence

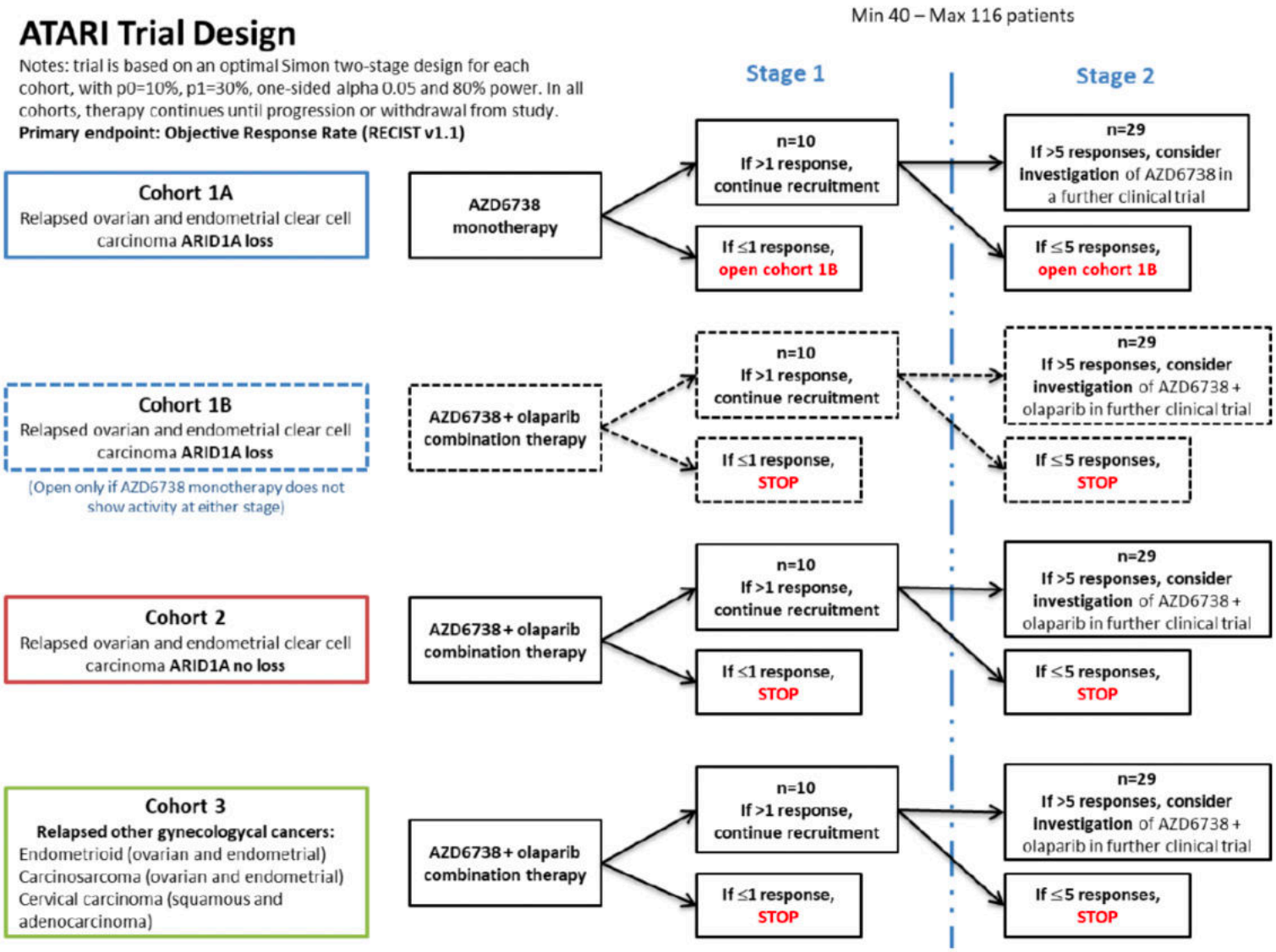

Figure 1.6 ATARI trial schema. Trial will follow a classical two-stage design with progression to stage 2 only taking place if the pre-defined stage 1 efficacy threshold is observed.

that combined PARP and ATR inhibition enhances cytotoxicity, theoretically compensating for the lack of ARID1A mutations. The BRCAness phenotype is not a feature of OCCC; cancers of this subtype are resistant to platinum-based chemotherapy, they do not display the genomic scars associated with HR deficiency (HRD) and, most importantly, do not harbour mutations in HR associated genes. Due in part to the abrogation of cell cycle checkpoints in response to the DNA damaging effects of PARPi (Horton, Stefanick et al. 2007), *in vitro* silencing of ATR has been shown to synergise with PARP inhibition (McCabe, Turner et al. 2006). ATR inhibition has also been shown to impede BRCA1-independent loading of DNA repair protein RAD51 homolog 1 (RAD51), enabling restoration of stalled replication forks, a mechanism that has been linked with overcoming PARPi resistance in *BRCA1* and *BRCA2* mutant cells (Yazinski, Comaills et al. 2017).

1.4 Identification of genetic determinants of ATRi resistance and sensitivity using CRISPR/Cas9 mutagenesis

1.4.1 Overview of CRISPR/Cas9

Clustered regularly interspaced short palindromic repeats (CRISPR)/Cas9 technology has been used to model multiple aspects of the cancer phenotype (Stewart, Banerjee et al. 2020). The system exploits a nuclease (Cas9) first identified in bacteria to protect against exogenous, and potentially deleterious DNA, such as that introduced by viruses (Jansen, Embden et al. 2002, Mojica,

Diez-Villasenor et al. 2005, Barrangou, Fremaux et al. 2007). The simplest iteration of the system as an experimental tool consists of Cas9 nuclease and a single guide RNA (sgRNA), both of which can be transiently transfected or transduced into a cell. The sgRNA has homology with a specific DNA sequence within the genome and also forms a complex with the Cas9 nuclease, guiding the Cas9 to the site of interest (Jinek, Chylinski et al. 2012). Cas9 then cuts both DNA strands at the target site producing a DSB (Mali, Yang et al. 2013). Inherent DDR within cells often repairs these DSBs in a conservative manner, restoring the native DNA sequence. However, in some instances mutations, often insertions and deletions, are introduced. CRISPR-Cas9 exploits this mutagenic potential of DSB repair to disrupt the endogenous DNA sequence leading to the translation of abnormal proteins the function of which is perturbed or, in some cases, resulting in no translation of the gene at all (a functional knock-out) (Figure 1.7) (Cong, Ran et al. 2013). This type of CRISPR-Cas9 mutagenesis is referred to CRISPRn.

More recently, researchers have employed a catalytically inactive form of Cas9 (dead-Cas9; dCas9) which is unable to produce DSBs but is instead fused to one of an array of effector proteins which are capable of both promoting and repressing transcription, referred to as CRISPR-activation (CRISPRa) (Mali, Aach et al. 2013) or CRISPR-interference (CRISPRi) (Gilbert, Larson et al. 2013) respectively. With, CRISPRa/i, the sgRNA directs the dCas9 to the promoter region of the gene of interest, where the effector proteins, VP64-p65-Rta (VPR) in the case of CRISPRa and Krüppel-associated box (KRAB) in the case of

CRISPRi, promote or repress gene expression (Gilbert, Larson et al. 2013, Chavez, Scheiman et al. 2015). Epigenetic modifications, such as methylation, can be introduced by fusing dCas9 to alternative effector proteins (Kang, Park et al. 2019) (Figure 1.8).

Dissecting various aspects of the cancer phenotype using CRISPR-Cas9 technology has a number of advantages over siRNA approaches, such as that employed in the identification of the ARID1A-ATR synthetic lethal interaction (Williamson, Miller et al. 2016). siRNA reduces gene expression at the messenger RNA (mRNA) level through the RNA-Induced Silencing Complex (RISC) (Meister, Landthaler et al. 2004), whereas CRISPRn targets the genomic DNA itself, producing a functional knock-out of the gene (Jinek, Chylinski et al. 2012). Thus, low level protein expression in the context of siRNA-mediated gene silencing may hinder the ability to detect an effect. One drawback of CRISPRn mediated mutagenesis in comparison to siRNA gene interference, is the relative inability to study essential genes (Hart, Chandrashekhar et al. 2015), that is genes encoding proteins that are required for cell survival. However, the development of CRISPR interference has provided a means to overcome this challenge (Gilbert, Larson et al. 2013). Of course, CRISPR activation has afforded the opportunity to study gain of function mutations, something which could not be achieved via siRNA. The interpretation of any genetic perturbation study relies on the specificity of the technique employed. The most significant limitation to the use of siRNA is off-target gene silencing. This can arise through the degradation of mRNA with partial homology to the siRNA (Birmingham,

Anderson et al. 2006, Fedorov, Anderson et al. 2006) but also via the microRNA pathway with the potential to reduce the expression of a much larger number of genes (Doench, Petersen et al. 2003). Although CRISPR-mediated mutagenesis has been reported at off target sites, this occurs at a much lower frequency that with siRNA (Hsu, Scott et al. 2013, Zhang, Tee et al. 2015) and has been reduced by the use of computational algorithms to rationally design sgRNAs with sequences less likely to bind DNA at off-target sites (Doench, Hartenian et al. 2014, Doench, Fusi et al. 2016).

sgRNAs can now be synthesised en masse relatively efficiently. This has enabled the generation of large sgRNA libraries which afford the opportunity to perform high-throughput CRISPR-Cas9 screens to identify genetic determinants of drug responses. In such screens, Cas9 expressing cells are infected with an sgRNA library packaged in lentivirus. The entire coding genome can be targeted using such sgRNA libraries, which can consist of more than 200 000 sgRNAs where 5-10 sgRNAs target each gene. In order to ensure that the observed phenotype is due to the alteration of a single gene, a multiplicity of infection is used so as to ensure than on average one virus particle infects each cell. The infected cells are then exposed to a drug concentration designed to a predefined surviving fraction at the end of the assay.

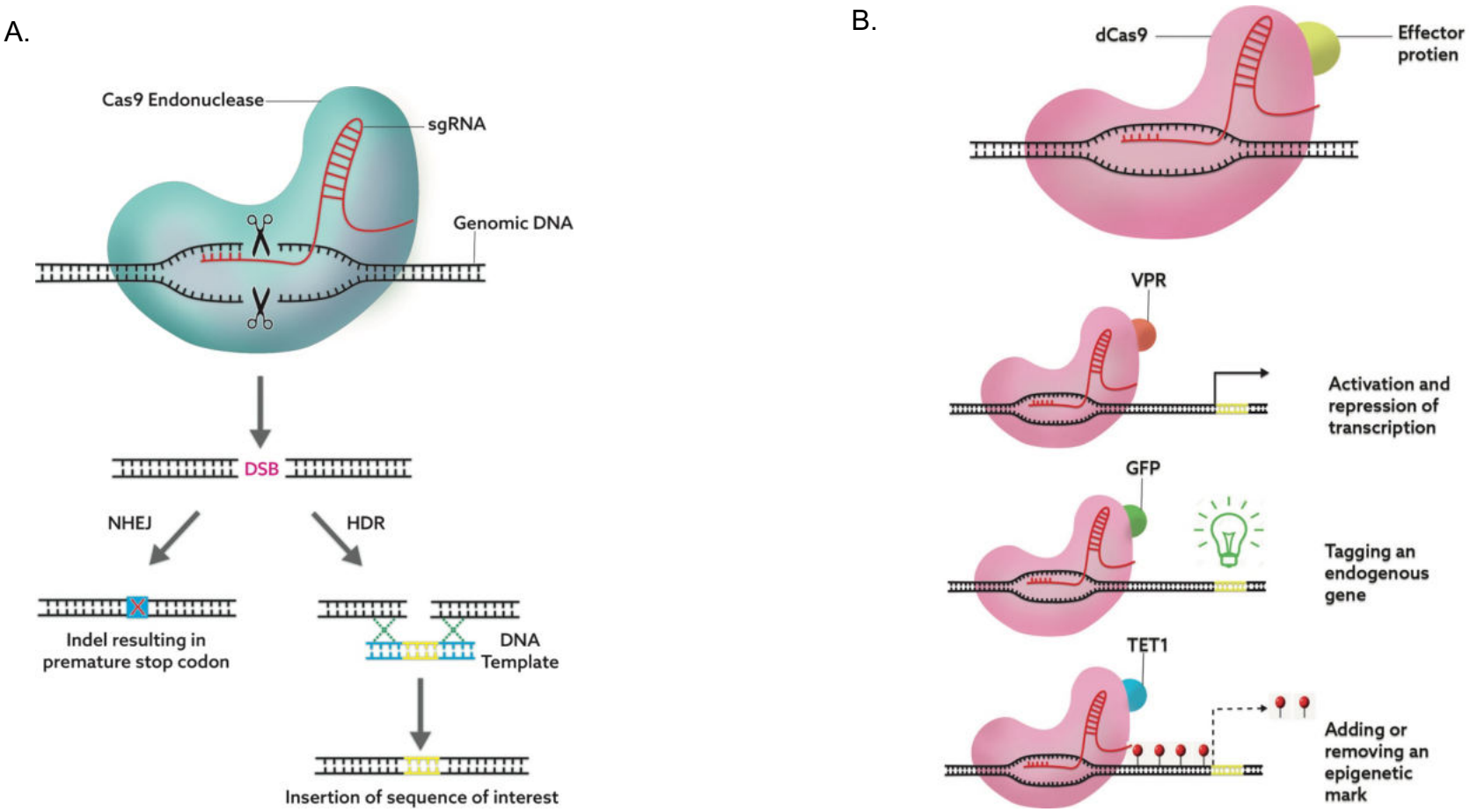

Figure 1.7 CRISPR-Cas9-mediated gene editing. Cas9 endonuclease is directed to the region of interest in the genome by a single-guide RNA(sgRNA). The enzymatic activity of Cas9 cleaves both strands of genomic DNA, resulting in a double-strand break (DSB). If this DSB is repaired by non-homologous end-joining (NHEJ), its error prone nature leads to insertion/deletion mutations, which can produce a functional gene knockout. If a DNA template is also introduced to the cell, homologous recombination (HR) can incorporate the desired sequence into the genome. (b)dead-Cas9 (dCas9) facilitates gene perturbation without causing DSBs. An enzymatically inactive form of Cas9, dCas9, generated through the mutation of its endonuclease domain is guided to the genomic region of interest by a sgRNA but does not cause a DSB. Instead, effector proteins fused to dCas9 modify the target region of the genome in the desired manner. Examples include activation or repression of transcription or even methylation. Taken from Stewart *et al (2020).*

1.3.1 Using CRISPR/Cas9 to identify genetic determinants of ATRi resistance and sensitivity

Several groups have reported on the use of CRISPRn screens in the identification of the genetic determinants of response to ATRi. Ruiz *et al* utilised the genome-wide CRISPRn screen in mouse embryonic stem (ES) cells to identify genes implicated in ATRi resistance. Using this approach, loss of function mutations in *CDC25A*, which encodes M-phase inducer phosphatase 1, resulted in ATRi resistance, a phenotype that was reversed by inhibition of WEE1 (Ruiz, Mayor-Ruiz et al. 2016).

In an effort to determine a consensus set of genetic determinants of ATRi sensitivity Hustedt *et al* performed genome-wide CRISPRn screens in immortalised retinal pigment epithelial (RPE), HCT116 and HeLA cells using two ATRi, AZD6738 and VE-821 (Hustedt, Alvarez-Quilon et al. 2019). By integrating the results of these CRISPRn screens a candidate list of 117 genes was generated that, when subjected to CRISPR mutagenesis, enhanced ATRi sensitivity. From this list, 14 genes validated as novel genetic determinants of ATRi sensitivity, namely *APEX2, c17orf53, CABIN1, CIP2A, DSCC1, POLE4, TOPBP1, TYMS NAE1, DPH1, DTYMK, PPP1R8, POLE3* and *POLE4* (Hustedt, Alvarez-Quilon et al. 2019).

The mechanism underlying ATRi induced cytotoxicity in ARID1A-deficient cells, proposed by Williamson *et al,* entails a reduction in ARDI1A-dependent recruitment of TOP2A to DNA, with a resulting inability to resolve complex structures arising during DNA replication and an increased reliance on ATR (Williamson, Miller et al. 2016). The results from the CRISPRn screens described by Ruiz *et* al and Hustedt *et al* build on this and suggest that the response

to ATRi in general are driven by a combination of the generation of replication stress and forced mitotic entry (Ruiz, Mayor-Ruiz et al. 2016, Hustedt, Alvarez-Quilon et al. 2019). Loss of function mutations of genes encoding proteins involved in DNA replication including *POLE3* and *POLE4*, components of the DNA polymerase ε, which is responsible to leading strand extension during DNA replication (Pursell, Isoz et al. 2007, Lujan, Williams et al. 2016), and *TOPBP1*, which ensures genome integrity during normal S phase (Kim, McAvoy et al. 2005), result in ATRi sensitivity (Hustedt, Alvarez-Quilon et al. 2019). Meanwhile, the loss of CDC25A function, which is responsible for the dephosphorylation of CDK1, a rate limiting step in the G_2/M transition, drives ATRi resistance (Shen and Huang 2012). This refined view of how ATRi exert their cytotoxic effect will aid future work to identify prognostic biomarkers for this class of drugs.

1.4 Aims of this work

The clinical outcomes for women diagnosed with OCCC remain poor and there are currently no targeted therapies licensed for this indication. The identification of a novel synthetic lethal interaction between ARID1A and ATR offers a potential treatment strategy given the relatively high prevalence of *ARDI1A* mutations present in this tumour type. The activity of ATRi in *ARID1A* mutant OCCC is currently being assessed in ATARI.

The aim of this project is to generate data that could help refine how ATRi are used in the context of OCCC and other gynecological cancers. This will entail the use of CRISPR-Cas9 mutagenesis screens, which have hitherto not been performed in an ARIDA-deficient context, to identify biomarkers for ATRi response and resistance which will be validated in

the pre-clinical setting. This pre-clinical work will be used to inform how the results of the ATARI clinical trial are interpreted and it is hoped will inform how future clinical trials are designed.

Chapter 2. Materials & Methods

2.1 Reagents

2.1.1 General Chemicals and solutions

All reagents were purchased from Sigma unless otherwise stated.

PBS: 137 nM NaCl, 2 mM KCL, 8 mM Na_2HPO_4 in H_20 with pH adjusted to 7.4 using HCl.

RIPA buffer: 50 mM Tris pH 8.0 , 150 nM NaCl, 0.1% SDS, 0.1% deoxycholic acid, 1% Triton-X-100, 50 mM NaF, 1 mM Na_3V0_4 with 1 x MiniComplete® Protease Cocktail tablet (Roche) added per 10mL buffer.

EDTA 0.5 M: di-sodium salt of ethylenemiaminetetracetate in H_20, pH adjusted to 8.0 with NaOH.

MOPS: 3-(N-morpholino)propanesulfonic acid (Invitrogen)

PFA: 4% (w/v) paraformaldehyde in PBS

DAPI: 4'6-Diamidino-2-Phenylindole, dihydrochloride

IFF (Immunofluorescence buffer): PBS with 1% bovine serum albumin and 2% foetal bocine serum (Life Technologies, UK).

PI staining solution: Propidium iodide 20 µg/mL with RNase A 100 µg/mL in PBS

Triton solution: 0.25% Triton-X-100 in PBS

Transfer buffer: 14.4 g glycine, 3.03 g Tris, 200 mL methanol made up in 1 litre with H_20

10 x TBS-T: 200 mL 1 M Tris pH 7.5, 300 mL 5 M NaCl, 10 mL tween in 1 L H_20

TRIS: Tris(hydroxymethyl)aminomethane (Invitrogen)

2.1.2 Drugs and therapeutics

AZD6738 and VX970 were obtained from Selleckchem.

2.1.3 Antibodies

The antibodies used during the course of this PhD project are summarised in table 2.1 Horseradish peroxidase secondary antibodies were obtained from Sigma and diluted 1:10,000. For images obtained using the Odyssey Infrared

Imaging system from Licor® fluorescent dye labelled secondary antibody were purchased from Odyssey and diluted 1:5000.

Antibody	Supplier	Product number	Dilution
Primary antibodies for Western blot			
Cas-9 N-terminus	Novus Biologicals	NBP2-36440	1:1000
Vinculin	Santa Cruz	SC-73614	1:1000
PPP2R1A	Cell signaling	2041S	1:1000
PPP2R2A	Cell signaling	5689S	1:1000
PPP2CA	Abcam	Ab106262	1:1000
Myc	Abcam	Ab32072	1:1000
WEE1	Cell signaling	13084S	1:1000
Primary antibodies for immunofluorescence			
53BP1	Cell signalling	4937S	1:50
Cyclin A	Santa Cruz	SC-217682	1:100
Primary antibodies for cell cycle analysis by FACS			
Phosphohistone-H3 (S10)-alexa488	Cell signalling	3465S	1:50

Table 2.1Summary of antibodies used in the course of this thesis.

2.1.4 Genome-wide CRISPRn library

The previously published and validated genome-wide human lentiviral library (Kosuke Yusa Human GW CRISPR guide RNA library V1)(Koike-Yusa, Li et al. 2014) provided directly by Dr Kosuke Yusa.

2.1.5 Recombinant Cas9 endonuclease

TrueCut® v2 recombinant Cas9 endonuclease was purchased from Invitrogen and stored at –20^{0}C.

2.1.6 EditR sgRNAs

Custom designed CRISPR RNA (crRNA) and tracrRNA (trRNA) were obtained from Horizon discovery and reconstituted to 20 µM in Tris pH 7.4. Edit-R non-targeting control crRNA 1 and 2 (Horizon Discovery) with no homology to any known sequence in the human genome were used as negative controls. A *PLK1*-specific crRNA (Horizon Discovery) was used as a control for successful transfection.

2.1.7 siRNA library targeting the human genome

The Dharmacon® SMARTpool® kinase library was purchased from Dharmacon. An siRNA library targeted 953 genes encoding protein kinases and kinase-related genes, tumour suppressor genes and included in the Cancer Gene Census

(Sondka, Bamford et al. 2018) were supplied in 96 well plate format with each gene represented by one well, with 80 genes per plate. Each well contained an siRNA SMARTpool® with four individual siRNAs targeting the same gene but with different target sequences. Target sequence information was not provided. Prior to performing the screen, the library was supplemented with additional control siRNAs and aliquoted using the Hamilton Robot in to 384 well plates, which were then used to perform the screen.

2.1.8 siRNA oligonucleotides

siRNA oligonucleotides were purchased from Horizon Discovery and were supplied 2'ACE protected and lyophilized. These were reconstituted to 20 μM in diethyl pyrocarbonate (DEPEC) treated water (Ambion) and stored at -20 ^{o}C. The following non-targeting siRNA controls are used in this thesis and target no known human genes: siControl1 or siControl2 (Horizon Discovery). The siRNAs used in this thesis are summarised in Table 2.2.

Target	Type	Product code
siCON1	Non-targeting	D-001206-13-05
siCON2	Non-targeting	D-001206-14-05
PLK1	SMARTpool	M-003290-01-0005
WNK1	SMARTpool: siGENOME siRNA	M-005362-01-0005
WNK1	Set of 4: ON-TARGET-PLUS siRNA	LQ-005362-02-0005

Table 2.2 Summary of siRNAs used in the course of this thesis.

2.1.9 Culture media

Roswell Park Memorial Institute (RPMI) 1640 medium was supplied by Gibco and supplemented with 10% foetal bovine serum (FBS) and and penicillin-streptomycin 100 units/mL. Optimem medium was supplied by Gibco.

2.1.10 Cell lines

TOV21G cell line was obtained from American Type Culture Collection (ATCC) and was cultured in regular RPMI medium. HCT116 *ARID1A* isogenic pair was obtained from Horizon Discovery and cultured in RPMI medium. OVISE and OVTOKO cell lines were obtained from Dr Hiroaki Itamochi (Tottori University School of Medicine, Yonago, Japan) and cultured in RPMI.

2.2 Protocols

2.2.1 General cell culture

All cell culture was performed under sterile conditions in a tissue culture hood. Cells were grown in 5% CO_2 at 37^0C in their respective media. Cells were allowed to reach approximately 80% confluency before passaging as follows: culture medium was aspirated before cells were washed with a covering volume of PBS. Cell detachment was achieved by incubating with a covering volume of trypsin-EDTA at 37^0C. Trypsin was neutralised by the addition of culture medium

containing FBS before cells were re-seeded in to a new flask or plate. Counting of cells was performed using Countess automated cell counter (Invitrogen). 10 µL of cell suspension was mixed with 10 µL tryphan blue (Invitrogen) before counting. Frozen cell stocks were maintained in liquid nitrogen in freezing media (90% FBS with 10% DMSO). Mycoplasma testing was carried out periodically using Mycoalert Mycoplasma Testing Kit (Lonza). Cell identity was confirmed by short tandem repeat (STR) typing every 6 months.

2.2.2 Short term cell viability assay

Cells were seeded to 96-well or 384-well plate at a density of 500 cells per well in 200 µL or 50 µL respectively. 24 hours after seeding, drug was added at indicated concentrations using the Echo liquid handler (Labcyte). In the case of 96-well plates this entailed the removal of culture medium, addition of drug before 200 µL fresh medium added to bring drug to intended concentration. This process was repeated after 3 days. For 384-well plates, drug was added directly to the plate (i.e. medium was not removed). After 7 (96-well) or 5 (384-well) days cell viability was measured using CellTiter-Glo® (CTG). Medium was removed from each well before 50 µL (96-well) or 25 µL (384-well) CTG (diluted 1:4 in PBS) was added to the plate which was subsequently incubated at room temperature for 20 minutes under constant agitation. Luminescence was measured using the Victor X5 Multilabel plate reader (Perkin Elmer). From these luminescence readings a surviving fraction was calculated by normalising the luminescence reading for each well to that of the vehicle treated well. Dose

response curves were then generated using GraphPad Prism and significance determined using two-way ANOVA.

2.2.3 Long term cell viability assay

Cells were seeded to 24 well plate at density of 500 cells per well in 1 mL culture medium. 24 hours after seeding medium was removed and replenished with medium containing drug at indicated concentration. This process was repeated every 3 days until vehicle treated well became confluent (typically 14-21 days). Cell viability was then assessed using CTG. 150 µL CTG (diluted 1:2 in PBS) was incubated at room temperature for 1 hour under constant agitation. 100 µL of resulting suspension was transferred from each well to a 96 well plate before luminescence was measured, surviving fraction calculated and dose response curves generated as previously described.

2.2.4 Genome-wide CRISPRn screen

Doxycycline inducible Cas9 TOV21G cells were generated prior to the commencement of the fellowship by Dr Feifei Song. Briefly, TOV21G cells were transduced with the Edit-R inducible Lentiviral hEF1a-Blast-Cas9 Nuclease (Dharmacon) and selected in Blasticidin 7 µg/mL. Cas9 expression was confirmed via Western blot.

The genome-wide CRISPRn screen was performed as previously described (Hustedt, Alvarez-Quilon et al. 2019). Inducible Cas9 expressing cells were seeded for 1000x representation per sgRNA, and infected at a multiplicity of infection (MOI) of 0.3, to avoid multiple sgRNA infections per cell, using the previously published and validated genome-wide human lentiviral library (Kosuke Yusa Human GW CRISPR guide RNA library V1) (Koike-Yusa, Li et al. 2014). After puromycin selection (1 μg/mL), cells were harvested at day 0 (T0) and on day 14 (T1). Cells were exposed to AZD6738 0.1 μM (the concentration of AZD6738 that resulted in a reduction in the Surviving Fraction (SF) by 50%, SF_{50}) or DMSO between days 0 and 14. Media containing AZD6738 or DMSO was replenished twice per week. DNA was extracted from the T=0 and T=1 samples. sgRNAs in each sample were sequenced by the Tumour Profiling Unit (The Institute of Cancer Research) using a custom U6 primer. Bioinformatic analysis was performed by the Breast Cancer Bioinformatics Research Group (Institute of Cancer Research). Z score analysis was used for the downstream analysis of sgRNA raw read data.

For the Z score analysis (where Z = 0 represents no effect on viability and positive Z scores represent a gain in viability), guides with a maximum read count of zero in the T=0 sample were first identified and removed from the analysis. Subsequently, raw read rounds were converted to parts per ten million (pptm) in order to take in to account any differences in the amount of DNA sequenced between samples. The raw pptm counts for each sgRNA were log2 transformed before calculating viability effect (VE) and drug effect (DE) Z scores (Equations 1

and 2). VE refers to the rate of decline in sgRNA abundance in the absence of any drug exposure, i.e. in the presence of vehicle alone. DE refers to the difference in the sgRNA abundance between the vehicle and drug exposed time point during the screen, e.g. T = 0, T = 1. In order to remove any difference in DE that can be attributed to VE, a linear model of DE ~ VE was fitted and then adjusted to give a DE corrected for VE (DE'[DE corrected]) (Equation 3). Gene level NormZ score analysis was used for the downstream analysis of sgRNA read count data as described previously (Colic, Wang et al. 2019). In brief, the guide DE'[DE corrected] of all gRNA across all replicates is summed to get a gene-level sumZ score, which is then normalized (by dividing by the square root of the number of summed terms) to the final NormZ score (Equation 4).

Equation 1:

$$VE = \frac{(DMSO(T1) - DMSO(T2) - median(DMSO(T1) - DMSO\ (T0)}{MAD(DMSO(T1) - DMSO(T2))}$$

Equation 2:

$$DE = \frac{(Drug(T) - DMSO\ (T) - median(Drug(T) - Drug\ (T)}{MAD(Drug(T) - DMSO(T)}$$

Equation 3:

$$DE'(DEcorrected) = (DE - c\ ) - (VE\ x\ m)$$

Equation 4:

$$Norm\ Z = \frac{\Sigma(DE'(DEcorrected)}{\sqrt{n}}$$

*Being DMSO: log2 PPTM count of DMSO samples at time points T1 and T0; Drug: log2 PPTM counts of drug exposed samples at the time point T; MAD:

mean absolute distribution; c: intercept; m: slope; n: number of sgRNA targeting given gene.

2.2.5 Edit R revalidation of screen hits

TOV21G cells were reverse transfected in 6 well plates. For each transfection the contents of transfection mix 1 and transfection mix 2 (Table 2.3) were combined and incubated at room temperature for 10 minutes. Transfection mix 1 and transfection mix 2 were then combined and incubated for a further 10 minutes at room temperature. 300,000 TOV21G cells suspended in 2 mL of antibiotic free medium was then added to combined transfection mix and cells incubated at 37^0C overnight. After 24 hours, medium containing transfection mix was removed and fresh medium replenished. 72 hours after transfection, cells were seeded to 24 well plate and long term cell viability performed as outlined in section 2.2.4. The sgRNA sequences used in the work contained in this thesis are outlined in Table 2.4.

Transfection Mix 1	**Transfection Mix 2**
250 µL optimem	250 µL optimem
1.25 µL trRNA (20 µM)	5 µL CRISPRmax reagent
1.25 µL crRNA (20 µM)	
1 µL recombinant Cas9 (20 µM)	
10 µL CRISPRmax plus	

Table 2.3 EditR transfection mix components.

sgRNA	Oligonucleotide sequence
sgPPP2R2A 1	GAAGGGTATAACTTGAAAG
sgPPP2R2A 2	GCATCTGGAAATTACAGAC
sgATM	GAAGGGTATAACTTGAAAG

Table 2.4 Summary of editR sgRNA oligonucleotide sequences.

2.2.6 Genomic DNA extraction from cell lines

Genomic DNA was extracted using DNeasy blood &tissue kit (Qiagen) according to the manufacturer's instructions and eluted in 200 µL nuclease free water (Ambion) before DNA concentration was determined by measuring absorbance at 260 nm using NanoDrop 1000 (Thermo).

2.2.7 Genomic DNA from FFPE tumour samples

Genomic DNA was extracted from formalin-fixed paraffin-embedded (FFPE) tumour samples collected from patients enrolled Royal Marsden Hospital (RMH) NHS Foundation Trust study: CCR3705 "Analysis of tumour specimens for biomarkers in gynaecological cancers" by Dr Saira Khalique prior to the commencement of this fellowship (Khalique, Nash et al. 2021). Briefly, DNA extraction and Next Generation Sequencing (NGS) took place in Good Clinical Laboratory Practice (GCLP) accredited laboratories at The Centre for Molecular Pathology, The Royal Marsden NHS Foundation Trust, Sutton. Genomic DNA from FFPE tissue sections was extracted using QIAamp FFPE Tissue Kit

(Qiagen) according to the manufacturer's instructions for both tumour and non-malignant content. Genomic DNA from blood was extracted using the QIAamp Blood mini kit (manual) or QIAsymphony DNA MidiKit (automated) (Qiagen) according to the manufacturer's instructions. DNA quality was assessed on the Agilent 2200 Tapestation (Agilent) and the Qubit Fluorometer (Fisher Scientific).

2.2.8 Polymerase chain reaction (PCR)

PCR amplicons were generated using 100 ng DNA in 50 μL reactions, using Q5® high-fidelity polymerase kit (New England Biolabs), according to manufacturer's protocol. Primers used are summarized in Table 4. PCR was carried out on a thermocycler as follows: 98^0C for 30 seconds, followed by 25 cycles of 98^0C for 10 seconds (melting), 65^0C for 30 seconds (annealing) and 70^0C for 20 seconds, before 72^0C for 2 minutes (final extension). PCR products were analyzed by agarose gel electrophoresis by mixing with 6x loading dye (New England Biolabs) and separation by gel electrophoresis. Agarose gels were made by dissolving 1 gram ultra pure agarose (Life Technologies) in 100 mL 1 x TAE buffer with 1:10,000 GelRed nucleic acid stain (Biotium). Hyperladder 1 (Bioline) was used to estimate size of PCR product. PCR product purified using QIAquik PCR purification kit (Qiagen) and eluted in 50 μL nuclease free water (Ambion). The primers used for PCR in the work contained in this thesis are summarised in Table 2.5

	Forward primer	Reverse primer
PPP2R2A (sgPPP2R2A 1)	GCCACCAATCTTTGCATTAT	TTCAAGCTCTGCTCAGGATTT
PPP2R2A (sgPPP2R2A 2)	TTCAGCACTCGAAAGGATCAA	CCTTCTTCACCAAACACCACCA AAG
PPP2R1A	ACTGTTACTATCAGCTCCGTT TC	CTCATCTACCTCTGTGAACTTGTC

Table 2.5 Summary of primer sequences used in this work.

2.2.9 TIDE analysis

Tracking indels by decomposition (TIDE) analysis was performed using ICE V2 CRISPR analysis tool (Synthego).

2.2.10 CRISPR prime gene editing

CRISPR prime gene editing performed using PE2 system as described by Anzaolone *et al (Anzalone, Randolph et al. 2019)*. Briefly, TOV21G cells were reverse transfected with CRISPR prime gene editing machinery. 375 ng pegRNA, 124.5 ng nicking gRNA and 2 µL P3000 (Invitrogen) mixed in 250 µL Optimem and incubated at room temperature for 10 minutes. 5 µL lipofectamine 3000 mixed with 250 µL optimum and incubated at room temperature for 10 minutes. The CRISPR prime editing mix and transfection mix were then combined in a 6 well plate and incubated at room temperature for 10 minutes. 300,000 TOV21G cells suspended in serum free medium and added to combined transfection mix. 5 days post transfection, cells were single cell sorted in to 96 well plates and

expanded. Once 90% confluency was reached, cells were trypsinised and resuspended and transferred in to two replicate plates. Genomic DNA was extracted from one plate, whilst the duplicate plate was viably frozen as previously described and stored at –80^{0}C. PCR based genotyping of clones was performed as previously described. PCR products were purified using QIAquick PCR Purification Kit (Qiagen) eluted in 50 µL nuclease free water as per the manufacturer's instructions. For Sanger sequencing, 15 µL purified PCR product mixed with 2 µL *PPP2R1A* forward primer (10 µM) described in section 2.2.8. Sanger sequencing was performed by Eurofins Genomics and results were analyzed using SnapGene software. The pegRNA sequences used in this work are summarized in Table 2.6.

Mutation	**PEG-RNA sequence**
PPP2R1A p.R183P	AGGCTGCGGCGGGCCGCACCATGGGGGT
PPP2R1A p.R183W	AGGCTGCGGCCCACCGCACCATGGGGGT

Table 2.6 Summary of pegRNA sequences used in this thesis.

2.2.11 TOPO-cloning

100 ng PCR products cloned in to pCR-Blunt II TOPO vector using Zero Blunt TOPO PCR Cloning Kit (Invitrogen) as per manufacturer's instructions. The final mix was incubated for 1 hour at room temperature and prepared for transformation. For transformation, 50 µL of competent bacteria were place into a sharp-bottom 14 mL round bottom polystyrene tube and mixed gently with 5 µL

cloned PCR product. Following 30 minutes of incubation on ice, tubes were heated to 42^{0}C for 50 seconds before being incubated on ice for 15 minutes. 500 µL SOC medium was added and bacteria were shaken at 37^{0}C for 1 hour. 50 µL bacterial suspension was plated on to agar plate containing ampicillin (100 µg/mL). Plates were then incubated upside-down at 37^{0}C overnight. The following day 10 colonies were picked and, expanded in SOB medium containing ampicillin 100 µg/mL. after incubating for 16 hours at 37^{0}C. Plasmid DNA was extracted using Qiaprep Spin Miniprep Kit (Qiagen) as per manufacturer's instructions. Sanger sequencing of isolated plasmid was performed by Eurofins Genomics using a U6-forward primer (GGCCTATTTCCCATGATTCCTTC). Results were analysed using SnapGene software.

2.2.12 Western blot analysis

Whole cell lysates were extracted using Radioimmunoprecipitation assay (RIPA) buffer (Thermo scientific) supplemented with Complete mini proteinase inhibitor (Roche). Protein concentration calculated using Bradford's reagent. Lysates separated using 4-12% SDS-PAGE BIS-TRIS gel and transferred to nitrocellulose membrane. Membranes were blocked in 5% milk and incubated in primary antibody in 5% BSA overnight at 4^{0}C. The following day a fluorescent or HRP-conjugated secondary antibody was added and incubated for one hour at room temperature followed by 3 x 20-minute washes with TBST. For Western blots performed with HRP-associated secondary antibodies a covering volume of Thermo Scientific SuperSignal West Femto Maximum Sensitivity Substrate

(ThermoFisher) was added immediately before measuring chemiluminescence. Signal was measured using the Licor system (Odyssey).

2.2.13 Cell cycle analysis by FACS

For the cell cycle analysis, 150,000 cells were seeded to 6 well plates. 24 hours later, medium was removed and replenished with medium containing drug or DMSO. Cells were then exposed to drug or DMSO for 24 hours. For the final 2 hours of drug exposure 5-ethynyl-2'-deoxyuridine (EdU) 20 μM (ThermoFisher) was added to the culture medium. Cells were harvested, washed in ice cold PBS before being fixed in 70% ethanol at 4^0C overnight. Staining of cells was carried out using Click-iT™ Plus EdU Alexa Fluor™ 647 Flow Cytometry Assay Kit (Invitrogen) as per manufacturer's instructions. Briefly, cells were permeabilised in 1 x saponin diluted in PBS before being stained with Alexa Fluor™ 647. Cells were washed and then incubated with Alexa Fluor™ 488-conjugated anti-phosphohistone H3 (S10) antibody (Invitrogen) at 1:50 concentration for 1 hour at room temperature, protected from light. Cells were then digested and stained with PI for DNA content with FxCycle™ PI/RNase Staining Solution (ThermoFisher). Detection of EdU staining, phosphohistone H3 staining, or PI was performed on a BD LSR II flow cytometer (BD biosciences). EdU was detected with the red laser detecting Alexa 647 blue at 635 nm using the 600/20 nm filter, phosphohistone H3 was detected using the blue laser detecting Alexa 488 at 520 nm using 530/30 nm filter and PI was measured at 488 nm detecting PE/Texas using the 610/20 filter. Debris and doublets were gated out from a

forward scatter (FSC)/side scatter (SSC) plot and DNA dye area/width plot respectively and the selected population was analysed regarding its cell cycle distribution using FlowJo (BD) FACS analysis software.

2.2.14 Immunofluorescence

Cells were seeded to polylysine coated cover slips (Corning). Once cells reach 60% confluence medium was removed and replenished with medium containing drug or DMSO. After 24 hours cells were fixed in 4 % PFA for 15 minutes at room temperature. Fixed cells were washed in PBS 3 times and then stored in PBS at 4 degrees. For staining of intracellular proteins and DNA, cells were first permeabilised in 0.25 % Triton-X in PBS for 15 minutes before being washed 3 times and blocked in IFF for 1 hour at room temperature. Cells were then incubated in primary antibody overnight at 4^0C. Cells were washed again in PBS 3 times before being incubated with Goat anti-Mouse IgG (H+L) Cross-Adsorbed Secondary Antibody, Alexa Fluor™ 555 (Thermo Fisher Scientific) and Goat anti-Rabbit IgG (H+L) Cross-Adsorbed Secondary Antibody, Alexa Fluor™ 488 (ThermoFisher) secondary antibody (1:1000 dilution) for 1 hour at room temperature. After a further 3 washes in PBS, cells were mounted on glass cover slips using ProLong™ Gold Antifade Mountant with DAPI (Invitrogen). Mounted coverslips were stored in the dark at 4^0C until imaging. Z stack images were acquired using Marianas advanced spinning disc microscopy (3i) with the generation of maximum projections performed using Slidebook6 (3i) software. Quantification of 53BP1 bodies was performed using CellProfiler imaging

analysis software. Micronuclei were measured manually and expressed as proportion of cells in visual field (minimum 100 cells).

2.2.15 Time lapse microscopy

Cells were seeded to flat bottom 96-well imaging plates (Perkin Elmer) in phenol-free RPMI medium (Gibco). Once cells reached approximately 60% confluency medium was removed and replenished with medium containing SPY505-DNA nuclear stain (Tebubio), SPY650-tubulin Probe (Universal biologicals) and SPY555-actin Probe (Universal biologicals) all at 1:1000 dilution. After culturing for four hours either DMSO or AZD6738 to a final concentration of 500 nM was added to each well. Cells were imaged every 5 minutes for 24 hours with the Marianas basic spinning-disk microscope system (Intelligent Imaging Innovations, 3i) with the generation of maximum projections performed using Slidebook6 (3i) software. Throughout imaging, cells were maintained at 37^0C in 5% CO_2. Duration of metaphase for 50 mitotic cells was measured manually.

2.2.16 Phospho-proteomic analysis

Protein extraction, preparation and mass spectrometry processing and analysis were performed by the Proteomics and Metabolomics Laboratory (Institute of Cancer Research, London, UK). In brief, snap frozen cell pellets were lysed by probe sonication and protein extracts were subjected to trypsin digestion. The tryptic peptides were labelled with amine-reactive TMT10plex Isobaric Label

Reagent (Thermo), which the multiplexed identification of up to 9,410 proteins. Labelled peptides were then combined in equal quantities and subjected to fractionation with high-pH C18 high-performance liquid chromatography (HPLC). LC-MS analysis was performed on the Dionex Ultimate 3000 system coupled with the Orbitrap Fusion Mass Spectrometer. Perseus software (Max Plank Institute) was used for data analysis.

2.2.17 High-throughput siRNA screen

An siRNA library targeting 953 genes encoding kinases and kinase-related genes, tumour suppressor genes (Dharmacon) and included in the Cancer Gene Census was used. Each well contained a smartpool of four distinct siRNAs which targeted different sequences within the same target gene. Additional positive and negative control siRNAs were added to the plate as previously described. 100 nL of 10 μM siRNA transferred to 364 well plate using Echo liquid handler (Labcyte). 5 μL Optimem was added to each well and plates agitated for 30 minutes at room temperature. A 2 x concentration transfection mix consisting of 4.95 μL Optimem and 0.05 μL RNAi Max (Invitrogen) combined per well and incubated at room temperature for 10 minutes. Optimem was then added to transfection mix to bring to a 1 x concentration. 10 μL of 1 x transfection mix added to each well and incubated at room temperature for 10 minutes. 500 cells suspended in 35 μL of antibiotic free medium was then added to each well and returned to incubator at 37^0C. 24 hours post transfection AZD6738 at a final concentration of 100 nM or

DMSO was added to each well. Cell viability was assessed after 5 days using CellTiter-Glo® as previously described.

When analysing the siRNA screen data the luminescence readings from each well were $\log_2$ transformed and centred to the median of the plate in order to account for any variability between plates. A drug effect (DE) score was then calculated by subtracting the median of plate centred scores of replicates for DMSO arms from the drug exposed arms of the screen. Robust z-normalisation method with median and mean absolute deviation (MAD) as the data is skewed due to the presence of outliers (Equation 5).

Equation 5:

$$DE\ z\ score = \frac{DE - median}{MAD}$$

Where median represents the median DE for all the siRNAs in the screen and MAD represents the an estimate mean of the standard deviations for all the siRNAs. As before, a DE z score of 0 represents no effect on viability whereas a negative DE score represents increased cell death and a positive DE score represents reduced cell death, i.e. drug resistance.

2.2.18 Reverse siRNA gene silencing

Reverse siRNA transfections were performed in 6-well plates. 5 µL of siRNA was combined with 250 µL optimem and incubated at room temperature for 5 minutes. 5 µL of RNAi max was combined with 250 µL optimem and incubated at room temperature for 10 minutes. Following their respective incubation periods the RNAi mixture and transfection mixture were combined in well of 6-well plate and incubated for 15 minutes under constant agitation at room temperature. 250,000 cells suspended in 2 mL serum free medium was then added to each well and plates returned to incubator at 37^0C. After 24 hours, medium containing transfection mix was removed and replenished with fresh medium. 72 hours post transfection cells were seeded for cell viability assay or cell cycle analysis as previously described or harvested for protein extraction.

2.3 In vivo studies

2.3.1 Maximum tolerated dose (MTD) study for AZD6738

14 BALB/c nude mice aged between six and seven weeks were divided in to 4 groups (2 with 3 mice and 2 with 4 mice). Group 1 (3 mice) was treated with vehicle, consisting of 10% DMSO (Sigma) plus 40% Propylene Glycol (also known as 1,2 Propan-diol) (Merck) + 50% de-ionised sterile water. Group 2 (3 mice) was treated with AZD6738 25 mg/kg on a 3 days on, 4 days off regime. Group 3 (4 mice) was treated with AZD6738 25 mg/kg 5 days on, and 2 days off regime. Group 4 (4 mice) was treated with AZD6738 25 mg/kg on a 7 days on, 7

days off regime. AZD6738 was reconstituted in vehicle and administered by oral gavage. Animals were treated for 30 days with their weight being measured before each dose of vehicle/AZD6738 was administered. If more than a 20% relative weight loss was observed the animals were culled.

2.3.2 Generation of luciferase expressing cell lines

Cells were infected in 6-well plate with Lenti-ONE RFP-2A-Luc2 lentiviral vector (GEG Tech) encoding red fluorescent protein (artificial sequence derived from sea anemone Entacmaea quadricolor) and Luciferase2 (artificial sequence derived from Photinus pyralis genome). Cells were expanded for 1 week and then FACS sorted for RFP positive cells using BD FACS ARIA II cell sorter (BD).

2.3.3 Assessment of luciferase activity

Cells seeded using a serial dilution in triplicate to 96-well plate with a highest concentration of 10,000 cells per well decreasing by half with each dilution until 312.5 cells/well reached. 24 hours later luciferin (Perkin Elmer) was added to each well to give a final concentration of 150 µg/mL. After 2-3 minutes, total flux luminescence in photons/second was measured using IVIS® Spectrum In Vivo Imaging System (Perkins Elmer).

2.3.4 Pilot in vivo study

1 x 10^6 luciferase expressing TOV21G cells were diluted in 100 µL sterile PBS and injected directly in to the intraperitoneal cavity of three BALB/c nude mice per genotype. *In vivo* imaging using IVIS® Spectrum In Vivo Imaging System was performed three times per week. Ten minutes before imaging luciferin 150 mg/kg was injected into the peritoneum. Home office end points granted on the project licence were applied for decisions regarding culling. This followed signs linked to tumours such high IVIS signal, abdominal distention due to ascites, low body condition score and change in health status related to abdominal tumours.

2.3.5 Full *in vivo* study

1 x 10^6 luciferase expressing TOV21G cells were diluted in 100 µL sterile PBS and injected directly in to the intraperitoneal cavity of 30 BALB/c nude mice per *PPP2R1A* genotype. 6 days post inoculation animals were treated with vehicle or AZD6738 25 mg/kg on a 5 days on, days off regime as outlined in Section 3.3.2. *In vivo* imaging using IVIS® Spectrum In Vivo Imaging System was performed three times per week until 17 days post treatment initiation. Ten minutes before imaging luciferin 150 mg/kg was injected in to the peritoneum. Animals continued to be treated and monitored for survival assessment up until 30 days. Home office end points granted on the project licence were applied for decisions regarding culling. This followed signs linked to tumours such high IVIS signal, abdominal distention due to ascites, low body condition score and change in health status related to abdominal tumours. Throughout the study, body weight was measured

prior to the administration of vehicle/AZD6738, with animals being culled if more than a 20% relative weight loss was observed.

2.4 Statistical analysis

Statistical analysis was performed using GraphPad Prism. The statistical test used for each analysis is defined in the figure legend. Statistical significance set at $p < 0.05$.

Chapter 3. identify genetic determinants of ATRi sensitivity in ARID1A mutant ovarian clear cell carcinoma.

3.1 Introduction

Williamson and Lord have previously demonstrated that loss of *ARID1A* causes ATR inhibitor (ATRi) sensitivity in models of ovarian clear cell carcinoma (OCCC) (Williamson, Miller et al. 2016). This data led to a number of clinical trials, including NCT04065269 (ATARI) and NCT03682289. In order to better understand what, in addition to *ARID1A*, controls ATRi responses in OCC, I designed a genome-wide CRISPR-Cas9 mutagenesis ATRi chemosensitivity screen in ATRi-sensitive, *ARID1A* mutant TOV21G OCC cells (*ARID1A* p.549fs, p.756fs). My intention in doing this was to generate information that could be used to inform the analysis of trials such as ATARI.

3.2 Generation of Cas9 positive TOV21G cells

For the purposes of the screen, Cas9-positive TOV21G cells were generated by Dr Feifei Song (Lord Lab). Cells were transducted with EditR inducible lentiviral hEF1a-Blast-Cas9 nuclease (Dharmacon) and selected in blasticidin. This led to the generation of a Cas9-expressing daughter clone (Figure 3.1).

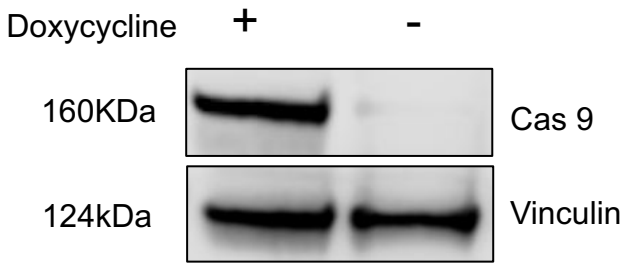

Figure 3.1 Western blot confirming induction of Cas9 following exposure to doxycycline. Whole cell extracts from iCas9 expressing TOV21G cells following exposure to doxycycline (1 µg/ml) for 24 hours.

Following the generation of the Cas9 positive TOV21G cells, I confirmed the sensitivity of these cells to either of two different clinical ATRi, AZD6738 and VX970, using *ARID1A* isogenic HCT116 cells as controls (HCT116 ARID1A$^{+/+}$ and HCT116 ARID1A$^{-/-}$) (Figure 3.2).

3.3 Screen overview

I designed a genome-wide CRISPR screen in which Cas9+ TOV21G cells were infected with a short guide RNA (sgRNA) library designed to target 18,010 genes, using a multiplicity of infection of 0.3 designed to introduce only one gRNA per cell (Figure 3.3). Here a representation (number of cells per sgRNA) of >1000 was used, to maximise the potential to identify sgRNAs that altered ATRi sensitivity. Transduced cells were then exposed to AZD6738 or the drug vehicle (DMSO) for two weeks, after which sgRNA frequency in the surviving cell populations was determined by deep sequencing.

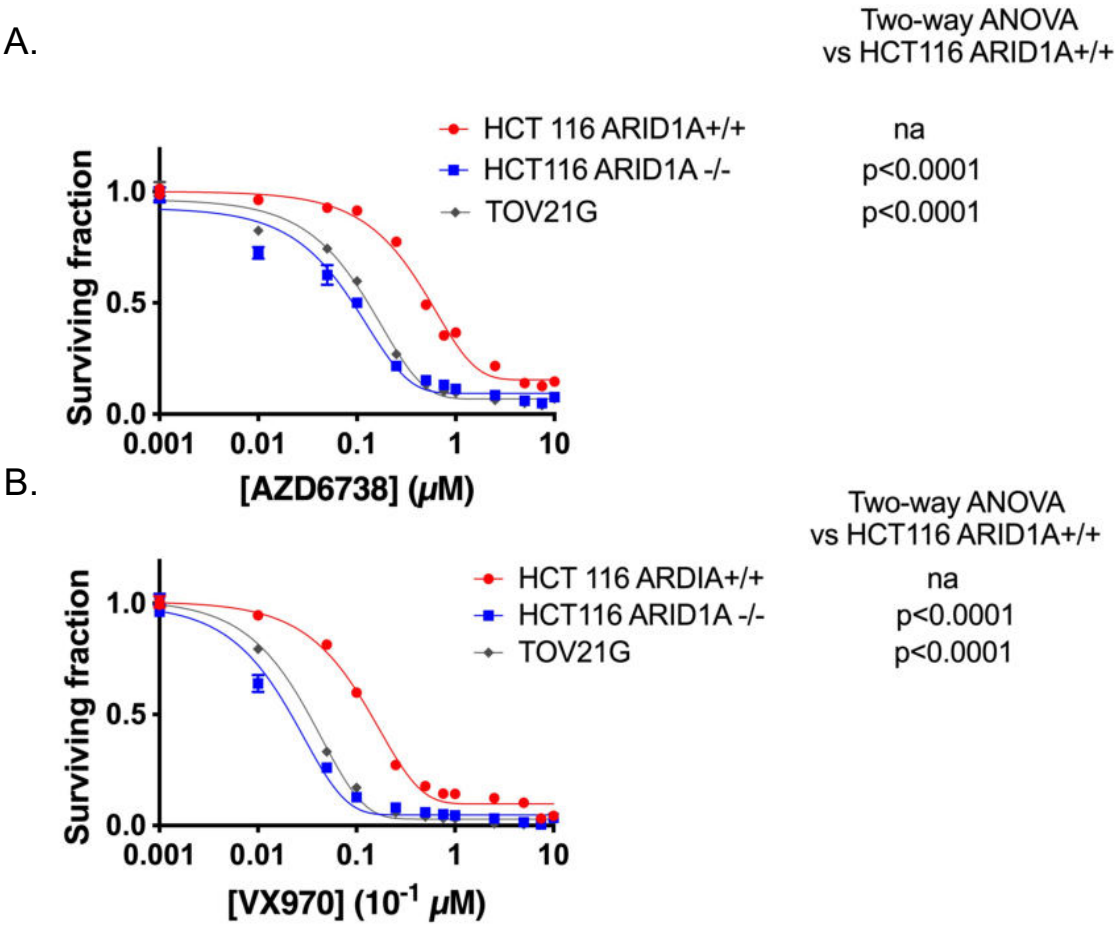

Figure 3.2 TOV21G cells are sensitive to ATRi. (A-B) Dose response curves illustrating the ATRi sensitivity of OCCC TOV21G cells. Cells were plated in 384 well plates and exposed to either AZD6738 (A) or VX970 (B) for five continuous days, at which point cell viability was assessed using CellTitre-Glo®. ARID1A$^{+/+}$ and ARID1A$^{-/-}$ HCT116 cells are included as controls. Error bars represent standard error of the mean (SEM) from 5 replicates. Significance determined via two-way ANOVA.

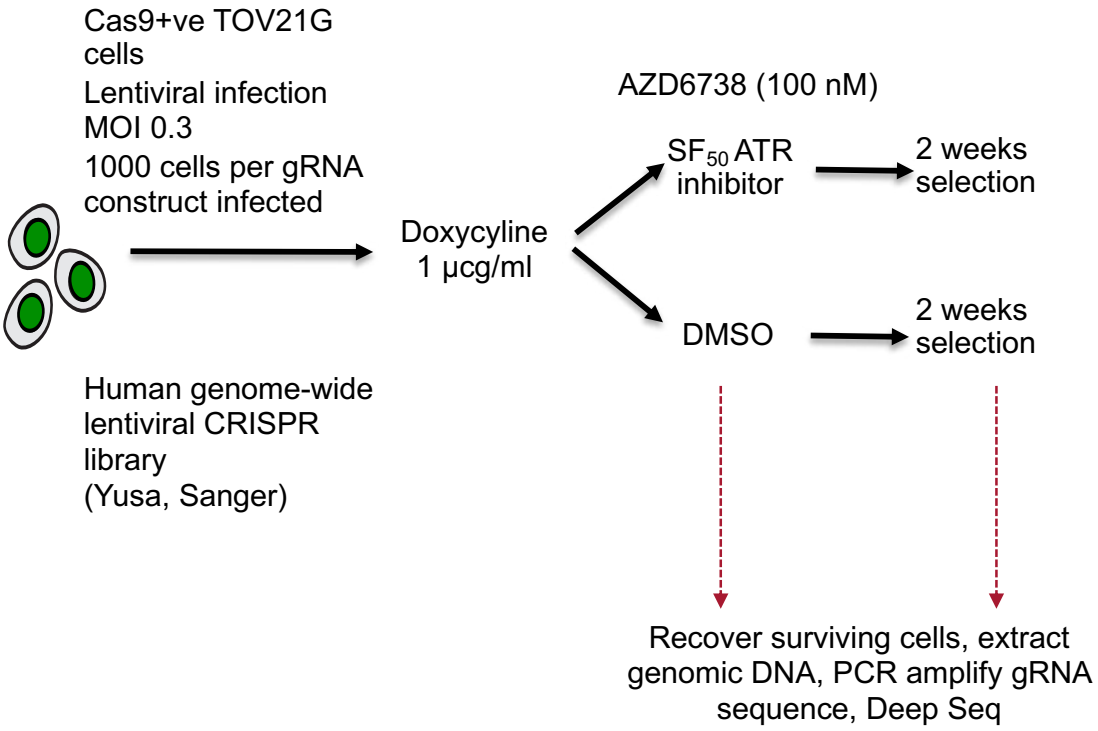

Figure 3.3 Screen schema for genome wide CRISPRn screen. Cas9 expressing TOV21G cells infected with lentiviral library targeting 20,000 genes with representation of 5 sgRNA per gene. Following induction of Cas9 with doxycycline cells were exposed to AZD6738 100 nM or DMSO for two weeks. Cells were harvested prior to drug/DMSO exposure and after 2 weeks for genomic DNA extraction and next-generation sequencing.

3.4 Data analysis

sgRNA abundance was determined in the populations exposed to AZD6738 or DMSO using a gene-based depletion score termed Norm Z (Colic, Wang et al. 2019). I assessed the quality of this screen by assessing the performance of sgRNA designed to target "core essential genes" – i.e. those genes that are essential in most cell lineages (Hart, Chandrashekhar et al. 2015), observing significantly lower Norm Z scores in the core essential genes when compared to the non-essential genes ($p < 0.0001$, unpaired Wilcoxon rank sum test) (Figure 3.4).

By comparing sgRNA frequencies in DMSO and ATRi-exposed cultures, I determined the identity of genes that controlled ATRi sensitivity/resistance. In TOV21G cells, sgRNA designed to target *POLE3* or *POLE4* (DNA polymerase ε accessory subunit encoding genes) caused AZD6738 sensitivity (Figure 3.5), consistent with similar ATRi chemosensitvity screens carried out in other cell lines (Hustedt, Alvarez-Quilon et al. 2019). Similarly, gRNA designed to target *CDC25B* and *CDK2* caused AZD6738 resistance (Figure 3.5), consistent with previous reports (Ruiz, Mayor-Ruiz et al. 2016), indicating that the screen was able to detect genetic determinants of both sensitivity and resistance to ATRi.

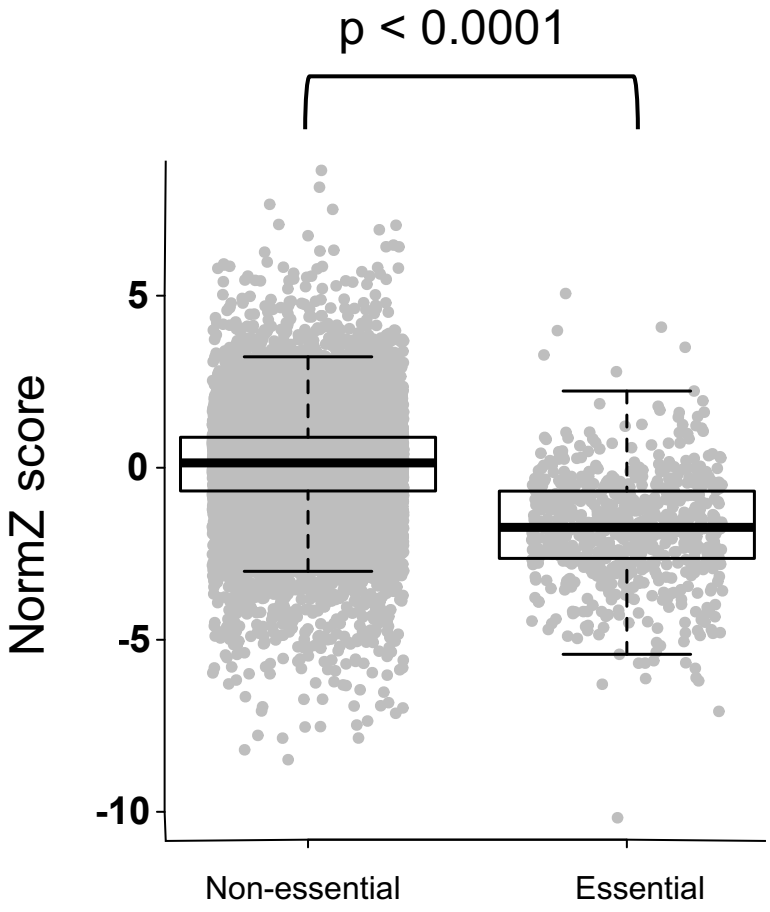

Figure 3.4 . CRISPR-Cas9 screen quality control plot. Jitter box plots showing gene level normalised Z scores (NormZ) scores for 18,009 genes classified as either “core essential” or “non-core essential”(Hart et al., 2015). Core essential genes had significantly lower NormZ scores than non-core essential genes ($p < 0.001$, non-parametric unpaired Wilcoxon rank sum test).

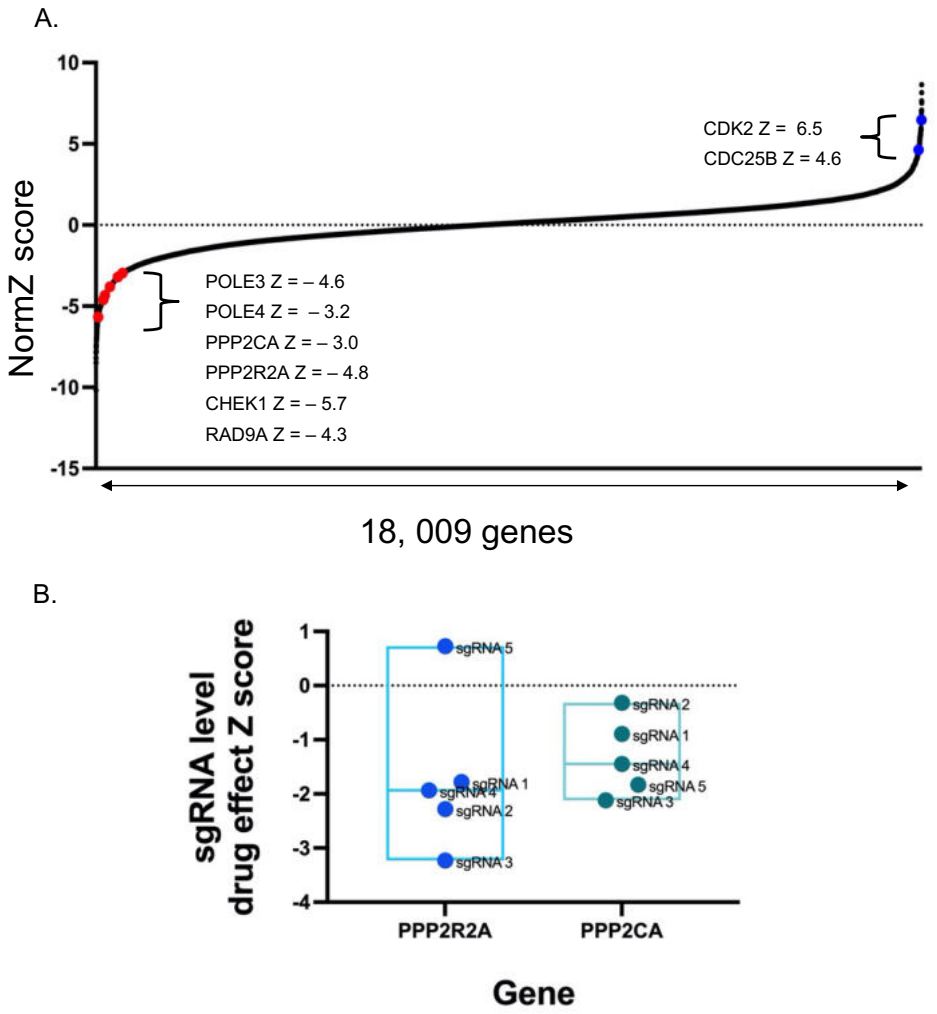

Figure 3.5 Genome wide CRISPRn screen identifies several genes encoding PP2A subunits as ATRi response genes. (A) Scatter plot showing the ranked gene-level NormZ scores from the genome wide CRISPR-Cas9 screen. PPP2R2A and PPP2CA were identified as sensitising ”hits” along with several other genes previously known to cause sensitivity to ATRi such as POLE3, POLE4, CHEK1 and RAD9A . (B) Guide level Z scores from the genome wide CRISPR screen for the sgRNAs designed to target PPP2R2A or PPP2CA.

3.5 Genes encoding Protein phosphatase 2A genes identified as ATRi response genes

Using a Norm Z score of less than -2.0 as a threshold for indicating a significant sensitizing effect, I noticed that sgRNA targeting the protein phosphatase 2A (PP2A) subunits *PPP2CA* and *PPP2R2A* caused ATRi sensitivity in TOV21G cells (Figure 3.5), an effect analogous to the effect of *PPP2R2A* shRNA causing ATRi sensitvity in non-small cell lung cancer tumour cell lines (Qiu, Fa et al. 2020).

PP2A is a highly conserved serine/threonine phosphatase responsible for the majority of phosphatase activity in eukaryotic cells (Janssens and Goris 2001, Sontag 2001). The broad spectrum of cellular processes in which PP2A is involved is enabled by its complex structure. PP2A is a heterotrimeric holoenzyme consisting of a scaffolding subunit (A) which forms a core dimer with a catalytic (C) subunit (Cho and Xu 2007). Substrate specificity and subcellular localisation of PP2A is imparted through the incorporation of a regulatory (B) subunit, of which 19 have been described, into the holoenzyme complex (Martens, Stevens et al. 2004). Several isoforms of the scaffolding, regulatory and catalytic subunits have been previously described Table 3.1 and are either encoded by discrete genes or are a consequence of alternative splicing of the same gene (Janssens and Goris 2001, Sontag 2001, Martens, Stevens et al. 2004). Genes identified as ATRi response genes in a genome wide CRISPRn screen, namely *PPP2R1A* and *PPP2R2A*, encode the scaffolding and catalytic subunits respectively (Figure 3.6).

Subunit	Gene	Isoform	Alternative Name	Chromosome	Normal tissue distribution	Subcellular localization	Abnormal tissue distribution	Refs
Scaffold (A)	PPP2R1A	α	PR65α,PP2A-Aα	19q13.33	Ubiquitously expressed in all the tissues	Cytosol	Lung, breast, melanoma, endometrial and ovarian cancer	(Hemmings, Adams-Pearson et al. 1990, Wang, Esplin et al. 1998)
	PPP2R1B	β	PR65β,PP2A-Aβ	11q23.2	Ubiquitously expressed and highly expressed in ovary (oogenesis)	Cytosol	Lung, Breast, colon, ovarian, B-CLL	(Hemmings, Adams-Pearson et al. 1990, Wang, Esplin et al. 1998)
Catalytic (C)	PPP2CA	α	PP2Acα	5q31.1	Brain and Heart	Cytoplasm and Nucleus	Prostate	(Arino, Woon et al. 1988, Khew-Goodall and Hemmings 1988, Bhardwaj, Singh et al. 2011)
	PPP2CB	β	PP2Acβ	8p12	Brain and Heart	Cytoplasm and Nucleus	-	(Arino, Woon et al. 1988, Khew-Goodall and Hemmings 1988)
Regulatory (B)	PPP2R2A	α	PR55α,PP2ABα	8p21.1	Widely distributed in all tissues	Membranes, cytoplasm, Microtubules Nucleus. Golgi complex, endoplasmic reticulum and neurofilaments	AML, prostate	(Hemmings, Adams-Pearson et al. 1990, Cheng, Liu et al. 2011, Ruvolo, Ruvolo et al. 2014)
	PPP2R2B	β	PR55β,PP2ABβ	5q31-5q32	Brain and testis	Cytosol	-	(Hemmings, Adams-Pearson et al. 1990)
	PPP2R2C	γ	PR55γ, PP2ABγ	4p16.1	Brain	Mainly in Cytoskeletal fraction	Lung cancer, melanoma	(Zolnierowicz, Csortos et al. 1994, Banerjee, Read et al. 2007)
	PPP2R2D	δ	PR56/61δ, PP2AB'δ	6p21.1	Primarily exist in brain	Cytoplasm, Nucleus, Mitochondria, Microsomes	-	(Strack, Chang et al. 1999)
Regulatory(B')	PPP2R5A	α	PR56/61α,PP2AB'α	1q32.2-q32.3	Cardiac tissues and skeletal muscles	Cytoplasm	-	(McCright, Rivers et al. 1996)
	PPP2R5B	β	PR56/61β,PP2AB'β	11q12-q13	Brain	Cytoplasm	-	(Csortos, Zolnierowicz et al. 1996, McCright, Rivers et al. 1996)
	PPP2R5C	γl, 2,3	PR56/61γ, PP2AB'γ	14q32	Cardiac tissues and skeletal muscles (HE)	Cytoplasm and Nucleus	Lung cancer ,reduced level in melanoma cells	(Csortos, Zolnierowicz et al. 1996, McCright, Rivers et al. 1996, Francia, Poulsom et al. 1999)
	PPP2R5D	δ	PR56/61δ, PP2AB'δ	6p21.1	Primarily exist in brain	Cytoplasm, Nucleus, Mitochondria, Microsomes	-	(McCright, Rivers et al. 1996, Tanabe, Nagase et al. 1996)

	PPP2R5E	ε	PR56/61ε, PP2AB'ε	14q23.1	Primarily exist in brain	Cytoplasm	Breast cancer, Soft tissue sarcoma	(McCright, Rivers et al. 1996, Dupont, Breyer et al. 2010)
Regulatory(B")	PPP2R3A	α	PR130,B"α1	3q22.1	Brain(HE), heart, Lung, kidney and muscle	Centrosome and Golgi complex	-	(Mayer-Jaekel and Hemmings 1994)
	PPP2R3A	α	PR72, B"α2	3q22.1	Heart(HE) and skeletal muscle	Cytosol and nucleus		(Mayer-Jaekel and Hemmings 1994)
	PP2R3B	β	PR70, PR48, B"β	Xp22.33, Y11.3	Placenta	Nucleus	-	(Yan, Fedorov et al. 2000)
	PPP2R3C	γ	G5PR, G4-1	14q13.2	During developmental process expressed in fetal brain	Nucleus	-	(Kamnasaran, Chen et al. 2005)
	PPP2R3D	δ	PR59, B"δ		Cardiac tissue, Kidney and Lungs	Nucleus	-	(Voorhoeve, Watson et al. 1999)
Regulatory(B'")	STRN		Striatin, PR110	2p22.2	Brain	Membrane and cytoplasm	-	(Moreno, Park et al. 2000)
	STRN3		SG2NA	14q13-q21	Neurons	Nucleus	-	(Moreno, Park et al. 2000)
	PPP2R4		PTPA, PR53	9q34	Widely expressed	Cytosol, Nucleus	-	(Cayla, Van Hoof et al. 1994, Janssens and Goris 2001)

Table 3.1 Summary of PP2A subunits, along with their tissue distribution, subcellular localization together and abnormal tissue distribution in disease states.

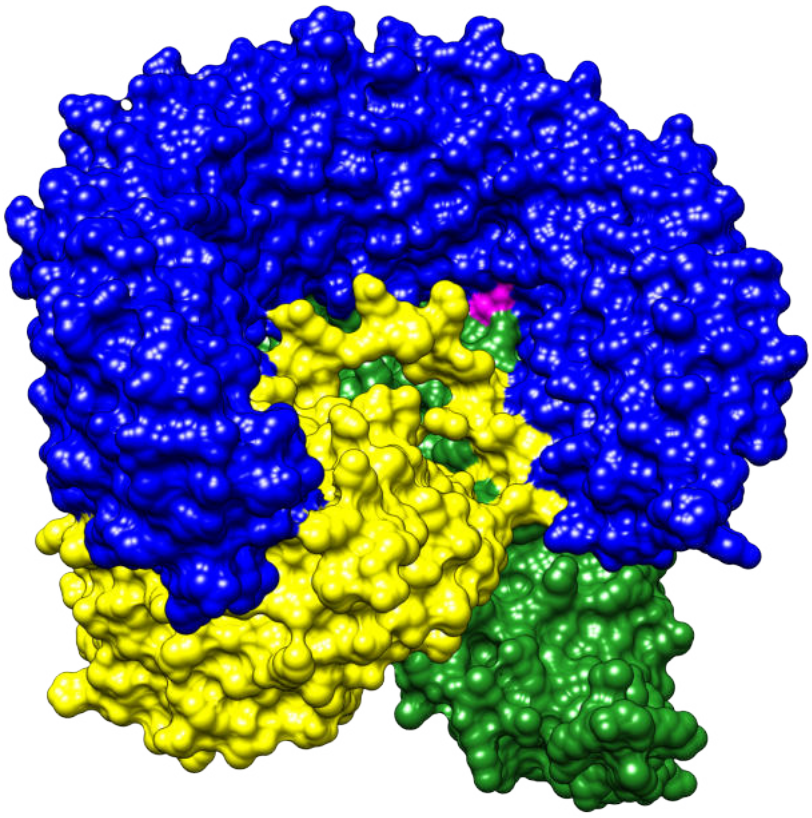

Figure 3.6 Crystal structure for the PP2A holoenzyme. Scaffolding subunit shown in blue, catalytic subunit shown in yellow and regulatory subunit shown in green. Conserved PPP2R1A p.R183 missense mutations, shown in pink, lead to amino acid substitutions at the site where the scaffolding subunit interacts with regulatory subunit. Xu *et al* (2006).

3.6 Revalidation of PPP2R2A as ATRi response gene using EditR approach

In subsequent experiments using *PPP2R2A* specific sgRNA, I confirmed the relationship between deleterious mutations in PP2A and ATRi sensitivity, finding that two different sgRNA targeting *PPP2R2A* caused a significant (two-way ANOVA, $p < 0.001$) increase in ATRi sensitivity, to a similar extent as that caused by sgRNA targeting the known ATR synthetic lethal gene, *ATM* (Figure 3.7). In order to confirm *PPP2R2A*-specific mutagenesis, I performed TIDE analysis on genomic DNA following transfection with the Cas9 nuclease and sgRNAs targeting *PPP2R2A*. This analysis revealed an editing efficiency of 18 % for both sgRNAs, which was sufficient to increase sensitivity to ATRi in this model (Figure 3.8).

3.7 Genes encoding PP2A subunits identified as ATRi response genes in multiple genome wide CRISPRn/i screens in molecularly distinct cell line

To assess whether PP2A-CRISPR ATRi sensitivity was private to TOV21G cells, or indeed a more generalisable effect, I re-analysed data from four additional genome-wide CRISPR screens carried out by Drs. Rachel Brough, Fei Fei Song and Joseph Baxter in the Lord Lab. These were carried out in an additional cell line, a non-tumour epithelial line with an engineered *p53* mutation, MCF10A *p53*^{mutant}. These were both CRISPR mutagenesis (CRISPRn) and CRISPR interference (CRISPRi) screens in MCF10A *p53*^{mutant} cells, using two different

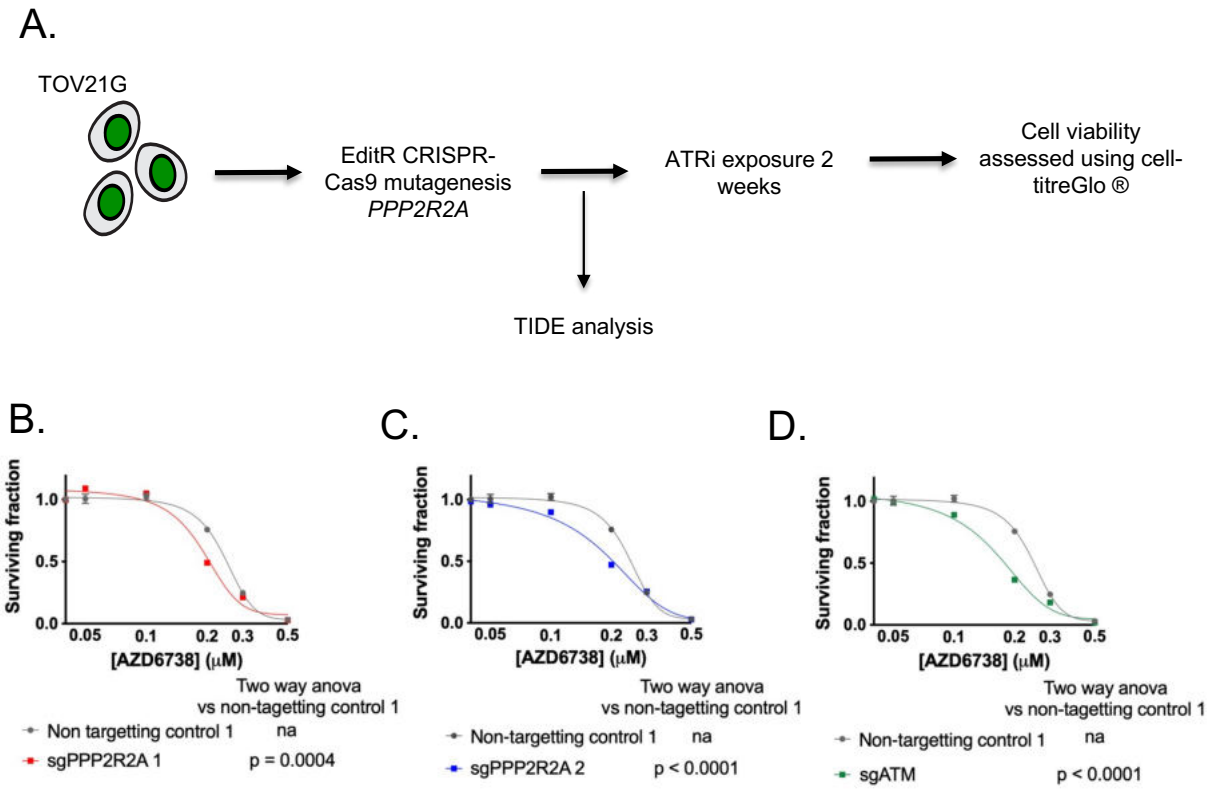

Figure 3.7 PPP2R2A revalidates as ATRi response genes using EditR approach. (A) Screen revalidation schema. TOV21G cells were transfected with either non-targeting, PPP2R2A specific or ATM– specific sgRNAs. 2 days after transfection, a fraction of cells were recovered for genomic DNA extraction and DNA sequencing analysis to confirm PPP2R2A mutation. Remaining cells were then exposed to AZD6738 for 14 days after which cell viability was assessed using using CellTitre-Glo®. (B-D) Dose response curves from experiment described in A. Curve for ATM is shown as positive control. Error bars represent standard error of the mean (SEM) from 4 replicates. Statisical significance determined via two-way ANOVA.

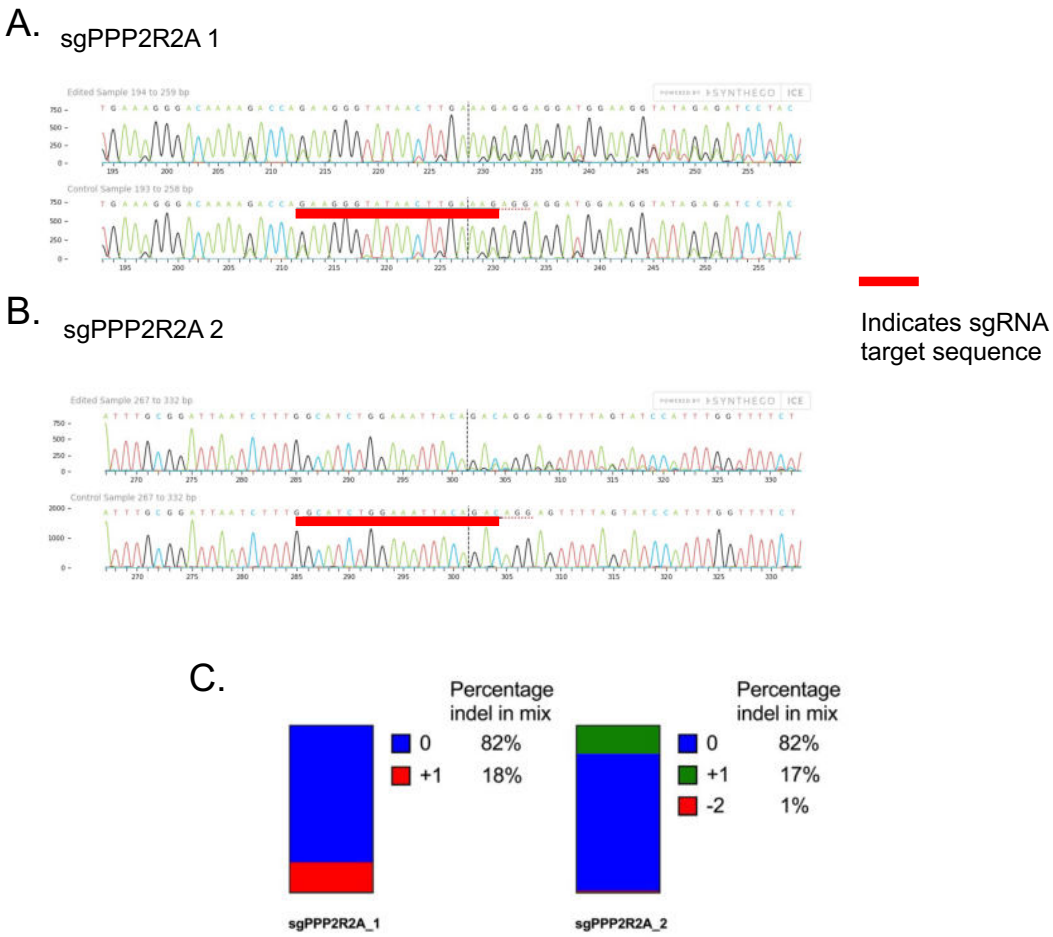

Figure 3.8 PPP2R2A mutagenesis confirmed using TIDE analysis. (A-B) Chromatogram showing sanger sequencing of sgRNA PPP2RP2A_1 and sgRNA PPP2R2A_2 (top) versus non-targeting control sgRNAs (bottom). Evidence of PPP2R2A specific gene editing in the PPP2R2A_1 and PPP2R2A_2 transfected cells. (C) TIDE analysis plot. The fraction of DNA sequence reads with either no indel mutation (0), an indel mutation of +1 base or an indel mutation of -2 bases is shown. Both PPP2R2A sgRNAs generated an indel rate of 18 %.

clinical ATR inhibitors, AZD6738 and VX970 (Figure 3.9). All four screens identified *PPP2CA* (encoding the catalytic subunit), *PPP2R1A* (scaffolding subunit) and *PPP2R2A* (regulatory subunit) as determinants of ATRi sensitivity (Figure 3.10). The NormZ scores (including the number of guides from the library with a drug effect Z score less than –2) for genes encoding PP2A subunits from genome wide CRISPRn and CRISPRi screens outlined in Figures 3.9 and 3.10 are summarised in Table 3.2. Taken together with the TOV21G screen data, this suggested that defects in protein phosphatase 2A cause a relatively penetrant (Ryan, Bajrami et al. 2018) synthetic lethal effect, operating in multiple, molecularly distinct settings.

3.8 Chapter 3 Discussion

In addition to known genetic determinants of ATRi sensitivity, the genome wide CRISPRn screen performed in the OCCC cell line TOV21G identified several genes encoding different PP2A subunits. The penetrance of this effect was demonstrated in a molecularly distinct non-cancerous cell line using both a CRISPRi and CRIPSRn approach, using two distinct ATRi (AZD6738 and VX970). In an independent experiment, transfection of two individual sgRNAs targeting *PPP2R2A* and recombinant Cas9 endonuclease significantly increased sensitivity to AZD6738 to a similar extent to sgRNA targeting ATM itself. *PPP2R2A*-specific mutagenesis was confirmed via TIDE analysis for both sgRNAs used in this revalidation experiment. This increased my

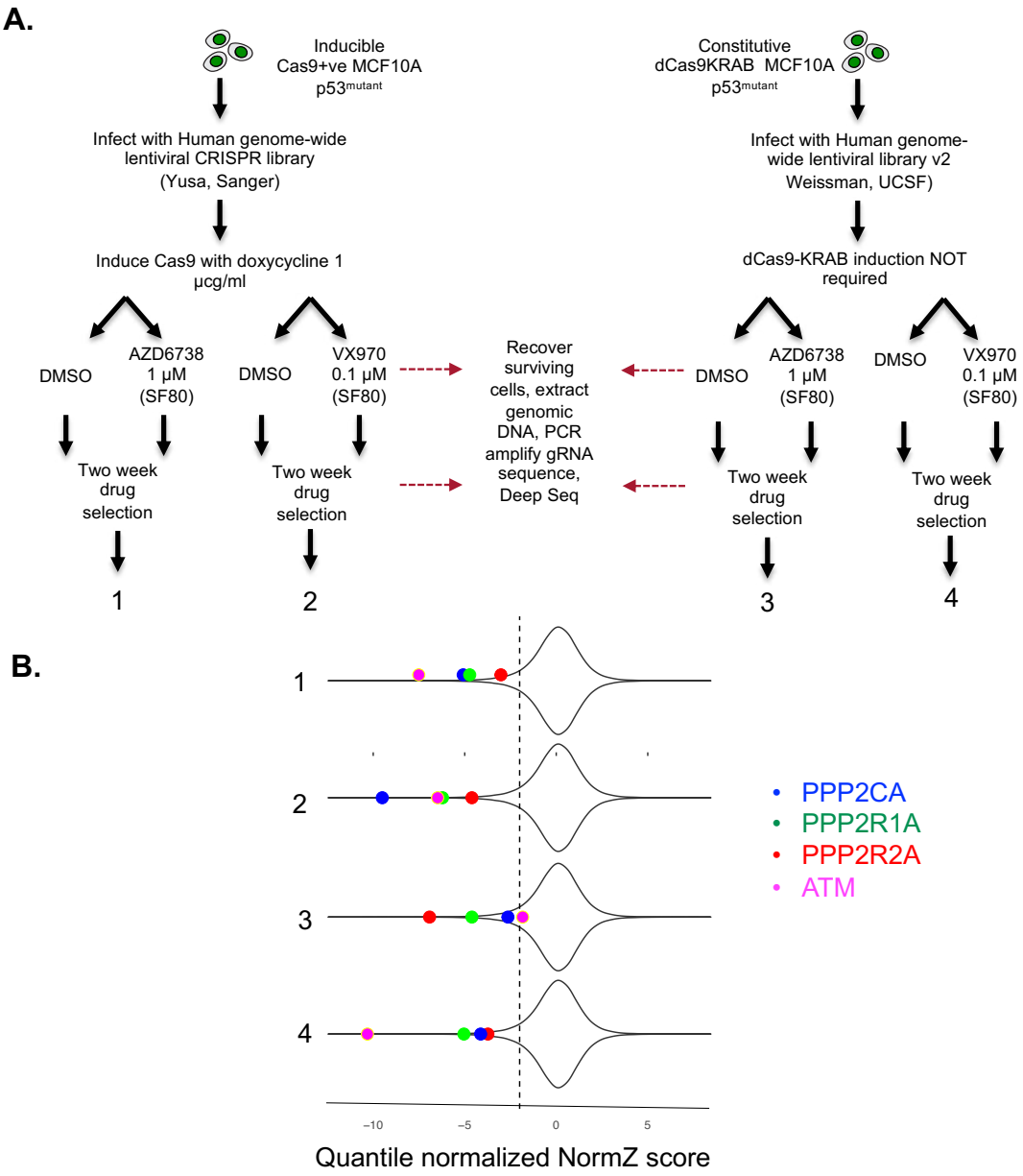

Figure 3.9 Genes encoding PP2A subunits identified in multiple genome wide CRISPRn/i screens performed in MCF10A cells. (A) Experimental scheme for additional CRISPR mutagenesis (CRISPRn) or CRISPR interference (CRISPRi) screens for genetic determinants of ATRi sensitivity. Non-tumour epithelial MCF10A cells, with a deleterious p53 mutation, expressing a doxycycline-inducible Cas9 transgene or constitutive dCas9-KRAB transgene were used as shown. AZD6738 SF80 was 1 µM. VX970 SF80 was 0.1 µM. (B) Violin plots showing the quantile normalized NormZ scores for either 18009 genes (CRISPRn screens) or 18905 genes (CRISPRi screens) from the screens described in (A).

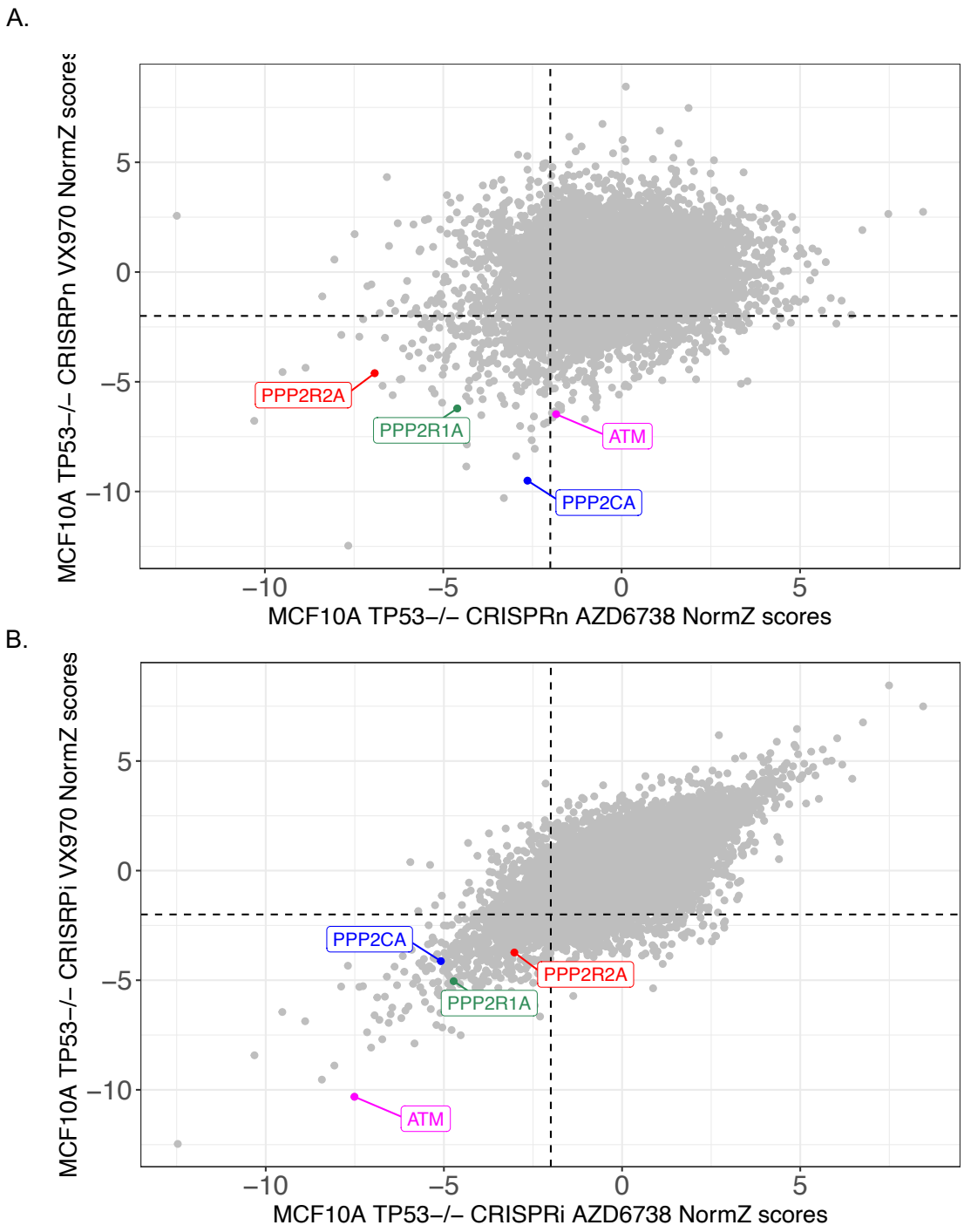

Figure 3.10 Quantile normalised NormZ scores from genome-wide CRISPRn/i screens with ATRi in MCF10A cells. Scatter plot showing the gene-level Norm Z score from the CRISPRN (A) and CRISPRi (B) screens performed with AZD6738 and VX970 described in Figure 8. Data points for PPP2R1A (green), PPP2R2A (red) and PPP2CA (blue) and ATM (magenta; positive control) are highlighted.

Cell line	p53$^{-/-}$ MCF10A								TOV21G	
Cas9	Nuclease				Interference				Nuclease	
Drug	VX970		AZD6738		VX970		AZD6738		AZD6738	
	NormZ	No Guides < 2	NormZ	No Guides < 2	NormZ	No Guides < 2	NormZ	No Guides < 2	NormalZ	No Guides < 2
PPP2CA	-16.77	5	-14.64	5	-6.19	2	-8.65	2	-2.9	1
PPP2CB	0.53	0	-0.95	1	-1.53	0	-0.10	0	0.13	0
PPP2R1A	-8.21	4	-6.35	4	-8.22	5	-7.62	4	-0.36	0
PPP2R1B	-0.53	1	-2.09	0	0.24	0	-0.34	0	-2.05	1
PPP2R2A	-4.94	4	-2.21	2	-5.28	3	-4.34	3	-3.8	3
PPP2R2B	2.97	0	1.32	0	0.70	0	1.35	1	3.1	0
PPP2R5E	-2.85	1	-4.61	1	-3.73	2	-3.51	2	-2.8	1

Table 3.2 Summary of the gene level NormZ scores, together with the number of guides in the library with a drug effect Z score less than 2, for genes encoding PP2A subunits included in genome wide CRISPRn or CRISPRi screens performed within our group.

confidence that the identification of PPP2R2A in the CRISPRn screen was not an artefact.

The selection of genetic determinants of drug sensitivity from CRISPR mutagenesis and other genetic perturbation screens demands that the genes selected meet a number of criteria:

1. Large effect size
2. Highly penetrant effect
3. Biological relevance to the tumour type of interest.

One potential caveat to the interpretation of the genome-wide CRISPRn screen results is the relative effect size of the effects delivered by sgRNAs targeting genes encoding PP2A subunits relative to other genes targeted. The gene-level Norm Z score for *PPP2RA* (–3.8) and *PPP2CA* (–2.9) rank these genes as the 304th and 584th most sensitizing effect respectively. Therefore, it could be argued that focusing on PP2A subunits for further validation excludes other genetic determinants of ATRi sensitivity with a greater effect size. However, as described in later chapters, genes encoding PP2A subunits have clinical significance in gynaecological malignancies, hence the focus on these.

With the advent of increasingly complex strategies for performing genetic perturbation screens, our ability to identify synthetic lethal interactions operating in cancer has increased. The penetrance of these effects refers to the extent to which they impact upon the genetic background of the cell model

they are observed in. Highly penetrant effects are ubiquitously observed irrespective of other genetic aberrations present, whilst effects with incomplete penetrance are highly context dependent, being heavily impacted by the presence of other mutations (Ryan, Bajrami et al. 2018). The identification of genes encoding PP2A subunits in five independent genome-wide CRISPRn/i screens performed with ATRi in two molecularly distinct backgrounds suggests that the observed effects are not private to TOV21G cells, gynaecological malignancies nor *ARID1A* mutant cells. This does not mean that this effect is not relevant in OCCC, other gynaecological malignancies or *ARID1A* mutant cancer but rather that is not dependent on these factors.

During the course of this project *Qui et al* published the results of a genome-wide pooled shRNA screen performed in preclinical models of non-small cell lung cancer to identify genetic determinants of ATRi and checkpoint kinase 1 inhibitors (CHK1i) (Qiu, Fa et al. 2020). In addition to identifying genes previously implicated in ATRi and CHK1i sensitivity, including replication proteins A1, A2 and A3 (RPA1-3) (Lee, Zhou et al. 2016) and WEE1 (Hustedt, Alvarez-Quilon et al. 2019), several PP2A components including genes encoding the scaffolding subunit (*PPP2R1A)* and two regulatory subunits (*PPP2R2A, PPP2R5B*) were identified as ATRi response genes. Mechanistically, *PPP2R2A* gene silencing was shown to increase basal levels of c-MYC at the post-translational level (Qiu, Fa et al. 2020) a known cause of replication stress (Dominguez-Sola, Ying et al. 2007) and a suspected cause of subsequent ATRi sensitivity (Young, O'Connor et al. 2019, Xing, Zhang et al. 2020, King, Southgate et al. 2021).

The putative relationship between PP2A and replication stress was explored further by *Li et al (Li, Kozono et al. 2020)* who reported that an endogenous PP2A inhibitor, FAM112A, is phosphorylated and inactivated by the CHK1. PP2A is known to dephosphorylate WEE1 on residues Ser53 and Ser153. Therefore, increased PP2A-phosphatase activity leads to a reduction in WEE1 phosphorylation, thereby blocking its ubiquitin mediated degradation and consequently increasing total cellular WEE1 levels (Li, Kozono et al. 2020). WEE1 is a known mediator of the G_2/M cell cycle checkpoint (Perry and Kornbluth 2007, Aarts, Sharpe et al. 2012). The authors therefore propose that loss of FAM122A constitutes a mechanism of acquired CHK1i resistance (Li, Kozono et al. 2020). CRISPR mediated mutagenesis or interference of gene encoded PP2A subunits could therefore be hypothesized to lead to decreased WEE1 levels, with the established effect of abrogating the G_2/M checkpoint and increasing sensitivity to ATRi (Bukhari, Lewis et al. 2019, Young, O'Connor et al. 2019). This will be explored in subsequent chapters.

Taken together, the data included in this chapter and published elsewhere supports a synthetic lethal interaction between ATR and PP2A. The relatively high prevalence of conserved *PPP2R1A* mutations in OCCC, as discussed in the following chapter, and published data suggesting that these mutations disrupt PP2A stoichiometry and function, led me to hypothesize that they may drive ATRi sensitivity in ARID1A-deficient OCCC. In subsequent chapters I describe the generation of isogenic models to explore the effect of *PPP2R1A* p.R183 mutation on the response to ATRi.

Chapter 4. PPP2R1A p.R183W and p.R183P mutations cause ATRi-induced S phase stress, premature mitotic entry, genomic instability and ATRi synthetic lethality in OCC tumour cells.

4.1 Introduction

In gynaecological cancers, deletions in *PPP2R2A*, which encodes a PP2A regulatory subunit, are recurrent in serous ovarian cancer (Berger, Korkut et al. 2018), whereas dominant negative missense mutations in the scaffolding subunit, encoded by *PPP2R1A,* are more frequent in non-serous gynaecological malignancies such as ovarian clear cell carcinoma (Murali, Soslow et al. 2014). For example, in a study of 42 OCCCs (of which the majority were primary tumours) 7% exhibited a heterozygous *PPP2R1A* mutation; the clustering of *PPP2R1A* mutations around the coding sequence for residue p.R183 of *PPP2R1A* suggested that *PPP2R1A* might act as an oncogene in OCC (Jones, Wang et al. 2010). Heterozygous *PPP2R1A* missense mutations are also observed in endometrial cancer and, similar to ovarian cancer, the prevalence varies according to histological subtype. In endometroid endometrial cancer, the most prevalent subtype, *PPP2R1A* missense mutations are observed in 2-7% of cases. However, in serous endometrial cancer, which accounts for approximately 10% of endometrial cancer cases, *PPP2R1A* missense mutations are observed in 20-60% of cases (McConechy, Anglesio et al. 2011, Zehir, Benayed et al. 2017).

Across cancer types *PPP2R1A* missense mutations are highly conserved and commonly result in amino acid substitutions in the scaffolding subunit at the site where it forms an interaction with the regulatory subunit (Jones, Wang et al. 2010). In preclinical models of serous endometrial cancer it has been demonstrated that the presence of *PPP2R1A* missense mutations leads to reduced incorporation of both the regulatory and catalytic subunits in to the PP2A holoenzyme complex and a subsequent reduction in PP2A-phosphatase activity (Taylor, O'Connor et al. 2019).

The identification of several PP2A subunits as ATRi response genes in the genome wide CRISPRn screen performed in TOV21G cells, along with the previous observations that heterozygous *PPP2R1A* missense occur in OCCC led me to explore how these mutations could impact the response to ATRi. Given the relative under-representation of OCCC cases in large publicly available cancer genomics data sets I sought to establish the incidence of *PPP2R1A* missense mutations and to determine the extent to which they co-occur with *ARID1A* mutations in an independent cohort of OCCC cases. I subsequently employed CRISPR prime gene editing to generate *PPP2R1A* isogenic models in an *ARID1A*-deficient OCCC background and assessed the response to ATRi in these newly generated models. Later, I established the phenotypic features associated with the ATRi response in *PPP2R1A-ARID1A* double mutant OCCC.

4.2 Assessment of PP2A subunit mutation frequency in ovarian clear cell carcinoma

As previously discussed, deletions affecting *PPP2R2A* are a frequent observation in serous ovarian cancer, seen in up to 17 % of cases (Figure 4.1A) (ICGC/TCGA 2020). *PPP2R1A* missense mutations have been reported to 7-20% of OCCC cases (Jones, Wang et al. 2010, Shih Ie, Panuganti et al. 2011, Kim, Lee et al. 2018). In order to independently assess the frequency of *PPP2R1A* mutations in OCC, genotyped genomic DNA from 23 primary OCCC tumours (patient details summarised in Table 4.1) which had received no prior therapy and were previously uncharacterised with respect to their *PPP2R1A* mutational status. Samples included in this analysis were collected as part of the Royal Marsden Hospital (RMH) NHS Foundation Trust study: CCR3705 “Analysis of tumour specimens for biomarkers in gynaecological cancers” and were used in the validation of the ARID1A immunohistochemistry assay utilised for patient stratification in ATARI (Khalique, Naidoo et al. 2018). As such, the *ARID1A* mutational status of these cases was already established.

In this case series 52% (12/23) had an established *ARID1A* mutation. I found that the same proportion, 52% (12/23), of cases exhibited a heterozygous missense mutation encoding residue p.R183 (Figure 4.1B). Of the *ARID1A* mutant cases in this OCC cohort, 33% (4/12) also had a PPP2R1A mutation (Figure 4.1B). In keeping with previous literature, the observed PPP2R1A missense mutations were anticipated to result in an arginine to proline, tryptophan, or glycine amino

acid substitution at position 183. This residue resides within one of the Huntington, elongation factor, PP2A, TOR kinase (HEAT) domains where the scaffolding subunit interacts with the regulatory subunit (Jones, Wang et al. 2010). This led me to explore the possibility that *PPP2R1A* mutations in OCC could cause ATRi synthetic lethality. Furthermore, as *ARID1A* and *PPP2R1A* mutations often co-occur and as *ARID1A* mutations in OCC have previously been linked to ATRi synthetic lethality (Williamson, Miller et al. 2016, Kurz, Miklyaeva et al. 2020, Yap, O'Carrigan et al. 2020) I also tested the hypothesis that PPP2R1A mutations could enhance the ARID1A/ATRi synthetic lethality.

4.3 Generation of TOV21G PPP2R1A isogenic models using CRIPSPR prime gene editing

Most prior functional studies have used gene silencing to model the effect of PPP2R1A dysfunction (McConechy 2013) or used the ectopic expression of mutant *PPP2R1A* cDNA to model cancer associated *PPP2R1A* mutations (Haesen, Abbasi Asbagh et al. 2016, Toda-Ishii, Akaike et al. 2016, Taylor, O'Connor et al. 2019, O'Connor, Leonard et al. 2020, Lenaerts, Reynhout et al. 2021). With the advent of CRISPR-Cas9 mutagenesis methods, such as CRISPR-prime editing (Anzalone, Randolph et al. 2019), the ability to introduce precise mutations into genes is now more achievable.

Sample ID	Diagnosis	FIGO Stage	Grade	Endometriosis	Tumour recurrence	PPP2R1A mutation	PPP2R1A mutation Details	ARID1A Mutation	ARID1A mutation details
3705-0416	OCCC	2	3	Yes	No	No	-	Yes	p.G191fs, p.T485*
3705-0464	OCCC	2	3	No	No	Yes	p.R183P	Yes	p.I2275S, p.G2070*
3705-0544	OCCC	1	3	No	Yes	Yes	p.R183P	No	-
3705-0558	OCCC	1	3	Yes	Yes	Yes	p.R183G	No	-
3705-0453	OCCC	2	3	Yes	Yes	No	-	No	-
3705-0435	OCCC	3	3	No	Yes	No	-	No	-
3705-0545	OCCC	3	3	Yes	Yes	Yes	p.R183P	Yes	p.G319fs, p.L1100fs
3705-0379	OCCC	1	3	Yes	No	Yes	p.R183P	No	-
3705-0383	OCCC	1	3	No	No	No	-	No	-
3705-0423	OCCC	3	3	Yes	No	Yes	p.R183W	No	-
3705-0461	OCCC	3	3	Yes	Yes	Yes	p.R183P	No	-
3705-0625	OCCC	3	3	Yes	Yes	No	-	Yes	p.A162fs; p.R1941*
3705-0646	OCCC	2	3	Yes	No	No	-	Yes	p.D1593fs
3705-0669	OCCC	2	3	No	No	Yes	p.R183P	Yes	p.G566*
3705-0673	OCCC	1	3	Yes	Yes	Yes	p.R183P	No	-
3705-0082	OCCC	3	3	Unknown	Yes	Yes	p.R183P	No	-
3705-0181	OCCC	2	3	No	No	No	-	No	-
3705-0559	OCCC	4	3	Unknown	Yes	Yes	p.R183P	No	-
3705-0635	OCCC	1	3	Yes	Yes	No	-	Yes	p.S1768*
3705-0719	OCCC	3	3	No	Yes	No	-	Yes	p.G13421*
3705-0720	OCCC	3	3	Yes	No	No	-	Yes	p.Y560*
3705-0713	OCCC	2	3	Unknown	Yes	Yes	p.R183P	Yes	p.S607*
3705-0459	OCCC	1	3	No	No	No	-	Yes	p.S280*

Table 4.1 Table 4.1. Patient characteristics for cohort summarized in Figure 4.1

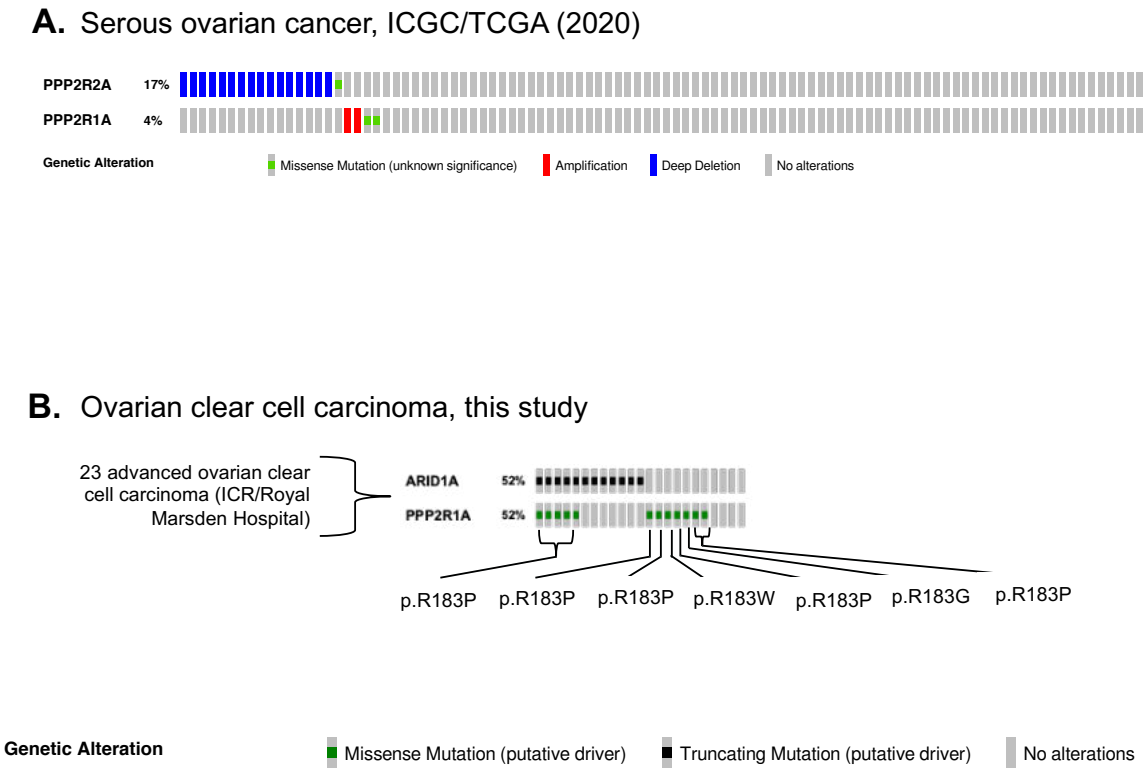

Figure 4.1 PPP2R1A missense mutations are prevalent in OCCC and co-occur with ARID1A mutations. Oncoprints illustrating prevalence of PPP2R2A deletions in serous ovarian cancer (A) or PPP2R1A mutations in ovarian clear cell carcinoma (OCCC – shown in B). Oncoprint in (A) generated from data in (ICGC/TCGA, 2020). Oncoprint in (B) generated by genotyping of 30 cases of advanced OCCC from the Royal Marsden Hospital.

In summary, CRISPR-prime editing is a technique which enables the introduction of a specific DNA sequence change without the need to provide donor DNA or the production of double strand DNA breaks. Cells are transfected with a modified Cas9 which produces a single strand DNA break (nick) fused to a reverse transcriptase (PE2), along with prime editing guide RNA (pegRNA), which guides PE2 to the sequence of interest and encodes the new genetic information that replaces the target sequence. Nicking of the target DNA sequence exposes the 3'-hydroxyl group, thereby initiating the process of the reverse transcription from the pegRNA. The product of this process is a branched intermediate containing two DNA flaps, one with the edited (newly synthesised) sequence and the other with the unedited (endogenous) sequence. The unedited flap is cleaved by specific endonucleases or 5'-exonucleases, enabling the process of 3'-strand ligation resulting in the formation of a heteroduplex double stranded DNA structure in which one DNA strand contains the edited sequence and the other the unedited sequence i.e. contains a nucleotide mismatch. Removal of the mismatch relies on the cell's intrinsic mismatch repair machinery (MMR), which can result in two outcomes. The genetic sequence in the edited strand can be copied onto the unedited strand thereby, indelibly installing the edited sequence. Alternatively, the reverse can occur, with the endogenous sequence being copied on to the edited strand, thereby permanently excluding the sequence change (Anzalone, Randolph et al. 2019). The addition of a nicking prime editing guide to the PE2 system creates a single strand DNA nick in the unedited strand, biasing the cell to using the edited strand as a template for repair

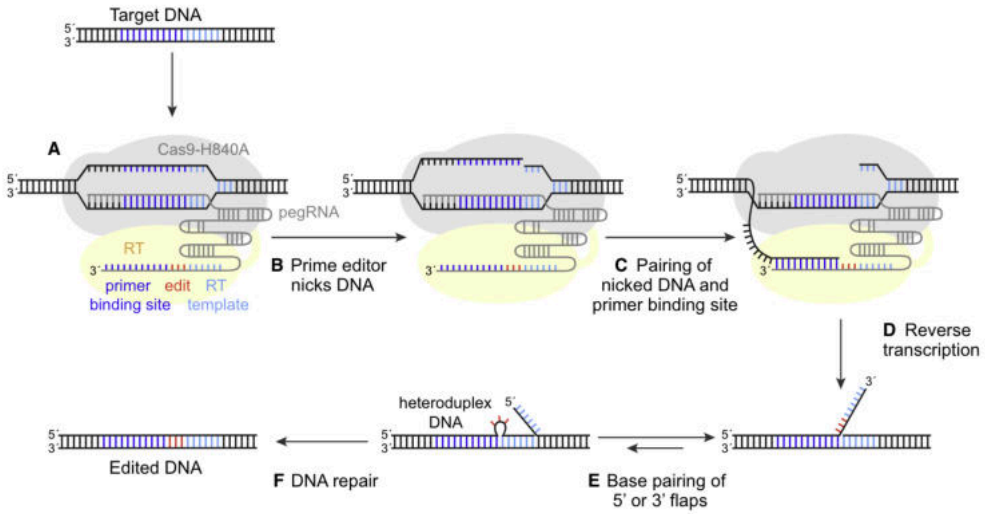

Figure 4.2 Schematic showing how CRISPR prime gene editing is considered to work.

(A) The prime editor (PE) composed of a Cas9-H840A fused to a reverse transcriptase (RT) and pegRNA bind to target DNA.

(B) The nuclease domain of the editor nicks one DNA strand.

(C) The nicked strand binds to the primer binding site on the extended 30 end of the pegRNA.

(D) The RT elongates the nicked DNA strand (incorporating the edit).

(E) The elongated strand competes for binding to the target DNA.

(F) A desired edit is installed after DNA repair of the heteroduplex DNA.

(*Adapted from Jan, Cirincione and Adamson. Mol Cell (2021)).*

and increasing the efficiency of gene editing (Anzalone, Randolph et al. 2019). A diagram describing how CRISPR-prime editing works is shown in Figure 4.2.

The pegRNA was designed as described by Anzalone *et al (Anzalone, Randolph et al. 2019).* Briefly, a guide sequence was designed to bring PE2 to a specific region of *PPP2R1A* 5' of the codon encoding amino acid residue R183 which was the target for editing. This guide sequence specifies the cut site, i.e. the region of *PPP2R1A* in which PE2 will produce a single strand nick, which is 4 base pairs 5' of the protospacer adjacent motif (PAM). This was added to the 5' end of the vector and placed under the transcriptional control of a U6 promoter. In order to construct the template for reverse transcription to introduce the desired mutation, I took the region of *PPP2R1A* encoding amino acid residue R183 and altered the sequence so that this codon now encoded a proline (p.R183P, CGG>CCC) or tryptophan residue (p.R183W, CGG>TGG). From this altered sequence I then took a region 12 base pairs 5' of the cut site and 10 base pairs extending from the desired edit on same strand that the PAM lies on. This entire region was then reverse complemented to give the non-PAM strand sequence and linked to the guide sequence via the scaffolding region, which is common to all pegRNAs. In this case, the native codon to be edited (CGG) also acted as the PAM site, therefore introduction of the altered sequence prevents further editing. This is followed by a DNA polymerase III terminator sequence (Pol III terminator) designed to stop reverse transcription once complete. The structure and sequence of the pegRNAs used to introduce PPP2R1A p.R813P and p.R183W missense mutations are summarised in Figure 4.3.

Figure 4.3 pegRNA structure and design. (A) PegRNA General structure. Expression of pegRNA is driven from an U6 promoter (Grey). Guide sequence (blue) directs PE2 enzyme to the gene of interest. Scaffolding region (magenta) connects guide sequence of edited region on the non-PAM DNA strand (red). DNA polymerase III terminator (yellow) ensures cessation of reverse transcription complete. (B) PegRNA sequence used to introduce *PPP2R1A* p.R183P mutation. Colour coded as described in (A). ^ shows cut site on sgRNA and corresponding position in reverse-complemented template sequence. Edited codon highlighted in green. (C) PegRNA sequence used to introduce *PPP2R1A* p.R183W mutation. Colour coded as described in (A). Edited codon highlighted in green. ^ shows cut site on sgRNA and corresponding position in reverse-complemented template sequence.

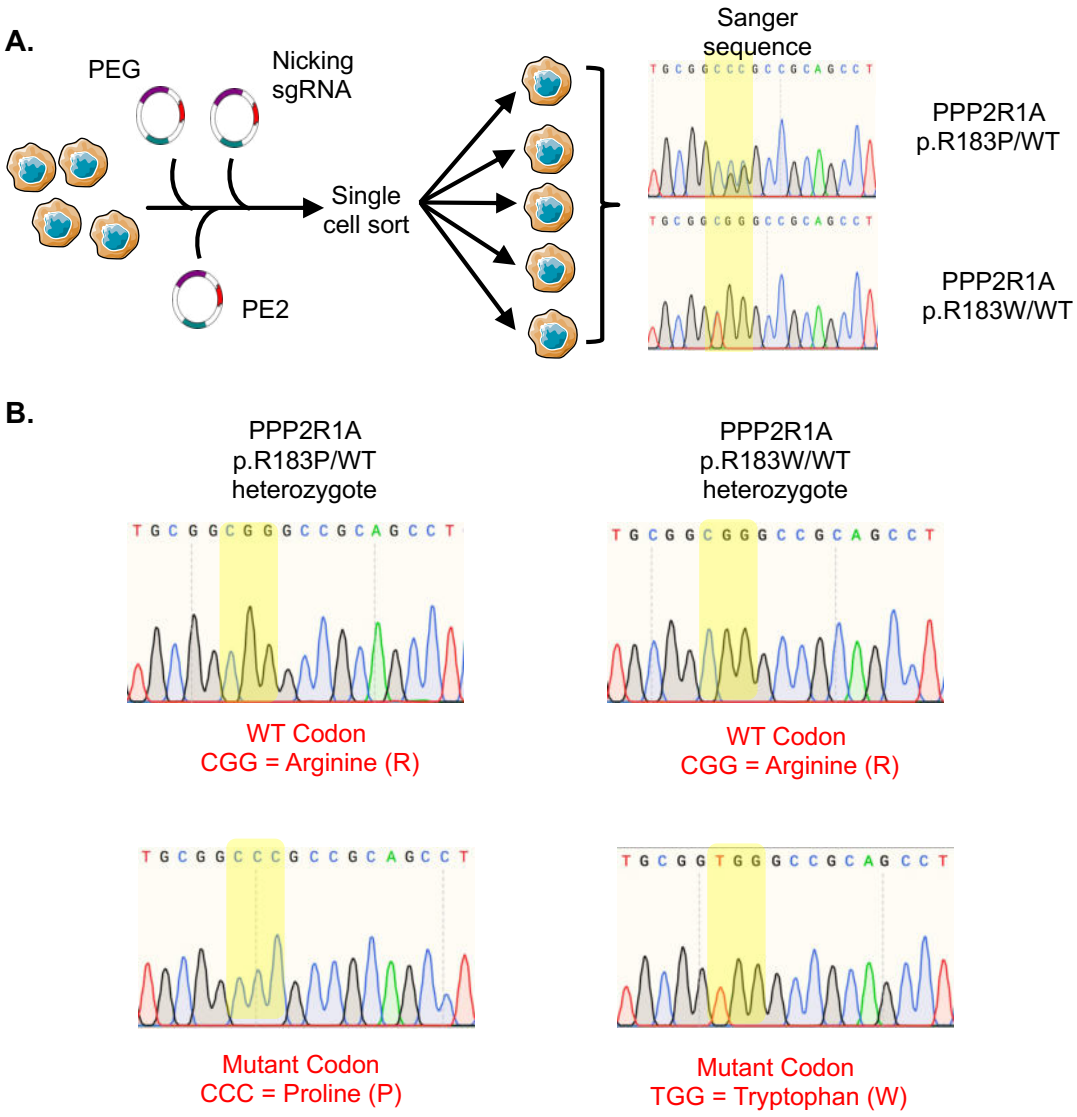

Figure 4.4 Heterozygous PPP2R1A missense mutations introduced to TOV21G cell line using CRISPR-prime gene editing. (A) Cells were transfected with plasmids encoding prime editing guide (PEG), PE2 and nicking sgRNA before being single cell sorted. The resultant clones were genotyped to confirm successful introduction of heterozygous PPP2R1A p.R183P or p.R183W missense mutations. (B) DNA sequence traces from PPP2R1A mutant clones generated in (A). Each mutation is heterozygous, present in 5/10 or 4/9 TOPO-cloned sequences for the PPP2R1A p.R183P or p.R183W models respectively.

I therefore used CRISPR-prime editing to introduce residue p.R183 missense mutations into *PPP2R1A* wild type, *ARID1A* mutant TOV21G OCC cells, generating daughter clones with either heterozygous PPP2R1A p.R183P or p.R183W mutations (Figure 4.4A). Topo-cloning was employed to confirm the heterozygous nature of *PPP2R1A* p.R183P and p.R183W mutations introduced (Figure 4.4B).

4.4 Introduction of heterozygous PPP2R1A missense mutations impacts PP2A structure and function.

Previous studies in pre-clinical models of serous endometrial cancer have demonstrated that the presence of dominant negative *PPP2R1A* missense mutations, affecting residues 183 and others, disrupts PP2A complex stoichiometry (Taylor, O'Connor et al. 2019). Commensurate with this data, I found that the total levels of other PP2A subunits was significantly decreased (Dunnett's test, $p < 0.001$) in both the TOV21G *PPP2R1A* p.R183P and p.R183W models when compared to the PPP2R1A WT cells (Figure 4.5).

Given these findings and the previous observation that *PPP2R1A* mutations lead to reduced incorporation of both regulatory and catalytic subunits in the PP2A complex (Taylor, O'Connor et al. 2019), I hypothesised that the introduction of PPP2R1A p.R183 mutations in TOV21G cells would lead to a reduction in PP2A-phosphatase activity. To assess this, I carried out mass spectrometry based phospho-proteomic profiling in *PPP2R1A* p.R183P and wild type isogenic cells and found PP2A-specific phospho-sites on substrates including HDAC5 (Greco,

Yu, Guise, & Cristea, 2011), IL6ST (Mitsuhashi et al., 2005) and SPRY1 (Lao et al., 2007) were significantly enriched (log2 fold change > 0, unpaired t-test, $p < 0.05$) in p.R183P mutant cells (Figure 4.6) consistent with a PP2A defect in these cells.

4.5 PPP2R1A mutation in TOV21G cells causes ATR inhibitor sensitivity and cell cycle defects

When I assessed ATRi sensitivity in PPP2R1A mutant cells, I found that TOV21G clones with a heterozygous p.R183P or p.R183W mutation were more sensitive to the ATRi AZD6738 than PPP2R1A wild type TOV21G cells (two-way ANOVA, $p < 0.001$) (Figure 4.7). PP2A has been described as a master cell cycle regulator with over 300 of its substrates being implicated in the regulation of cell cycle progression (Krasinska, Domingo-Sananes et al. 2011, Wlodarchak and Xing 2016, Kamenz, Gelens et al. 2021). Additionally, ATRi sensitivity in tumour cells is often associated with a decrease in the replicating S phase fraction of cells and premature mitotic entry (Saldivar, Hamperl et al. 2018). Using Edu labelling to label cells in replicating S phase and phosphorylation of histone H3 (pH3) as a marker of cells in mitosis, these two phenotypes were assessed in the newly generated TOV21G *PPP2R1A* isogenic models.

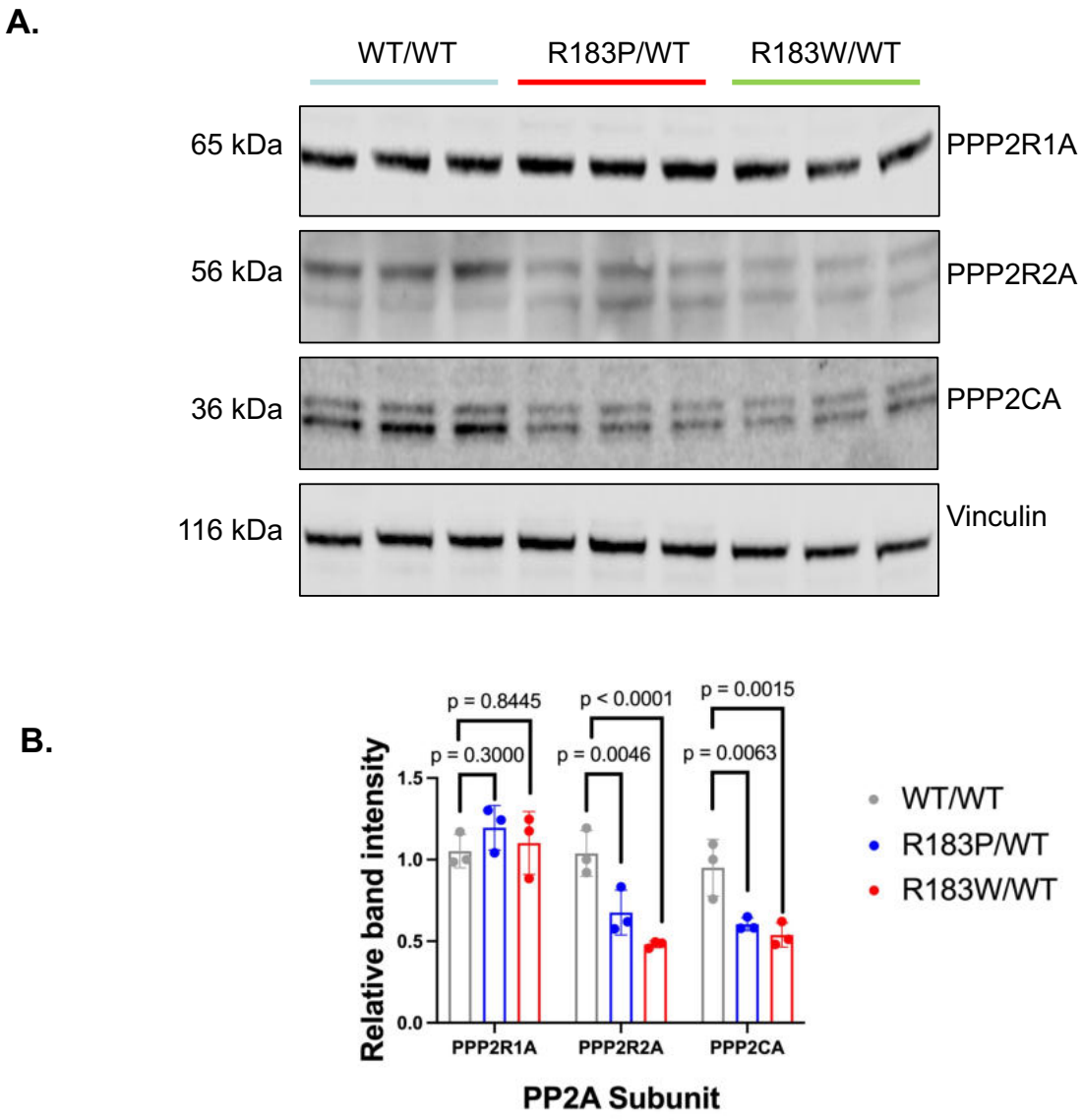

Figure 4.5 . Introduction of heterozygous PPP2R1A missense mutations leads to a reduction in total levels of PPP2R2A and PPP2CA in TOV21G cells. (A) Western blot illustrating that PPP2R1A p.R183P mutation causes reduced levels of PPP2R2A and PPP2CA (B) Quantification of band Western Blot band intensity from (A). Band intensity expressed relative to median intensity of the WT/WT samples for the indicated protein. Error bars represent mean and standard deviation from the 3 Western blot bands quantified. Statistical significance determined via Dunnett's test.

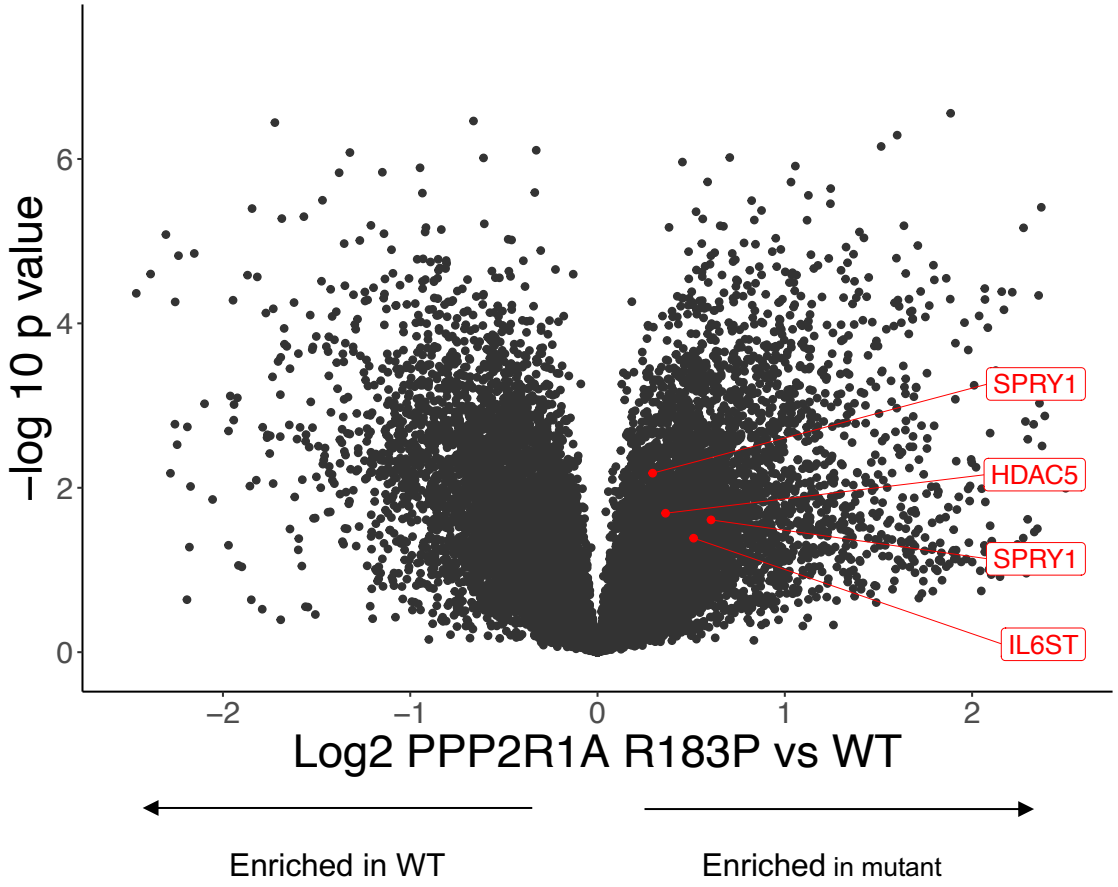

Figure 4.6 Known PP2A substrates are enriched in PPP2R1A mutant cells. Volcano plot illustrating results from phosphoproteomic profiling of PPP2R1A mutant cells, indicating a significant enrichment (Log2 fold change > 0, unpaired t-test <0.05) of known PP2A phosphorylation sites (highlighted)

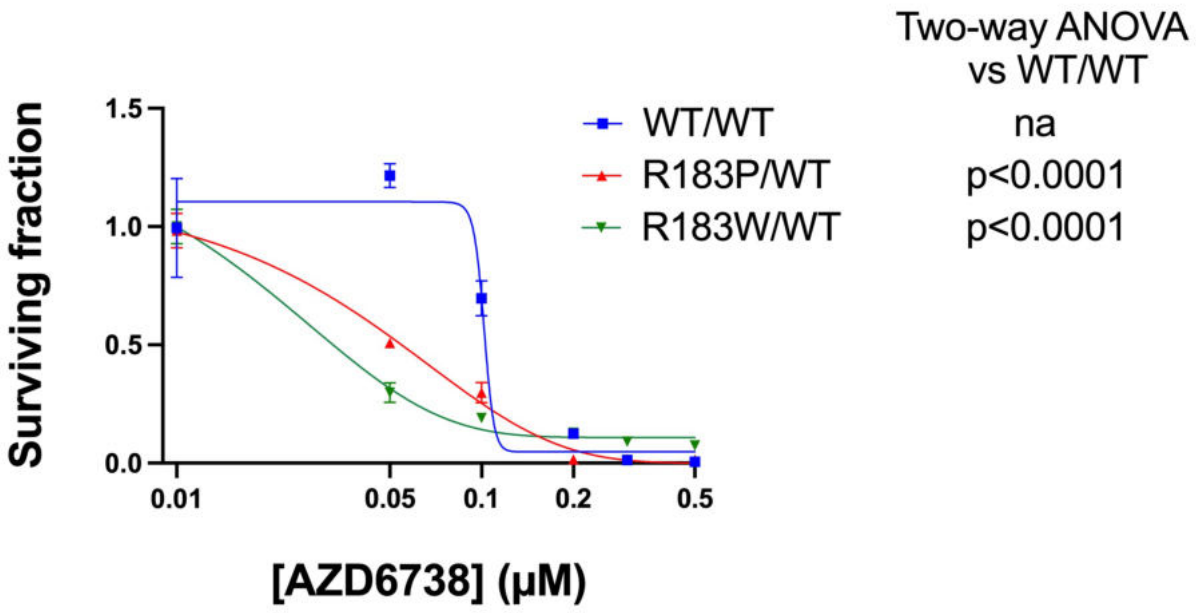

Figure 4.7 Introduction of PPP2R1A p.R183 mutation results in enhanced ATRi sensitivity in vitro. Dose response curve for cells from (D, E) exposed to AZD6738 for two weeks. Error bars represent SEM from 4 replicates. Significance determined using two-way ANOVA.

Using this approach, no significant different in the total S phase, replicating or non-replicating S-phase population was observed between TOV21G PPP2R1A WT and p.R183P mutant cells at baseline (Figure 4.8 A-D). Upon exposure to ATRi the most striking observation was a significant increase in the total S phase population in cells with a PPP2R1A p.R183P missense mutation compared to WT. On closer examination, the increase in the S phase population encompassed a significant expansion of the non-replicating S phase population at the expense of the replicating S phase population (Figure 4.8 A, C, D).

In addition, *PPP2R1A* p.R183P mutation caused a modest increase in pH3-positive cells, an effect that was exacerbated by ATRi exposure (Figure 4.9 A, B), and an increase in the proportion of pH3-positive cells with a genetic content of <4N (Figure 4.9 A, C), consistent with premature mitotic entry.

Chromosomal lesions, such as those that are generated prior to mitosis but transmitted to daughter cells, are often sequestered in nuclear compartments marked by p53-binding protein 1 (53BP1) (Lukas et al., 2011), referred to as 53BP1 bodies. I found that the combination of PPP2R1A p.R183 mutation and ATRi exposure caused a significant increase the proportion of cells with more than one 53BP1 body but did not in similarly treated *PPP2R1A* wild type cells (Figure 4.10A, B). In keeping with previous literature, 53BP1 bodies were observed in cells which stained negative for Cyclin A (Figure 4.10A) consistent

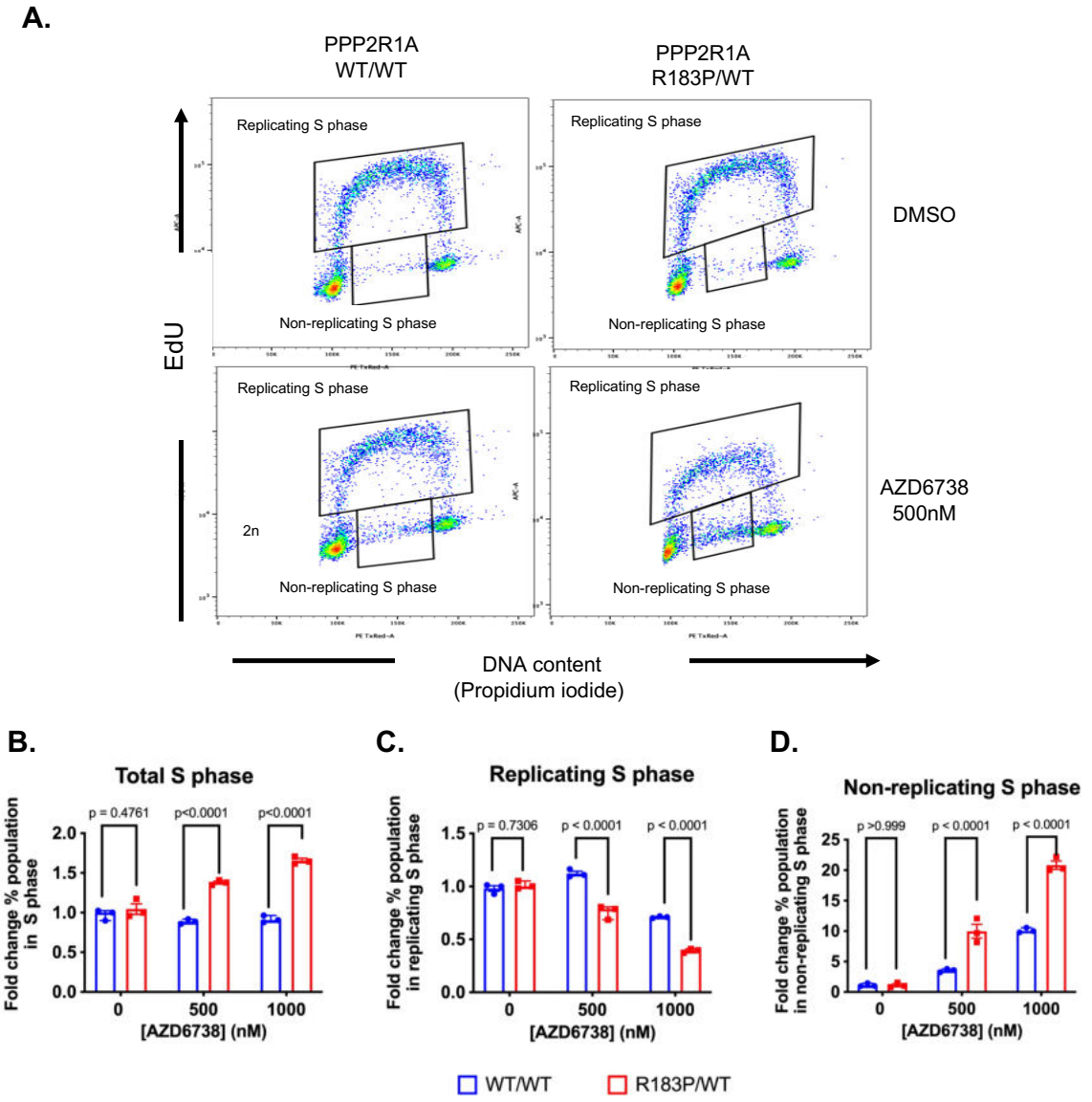

Figure 4.8 PPP2R1A R183P mutation and ATRi exposure causes an increase in the in non-replicating S phase fraction at the expense of the replicating S phase fraction. (A) FACS plots illustrating that PPP2R1A R183P mutation and ATRi exposure causes an increase in the in non-replicating S phase fraction at the expense of the replicating S phase fraction. (B-D) Quantification of changes in fraction of cells in total S phase (B) replicating S phase (C) or non-replicating S phase (D) from the experiment described in (A). Error bars represent mean and SD from three replicate experiments. Pairwise significance determined by two-way ANOVA with Šídák correction for multiple comparisons.

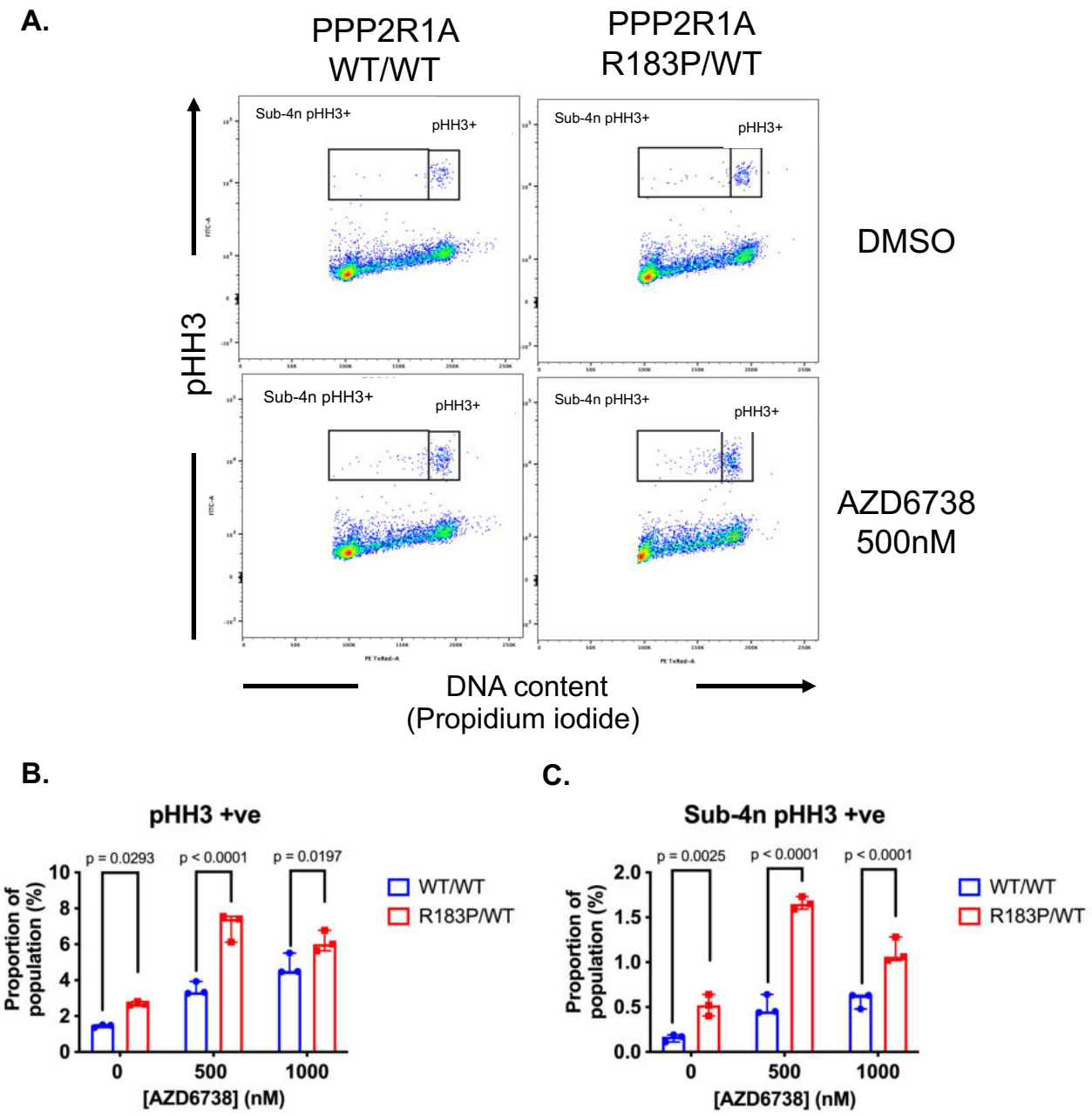

Figure 4.9 PPP2R1A cells entire mitosis with sub-4n genomic content in response to ATRi. (A) FACS plots illustrating that PPP2R1A R183P mutation and ATRi exposure causes an increase in the in non-replicating S phase fraction at the expense of the replicating S phase fraction. (B-D) Quantification of changes in fraction of cells in total S phase (B) replicating S phase (C) or non-replicating S phase (D) from the experiment described in (A). Error bars represent mean and SD from three replicate experiments. Pairwise significance determined by two-way ANOVA with Šídák correction for multiple comparisons.

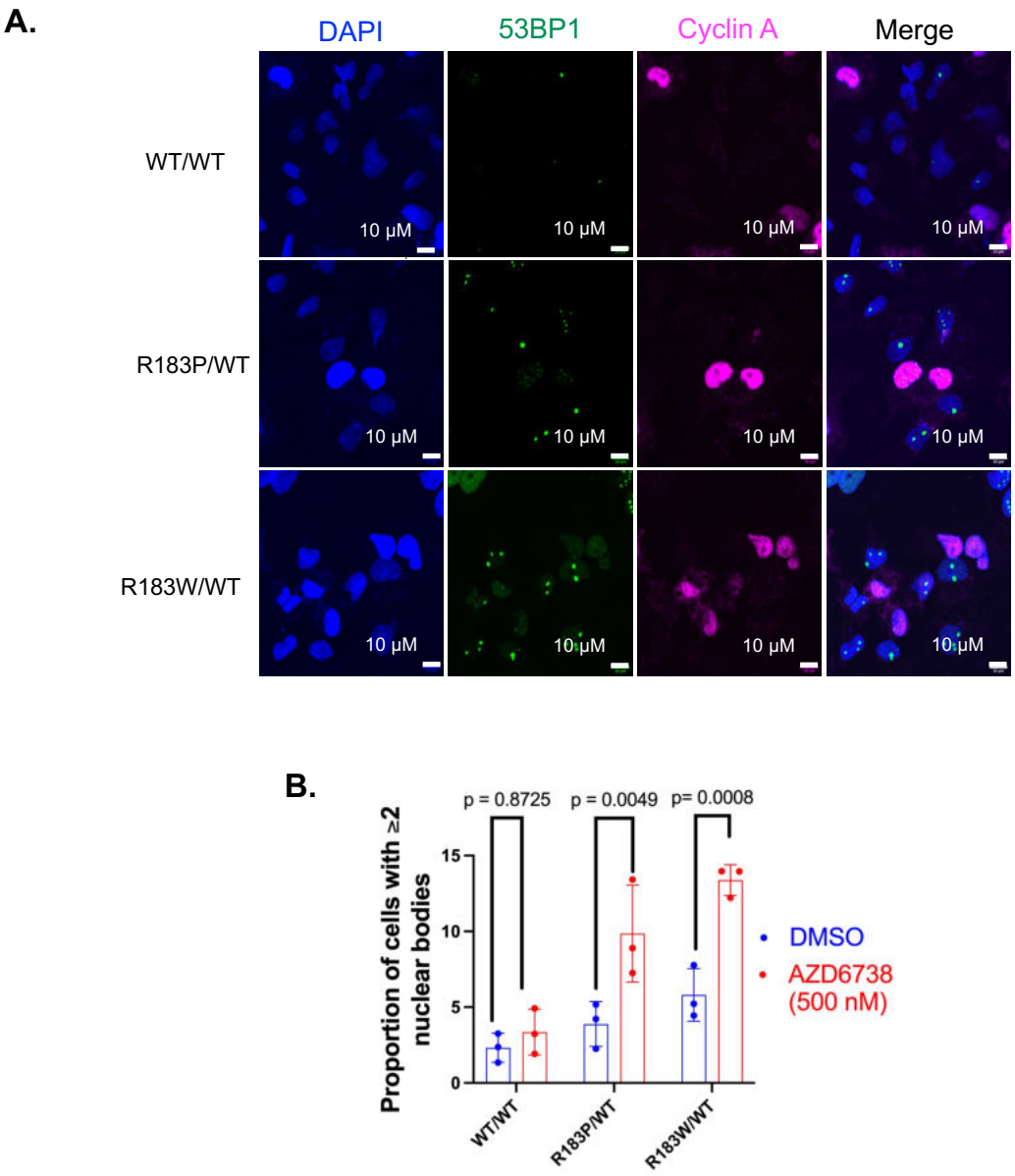

Figure 4.10 53BP1 bodies accumulate in PPP2R1A mutant cells in response to ATRi. (A) TOV21G PPP2R1A p.R183P isogenic cells were exposed to either DMSO or AZD6738 (500 nM) for 24 hours before being fixed and immunostained for 53BP1, cyclin A and with DAPI. Confocal microscopy images are shown. (B) Quantification of 53BP1 bodies from experiment described in (A). Error bars represent the mean and standard deviation from three replicate experiemts. Pairwise significance determined via Two-way ANOVA with Šídák's multiple comparison test.

with their accumulation in the G1 phase of the cell cycle (Lukas, Savic et al. 2011, Moreno, Carrington et al. 2016).

Given the observed S phase defects and premature mitotic entry in *PPP2R1A* mutant cells, I proceeded to perform time-lapse microscopy in order to examine mitotic kinetics. TOV21G *PPP2R1A* isogenic cells were labelled with fluorescent probes for DNA, tubulin and actin before being imaged via confocal microscopy at 5 minute intervals for 24 hours in the presence or absence of ATRi. Exposure to ATRi significantly increased the metaphase duration in *PPP2R1A* mutant cells (Figure 4.11 and 4.12). Indeed, in a proportion of *PPP2R1A* mutant cells, ATRi exposure led to cells failing to progress beyond metaphase and ultimately undergoing apoptosis (Figure 4.13). Commensurate with ATRi having a more deleterious effect in PPP2R1A p.R183P and p.R183W mutant cells than in wild type cells, I also found that ATRi exposure in PPP2R1A mutant cells caused a 12- (p.R183P) or 10-fold (p.R183W) increase in micronuclei, a common form of genomic instability caused by ATRi (Dillon, Barker et al. 2017) (Figure 4.14).

4.6 Discussion

In this chapter, I characterised a cohort of *ARID1A* WT and mutant OCCC cases with respect to their *PPP2R1A* p.R183 mutational status, observing a higher incidence of p.R183 missense mutations than previously reported. Using CRISPR prime gene editing, I successfully introduced heterozygous *PPP2R1A* p.R183P and p.R183W missense mutations in to the ARID1A-deficient cell line

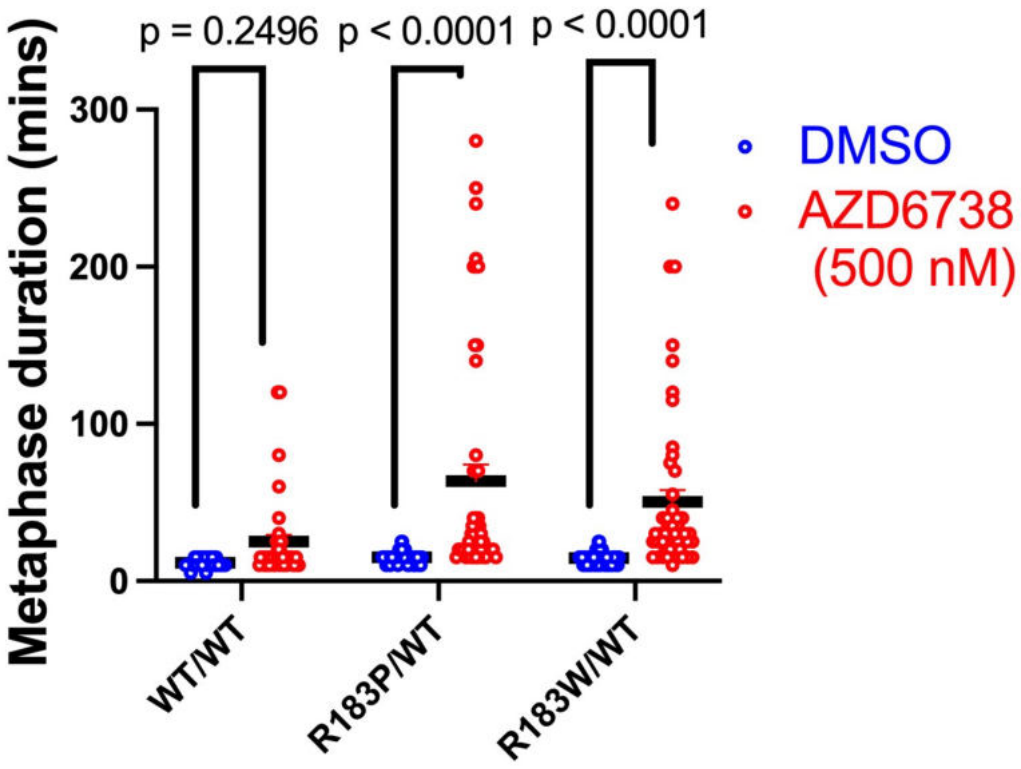

Figure 4.11 Exposure to ATRi increases the duration of metaphase in PPP2R1A p.R183 mutant cells. Quantification of metaphase duration from timelapse microscopy. TOV21G *PPP2R1A* WT, p.R183P and p.R183W labeled with fluorescent probes for DNA, tubulin and actin before being imaged via confocal microscopy every 5 minutes for 24 hours in the presence of AZD6738 500 nM or DMSO. Duration of metaphase measured for 50 cells per condition. Significance determined via Dunnett's test.

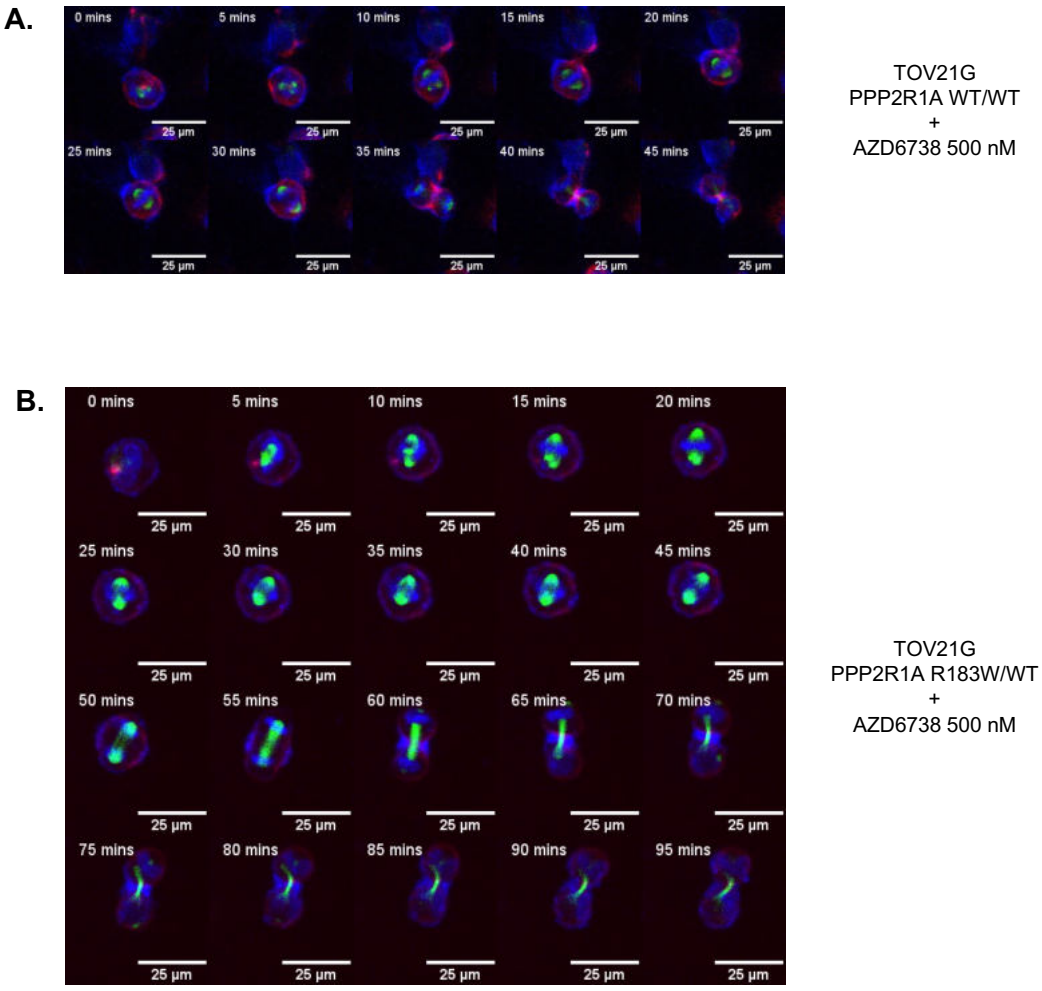

Figure 4.12 Exposure to ATRi increases the duration of metaphase in PPP2R1A p.R183 mutant cells. Representative images from time lapse confocal microscopy showing TOV21G PPP2R1A WT (A) or TOV21G *PPP2R1A* p.R183W (B) cells labeled for tublin, actin and DNA in the presence on AZD 6738 500 nM. Each frame represents a 5 minute time period. Time point 0 mins represents the start of metaphase

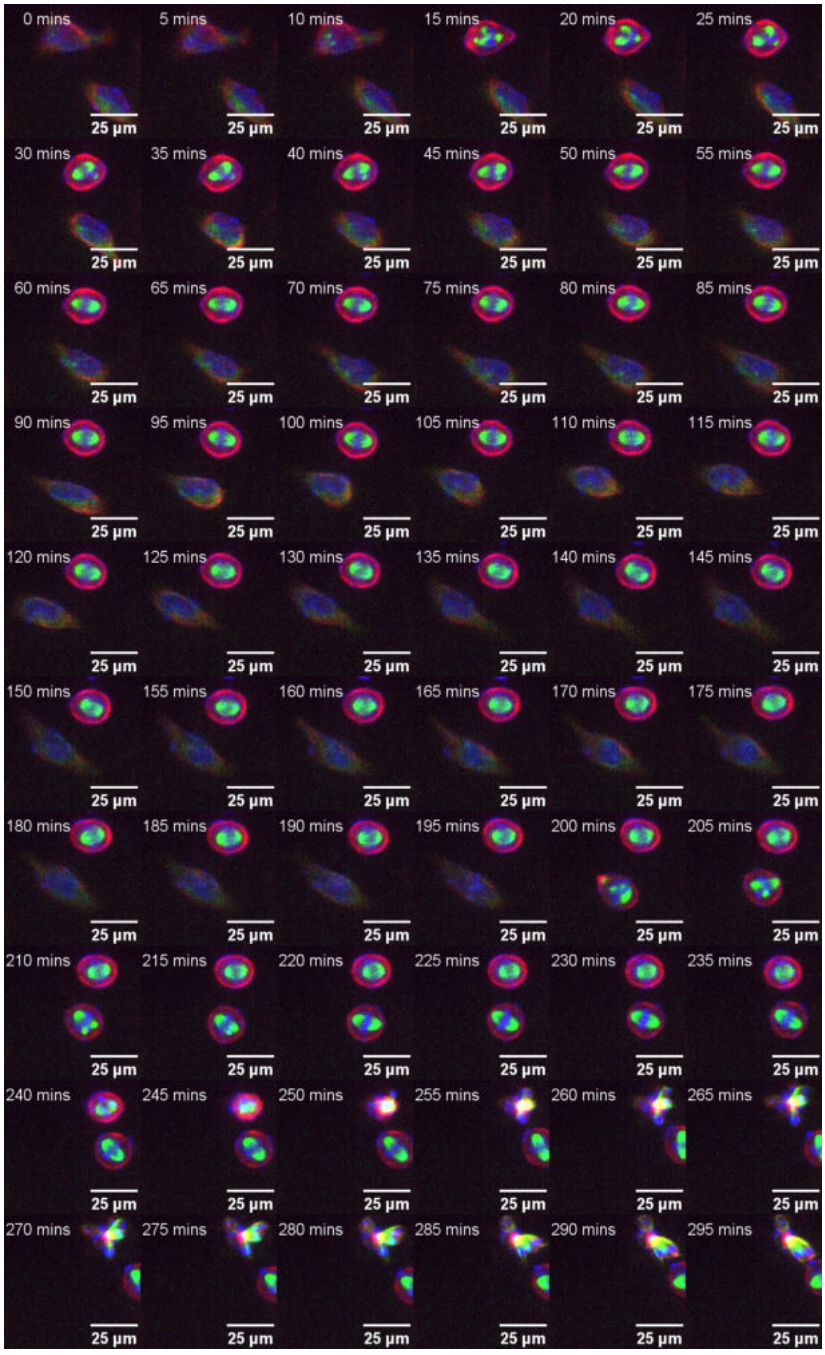

TOV21G
PPP2R1A R183W/WT
+
AZD6738 500 nM

Figure 4.13 A proportion of PPP2R1A mutant cells fail to progress through to anaphase in response to ATRi. Representative images from time lapse confocal microscopy showing TOV21G PPP2R1A p.R183W cells labeled for tublin, actin and DNA in the presence on AZD 6738 500 nM. Each frame represents a 5 minute time period. Cell remains in metaphase for 250 minutes before undergoing apoptosis. . Time point 0 mins represents the start of metaphase

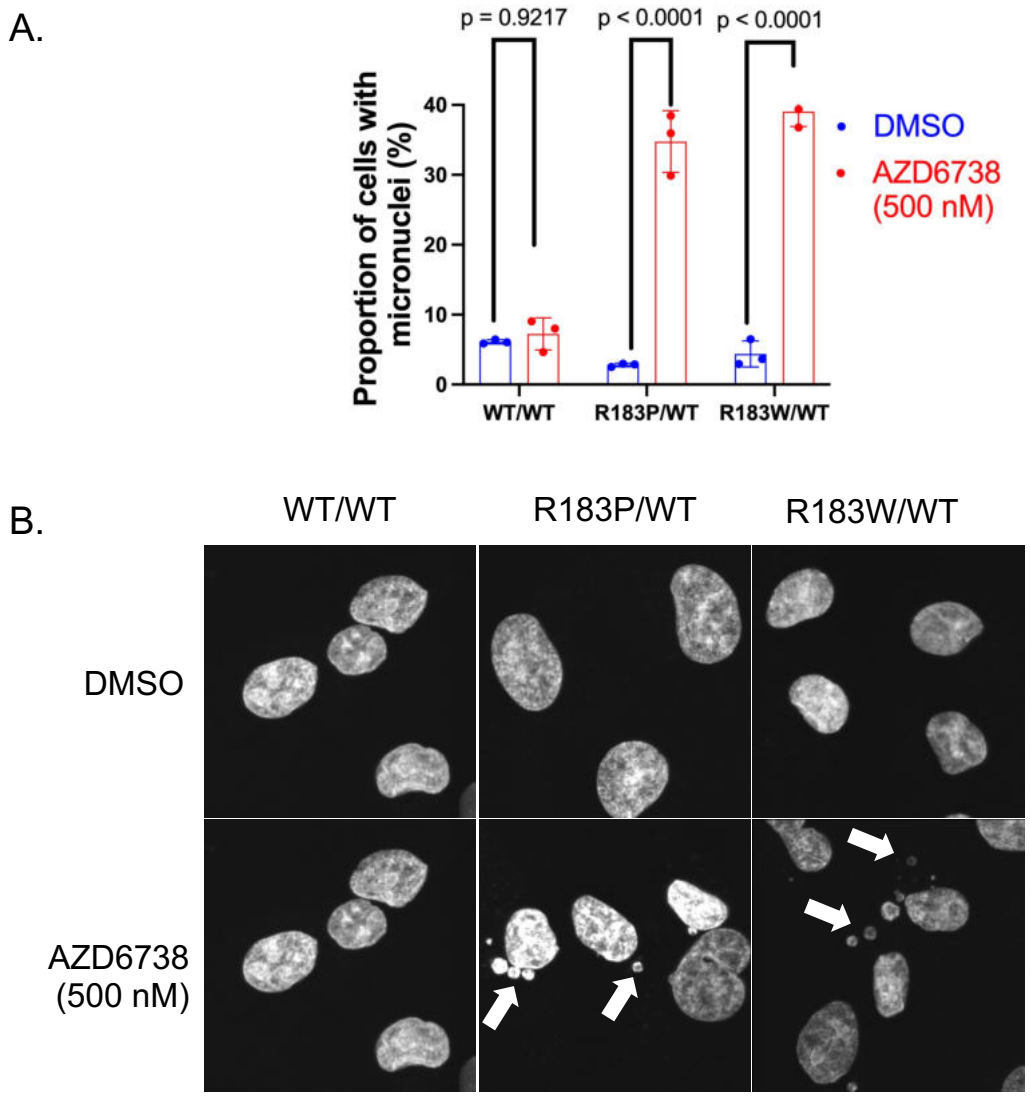

Figure 4.14 Exposure to ATRi leads to a significant increase in the proportion of cells with micronuclei in cells with a PPP2R1A mutation. (A) TOV21G PPP2R1A isogenic cells were exposed to either DMSO or AZD6738 (500 nM) for 24 hours before being fixed and stained with DAPI. Error bars represent SEM from three triplicate experiments. (B) Representative images for TOV21G PPP2R1A WT, p.R183P and p.R183W cells following exposure to AZD6738 (500 nM) or DMSO from experiment described in (A). Micronuclei indicated with arrows.

TOV21G. PPP2R1A p.R183 mutation in this cell line led to reduced total levels of PPP2R2A and PPP2CA and led to an enrichment of phospho-sites previously reported to PP2A phosphatase targets, in keeping with *PPP2R1A* missense reducing PP2A phosphatase activity. Furthermore, I demonstrated that the introduction of *PPP2R1A* p.R183 mutations led to increased sensitivity to ATRi *in vitro*. Taken together, observations presented in this chapter suggest that in *PPP2R1A* mutant OCCC cells, ATRi elicits S phase stress, premature mitotic entry, and genomic instability.

In a new cohort of OCCC cases, I observed a *PPP2R1A* p.R183 mutation frequency of 52 %. In contrast, three relatively small case series consisting of 15, 40 and 42 OCCC patients, *PPP2R1A* missense mutations were observed at frequencies of 20% (Kim, Lee et al. 2018), 9% (Shih Ie, Panuganti et al. 2011) and 7% (Jones, Wang et al. 2010) respectively. Whilst comparisons between small case series can be challenging, in part due to variations in the reporting of patient characteristics, the reasons for the observed differences are not entirely clear. These differences may simply reflect the expected variability when low numbers of patients are included in such studies. In similarity to the patients included in the analysis described in this chapter, mostly primary OCCC cases with no prior therapy were included in the series presented by *Kim et al (Kim, Lee et al. 2018)* and *Jones et al (Jones, Wang et al. 2010).* It should also be noted that the series presented between by *Kim at al (Kim, Lee et al. 2018)* and *Shih et al (Shih Ie, Panuganti et al. 2011)* contained a high proportion of Asian patients, whereas all of the patients included in the series included in this chapter were of

Caucasian ethnicity. Therefore, variability in the *PPP2R1A* mutation frequency due to the genetic background of the patient cohort cannot be excluded. Similarly, 52 % (12/23) of patients included in the case series described in this chapter had a confirmed diagnosis of endometriosis. Only *Kim et al* report the incidence of endometriosis (33 % [5/15]) amongst the patient cohort included in their analysis (Kim, Lee et al. 2018). Therefore, differences in the rates of OCCC arising from endometriosis also cannot be excluded as an explanation for the differences in observed *PPP2R1A* mutation frequency.

PPP2R1A mutations have previously been implicated in the disruption of the PP2A complex and in promoting the development of serious endometrial cancer (Taylor, O'Connor et al. 2019). Furthermore, a synthetic lethal interaction between *PPP2R1A* and ribonucleotide reductase inhibitors (RNRi) has been reported in preclinical models of serous endometrial cancer (O'Connor, Taylor et al. 2022). In both instances, modelling of these mutations has involved the expression of either mutant (Taylor, O'Connor et al. 2019) or wild-type PPP2R1A (O'Connor, Taylor et al. 2022) from a lentiviral vector. This approach places *PPP2R1A* expression under the control of the cytomegalovirus (CMV) promoter and therefore endogenous levels of expression cannot be guaranteed (Yang, Boehm et al. 2011). To the best of my knowledge, the use of CRISPR prime gene editing is the first instance in which a truly isogenic *PPP2R1A* model system has been generated, with expression of the WT or mutant gene being driven by the endogenous promoter. Although off-targeting gene editing is reported to be much lower with PE2 than with Cas9 nuclease (Anzalone, Randolph et al. 2019), it

should be noted that no formal assessment for this event was undertaken or was practicable, as it could occur throughout the entire genome. A functional rescue experiment, in which the mutant allele (i.e. the allele containing the CRISPR prime gene edited sequence) is inactivated, would increase confidence that the observed phenotype, in the case ATRi sensitivity, is caused by *PPP2R1A* p.R183 mutation.

In keeping with previous literature, the introduction of heterozygous *PPP2R1A* p.R183 mutations resulted in reduced total levels of the regulatory, PPP2R2A, and catalytic, PPP2CA, subunits (Taylor, O'Connor et al. 2019). One caveat to the observations presented in this chapter is that I was unable to demonstrate reduced incorporation of both PPP2R2A and PPP2CA in to the PP2A holoenzyme complex, in part due to an inability to immunoprecipitate endogenous WT or mutant PPP2R1A for Western blot analysis. This, in part, may reflect lower total levels of PPP2R1A when expression is driven from the endogenous promoter rather than the CMV promoter described above. Additionally, the lentiviral vector utilised by *Taylor et al*, allowed for the tagging of PPP2R1A with an exogenous epitope (in this case V5) which would facilitate immunoprecipitation (Taylor, O'Connor et al. 2019). In preclinical models of *PPP2R1A* mutant neurodevelopmental disorders, p.R183W mutant PPP2R1A reduced PP2A phosphatase activity as determined by phosphate released following the supplementation of immunoprecipitated PP2A with exogenous phospho-peptides (Lenaerts, Reynhout et al. 2021). In keeping with this data, I

observed an enrichment of known PP2A phospho-sites in keeping with *PPP2R1A* mutations having a deleterious impact on PP2A phosphatase activity.

PPP2R1A p.R183P/W mutation in the ARID1A mutant TOV21G cell line leads to an enhanced response to AZD6738. Phenotypically, the most striking feature of the ATRi response in *PPP2R1A* mutant cells is a reduction in the replicating S phase population. ATRi cause a modest reduction in the replicating S phase population in *PPP2R1A* mutant cells but the combination of *PPP2R1A* missense mutation and ATRi results in a supra-additive decrease in the replicating S phase population, suggesting that the effect is, at least in part, due to an effect on this phase of the cell cycle.

In order to understand how ATRi can affect the replicating S phase population it is important to establish the role that ATR plays in DNA replication during unperturbed cell division. Initiation of DNA replication at origins is a two-step process, beginning with licensing in late M phase and early G1 phase, followed by firing during S phase (Fragkos, Ganier et al. 2015). Origin licensing entails the loading of the pre-replicative complex, which includes the origin recognition complex (ORC) and the core replicative helicase minichromosome maintenance 2-7 complex (MCM2-7) on to chromatin. Activation of MCM2-7 helicase activity during origin firing in S phase requires loading of the pre-initiation complex (pre-IC), comprised of cell division cycle 45 (CDC45), the GINS complex (SLD5–PSF1–PSF2–PSF3), topoisomerase II binding protein 1 (TOPBP1), Treslin (a DNA polymerase), and other replication factors (Heffernan, Unsal-Kacmaz et al.

2007, Yekezare, Gomez-Gonzalez et al. 2013, Deegan, Yeeles et al. 2016). Origin firing is a tightly regulated process, both temporally and spatially, ensuring an adequate supply of the replicative machinery components and nucleotides to ensure faithful DNA replication (Saldivar, Cortez et al. 2017).

ATR-CHK1 signalling leads to the inhibition of CDC25A and the subsequent inactivation of its downstream substrate CDK1, culminating in cell cycle arrest (Liu, Guntuku et al. 2000, Mailand, Falck et al. 2000). During unperturbed DNA replication, low-level ATR-CHK1 signalling has been shown to restrict origin firing the dominant origin in a replisome via suppressing firing at dormant, i.e. non-dominant, origins (Syljuasen, Sorensen et al. 2005, Petermann, Woodcock et al. 2010, Moiseeva, Hood et al. 2017, Moiseeva, Yin et al. 2019). Moiseeva *et al* demonstrated that ATR inhibition resulted in a decrease in the inter-origin distance, as assessed by DNA fibre assays, suggesting firing of an increased number of origins across the replisome. Firing at these non-dominant origins was characterised by the CDC7-dependent hyperphosphorylation of MCM4 (Moiseeva, Hood et al. 2017). In a subsequent report, the same author demonstrated that both ATRi and CHK1i result in phosphorylation of RIF1 on residue S2205, which disrupts the interaction between RIF1 and protein phosphatase 1 (PP1). PP1 is proposed to antagonize the activity of CDC7 at non-dominant origins, thus RIF1 phosphorylation in response to ATRi results in the uncoordinated firing at dormant origins (Moiseeva, Yin et al. 2019).

If ATR inhibition results in widespread firing of origins of replication, one could surmise that this would lead to an increase in the active S phase population rather than the decrease outlined in this chapter. However, it should be noted that there is only a finite amount of cellular replicative machinery components and nucleotides to fulfil DNA replication. Indeed, unscheduled firing of dormant origins has been shown to create an excess of ssDNA, a common intermediate formed at stalled replication forks, which in turn becomes coated in RPA (Toledo, Altmeyer et al. 2013, Bhat and Cortez 2018). This process culminated in the exhaustion of the nuclear RPA pool and *RPA* gene silencing exacerbated the associated replication stress (Toledo, Altmeyer et al. 2013). Yin *et al* used computational analysis of single-molecule localization microscopy to quantify the composition of individual replisomes in single cells during unperturbed replication and under replicative stress (Yin, Lee et al. 2021). During unperturbed DNA replication ATR activity limits RPA accumulation at replication forks. This function of ATR was not reversed by CDC7 inhibition suggesting that it is independent of the ATR activity in limiting origin firing (Moiseeva, Yin et al. 2019, Yin, Lee et al. 2021). Furthermore, the ability of ATR to restrain RPA accumulation at replication forks functioned independently of canonical ATR-CHK1 signalling (Toledo, Altmeyer et al. 2013) but did require an ATR-ATRIP interaction (Yin, Lee et al. 2021). ATR inhibition therefore results in the accumulation of RPA at replication forks, further exhausting the nuclear RPA pool

The supply of nucleotides to facilitate DNA replication relies on two pathways, de novo synthesis and salvage, of which deoxycytidine kinase (dCK) and

ribonucleotide reductase (RNR) are the rate limiting enzymes for each pathway respectively (Amsailale, Van Den Neste et al. 2012). In pre-clinical models of Ewing sarcoma and leukaemia, ATR inhibition has been shown to reduce the cellular pool of nucleotides through the reduced activity of both dCK and RNR, resulting in an accumulation of DNA damage and ultimately cell death (Le, Poddar et al. 2017, Koppenhafer, Goss et al. 2020).

Beyond its role in limiting firing to a dominant origin and ensuring adequate resources to perform DNA replication, ATR also interacts with an array of replisome components and DNA repair factors that protect the replication fork from collapse and control replisome function (Saldivar, Cortez et al. 2017). Stabilization of a replication fork refers to the ability of stalled DNA synthesis following the removal of the insult, with the term “collapsed fork” referring to a fork which is unable to recommence DNA replication. Inhibition of nuclease dependent fork collapse is one mechanism through which ATR may improve fork stability. For instance, ATR phosphorylates the putative fork reversal enzyme SWI/SNF-related matrix-associated actin-dependent regulator of chromatin subfamily A-like protein 1 (SMARCAL1), reducing its ability to reverse forks and limiting aberrant fork processing via structure-specific endonuclease subunit (SLX4) (Couch, Bansbach et al. 2013, Ragland, Patel et al. 2013). Additionally, Fanconi anemia group D2 protein (FANCD2) has been shown to associate with the MCM complex in an ATR-dependent manner (Lossaint, Larroque et al. 2013). FANCD2 delays the progression of the replisome under conditions of replication stress, such as a depleted nucleotide pool, thereby limiting the accumulation of

ssDNA and limiting MRE11 dependent degradation of stalled forks (Ying, Hamdy et al. 2012, Lossaint, Larroque et al. 2013)

Thus, the uncoordinated firing of origins of replication, with the ensuing depletion of RPA and nucleotides, together with reduced replication fork stability are important mechanisms through which ATR inhibition can result in a reduced replicating S phase population. This phenotype is exacerbated in the TOV21G *PPP2R1A* p.R183P and p.R183W cell line models as compared to their WT counterparts. Xenopus egg extracts function as a model cell free system to study protein-protein interactions and was employed by Wang *et al* to determine the interactome of the PP2A regulatory subunits PPP2R2A (B55α) and PPP2R2B (B55β) (Wang, Zhu et al. 2018). In this study, PPP2R2A/PPP2R2B was demonstrated to co-immunoprecipitate with multiple proteins involved in DNA replication including RPA1, RPA2 Cdc6, Cdc45, DNA primase, and the minichromosome maintenance (Mcm) complex (Wang, Zhu et al. 2018). N terminal phosphorylation of RPA2 (an RPA subunit) on residues S4 and S8 facilitates the stabilization, repair, and recovery of stalled replication forks in response to replication stress (Ashley, Shrivastav et al. 2014). Consistent with PP2A-mediated dephosphorylation of these RPA2 residues, overexpression of PPP2R2A resulted in reduced RPA2 S4 and S8 phosphorylation (Wang, Zhu et al. 2018). Given that *PPP2R1A* p.R183 missense mutations have been shown to result in reduced incorporation of both PPP2R2A and PPP2R2B into the PP2A complex (Taylor, O'Connor et al. 2019), one could hypothesize that they would also disrupt the interaction between PP2A and these DNA replication-associated

proteins, including RPA2. The ensuing increased RPA2 S4/S8 phosphorylation would be expected to promote replication checkpoint arrest and a subsequent reduction in the replicating S population.

In somewhat of a contradiction to the data presented in this chapter and to the mechanistic hypothesis outlined above, Perl *et al* report that the presence of *PPP2R1A* missense mutations results in delayed S phase progression, and that increased PP2A activity results in replication stress through disruption of the replisome (Perl, O'Connor et al. 2019). Small molecule activators of PP2A (SMAPs) induce PP2A-dependent dephosphorylation of PP2A substrates and have been proposed as a potential therapy for cancers harbouring PP2A defects, such as castrate resistant prostate cancer (McClinch, Avelar et al. 2018) and MYC driven cancers, including Burkitt's lymphoma and *KRAS* mutant colorectal cancer (Farrington, Yuan et al. 2020). Perl *et al* showed that treatment with the putative SMAP DT-061 resulted in reduced incorporation of bromodeoxyuridine (BrdU) during S phase, which was associated with replication stress as assessed by DNA fibre assay (Perl, O'Connor et al. 2019). Mechanistically, this phenotype was attributed to a SMAP-induced reduction in chromatin bound CDC45, a key component of the replisome which links the helicase to the MCM complex (Broderick and Nasheuer 2009, Perl, O'Connor et al. 2019). It is, perhaps, an oversimplification to suggest that *PPP2R1A* missense mutations will result in a complete opposite phenotype to the one observed with SMAP-induced PP2A activation. Future work would focus on addressing these contradictory reports. DNA fibre assays performed in the *PPP2R1A* isogenic models in the presence

and absence of ATRi would allow for the assessment of replication fork dynamics. Western blot of immunoprecipitation (IP-Western) could provide a means of assessing the impact of *PPP2R1A* and ATRi on the replisome composition, including chromatin bound CDC45.

Finally, in addition to reducing incorporation of EdU during S phase, ATRi have been shown to cause the premature phosphorylation, and activation, of FOXM1, thereby promoting the S/G_2 transition (Saldivar, Hamperl et al. 2018). Indeed, PP2A is known to dephosphorylate both FOXM1 (Alvarez-Fernandez, Halim et al. 2011) thereby restraining the S/G_2 transition. Thus, in the context of PP2A dysfunction increased FOXM1 activity may contribute to the observed S phase defect. Unresolved DNA damage, arising in S phase that persists as the cells enter mitosis has the potential to impair the fitness of cells and elicit the observed accumulation of 53BP1 bodies. This process may well be exacerbated by the forced mitotic entry associated with ATR inhibition (Schoonen, Kok et al. 2019).

Chapter 5. PPP2R1A/ATRi synthetic lethality is a WNK1 dependent process

5.1 Introduction

So far, I have described the generation *PPP2R1A* isogenic models of ARID1A-deficient OCCC, along with the phenotypic features associated with the ATRi response in these cells. Several mechanisms through which PP2A defects could impact the response to ATRi have been described in the literature, namely elevated Myc expression (Qiu, Fa et al. 2020) and reduced WEE1 levels (Li, Kozono et al. 2020). First, I sought to determine whether either of these potential mechanisms could provide an explanation for the ATRi-sensitive phenotype observed in the TOV21G *PPP2R1A* p.R183 mutant models. In this Chapter, I show that neither of these potential mechanisms provide a suitable explanation for the effects seen in OCCC. I then used several agnostic approaches to identify the molecular determinants of ATRi sensitivity; a short interfering RNA (siRNA) screen and mass-spectrometry based phospho-proteomic profiling.

The use of siRNA screens has provided a means for the identification of genes involved in a multitude of biological processes. They have been used in research which led to the discovery of the synthetic lethal interaction between *ARID1A* and *ATR (Williamson, Miller et al. 2016)*, the identification of dasatinib as a potential therapy in ARID1A-deficienct OCCC (Miller, Brough et al. 2016) and more recently the elucidation of genetic determinants of the response to DNA polymerase theta inhibitors (Polθi) (Zatreanu, Robinson et al. 2021).

The phenotype of any cancer is not solely determined by the presence or absence of certain gene mutations. The array of proteins expressed, or proteome, along with their post-translational modifications, have emerged as important determinants of the malignant phenotype. Phosphorylation of serine, threonine and tyrosine residues within peptide motifs represent one of the most commonly observed post-translational modifications (Narushima, Kozuka-Hata et al. 2016). Changes in the phospho-proteomic profile in cancer have been used to identify signalling pathways implicated in the development of cancer (Harsha and Pandey 2010) and in the molecular events underpinning drug resistance (Boulos, Yousof Idres et al. 2020). Given the prominent role that PP2A plays in the overall phosphatase activity carried out in eukaryotic cells, I surmised that distinct changes in the phospho-proteome could be detected following ATRi exposure in the TOV21 *PPP2R1A* isogenic cells.

Using this parallel approach, With No Lysine Kinase 1 (WNK1) was identified as a potential mediator of the ATRi response in *PPP2R1A* mutant cells. WNK1 depletion rescued drug sensitivity and restored the replicating S phase population in response to ATR inhibition.

5.2 PP2R1A/ATR inhibitor synthetic lethality in OCC cells is not explained by changes in total WEE1 or Myc levels

Substrates of the PP2A holoenzyme have previously been implicated in modulating proteins such as Myc which control the extent of replication fork stress, a potential driver of ATRi sensitivity (Cottini et al., 2015; Dominguez-Sola et al., 2007; Hustedt et al., 2019; Sanjiv et al., 2016; Srinivasan, Dominguez-Sola, Wang, Hyrien, & Gautier, 2013). For example, PP2A is thought to dephosphorylate Myc on residue S62. In addition, *PPP2R2A* gene silencing has been shown to cause an increase in Myc protein levels (Qiu et al., 2020). Conversely, PP2A dephosphorylates WEE1 on residues S53 and S153, and PP2A defects cause decreased WEE1 levels via ubiquitin mediated degradation (Li et al., 2020). In principle, changes in either WEE1 and/or Myc could explain the ATRi sensitivity of PPP2R1A mutant OCCC cells. However, I found that neither p.R183P or p.R183W mutant cells exhibited elevated cMyc levels (Figure 5.1) or decreased WEE1 levels that could trivially explain the PPP2R1A/ATRi synthetic lethality (Figure 5.2).

5.3 siRNA screen identifies WNK1 as mediator of ATRi resistance in *PPP2R1A* mutant cells

As neither changes in Myc nor WEE1 could robustly explain ATRi synthetic lethality in *PPP2R1A* mutant cells, I took a more empirical approach to understand this phenotype. In the first instance, I used an RNA interference

A.

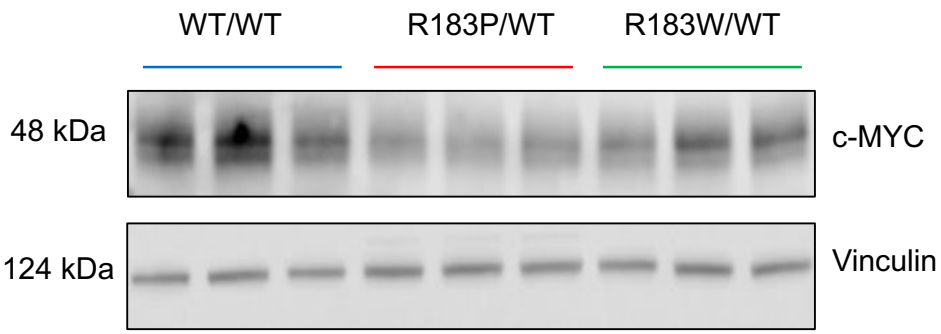

B.

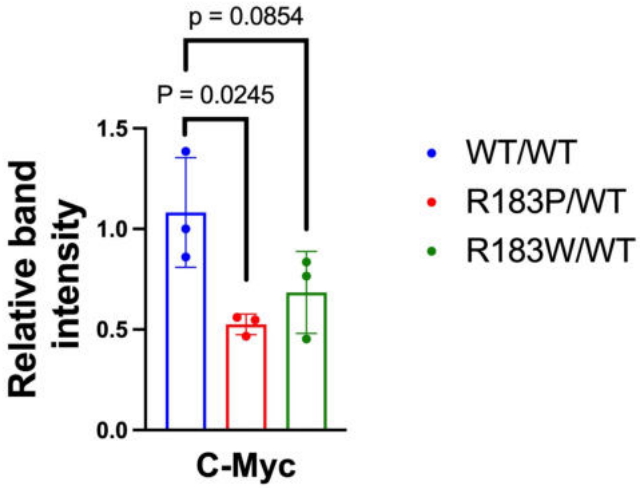

Figure 5.1 Total c-MYC levels decreased in PPP2R1A mutant cells. (A) Western blot for c–MYC from whole cell lysates from TOV21G PPP2R1A isogenic cells . (B) Quantification of band intensity from Western blot in (A). Band intensity calculated relative to median of WT/WT sample. Error bars represent mean and SD. Statistical significance determined by one-way ANOVA.

A.

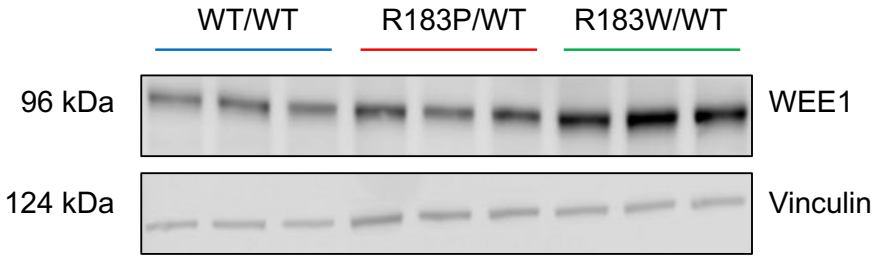

B.

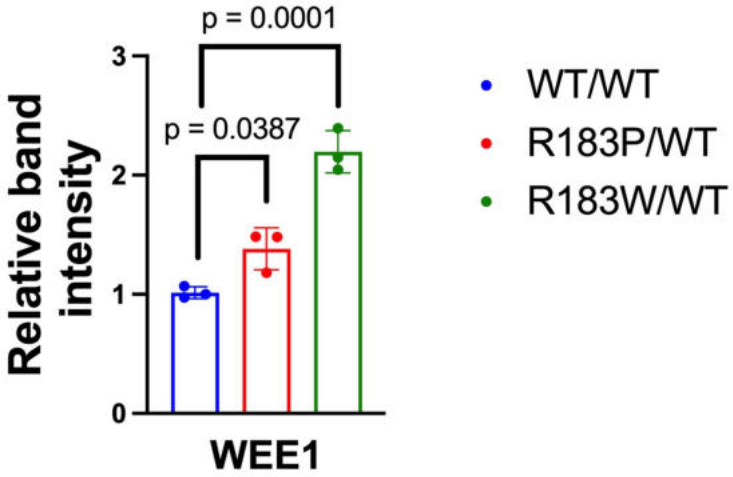

Figure 5.2 Total WEE1 levels increased in TOV21 PPP2R1A mutant cells. (A) Western blot for total WEE1 from whole cell lysates extracted from TOV21G PPP2R1A isogenic cells. (B) Quantification of band intensity from Western blot in B. Band intensity calculated relative to median of WT/WT sample. Error bars represent mean and SD. Statistical significance determined by one-way ANOVA

(siRNA) screen to identify genes that caused resistance to ATRi in *PPP2R1A* mutant and wild type cells, using a screening siRNA library designed to target 953 genes, including those involved in DNA repair and cell cycle control. Cells were reverse transfected with siRNA in 384 well plate format. They were then exposed to AZD6738 at a SF_{50} concentration (designed to decrease cell survival by 50 %) for 5 subsequent days, after which cell viability was determined by CellTitre Glo® reagent (Figure 5.3).

The effect of each gene silencing event on AZD6738 resistance was estimated by calculation of Drug Effect (DE) Z scores, with positive scores representing resistance-causing effects. This analysis indicated that siRNA designed to target the with no Lysine 1 Kinase (WNK1) caused ATRi resistance in *PPP2R1A* mutant cells (DE Z score = 1.78) but had minimal effects in wild type cells (DE Z score = – 0.21) (Figure 5.4).

5.4 Phospho-proteomic profiling of TOV21G *PPP2R1A* isogenic models

Given heterozygous *PPP2R1A* mutations are considered to reduce PP2A phosphatase activity, I speculated that distinct changes to the phosphor-proteome would be detectable upon ATR inhibition in the *PPP2R1A* isogenic model. Mass spectrometry-based phospho-proteomic profiling was therefore performed on TOV21G *PPP2R1A* WT and p.R183P cells following exposure to either DMSO or AZD6738 (5 μM) for 16 hours. Samples were analysed in

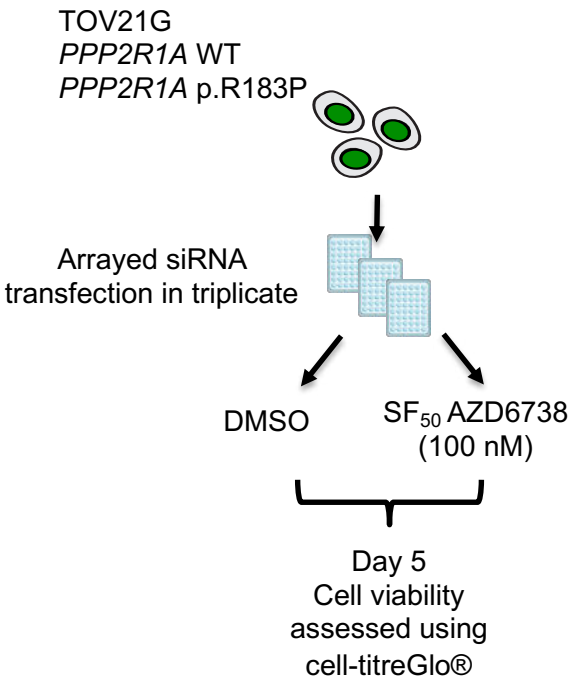

Figure 5.3 siRNA screen schema. TOV21G PPP2R1A WT and p.R183P cells were reverse transfected with siRNA library targeting 953 genes before being exposed to either DMSO or AZD6738 100 nM for five continuous days after which cell viability was assessed using cell-titer Glo® .

A.

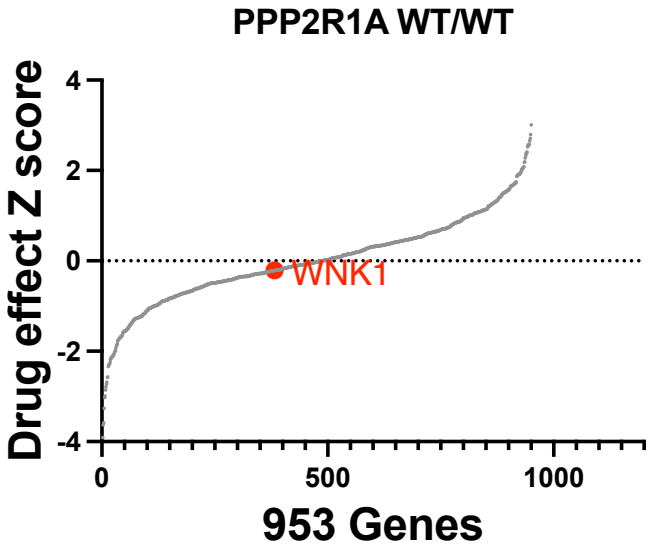

B.

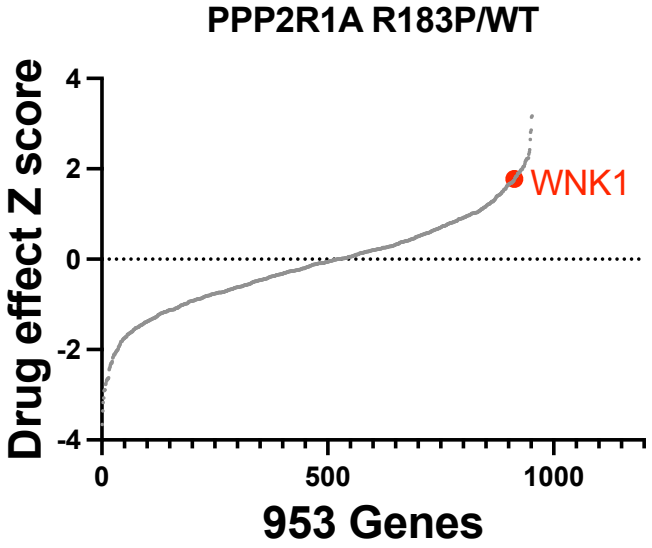

Figure 5.4 siRNA screen identifies WNK1 silencing as a cause of ATRi resistance in PPP2R1A p.R183P mutant cells. Ranked drug effect Z scores from siRNA screen described in (Figure 25) performed in TOV21G PPP2R1A WT cells (A) and TOV21G PPP2R1A p.R183P cells (B). Drug effect Z score for WNK1 highlighted in red.

Triplicate by Dr Theo Roumeliotis (ICR, London) and the mass spectrometry pipeline is summarised in Figure 5.5 and described below.

For each phospho-peptide sequence, a scaled abundance was determined. The total signal for each of the tandem-mass tag (TMT) channel is determined and normalized so that the total signal from each channel is equal to the value of the highest channel. In this way, changes to peptide/phospho-peptide abundances can be compared even when the proteins from which they are derived are expressed at differing levels in the cell (O'Connell, Paulo et al. 2018). For each phospho-peptide a Log2 fold change between DMSO- and ATRi-exposed cells was calculated allowing the DE to be determine with statistical significance being assessed via an unpaired t-test. Finally, to ensure that any changes in phospho-peptide enrichment were not simply due to increases or decreases in the total levels of the protein from which it was derived, I assessed the scaled relative abundances of the corresponding peptide in the complimentary total proteomic profile.

A principle component analysis (PCA) was performed on both the total proteomic and phospho-proteomic data sets. Interestingly, this analysis demonstrated that the total proteomic profiling separated samples strongly by genotype (*PPP2R1A* WT vs *PPP2R1A* p.R183P), whereas phosphor-proteomic analysis separated samples best by the drug exposure (DMSO vs AZD6738) (Figure 5.6). This

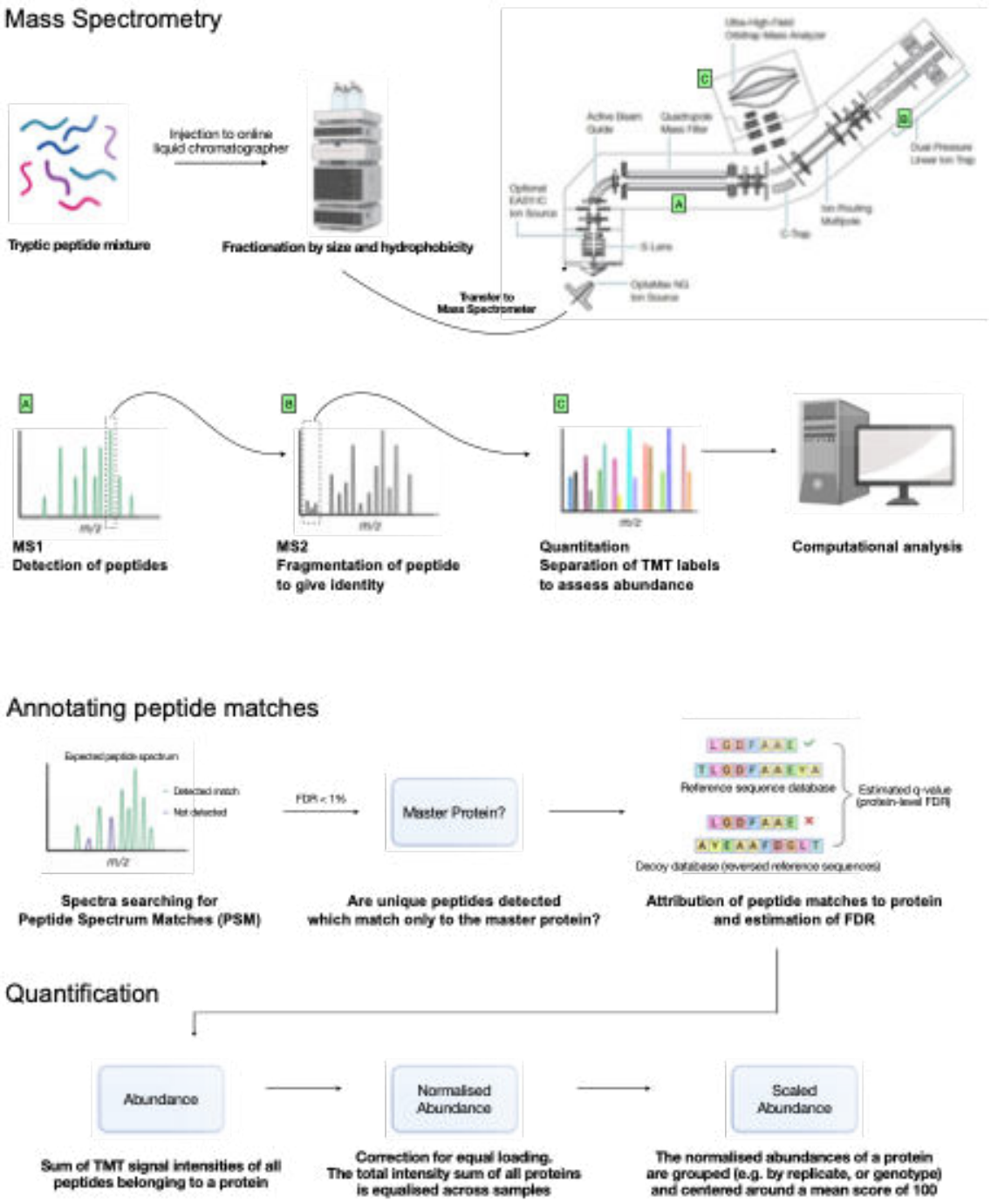

Figure 5.5 Schematic illustrating the mass spectrometry pipeline

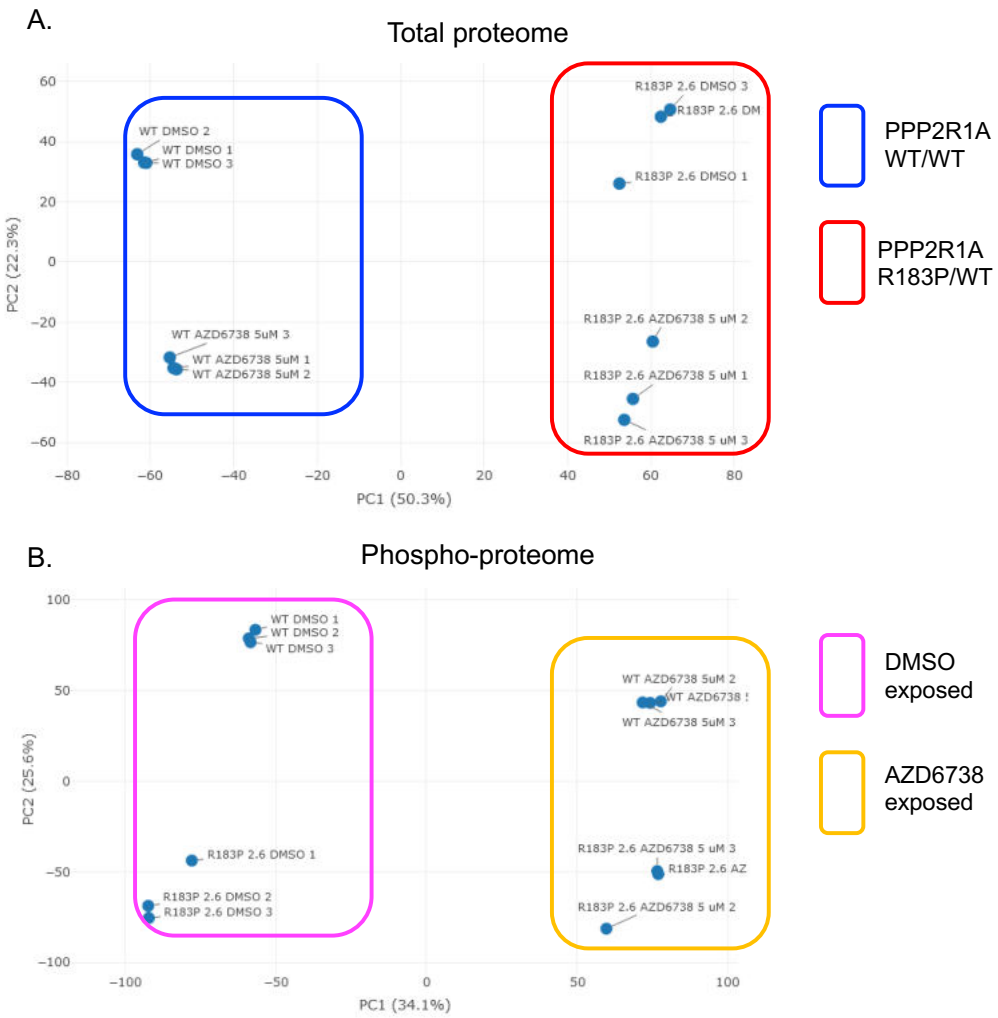

Figure 5.6 PCA analysis demonstrates that the total proteome separates samples strongly by cell line, whereas phospho-proteomics separates samples best by the ATRi treatments. (A) Principle component analysis (PCA) plots for the total proteomic profile. (B) PCA plot for phosphoproteomic profile.

suggests that exposure to ATRi leads to distinct changes in the phospho-proteomic profile of the *PPP2R1A* mutant cells when compared to WT cells.

When I cross-referred data from the siRNA screen to the phospho-proteomic analysis of *PPP2R1A* mutant and wild type cells, I noted that one of the most profound phospho-proteomic changes in *PPP2R1A* p.R183P mutant cells following ATRi exposure was an increase in a single WNK1 phosphorylation site (p.S183). In addition, there was an increase in phosphorylation of the WNK1 substrate OSR1 at residue p.S324, the WNK1 phosphorylation target site (Figure 5.7). These changes in WNK1 and OSR1 phosphorylation were not matched by changes in total protein level (Figure 5.8).

5.5 WNK1 depletion rescues ATRi sensitivity and restores the replicating S phase

The identification of WNK1 in both the siRNA screen and in the phospho-proteomic profiling was of interest as PPP2R1A has previously been shown to interact with WNK1 (Chi et al., 2020). Furthermore, in pre-clinical models of gastrointestinal stromal tumours (GIST), *PPP2R1A* mutations have also been associated with elevated WNK1 phosphorylation (Toda-Ishii et al., 2016). Although the WNK1 p.S183 phospho-site has not previously been described and does not lie within the catalytic (phosphatase) domain or any known regulatory domain (Figure 5.9), the observation that the WNK1 target phospho-site (OSR1 p.S324) was enriched in the PPP2R1A mutant cells following ATRi led me to

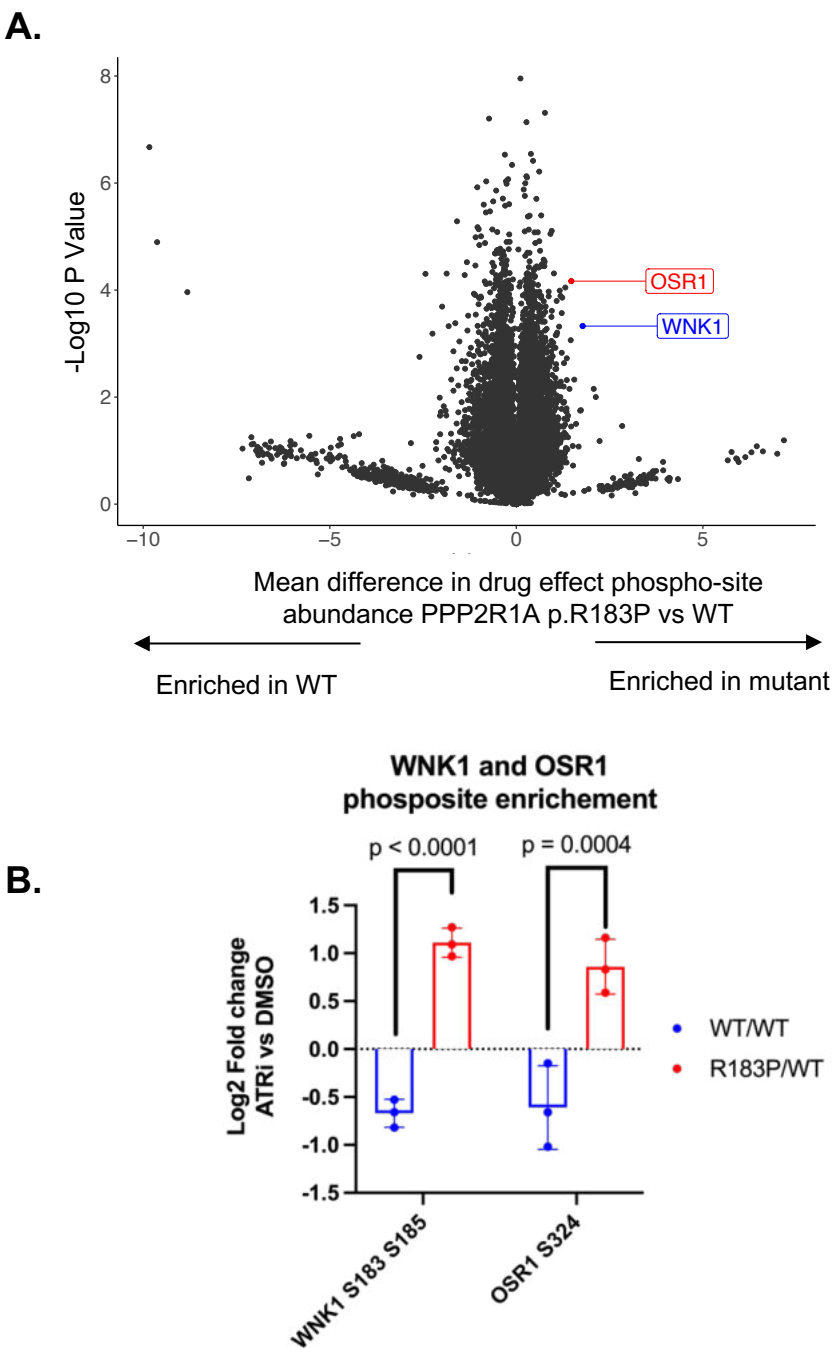

Figure 5.7 Single phosphosite on WNK1 and its downstream substrate OSR1 enriched in PPP2R1A mutant cells upon ATRi exposure. (A) Volcano plot showing the mean difference in drug effect on phospho-site abundance between TOV21G *PPP2R1A* WT and p.R183P cells. WNK1 and OSR1 among the most differentially phosphorylated peptides observed. (B). Log2 fold change in indicated phospho-site on WNK1 and OSR1 between AZD6738 and DMSO exposed TOV21G PPP2R1A WT and p.R183P cells. Analysis reveals that single phospho-site on each protein is differentially phosphorylated upon ATRi exposure. Error bars represent mean and SD. Significance determined via two-way ANOVA with Šídák's correction for multiple comparisons.

A. B.

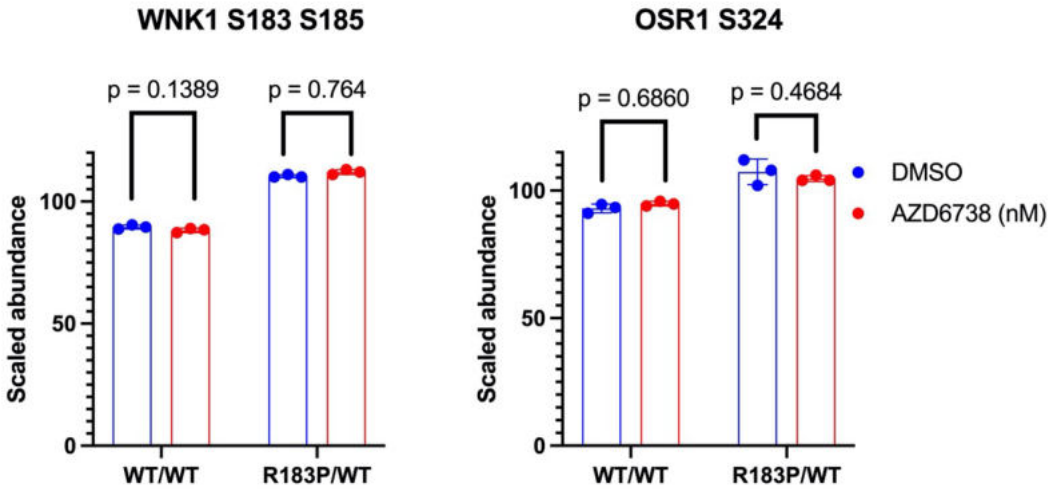

Figure 5.8 Increases in WNK1 and OSR1 phospho-site enrichment following ATRi exposure not due to increases on total peptide abundance. Histograms showing scaled abundance for peptides corresponding to WNK1 S183/S185 (A) and OSR1 S324 phospho-sites following exposure to DMSO or AZD6738. No significant difference observed. Error bars represent mean and SD. Significance determined via two-way ANOVS with Šídák's multiple comparisons test.

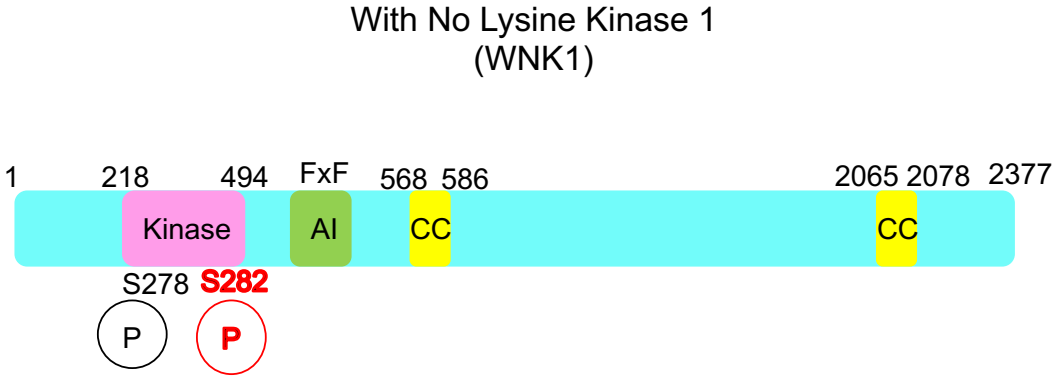

Figure 5.9 WNK1 structure. Numbers indicate amino acid residues. Homologous kinase domain (shown in pink) shared with all WNK family proteins. Autoinhibitory (AI) domain, with two essential phenylalanine residues (F) shown in green. Coiled coil (CC) domains shown in yellow. Activation of WNK1 is dependent on phosphorylation of two serine residues within the kinase domain, S278 and S282. S282 phosphorylation considered to be the most important activating event (highlighted in red). Adapted *from McCormick,Yang and Ellison. Hyertension. (2008)*

hypothesize that phosphorylation of this WNK1 residue reflected an activating event. I therefore sought to determine if depleting WNK1 using siRNA would rescue ATRi sensitivity and some of the other phenotypic features of the ATRi response in *PPP2R1A* mutant cells. Knock down of WNK1 via siRNA was confirmed via Western blot from whole cell extract (Figure 5.10). Having confirmed that transfection with the WNK1 siRNA smartpool used in the siRNA screen led to ATRi resistance in PPP2R1A mutant cells (Figure 5.11), I found that multiple distinct WNK1 siRNA also caused ATRi resistance in the same genetic background (Figure 5.12).

I proceeded to assess the impact of WNK1 on the cell cycle defects in PPP2R1A in response to ATRi. I found that WNK1 gene silencing reversed the decrease in the replicative S phase fraction caused by ATRi in PPP2R1A mutant cells (Figure 5.13), suggesting that the PPP2R1A/ATRi synthetic lethality was a WNK1-dependent process.

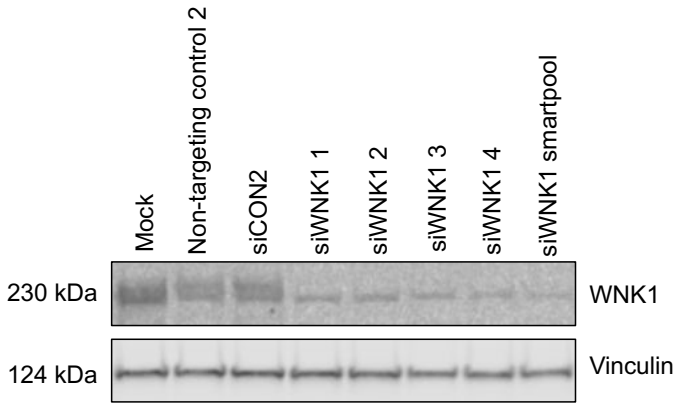

Figure 5.10 Western blot confirming gene silencing of WNK1 following transfection with WNK1 specific siRNAs. Whole cell lysates generated from TOV21G PPP2R1A WT cells 72 hours post transfection with indicated siRNA.

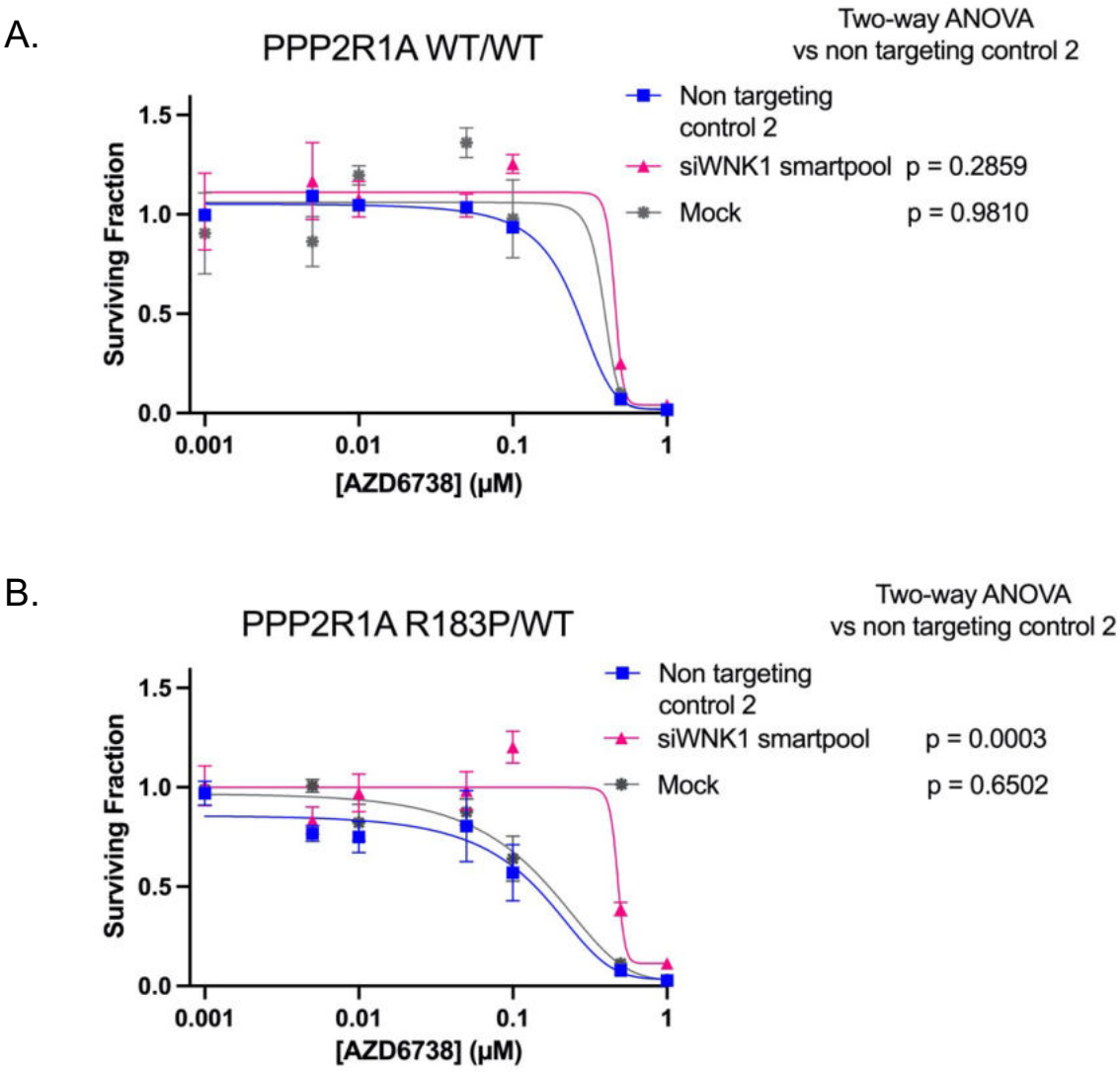

Figure 5.11 WNK1 gene silencing rescues ATRi sensitivity in PPP2R1A mutant cells. Dose response assay for TOV21G PPP2R1A WT (A) and p.R183P (B) cells exposed to increasing concentrations of AZD6738 following transfection with either WNK1 siRNA smartpool, non-targeting control 2 or mock transfected. Transfection with WNK1 siRNA smart pool led to significant (two-way ANOVA) resistance in PPP2R1A p.R183P cell line but not WT cells. Error bars represent mean and SEM from 5 replicates.

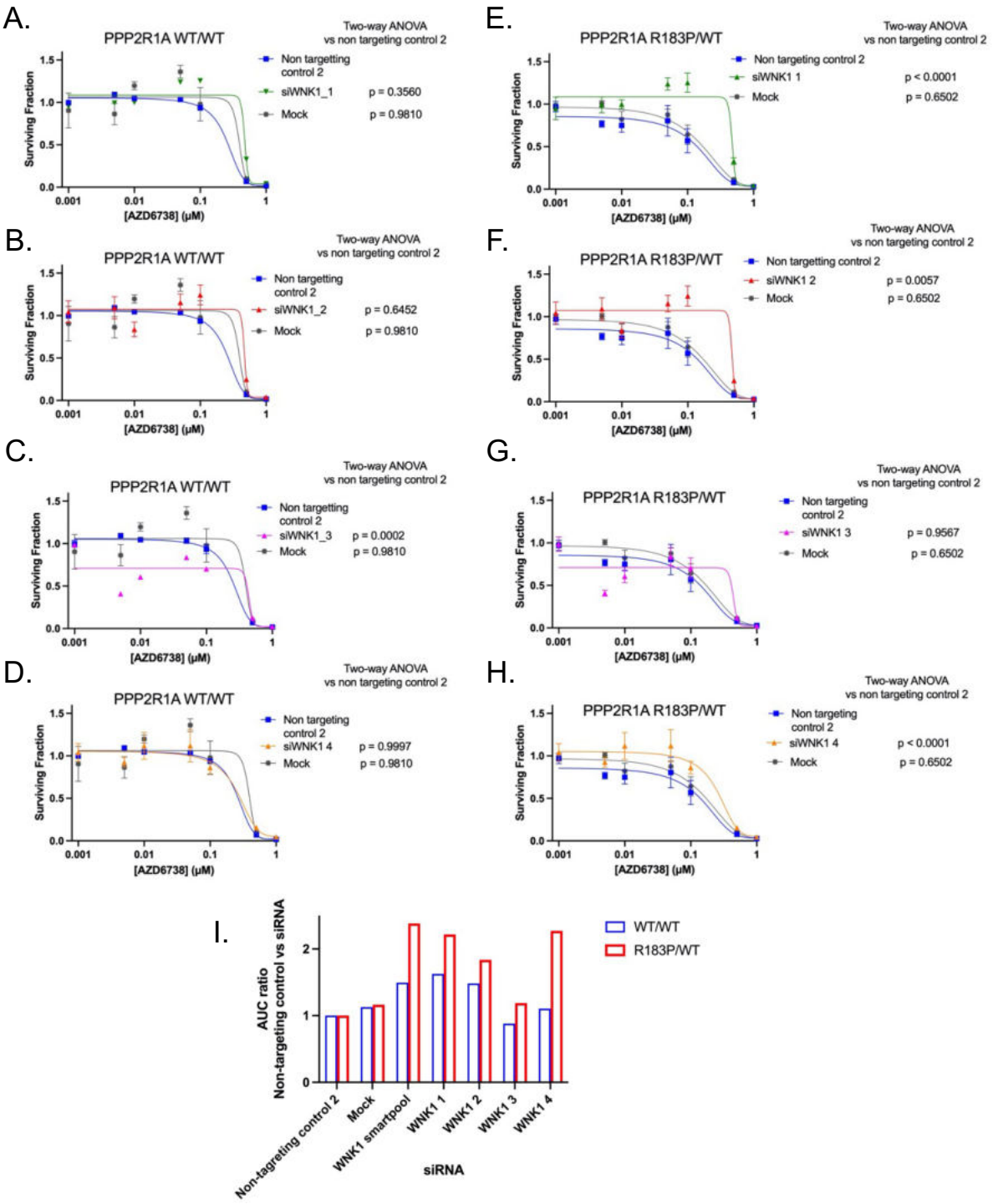

Figure 5.12 WNK1 gene silencing with individual siRNAs rescues ATRi sensitivity in PPP2R1A mutant cells. Dose response assay for TOV21G PPP2R1A WT (A-D) p.R183P (E-H) cells exposed to increasing concentrations of AZD6738 following transfection with either one of two individual WNK1 siRNAs, non-targeting control 2 or mock transfected. Error bars represent SEM from four replicate experiments. Significance determined via two-way ANOVA. (I) Histogram summarizing the AUC ratio, non-targeting control 2 vs indicated siRNA from experiments described in Figure 5.11 and 5.12 A-H.

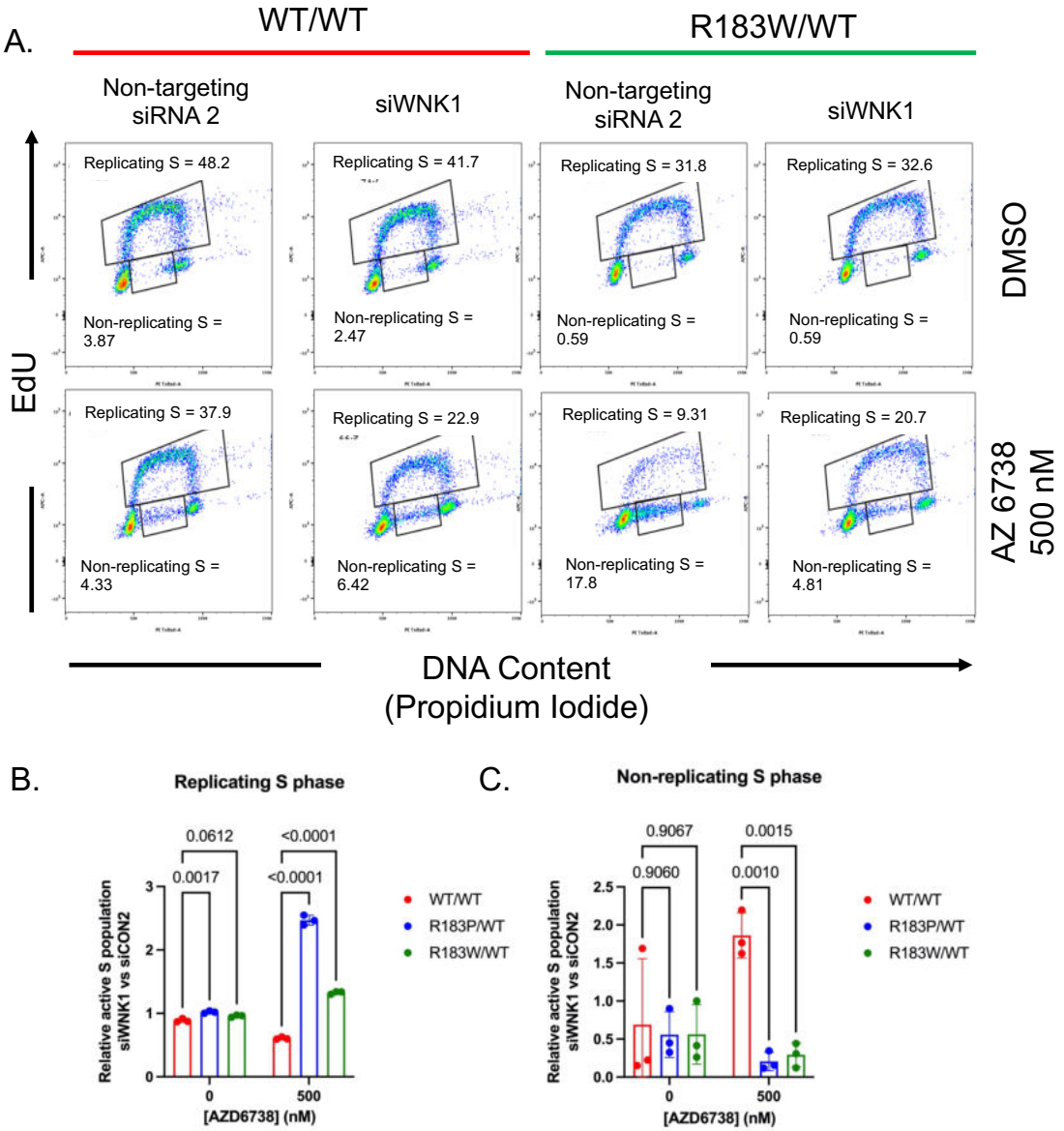

Figure 5.13 Silencing of WNK1 restores replicating S phase in PPP2R1A p.R183P and p.R183W cell lines but not in PPP2R1A wild type cells in response to ATRi. (A) Representative FACS plots with DNA content (PI) on the X-axis vs. EdU intensity on the Y-axis for TOV21G PPP2R1A WT and PPP2R1A p.R183W cell lines following transfection with indicated siRNA and following exposure to increasing concentrations of AZD6738. (B-C) Silencing of WNK1 leads to a relative increase in the proportion of cells in replicating S phase (B) and a corresponding decrease in the proportion of cells in non-replicating S phase (C) in PPP2R1A mutant cells following exposure to AZD6738 compared to non-targeting siRNA. Error bars represent SEM from four replicates. Significance determined by two-way ANOVA with Šídák's correction for multiple comparisons.

5.6 WNK1 silencing rescues ATRi sensitivity in *ARID1A* mutant OCCC cell lines with naturally co-occurring *PPP2R1A* mutations.

To assess the generalisability of these observations, I assessed whether silencing of WNK1 would reverse ATRi sensitivity in additional OCC cell lines with *PPP2R1A* mutations, other than the genetically engineered TOV21G model described above. OVTOKO and OVISE are two commonly used OCCC cell line models which harbour *ARID1A* p.F1991fs and p.Q543fs mutations respectively. Both cell lines also possess heterozygous *PPP2R1A* missense mutations, p.R183W in the case of OVISE and p.R183G for OVTOKO. Both OVTOKO and OVISE were sensitive to AZD6738, and WNK1 gene silencing led to significant resistance compared to non-targeting control 2 siRNA (two-way ANOVA, $p < 0.0001$) (Figure 5.14).

5.7 Chapter 5 Discussion

In this chapter I sought to determine the molecular basis for ATRi sensitivity in *PPP2R1A* mutant cells. Western blot analysis suggests that neither a reduction in total WEE1 levels nor elevated Myc expression, two potential mechanisms described in the literature (F. Li et al., 2020; Qiu et al., 2020), could provide a robust explanation for the observed phenotype. Through the integration of data generated through an siRNA resistance screen and the phospho-proteomic profiling of *PPP2R1A* isogenic cell lines, WNK1 was identified as a potential

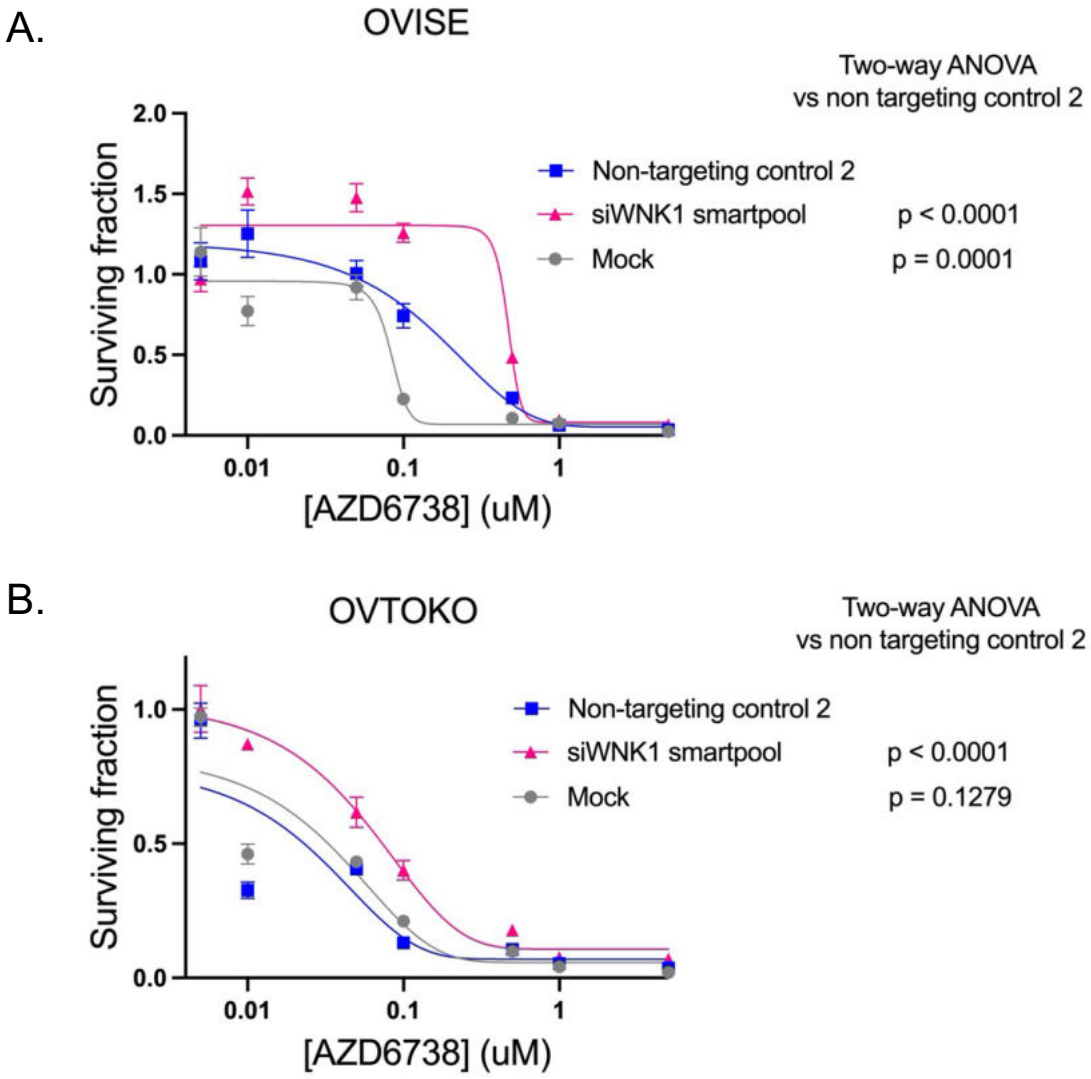

Figure 5.14 WNK1 gene silencing rescues ATRi sensitivity in OCCC cell lines with naturally occurring PPP2R1A missense mutations. Dose response assay for OVISE (A) and OVTOKO (B) cells exposed to increasing concentrations of AZD6738 following transfection with either WNK1 siRNA smartpool, non-targeting control 2 or mock transfected. Transfection with WNK1 siRNA smartpool led to significant increase in sensitivity to AZD6738 in both cell lines. Significance determined via two-way ANOVA. Error bars represent mean and SEM from 5 replicates.

mediator of ATRi sensitivity in *PPP2R1A* mutant TOV21G cells. Given WNK1 has previously been shown to interact with *PPP2R1A* and that the introduction of exogenous mutant PPP2R1A results in increased WNK1 phosphorylation, this kinase was chosen for further interrogation. I found that knock down of WNK1 rescued ATRi sensitivity in TOV21G *PPP2R1A* mutant cells but not WT. Furthermore, silencing of WNK1 rescued the replicating S phase population in *PPP2R1A* mutant cells following ATRi exposure, further supporting a novel role for the kinase in mediating the ATRi response. The rescue of ATRi sensitivity upon WNK1 depletion was also observed in two cell line models of *ARID1A*-mutant OCCC with naturally occurring *PPP2R1A* p.R183 mutations suggesting that this effect may be more generalisable.

With No Lysine Kinases (WNKs) are a family of conserved serine-threonine kinases so-named because of the atypical placement of a lysine residue within the catalytic domain. Four WNK family proteins (WNK1-4) have been described, with WNK1 and WNK4 being the most extensively studied due to their role in a rare form of familial hypertension, pseudohypoaldosteronism type II (PHA II) (Wilson, Disse-Nicodeme et al. 2001, Susa, Sohara et al. 2014). Given their association with the familial endocrine disorder, it is perhaps unsurprising that WNK1 signalling has most extensively been described in relation to cells response to hyperosmolar stress through the regulation of trans-membrane ion transport (Shekarabi, Zhang et al. 2017). However, more recently WNK signalling has been implicated in a variety of processes involved in tumorigenesis including

the epidermal-mesenchymal transition (Li, Li et al. 2021), angiogenesis (Sie, Li et al. 2020), and invasion and migration (Jaykumar, Jung et al. 2021).

Known WNK1 substrates include the Oxidative Stress Response Kinase 1 (OSR1) (Chen, Yazicioglu et al. 2004, Anselmo, Earnest et al. 2006) and STE20/SPS1-related proline/alanine-rich kinase (SPAK) (Vitari, Thastrup et al. 2006), through which they influence the activity of Na-Cl (NCC) and Na-K-2Cl (NKCC2) co-transporters (Zhang, Siew et al. 2015). The WNK1 signalling cascade has previously been shown to interact with several oncogenic pathways, including the Phosphoinositide 3-kinase (PI3K) network (Jiang, Zhou et al. 2005, Xu, Stippec et al. 2005), Nuclear factor kappa-light-chain-enhancer of activated B cells (NFκB) network (Miller, Brough et al. 2016) and Transforming growth factor β (TGF-β) network (Lee, Chen et al. 2007), further supporting its role in cancer formation. However, WNK1 has not hitherto been linked to ATR signalling, nor the response to ATRi.

Results for the siRNA screen suggested that WNK1 silencing led to ATRi resistance in *PPP2R1A* mutant cells but not WT. One limitation of the use of such an experimental technique is potential off-target gene silencing which may confound the interpretation of results (Birmingham, Anderson et al. 2006, Fedorov, Anderson et al. 2006). Confidence that the observed phenotype can be attributed to silencing of the target gene can be increased when multiple distinct siRNAs, targeting unique regions of the target mRNA, produce the same biological effect. When two or more such siRNAs lead to a phenotype, an

assumption that the effect is on-target can be made (Echeverri, Beachy et al. 2006). I validated screen findings using three distinct WNK1 specific siRNAs, and this gave me confidence that the effect was real and not an off-target effect nor screen artefact.

ATR inhibition in *PPP2R1A* mutant cells was associated with distinct changes to the phospho-proteome. WNK1 phospho-site p.S183/185 was enriched in the *PPP2R1A* mutant cell line following exposure to AZD6738, but depleted in WT cells under the same conditions. This phospho-site has not been previously described and does not lie in a known regulatory or catalytic domain of the kinase. However, the same pattern of enrichment in mutant cells but depletion in WT was observed for the established WNK1 substrate, OSR1 p.S324. I therefore concluded that the increased phosphorylation of WNK1 was an activating event. From the data presented in this chapter I am unable to specify whether this assumed increase in WNK1 kinase activity arises through increased phosphatase activity or some other mechanism, such as a change in subcellular localisation. The absence of a specific antibody for phospho-WNK1 (S183/185) precluded the validation of the mass spectrometry data by an orthogonal approach such as Western blot analysis.

WNK1 depletion reverses ATRi sensitivity in ARID1A-deficient cells with CRISPR primed-edited and naturally occurring *PPP2R1A* p.R183 mutations. Mechanistically, WNK1 gene silencing was associated with a restoration of the replicating S population in response to ATRi in PPP2R1A mutant cells but not

WT. I therefore hypothesise that, in the context of ATR inhibition, reduced WNK1 activity, either via hypo-phosphorylation or reduced protein levels, enables improved DNA replication during S phase *PPP2R1A* mutant cells. Consequently, cells entering mitosis would be able to segregate their chromosomes more readily, avoiding the deleterious consequences of ATR inhibition in ARID1A-deficient cells such as anaphase bridges and lagging chromosomes (Williamson, Miller et al. 2016). WNK1 has not previously been implicated in DNA replication or S phase progression. On the contrary, in previous studies, upon mitotic entry WNK1 has been shown to change its localisation from the cytoplasm to the mitotic spindles. Silencing of WNK1 resulted in aberrant segregation of chromosomes during anaphase, failure of abscission, and reduced viability (Tu, Bugde et al. 2011). These findings would appear to be at odds with the observations presented in this chapter. However, it is entirely possible that WNK1 plays functionally distinct roles in different phases of the cell cycle.

In the model described above, ATRi sensitivity in *PPP2R1A* mutant cells is driven by increased WNK1 activity. Therefore, future work could aim to establish which WNK1 substrate is responsible for the ATRi sensitive phenotype. Multiple CRISPR screens, described in this thesis or published elsewhere (Ruiz, Mayor-Ruiz et al. 2016, Hustedt, Alvarez-Quilon et al. 2019) have identified a compendium of genes that control ATRi sensitivity. WNK1 phosphorylation events that are critical for ATRi sensitivity could be identified by carrying out phosphoproteomic profiling in the *PPP2R1A* isogenic models in the presence and absence of WNK1 gene silencing. Integration of data provided through these two

approaches will likely generate testable hypotheses to explain the *PPP2R1A/ATR* synthetic lethal interaction.

Alternatively, a hypothesis driver approach could be adopted to establish the role of WNK1. As discussed in Chapter 4, the routes through which ATR inhibition can result in a decrease in the replicating S phase population include the unscheduled firing of dormant origins and the ensuing depletion of replisome components and nucleotides, together with the protective role ATR plays at the replication fork. Addressing which of these processes WNK1 participates in could be addressed in future work. DNA fibre assays would provide a means to assess both replication stress and origin firing in the in response to ATRi in the presence and absence of *WNK1* gene silencing. Sugitani *et al* have recently proposed the use of a Western blot for phospo-MCM4 and phospho-RIF1 as surrogate biomarkers for origin firing (Sugitani, Vendetti et al. 2022) providing an orthogonal means to assess origin firing. Assessment of the chromatin bound replisome components in the context of normal or repressed WNK1 expression would afford the opportunity to assess whether WNK1 participates in unperturbed DNA replication. Finally, repeating the phosphoproteomic profiling as described above would provide a means to assess changes in both the proteome and phosphoproteome, which could account for the discrepancies in replicating S phase populations between *PPP2R1A* mutant and WT cells in response to ATRi.

Data presented in this chapter suggests a novel role for WNK1 in mediating the ATRi response in *PPP2R1A/ARID1A* double mutant OCCC. In the subsequent

chapter I sought to determine whether the synthetic lethal interaction between ATR and PPP2R1A identified and characterised in previous chapters could also be observed *in vivo,* in xenograft models of ARID1A deficient OCCC.

Chapter 6. In vivo assessment of PPP2R1A/ATR synthetic lethal interaction.

6.1 Introduction

Having established a synthetic lethal interaction between PPP2R1A and ATR in a tumour cell line model of ARID1A-deficient OCCC, I sought to determine if this effect could also be observed i*n vivo*. Luciferase-expressing TOV21G cells have previously been shown to form diffuse miliary intraperitoneal disease when introduced to immunocompromised mice by intraperitoneal injection (Miller, Brough et al. 2016) mirroring the clinical presentation in patients with OCCC. I generated an orthotropic intraperitoneal model involving the xenografting of TOV21G PPP2R1A WT, p.R183P or p.R183W cells into immunocompromised mice. Using this model system, treatment with the ATRi AZD6738 significantly slowed tumour growth following transplantation of *PPP2R1A* mutant cells but not WT. This work was carried out by Asha Konde, Lord Lab, with my assistance and I analysed data emerging from this study.

6.2 Generation of luciferase-expressing TOV21G PPP2R1A isogenic cell lines

To facilitate the assessment of tumour burden using IVIS® imaging system *in vivo*, I first generated luciferase expressing TOV21G *PPP2R1A* WT (WT/WT), p.R183P (R183P/WT) and p.R183W (R183W/WT) cells. Cells were infected with a lentiviral vector encoding luciferase and red-fluorescent protein (RFP).

Luciferase catalyses the degradation of luciferin substrates, emitting photons in the process, which can be measured. 72 hours following infection, RFP positive cells were harvested via fluorescence-activated cell sorting (FACS). Prior to in vivo inoculation, the luciferase activity of these RFP positive cells was assessed *in vitro* with all three cell lines (Figure 6.1).

6.3 In vivo study optimization

A pilot study was performed to ensure that the genetic modifications introduced through CRISPR prime gene editing did not impact the ability of cells to xenograft. 1 x 10^6 luciferase-expressing TOV21G cells with WT *PPP2R1A* or those with heterozygous p.R183P or p.R183W mutations were inoculated via intraperitoneal injection in to 3 BALB/c nude mice per genotype. Luciferase activity was measured by the intraperitoneal injection of luciferin and IVIS imaging 24 hours following intraperitoneal tumour inoculation and then bi-weekly. All three cell lines xenografted successfully with an increase in luminescence observed after day 7 (Figure 6.2). Within the full *in vivo* study, I elected to begin drug treatment on day 6 to allow for sufficient time to allow successful xenografting but also before exponential tumour growth occurred, in order to maximize the ability to observe a response.

A.

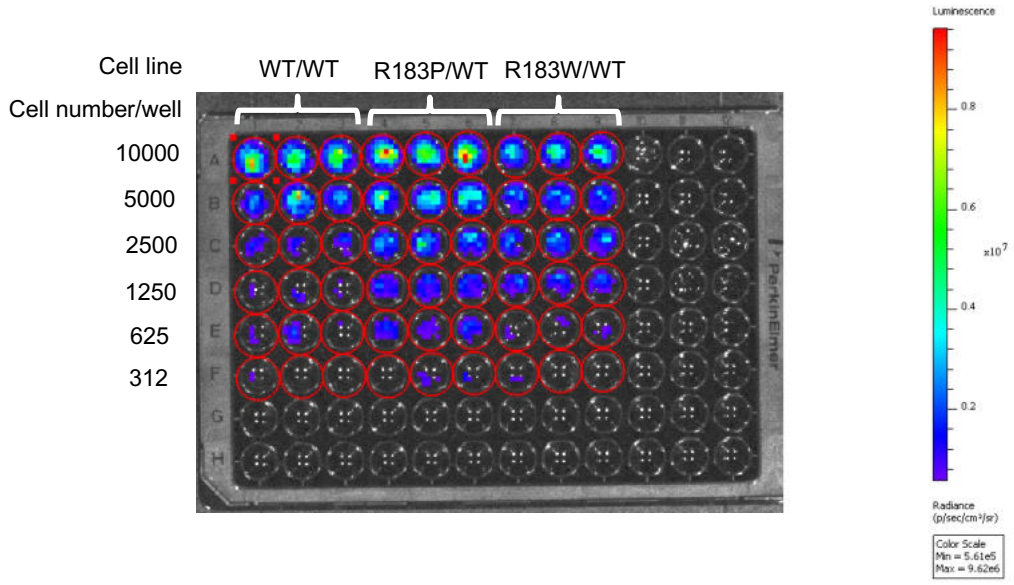

B.

Cell line	Mean luminescence (Photons/second/cel)l	Sufficient for in vivo assessment
TOV21G PPP2R1A WT/WT	1758.77	Yes
TOV21G PPP2R1A R183P/WT	3325.49	Yes
TOV21G PPP2R1A R183W/WT	2012.07	Yes

Figure 6.1 Luciferase activity of TOV21G PPP2R1A isogenic models satisfactory for iVIS imaging. (A) Luciferase activity confirmed in TOV21G PPP2R1A WT, p.R183P and p.R183W cells. Following infection and FACS sorting, cells seeding to 96 well plate at indicated densities. After 24 hours, luciferin (150 µcg/ml) added to each well. Luminescence measured via IVIS imaging 10 minutes after addition of luciferin. (B) Quantification of luminescence from experiment described in (A). All three cell lines exceed the minimum threshold stipulated in manufactured recommendations (500 photons/second/cell).

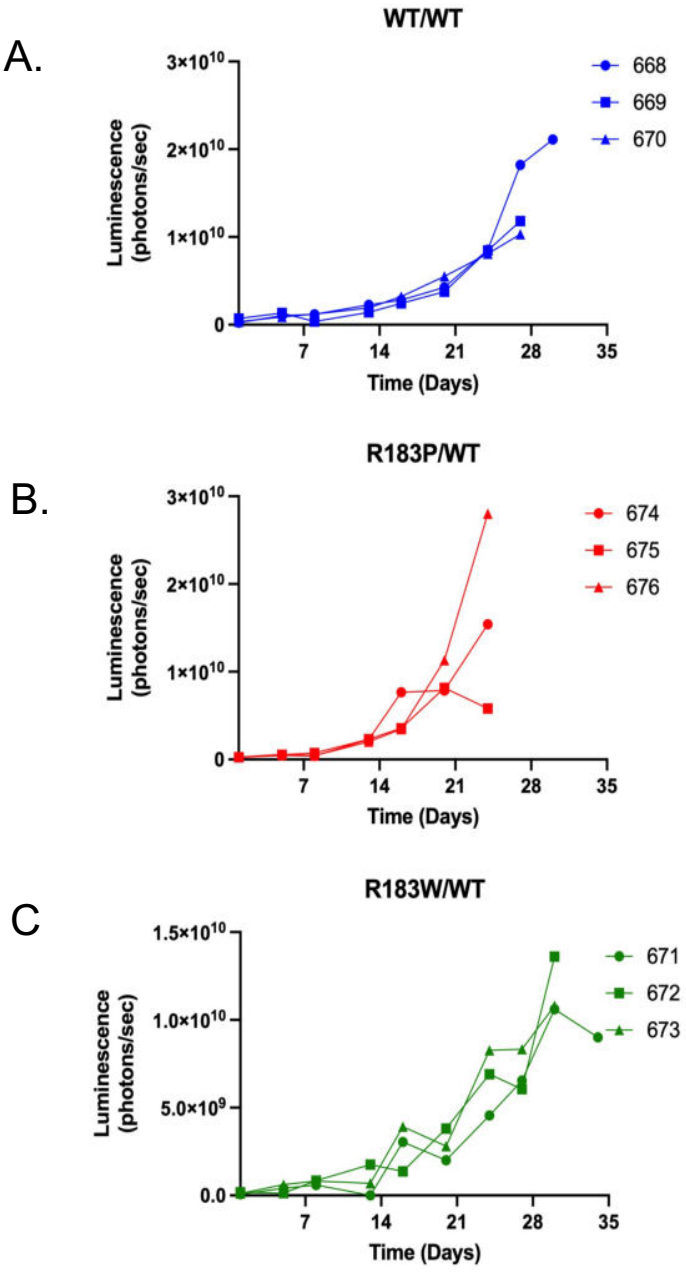

Figure 6.2 Luciferase expressing TOV21G PPP2R1A isogenic models successfully xenograft. Luciferase expressing TOV21G PPP2R1A WT (A), p.R183P (B) and p.R183W(C) cells successfully xenograft following intraperitoneal (IP) injection. 1 X 10^6 cells inoculated via IP injection on day 0. Tumour burden assessed by the IP injection of luciferin (150 mg/kg) followed by IVIS imaging after 10 minutes. Tumour burden assessment performed 24 hours after tumour cell inoculation and bi-weekly thereafter. Mice culled due to abdominal distension (ascites), poor body condition or > 20% weight loss compared to baseline.

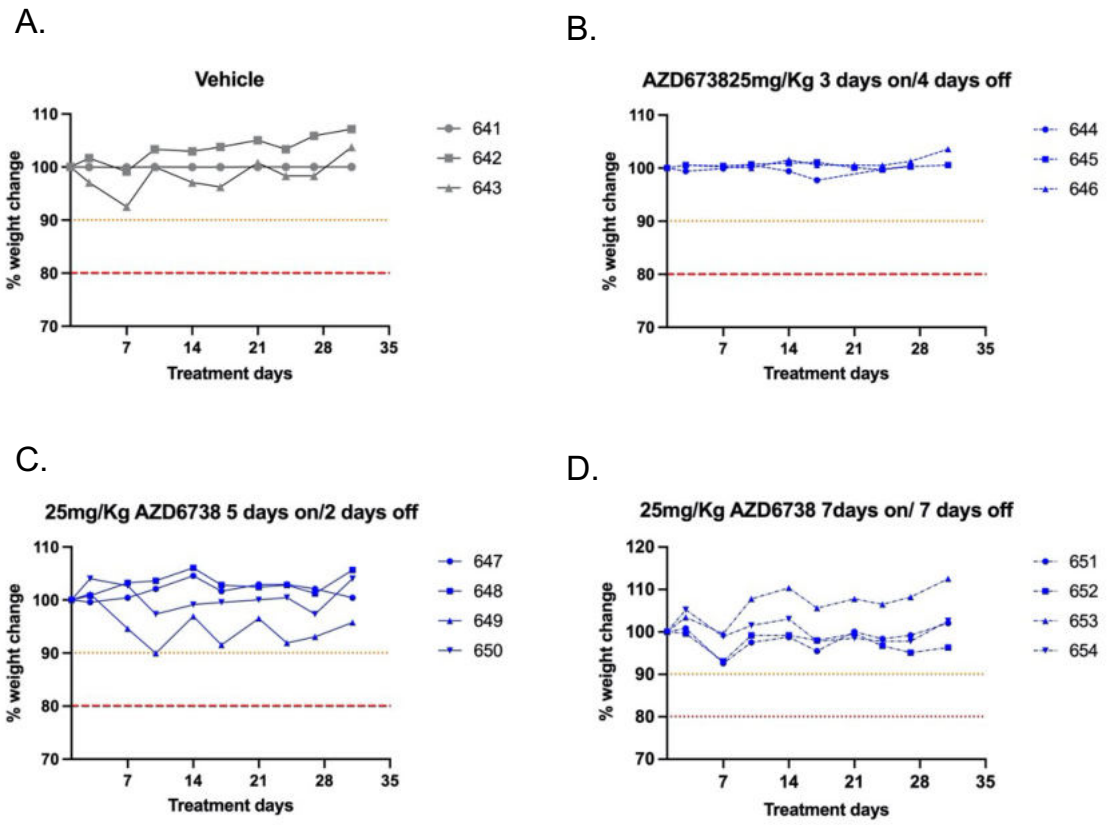

Figure 6.3 AZD6738 25mg mg/kg, using cycles of five days on treatment followed by two days break was selected for the full in vivo study. Vehicle (A) or AZD6738 25 mg/kg given in 3 days on/4days off (B), 5 days on/2 days off(C) and 7 days on/days off (D) schedules for 30 days. Orange dashed line represents 10% weight loss relative to baseline, the threshold for extra monitoring. The red dashed line represents 20% weight loss, the threshold for culling. All regimes tolerare without >10% weight loss for any individual animal

AZD6738 has been associated with toxicity when used in mice for *in vivo* studies (Astrazeneca, personal communication, June 2021). A variety of AZD6738 doses and schedules have been reported in the literature (Checkley, MacCallum et al. 2015, Vendetti, Lau et al. 2015, Wallez, Dunlop et al. 2018, Qiu, Fa et al. 2020). As TOV21G OCC cells have an *ARID1A* loss-of-function mutation and are somewhat sensitive to ATRi, both *in vitro* and *in vivo* (Williamson, Miller et al. 2016), a relatively low dose of AZD6738 (25mg/kg) was selected to maximise the chance of seeing an increase in ATRi sensitivity in the context of a pre-existing ARID1A/ATRi synthetic lethality. Several dosing schedules were trialled, all of which were tolerated without >20% weight loss, a pre-defined threshold for culling (Figure 6.3). Ultimately, AZD6738 25mg mg/kg, using cycles of five days on treatment followed by two days break was selected for the full *in vivo* study.

6.4 PPP2R1A mutations enhance ATRi sensitivity *in vivo*

In order to assess whether PPP2R1A/ATRi synthetic lethality operated *in vivo,* I designed a xenograft and therapy experiment shown in Figure 6.4.

In this experiment, TOV21G cells and the daughter clones with a heterozygous *PPP2R1A* p.R183P or p.R183W mutations were transplanted into recipient mice. To model local metastasis in OCC, these cells were introduced into the peritoneal cavity of mice and tumour growth was monitored by IVIS-based luminescence. After tumours had established, tumour bearing animals were treated with AZD6738 or the drug vehicle DMSO and monitored tumour volume for 17 days. Given that the cell line xenografts displayed different growth kinetics in the pilot experiment (Figure 6.2) a fold change luminescence relative to a measurement

taken 24 hours prior to treatment inititation was calculated. In keeping with previous literature, the development of ascites in this orthotropic xenograft model rendered the measurement and interpretation of luminescence beyond 17 days unreliable (Baert, Verschuere et al. 2015).

I found that when compared to vehicle treatment, this low dose ATR inhibitor treatment had minimal effects on tumour growth in the absence of a *PPP2R1A* mutation but significantly suppressed tumour growth in the presence of a PPP2R1A mutation (two-way ANOVA, $p < 0.05$) (Figure 6.5 and 6.6). For both the TOV21G *PPP2R1A* p.R183P and p.R183W models a significant reduction in luminescence was observed from day 10 onwards (Figure 6.7). As expected, this low dose ATRi treatment had minimal effects on animal body weight or condition (Figure 6.8).

6.5 Treatment with AZD6738 improves survival irrespective of PPP2R1A status

Although the development of ascites in this orthotopic mouse model precluded IVIS imaging beyond day 17 of treatment, mice continued to be monitored for survival analysis. Mice were culled due to poor body condition, development of ascites or change in health status due to abdominal tumours. As previously discussed, TOV21G cells harbour a loss-of-function *ARID1A* mutation and have

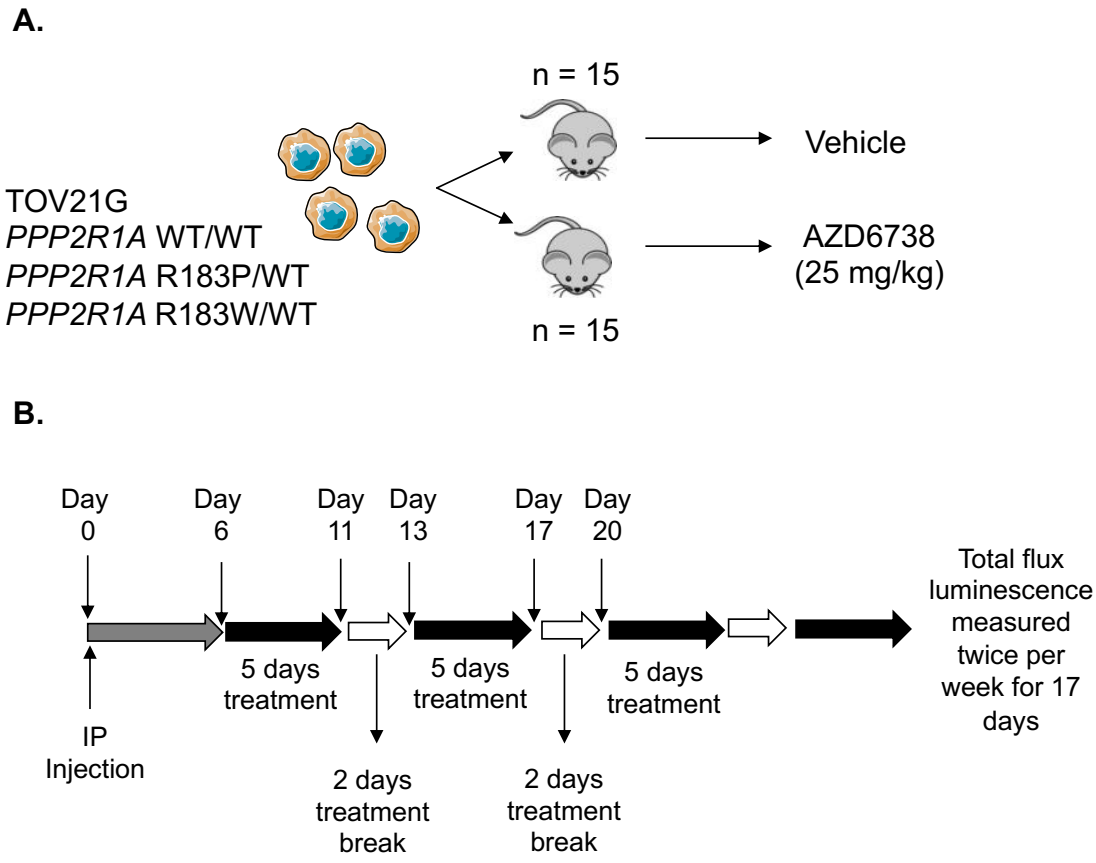

Figure 6.4 In vivo study schema. (A) *In vivo* schema. 1 x 10^6 Luciferase expressing TOV21G PPP2R1A WT, p.R183P and p.R183W injected into the peritoneum of BALB/c athymic mice and treated with either vehicle (n=15) of AZD6738 25 mg/kg (n=15). (B) Treatment schedule for the *in vivo* study described in (A). IP injection performed on day 0. Treatment initiated on day 6. Mice treated with either vehicle or AZD6738 25 mg/kg using cycles of five days on treatment followed by two days break. Tumour burden assessed via IVIS imaging bi-weekly for 17 days.

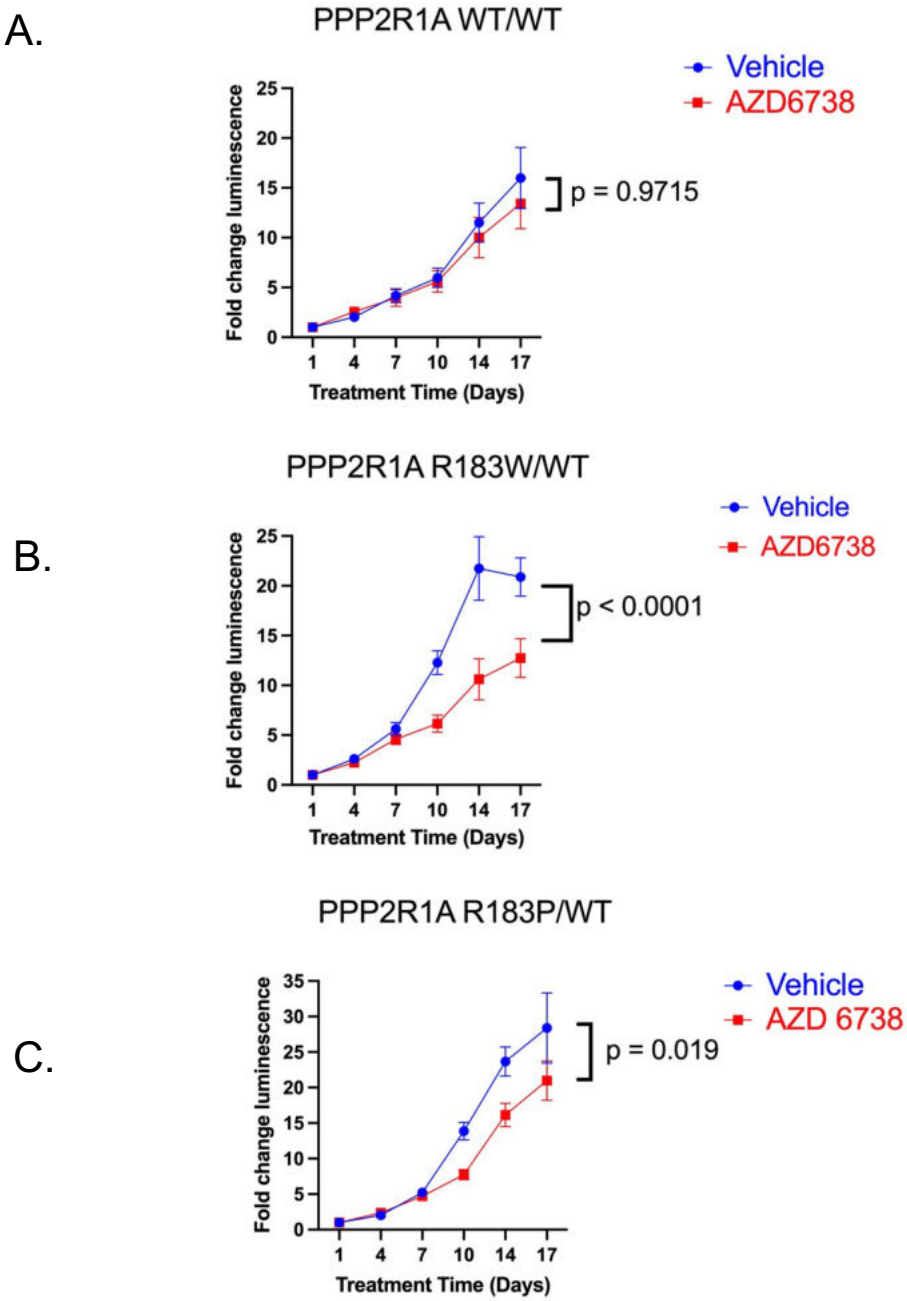

Figure 6.5 Treatment with AZD6738 impairs the growth of PPP2R1A mutant tumours but not WT. Line plots showing fold change in luminescence compared to pre-treatment level for TOV21G PPP2R1A WT (A), p.R183W (B) and p.R183P (C) cells. Error bars represent SEM. Significance determined by two-way ANOVA.

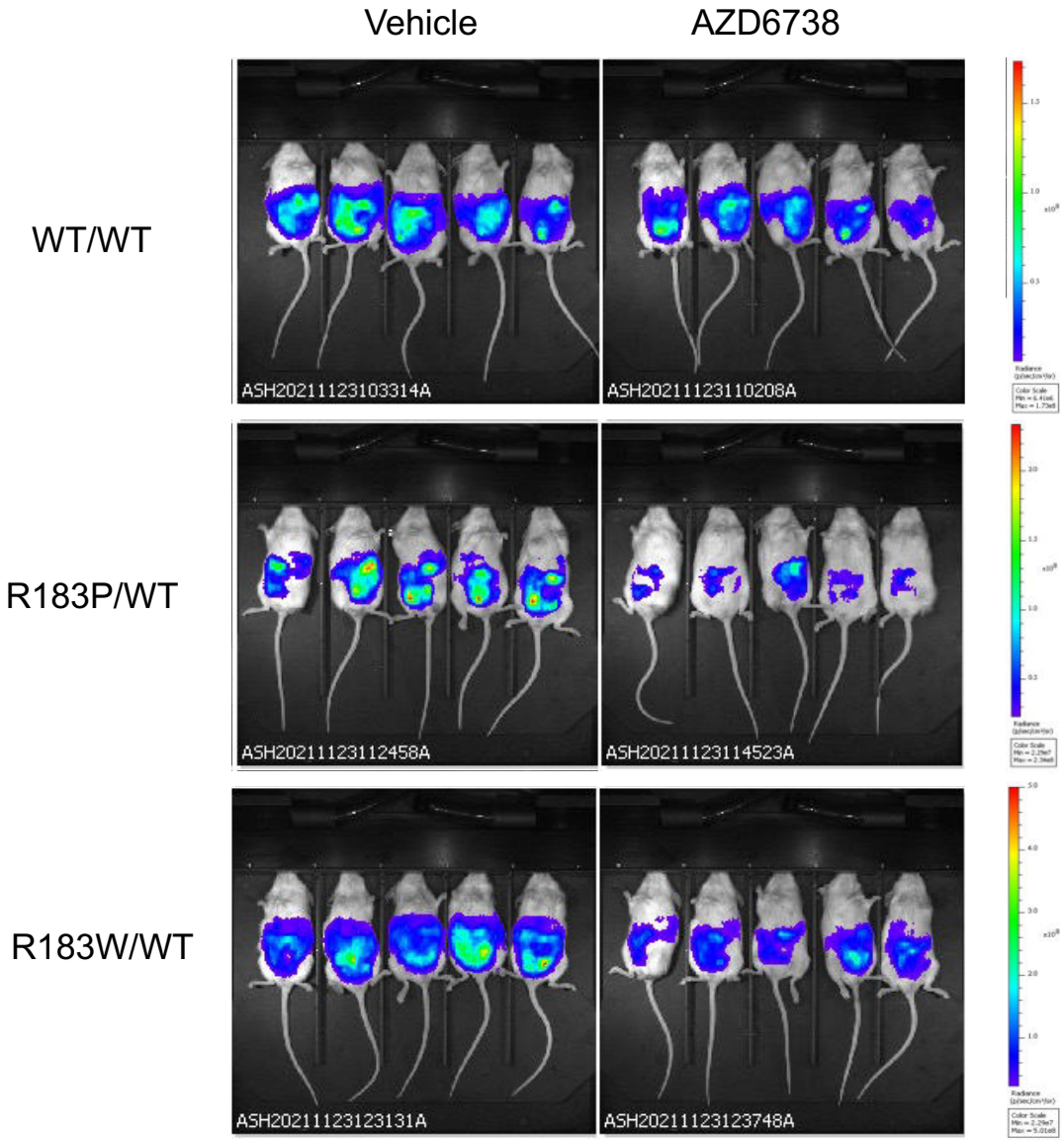

Figure 6.6 Treatment with AZD6738 impairs the growth of PPP2R1A mutant tumours but not WT (Continued). Representative images of vehicle and AZD6738 treated mice taken 14 days post initiation of treatment.

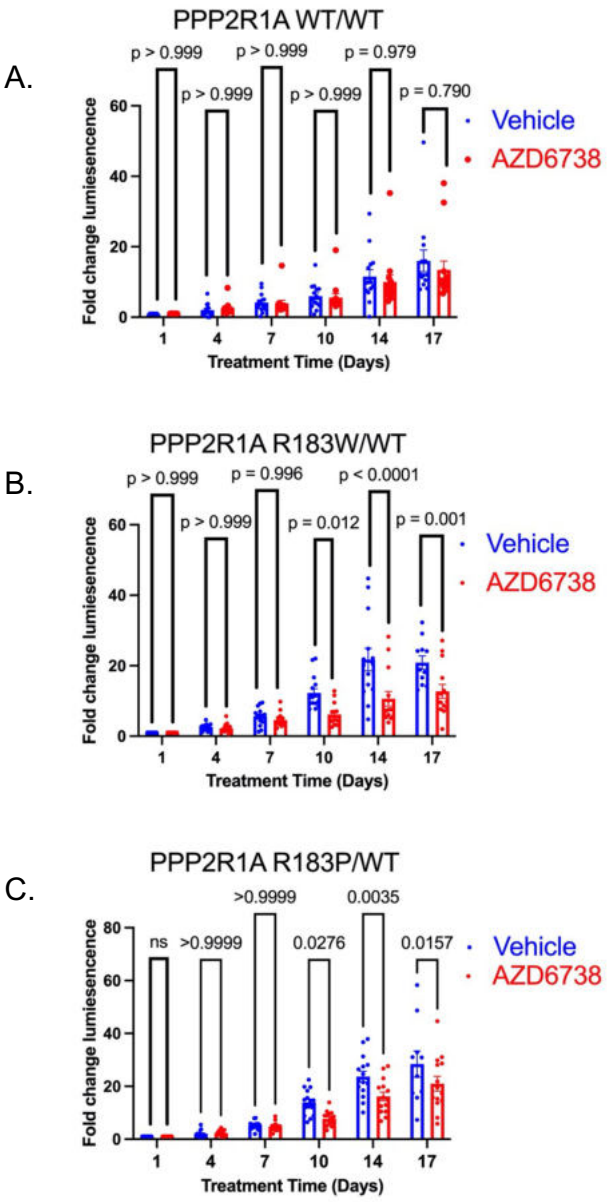

Figure 6.7 Treatment with AZD6738 limits growth of PPP2R1A mutant cells from day 10 onwards. Histogram showing the fold change luminescence for compared to pre-treatment level for TOV21G PPP2R1A WT (A), p.R183W (B) and p.R183P (C) cells in each arm. Error bars represent SEM. Pair-wise significance determined via two-way ANOVA with Šídák correction for multiple comparisons.

been shown to be sensitive to the ATRi VX970 *in vivo (Williamson, Miller et al. 2016)*. Treatment with AZD6738 resulted in significantly increased survival (Mantel-Cox test, $p < 0.05$) for all three genotypes Figure 6.9).

6.6 Chapter 6 Discussion

Using the TOV21G *PPP2R1A* isogenic models generated and characterised in previous chapters I developed an orthotopic xenograft model of OCCC. Treatment with the ATRi AZD6738 significantly reduced the tumour burden resulting from the inoculation of *PPP2R1A* mutant cells but not WT as assessed by IVIS imaging. Significantly longer survival was observed with AZD6738 treatment compared to vehicle irrespective of the *PPP2R1A* genotype of the xenotransplanted cells.

The primary focus of the work described within this thesis is the identification of prognostic biomarkers for ATRi response in ARID1A mutant OCCC, thereby helping to rationalise the future use of this class of drug. In proposing *PPP2R1A* mutations as such a biomarker, one must be mindful of the magnitude of benefit observed. Although the difference between tumour growth in the AZD6738 and vehicle treated arms for the *PPP2R1A* p.R183P and p.R183W models reached statistical significance, it should be noted that all xenografted tumours continued to progress despite treatment with ATRi. However, a relatively low dose of

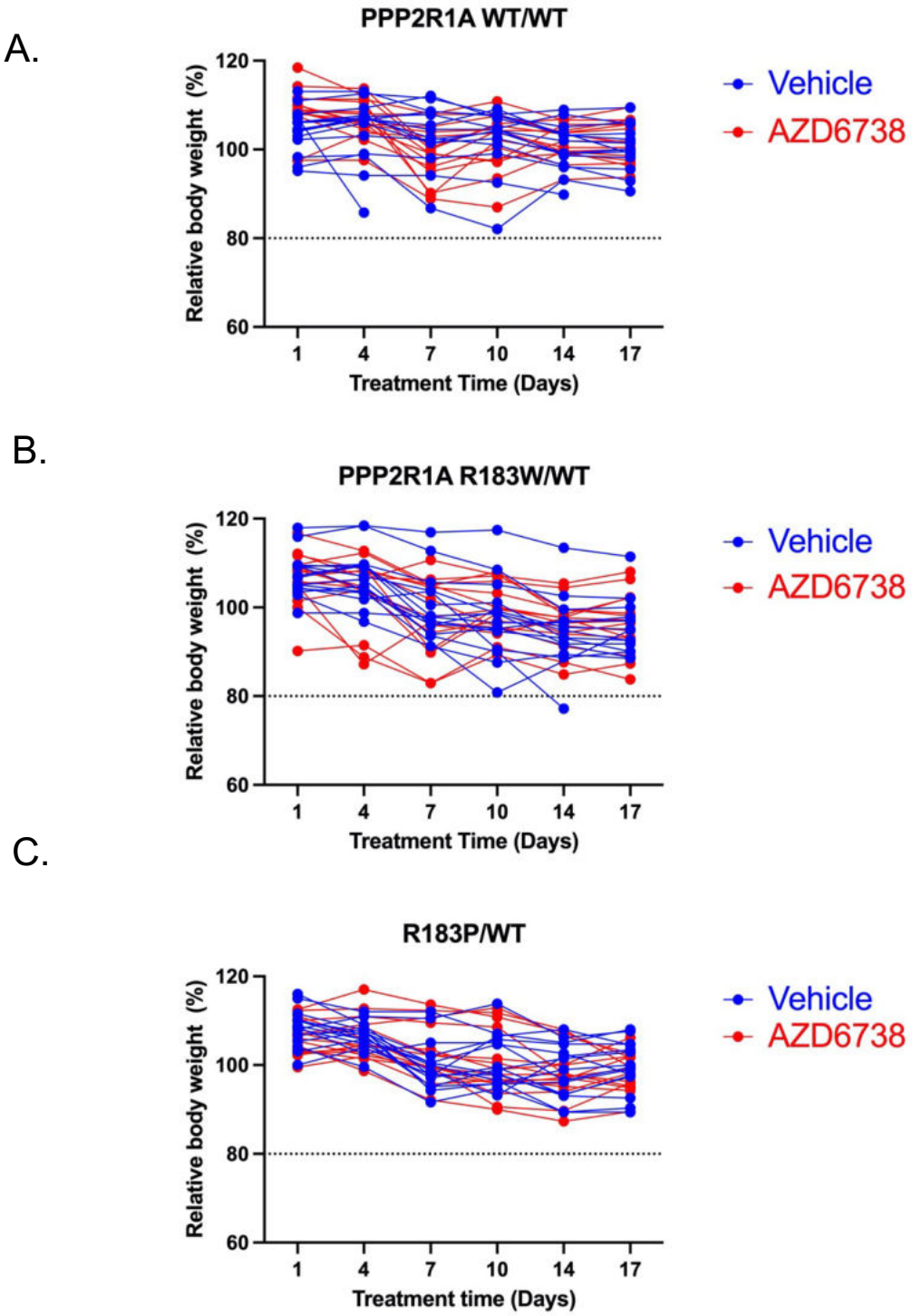

Figure 6.8 Low dose ATRi treatment had minimal effects on animal body weight. Body weight of each animal expressed relative to body weight at time of IP injection of tumour cells. One animal in the vehicle treated TOV21G PPP2R1A p.R183W group (B) culled due to >20% weight loss.

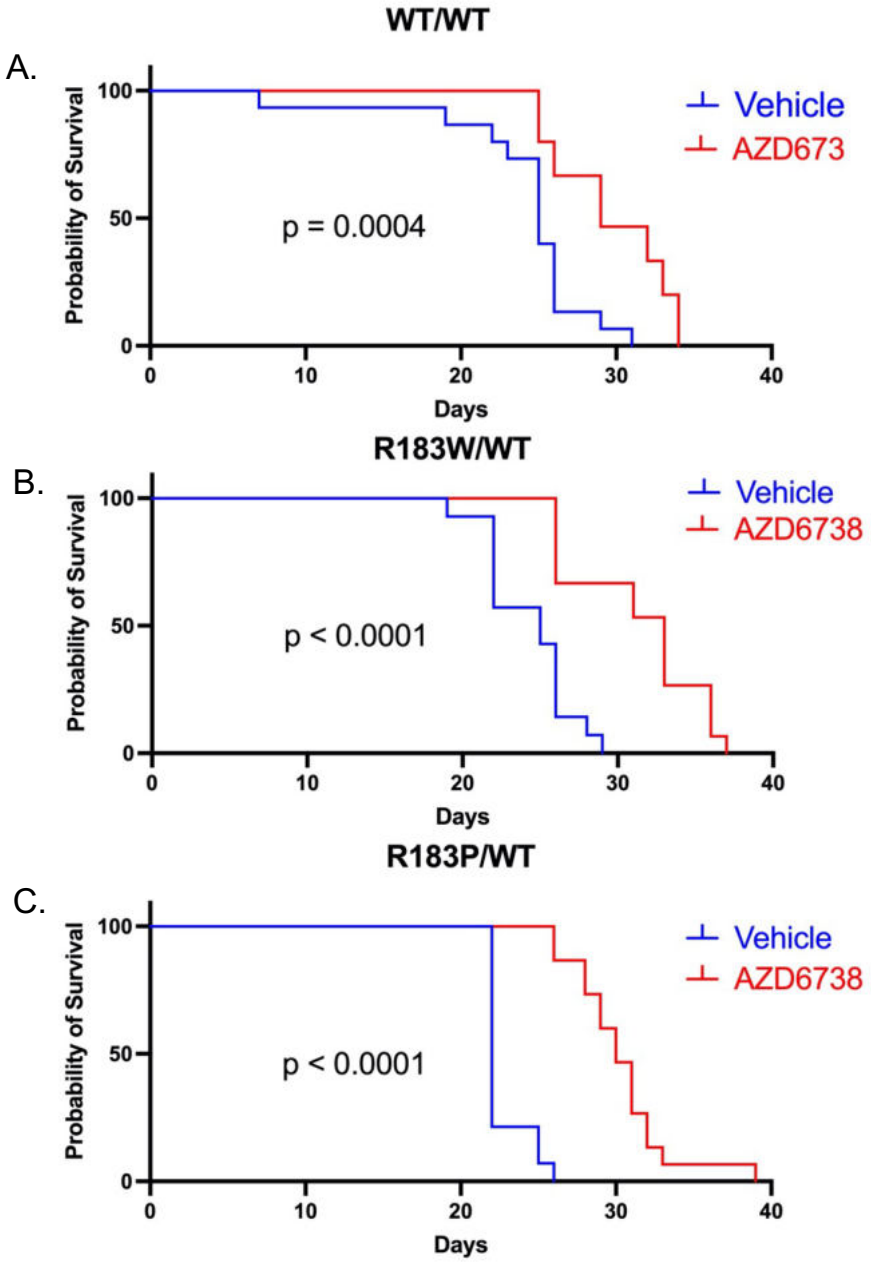

Figure 6.9 Treatment with AZD6738 results significantly improves survival irrespective of PPP2R1A genotype. Kaplan-Meier curves for mice inoculated with TOV21G PPP2R1A WT (A), p.R183W (B) or p.R183P(C) cells. Significance determined via Mantel-Cox test.

AZD6738 was used in this study compared to those published in the literature. This dose level was selected to increase the likelihood of observing synthetic lethality between PPP2R1A and ATR in the context of an *ARID1A* mutant background. Furthermore, the observed response to ATRi in the *PPP2R1A* mutant models was comparable to that reported in the publications which first identified ATR/ARID1A synthetic lethality (Williamson, Miller et al. 2016) and reported the therapeutic potential of dasatinib in ARID1A-deficient OCCC (Miller, Brough et al. 2016) both of which involved the xenotransplantation of unmodified TOV21G cells. The apparent low magnitude of benefit observed with drug treatment across all three *in vivo* studies perhaps reflects the aggressive nature of the TOV21G orthotopic xenograft model.

In keeping with previous literature (Baert, Verschuere et al. 2015), the development of ascites in this *in vivo* experiment rendered the assessment of tumour burden via IVIS imaging unreliable beyond 17 days of treatment. One unexpected observation from the *in vivo* study described in this chapter was the significantly improved survival of the mice inoculated with TOV21G *PPP2R1A* WT cells with AZD6738 compared to vehicle despite no significant reduction in tumour growth as assessed by IVIS imaging. It should be remembered that some of the criteria for culling, such as poor body condition and abdominal distension, are somewhat subjective, raising the prospect that the survival analysis will be confounded by inter-animal variability. Furthermore, survival assessments in orthotopic xenograft models involving Intraperitoneal injection of tumour cells has been shown to be heavily impacted by the development of ascites, which was a

relatively stochastic event in the *in vivo* study presented in this chapter. *Baert et al* reported that, in the context of a mouse model of serous ovarian cancer involving the intraperitoneal injection of ID8 cells, intermittent abdominal paracentesis not only increased luminescence readings, but also led to significantly extended survival (Baert, Verschuere et al. 2015). Abdominal paracentesis was not performed as part of the *in vivo* study presented in this chapter. Given that abdominal distention acted as predefined criterion for culling animals, variability in the development of ascites between animals could also have confounded survival analysis. Due to the potential issues with the survival analysis as outlined, assessment of tumour burden via IVIS imaging was selected as the main end point for assessing the impact of *PPP2R1A* mutations on the ATRi response.

Data presented in this chapter suggests that the observation of the synthetic lethal interaction between PPP2R1A and ATR is not limited to *in vitro* settings but can also be seen in *in vivo* model systems. Potential future work could explore whether pharmacological inhibition of WNK1 could rescue the ATRi sensitivity of *PPP2R1A* mutant cells *in vivo*. WNK-IN-11 is an allosteric inhibitor reported to possess high levels of specificity for WNK1 compared to other WNK family proteins (Yamada, Levell et al. 2017) and could be utilised to this end in a future *in vivo* approach.

Chapter 7. Overall discussion

7.1 Summary of work

OCCC represents a great unmet need in the treatment landscape of ovarian cancer. The relative rarity of OCCC and its unique molecular features compared to HGSOC, together with an inherent resistance to standard cytotoxic chemotherapy and a lack of approved targeted agents, all lead to the outcomes for women diagnosed with advanced OCCC being significantly worse than for women diagnosed with other EOC subtypes. The identification of a novel synthetic lethal interaction between ARID1A and ATR (Williamson, Miller et al. 2016) offers a promising therapeutic approach for women diagnosed with OCCC given that LOF *ARID1A* mutations are observed in approximately 50% of cases. The activity of ATRi is currently being assessed in the phase II, proof-of-concept trial ATARI (NCT04065269) (Banerjee, Stewart et al. 2021) with the results eagerly awaited.

In order to understand what, in addition to ARID1A status, might determine responses to ATRi in OCCC, my work in this area was initiated by a genome-wide CRISPRn ATRi chemosensitisation screen in an *ARID1A* mutant OCCC cell line (Chapter 3). Although other CRISPR-Cas9 screens for ATRi sensitivity/resistance have been carried out (Ruiz, Mayor-Ruiz et al. 2016, Hustedt, Alvarez-Quilon et al. 2019) , none have been in *ARID1A* mutant OCCC tumour cells. The *ARID1A* mutant/OCCC context of my screen seemed an important feature of my work, given that the variable penetrance of synthetic

lethal interactions in cancer can in part be explained by cell type specific variations in gene regulatory and signalling networks, many of which likely be controlled by the presence or absence of particular cancer driver genes (Ryan, Bajrami et al. 2018). Cross referencing the data generated from my own screens with similar CRISPR screens published in the literature, I identified genes previously implicated in both ATRi resistance, namely CDK2 (Ruiz, Mayor-Ruiz et al. 2016), and sensitivity, including *POLE3* and *POLE4* (Hustedt, Alvarez-Quilon et al. 2019*)*, indicating that the screen functioned as intended. Genes encoding several PP2A subunits, including *PPP2R2A* and *PPP2CA,* were identified as ATRi response genes. In order to ensure that this effect was not private to the TOV21G cell line, and before genes were taken forward for further interrogation, data generated from four independent genome-wide CRISPRn and CRISPRi screens, performed with the ATRi VX970 and AZD6738, in the molecularly distinct breast epithelial cell line MCF10A were examined (Chapter 3). Genes encoding multiple PP2A subunits were again identified, suggesting the synthetic lethal interaction between PP2A and ATR, although operating in the context of ARID1A mutant OCCC, was also a more generalisable effect, operating as it did in a variety of molecular settings.

The existence of a synthetic lethal interaction between ATR and PP2A was supported by two reports published during the course of this project. Qiu *et al* used an orthogonal shRNA screening approach in pre-clinical models of non-small cell lung cancer, finding the silencing of several genes encoding PP2A subunits resulted in ATR and CHK1 inhibitor sensitivity (Qiu, Fa et al. 2020).

Mechanistically this phenotype was attributed to elevated MYC expression an established cause of replication stress and ATRi sensitivity (Dominguez-Sola, Ying et al. 2007, Qiu, Fa et al. 2020). In another report CRISPR mutagenesis of *FAM122A* resulted in PP2A activation, which in turn leads to increased WEE1 phosphorylation, thereby protecting it from proteasomal degradation (Li, Kozono et al. 2020). Elevated total WEE1 was associated with reduced replication stress and resistance to CHK1i (Li, Kozono et al. 2020). Conversely, and consistent with the screen data presented in Chapter 3, reduced PP2A function would be assumed to be associated with reduced WEE1 levels, increased replication stress and, ATRi sensitivity (Li, Kozono et al. 2020).

I was led to focus on this complex due to the data generated from the genome wide screens summarised in Chapter 3, together with the published literature regarding a potential synthetic lethal interaction between PP2A and ATR (Li, Kozono et al. 2020, Qiu, Fa et al. 2020) and the previous reports that heterozygous *PPP2R1A* mutations are a relatively common observation in OCCC (Jones, Wang et al. 2010, Shih Ie, Panuganti et al. 2011, Kim, Lee et al. 2018). In the context of OCCC, *PPP2R1A* mutations cluster around residue R183 (Jones, Wang et al. 2010), leading to amino acid substitutions where the scaffolding subunit interfaces with the regulatory subunit, suggesting they may function as driver mutations. Taylor *et al* demonstrated that when p.R183 mutant PPP2R1A was expressed from a lentiviral vector it resulted in reduced incorporation of the regulatory (PPP2R2A) and catalytic (PPP2CA) subunits and reduced PP2A phosphatase activity (Taylor, O'Connor et al. 2019). Given that CRISPR

mutagenesis or interference of both PPP2R2A and *PPP2CA* was associated with increased ATRi sensitivity I hypothesised that the introduction of heterozygous *PPP2R1A* missense mutations would have a similar ATRi sensitive phenotype. If the observed increase in ATRi sensitivity is specific to these mutations, or indeed if complete loss of *PPP2R1A* is lethal, this effect would not be observed in the CRISPRn screen.

At this juncture, it is worth noting the potential relevance of the PP2A-synthetic lethal interaction in the wider cancer context. Whilst the scope of this project is limited to OCCC the identification of multiple PP2A subunits from the genome-wide CRISPRn/i is pertinent to other tumour types. *PPP2R1A* missense mutations that would be expected to impact PP2A complex stoichiometry have been observed across endometrial cancer subtypes, with a prevalence of 35-39% in serous endometrial cancer (Zehir, Benayed et al. 2017, ICGC/TCGA 2020), 17-30% in endometrial carcinosarcoma (Zehir, Benayed et al. 2017, ICGC/TCGA 2020), 21% in endometrial clear cell carcinoma (ICGC/TCGA 2020) and 10-13% of endometroid endometrial cancer (Zehir, Benayed et al. 2017, ICGC/TCGA 2020). Beyond gynaecological cancers, deleterious *PPP2R1A* missense mutations suspected to disrupt PP2A assembly and function are observed in approximately 3% of colorectal cancer cases (ICGC/TCGA 2020). Deletions in *PPP2R2A* have been observed at high frequencies in non-small cell lung cancer (NSCLC) (17%), colorectal cancer (12%), bladder cancer (17%), serous ovarian cancer (11%) and breast cancer (11%) (ICGC/TCGA 2020). Additionally, *PPP2R2A* loss of heterozygosity has been reported to result in

reduced expression of the corresponding protein in 60% of prostate cancers, 46% of ovarian cancers, and 43% of lung adenocarcinomas (Kalev, Simicek et al. 2012). Finally, deletions impacting *PPP2CA* are observed in both oesophagogastric cancer (4%) and lung cancer (2%) (ICGC/TCGA 2020). Thus, the therapeutic potential of the PP2A-ATR synthetic lethal interaction may be relevant to a far wider range of cancers than those within this thesis.

It should also be noted the co-occurrence of truncating loss of function *ARID1A* mutations and *PPP2R1A* missense mutations is not limited solely to OCCC being also seen in endometrial CCC. Although *PPP2R1A* is found in a higher proportion of serous endometrial cancer compared to the most common endometroid subtype, the co-occurrence of ARID1A and PPP2R1A does occur in the later (ICGC/TCGA 2020). Given that approximately 90% of endometrial cancer cases are of the endometroid subtype, this could greatly increase the number of patients for which the data presented in this thesis is pertinent to. The co-occurrence of *PPP2R1A* and *ARID1A* mutations is also observed at a much lower frequency of advanced colorectal cancer cases (Yaeger, Chatila et al. 2018). *ARID1A* and *PPP2R1A* encode components of multi-subunit complexes, namely cBAF and PPP2R1A respectively. In bladder cancer, truncating mutations in *ARID1A* are observed in 19% of cases with 5% of these also displaying deletions in *PPP2R2A (ICGC/TCGA 2020)*. *SMARCA4* encodes the ATPase subunit of the cBAF, PBAF and ncBAF complexes (Chabanon, Morel et al. 2020). Mutations predicted to have a deleterious effect on SMARCA4 function have been observed in 4% of non-small lung cancer cases, with 4 % of these also carrying a deletion in

PPP2R2A (Campbell, Alexandrov et al. 2016). The work contained in this thesis may therefore be relevant to a wider number of tumour types and be worthy of further exploration in subsequent work.

Given the relatively low patient numbers included in the case series which previously reported the prevalence of *PPP2R1A* mutations in OCCC, and in order to establish the rate at which they co-occur with *ARDI1A* mutations in this tumour type, in Chapter 4, I performed *PPP2R1A* genotyping on an independent cohort of OCCC patients, the *ARID1A* mutation status of which was already established (Khalique, Nash et al. 2021). This analysis revealed a higher prevalence (52%) than previously reported and importantly, these mutations were often observed in cases which also harboured an *ARID1A* mutation. The explanation for the higher *PPP2R1A* mutation rate amongst the cohort described in Chapter 4 compared to those from previously published case series (7-20%) (Jones, Wang et al. 2010, Shih Ie, Panuganti et al. 2011, Kim, Lee et al. 2018) is not entirely clear. This discrepancy may simply reflect the expected variations between case series involving low numbers of patients. However, potential explanations include differences in the genetic background of the patients included and the rates of endometriosis. Indeed, two groups have employed whole exome sequencing of endometriotic lesions to assess the prevalence of cancer-associated mutations even when no malignancy is present (Anglesio, Papadopoulos et al. 2017, Zou, Zhou et al. 2018). In both studies heterozygous *PPP2R1A* missense mutations were detected in invasive endometriotic lesions which were not present in the adjacent tissue (Anglesio, Papadopoulos et al. 2017, Zou, Zhou et al. 2018).

Determining whether PPP2R1A mutations are more commonly observed in cases of OCCC arising from endometriosis would require both a larger patient cohort as well as a detailed history of any endometriosis.

The first reported use of CRISPR prime gene editing as a means to introduce precise DNA sequence changes without the need to produce DSBs or provide a donor DNA template was made during the course of this project (Anzalone, Randolph et al. 2019). This afforded me the opportunity to impose heterozygous *PPP2R1A* missense mutations on an *ARID1A* mutant OCCC model, TOV21G. As far as I am aware, this is the first instance in which recurrent *PPP2R1A* missense mutations have been modelled by altering the coding sequence of the endogenous gene. The advantage of this approach is that expression of the mutated gene, in this case *PPP2R1A,* remains under the control of its endogenous promoter, thereby ensuring physiological levels of expression. In contrast, the studies which described the impact of *PPP2R1A* missense mutations on PP2A complex stoichiometry and function (Taylor, O'Connor et al. 2019) and drug (RNRi, MEKi) (O'Connor, Leonard et al. 2020, O'Connor, Taylor et al. 2022) have placed the expression of either WT or mutant PPP2R1A under the control of the CMV promoter, an approach which does not guarantee a biologically relevant level of transcription.

Whilst CRISPR prime gene editing remains an enormously powerful tool for modelling the cancer phenotype, the efficiency with which the desired sequence change can be introduced acts a significant barrier to its use. 0.5% of the screen

clones carried a *PPP2R1A* p.R183P mutation and this figure dropped to 0.25% for the p.R183W model. This low editing efficiency acted as a barrier to the number of models that could be generated using this approach. In contrast, Anzalone *et al* report an editing efficiency of 11 - 39% across all types of point mutations at six distinct genomic sites (Anzalone, Randolph et al. 2019). However, HEK-293 cells, an immortalised embryonic kidney epithelial cell line, were utilised in the study which first reported on the use and efficient of CRISPR prime gene editing (Anzalone, Randolph et al. 2019).HEK-293 cells are widely used throughout cell biology due to the high transfection efficiency associated with their use by a variety of techniques (Thomas and Smart 2005, Cheng, Mitchell et al. 2015). It is perhaps unsurprising that a lower editing efficiency is observed in different cell line models, given that three individual plasmids need to be transfected in order to deliver all the components of the CRISPR prime machinery. A more recent iteration of the CRISPR prime editing system entailed the co-transfection of a dominant negative MutL protein homolog 1 (MLH1) which reduced the cell's inherent ability to perform DNA mismatch repair, increasing the editing efficiency up to 7.7 fold compared to previous versions of the technology (Chen, Hussmann et al. 2021). This updated system could be employed in future work to model the *PPP2R1A* mutations in a more diverse set of genetic backgrounds, including *ARID1A* WT settings, in order to assess their impact on various aspects of the cancer phenotype.

Using the approach described above, a *PPP2R1A* isogenic model of the *ARID1A*-mutant OCCC cell line TOV21G was created. Two daughter clones harbouring

either a *PPP2R1A* p.R183P or p.R183W mutations demonstrated increased sensitivity to AZD6738 *in vitro* when compared to their WT counterpart. The ATRi-sensitive phenotype of the *PPP2R1A* mutant TOV21G models was recapitulated *in vivo* as described in Chapter 6. No formal assessment for off-target editing was made or was practicable due to the potential for it to occur throughout the entire genome. However, the observation that two independent pegRNAs designed to introduce different amino acid substitutions resulted in the ATRi sensitive phenotype, increases confidence that it is not a result of some off target effect. Rescue of the ATRi sensitive phenotype by selectively inactivating the mutant allele, for example using CRISPR-mediated mutagenesis, would provide an experiment approach to further increase confidence that the phenotype is indeed a consequence of the introduction of the *PPP2R1A* mutations.

In this model system, the synthetic lethal interaction between ATR and PPP2R1A in *ARID1A* mutant cells was characterised by a decrease in cells replicating S phase of the cell cycle, an increase in cells entering mitosis with sub-4n genomic content, and the accumulation of 53BP1 bodies. Neither elevated Myc levels nor reduced WEE1 levels could provide a trivial explanation for the ATRi sensitive phenotype. Mechanistically, this synthetic lethal effect and the cell cycle effects of ATRi appear to be dependent upon the kinase WNK1, which was implicated in this synthetic lethal interaction via the integration of data generated from a siRNA screen and phosphoproteomic profiling, and itself exhibits increased phosphorylation in *PPP2R1A* mutant OCC cells. Depletion WNK1 rescued ATRi sensitivity in *PPP2R1A* p.R183 mutant cells but not WT cells. Indeed, silencing

of WNK1 restored the replicating S phase population normally depleted by ATRi, implying that it is the main cause of the ATR-PPP2R1A synthetic lethal interaction. Exposure to ATRi can reduce the S population via the unscheduled firing of dormant origins of replication (Moiseeva, Hood et al. 2017, Moiseeva, Yin et al. 2019) with the ensuing depletion of cellular pools of nucleotides (Le, Poddar et al. 2017, Koppenhafer, Goss et al. 2020) and RPA (Toledo, Altmeyer et al. 2013, Yin, Lee et al. 2021) together with replication fork collapse (Saldivar, Cortez et al. 2017). The precise mechanism through which *PPP2R1A* missense mutations exacerbate the ATRi-induced reduction in the replicating S phase population remains to be established but could result from increased RPA2 phosphorylation (Wang, Zhu et al. 2018) and disruption of the replisome composition (Perl, O'Connor et al. 2019).

Data presented in Chapter 5 proposes that the synthetic lethal interaction between PPP2R1A and ATR is dependent on WNK1. Increased WNK1 phosphorylation in *PPP2R1A* mutant cells following ATR inhibition is assumed to result in its activation given the increase in phosphorylation of its target residue on OSR1. Depletion of WNK1 in *PPP2R1A* mutant cells restores the replicating S phase population in response to ATR inhibition and rescues the ATRi sensitive phenotype in these model systems. To date, the function of WNK1 has been most extensively explored in the context of the cell's response to hyperosmolar stress and in cases of familial hypertension (Wilson, Disse-Nicodeme et al. 2001, Vitari, Thastrup et al. 2006, Susa, Sohara et al. 2014). WNK1 has hitherto not been linked to ATR signalling, the response to ATRi or DNA replication. Data presented

in this thesis does not provide a mechanistic explanation as to how increased WNK1 activity mediates the ATRi response. Further phosphoproteomic profiling and cross referencing of this data with existing CRISRP data may identify the WNK1 substrate responsible for this phenotype. Alternatively, a hypothesis driven approach could be adopted to address whether WNK1 gene silencing reverses the aforementioned mechanisms through which ATRi cause a reduction in the replicating S phase population, namely suppression of non-dominant origins or replication, maintaining cellular pools of nucleotide and RPA and stabilizing replication forks,

7.2 Future directions

The work presented in this thesis suggests that the presence of *PPP2R1A* missense mutations enhances ATRi sensitivity in OCCC tumour cell line models with pre-existing *ARID1A* mutations. I therefore hypothesize that the co-occurrence of these two cancer driver mutations may be a better predictor of ATRi sensitivity than the presence of either mutation alone. Clinical samples provided through the ATARI trial and outcome data, once available, will provide the means to address this hypothesis.

Pre-treatment tissue samples, either archival samples or fresh biopsies where this is not available, have been collected for all patients undergoing screening to enter ATARI. Whole exome sequencing of tumour genomic DNA from these samples will provide an orthogonal route to determine the prevalence of

PPP2R1A missense mutations and their relationship with *ARID1A* mutations in OCCC but also in a range of other gynaecological malignancies recruited to cohort 3. Correlation of sequencing data with clinical outcome data may allow us to determine whether the ATR-PPP2R1A synthetic lethal interaction observed *in vitro* and *in vivo* also results in improved clinical outcomes in patients.

It is my hope that this work will be able to refine the ATRi response biomarker to improve how this class of drug is used in the future treatment of OCCC and other *PPP2R1A* mutant cancers. For instance, the ATARI protocol could be amended so that only patients with ovarian or endometrial clear cell carcinoma with loss of ARID1A expression and harbouring a PPP2R1A missense mutation would receive AZD6738 monotherapy, with the remaining patients being treated with the AZD6738/olaparib combination. An alternative approach would be to design a basket study for patients with cancers carrying both *ARID1A* mutations together with a *PPP2R1A* missense mutation, which could be expanded to include patients with cancers carrying defects in genes encoding both PP2A and PBAF subunits.

Cross referencing whole exome sequenced data from these pre-treatment specimens with CRISPR screen data generated as part of this thesis and published in the literature and clinical outcome data, affords the opportunity to identify novel genetic determinants of ATRi sensitivity and resistance. The availability of post-progression tissue biopsies arising through ATARI is limited due to a combination of patient preference, anatomical location of metastatic

OCCC largely in the peritoneal cavity and the aggressive nature of the disease. Liquid biopsies, i.e. the sampling of analytes from bodily fluids, most commonly blood, has enabled the longitudinal sampling treatment where serial tissue samples are not available (Pantel and Alix-Panabieres 2010, Kilgour, Rothwell et al. 2020). Next generation sequencing of circulating tumour DNA (ctDNA) has enabled the detection of *EGFR* mutations in cases of non-small cell lung cancers, which predict resistance to the tyrosine kinase inhibitors, gefitinib and osimertinib (Yu, Arcila et al. 2013) and *KRAS* mutations in colorectal cancer which predict resistance of EGFR-directed monoclonal antibodies (Yu, Xiao et al. 2013). A capture sequencing panel encompassing known and putative genetic determinants of ATRi resistance and sensitivity has been generated using CRISPR screen data produced during the course of this project and more widely by the Lord laboratory and published in the literature (Ruiz, Mayor-Ruiz et al. 2016, Hustedt, Alvarez-Quilon et al. 2019), Sequencing of ctDNA from serial on-treatment and post-progression plasma samples collected from patients enrolled in ATARI using this panel will provide another means to identify clinically meaningful biomarkers for ATRi resistance.

7.3 Final conclusions

At the time of completing this thesis, there remain no approved OCCC-specific targeted treatments. The results of ATARI will help guide whether ATRi have utility in the treatment landscape of OCCC, perhaps including *PPP2R1A* mutational status as a guide to patient selection. The results of several trials of

ICB are eagerly awaited whilst the full range of *ARID1A* synthetic lethal interactions have yet to be assessed in the context of clinical trials. Going forward, the challenge will not only be to assess which of these treatments demonstrate the greatest activity, but also how they should be sequenced to maximize patient benefit. It is entirely possible that a combination of these experimental strategies is needed. For instance, there is already rationale for augmenting the anti-tumour activity of ICB through combination with ATR inhibition (Sun, Yang et al. 2018, Dillon, Bergerhoff et al. 2019) and anti-angiogenic therapy (Allen, Jabouille et al. 2017), two therapies with potential in OCCC. Perhaps the greatest challenge will be the assessment of multiple potential therapies in a rare tumour type at a rate that can quickly improve outcomes for these patients. This may demand a rethink of the way in which clinical trials are designed. Rather than sequential trials, multi-arm modular clinical trials in which the activity of experimental therapies are assessed in parallel, allowing for the early termination of those drugs which display limited activity and the addition of novel treatments and combinations as they arise, may provide a means for more rapid drug development.

The success of any such novel therapy will rely on the identification of robust biomarkers to predict patients most likely to respond. In essence, the aim of this project was to pro-actively identify potential biomarkers for response to ATRi using CRISPR-Cas9, that could inform how ATARI will be interpreted. The advent of CRISPR-Cas9 technology has revolutionised our ability to model the cancer phenotype (Stewart, Banerjee et al. 2020) including drug sensitivity and resistance. However, it should be noted that know large sgRNA libraries are used,

we are in effect modelling the effect of one genetic alteration at a time. This oversimplifies the situation in cancer cells, where numerous driver and passenger mutations cooperate to promote cancer progression. The development of Cas12a, a modified Cas9 endonuclease with intrinsic RNA process abilities that facilitates simultaneous mutagenesis of multiple genes within the same cell from a single RNA transcript (Gier, Budinich et al. 2020), goes some way to address this shortcoming.

Finally, it is worth speculating on what the overarching challenges in the clinical development of ATRi might be. In general terms, novel personalised cancer treatments tend to have several “ideal” features. Firstly, these treatments should be able to elicit significant and sustained anti-tumour responses and a survival benefit, using dosing regimens that leave normal tissues relatively unaffected, i.e. they should possess a large therapeutic window. Secondly, these novel treatments should demonstrate a tolerable side effect profile so as to not have a detrimental impact on a patient’s quality of life. Thirdly, a biomarker or biomarkers should exist to distinguish patients most likely to benefit from those who will not. Even in phase I studies, ATRi were shown to elicit significant and sustained anti-tumour responses in isolated patients without delivering dose-limiting toxicity (Dillon, Guevara et al. 2019, Yap, O’Carrigan et al. 2020). Based on this promising phase I trial data, a plethora of phase II clinical trials have been initiated, despite the lack of robust predictive biomarkers for ATRi responses. What are the underlying reasons for the lack of such biomarkers? One simple explanation is that these phase II trials, including ATARI, are ongoing and data made

available through them may shed some light on the biomarkers needed to rationalise the use of ATRi in the future. However, it is also worth considering that the identification of ATRi predictive biomarkers may be more complex than, for example, the clinical PARPi that have been approved for use. This remains a possibility. For example, the burden of both pre-clinical and clinical data for the use of PARPi suggests that there is a singular driver for profound sensitivity, namely a defect in HR. This relatively stereotypic nature of PARPi sensitivity mechanisms has meant that explaining clinical responses to these agents, and thus the identification of predictive biomarkers, has been relatively simple. In comparison, a number of different drivers or ATRi sensitivity have been proposed including elevated replication stress caused by oncogene activation (e.g. Myc (Cottini, Hideshima et al. 2015), Cyclin E (Guerrero Llobet, van der Vegt et al. 2020, Xu, George et al. 2021)) defects in the composition of SWI/SNF complexes (e.g. ARID1A (Williamson, Miller et al. 2016), SMARCA4 (Kurashima, Kashiwagi et al. 2020)) or the increase in replication fork stress caused by the higher burden of transcription/replication conflicts (TRCs) in tumour cells (Hamperl, Bocek et al. 2017). Although each of these factors might drive a greater reliance upon ATR (and thus ATRi sensitivity) by causing some form of replication fork stress, these do so via different molecular routes. As such, the drivers of ATRi sensitivity, might be more varied than for drug classes such as PARPi.

The relative heterogeneity in drivers of ATRi sensitivity described above might in turn mean that ascribing anti-tumour responses in clinical trials to one particular driver difficult, especially when multiple driver events might be at play in any given

patient cohort. If such a scenario turns out to be the case, this might argue for the development of biomarkers that measure some form of cellular functionality. Indeed, determining cancers with high levels of replications stress whether this is caused by *ARID1A* mutations, elevated Cyclin E or other drivers, such as TRCs, as opposed to the development of a genomic biomarker, e.g. *ARID1A* or *PPP2R1A* mutation, may help to better identify patients most likely to benefit from ATRi.

Chapter 8. Reference List

Aarts, M., R. Sharpe, I. Garcia-Murillas, H. Gevensleben, M. S. Hurd, S. D. Shumway, C. Toniatti, A. Ashworth and N. C. Turner (2012). "Forced mitotic entry of S-phase cells as a therapeutic strategy induced by inhibition of WEE1." Cancer Discov **2**(6): 524-539.

Ablasser, A., M. Goldeck, T. Cavlar, T. Deimling, G. Witte, I. Rohl, K. P. Hopfner, J. Ludwig and V. Hornung (2013). "cGAS produces a 2'-5'-linked cyclic dinucleotide second messenger that activates STING." Nature **498**(7454): 380-384.

Academic, U. Community Cancer Research and I. National Cancer. (2022, September 30). "Olaparib in Treating Patients With Metastatic Biliary Tract Cancer With Aberrant DNA Repair Gene Mutations." Retrieved 20th July, 2022, from https://ClinicalTrials.gov/show/NCT04042831.

Ahel, D., Z. Horejsi, N. Wiechens, S. E. Polo, E. Garcia-Wilson, I. Ahel, H. Flynn, M. Skehel, S. C. West, S. P. Jackson, T. Owen-Hughes and S. J. Boulton (2009). "Poly(ADP-ribose)-dependent regulation of DNA repair by the chromatin remodeling enzyme ALC1." Science **325**(5945): 1240-1243.

Allen, E., A. Jabouille, L. B. Rivera, I. Lodewijckx, R. Missiaen, V. Steri, K. Feyen, J. Tawney, D. Hanahan, I. P. Michael and G. Bergers (2017). "Combined antiangiogenic and anti-PD-L1 therapy stimulates tumor immunity through HEV formation." Sci Transl Med **9**(385).

Allis, C. D. and T. Jenuwein (2016). "The molecular hallmarks of epigenetic control." Nat Rev Genet **17**(8): 487-500.

Alvarez-Fernandez, M., V. A. Halim, M. Aprelia, J. Laoukili, S. Mohammed and R. H. Medema (2011). "Protein phosphatase 2A (B55alpha) prevents premature activation of forkhead transcription factor FoxM1 by antagonizing cyclin A/cyclin-dependent kinase-mediated phosphorylation." J Biol Chem **286**(38): 33029-33036.

Amsailale, R., E. Van Den Neste, A. Arts, E. Starczewska, F. Bontemps and C. Smal (2012). "Phosphorylation of deoxycytidine kinase on Ser-74: impact on

kinetic properties and nucleoside analog activation in cancer cells." Biochem Pharmacol **84**(1): 43-51.

Anglesio, M. S., J. George, H. Kulbe, M. Friedlander, D. Rischin, C. Lemech, J. Power, J. Coward, P. A. Cowin, C. M. House, P. Chakravarty, K. L. Gorringe, I. G. Campbell, G. Australian Ovarian Cancer Study, A. Okamoto, M. J. Birrer, D. G. Huntsman, A. de Fazio, S. E. Kalloger, F. Balkwill, C. B. Gilks and D. D. Bowtell (2011). "IL6-STAT3-HIF signaling and therapeutic response to the angiogenesis inhibitor sunitinib in ovarian clear cell cancer." Clin Cancer Res **17**(8): 2538-2548.

Anglesio, M. S., N. Papadopoulos, A. Ayhan, T. M. Nazeran, M. Noe, H. M. Horlings, A. Lum, S. Jones, J. Senz, T. Seckin, J. Ho, R. C. Wu, V. Lac, H. Ogawa, B. Tessier-Cloutier, R. Alhassan, A. Wang, Y. Wang, J. D. Cohen, F. Wong, A. Hasanovic, N. Orr, M. Zhang, M. Popoli, W. McMahon, L. D. Wood, A. Mattox, C. Allaire, J. Segars, C. Williams, C. Tomasetti, N. Boyd, K. W. Kinzler, C. B. Gilks, L. Diaz, T. L. Wang, B. Vogelstein, P. J. Yong, D. G. Huntsman and I. M. Shih (2017). "Cancer-Associated Mutations in Endometriosis without Cancer." N Engl J Med **376**(19): 1835-1848.

Anselmo, A. N., S. Earnest, W. Chen, Y. C. Juang, S. C. Kim, Y. Zhao and M. H. Cobb (2006). "WNK1 and OSR1 regulate the Na+, K+, 2Cl- cotransporter in HeLa cells." Proc Natl Acad Sci U S A **103**(29): 10883-10888.

Anzalone, A. V., P. B. Randolph, J. R. Davis, A. A. Sousa, L. W. Koblan, J. M. Levy, P. J. Chen, C. Wilson, G. A. Newby, A. Raguram and D. R. Liu (2019). "Search-and-replace genome editing without double-strand breaks or donor DNA." Nature **576**(7785): 149-157.

Arino, J., C. W. Woon, D. L. Brautigan, T. B. Miller, Jr. and G. L. Johnson (1988). "Human liver phosphatase 2A: cDNA and amino acid sequence of two catalytic subunit isotypes." Proc Natl Acad Sci U S A **85**(12): 4252-4256.

Ashley, A. K., M. Shrivastav, J. Nie, C. Amerin, K. Troksa, J. G. Glanzer, S. Liu, S. O. Opiyo, D. D. Dimitrova, P. Le, B. Sishc, S. M. Bailey, G. G. Oakley and J. A. Nickoloff (2014). "DNA-PK phosphorylation of RPA32 Ser4/Ser8 regulates replication stress checkpoint activation, fork restart, homologous recombination and mitotic catastrophe." DNA Repair (Amst) **21**: 131-139.

Ashworth, A. (2008). "A synthetic lethal therapeutic approach: poly(ADP) ribose polymerase inhibitors for the treatment of cancers deficient in DNA double-strand break repair." J Clin Oncol **26**(22): 3785-3790.

Ayhan, A., T. L. Mao, T. Seckin, C. H. Wu, B. Guan, H. Ogawa, M. Futagami, H. Mizukami, Y. Yokoyama, R. J. Kurman and M. Shih Ie (2012). "Loss of ARID1A expression is an early molecular event in tumor progression from ovarian endometriotic cyst to clear cell and endometrioid carcinoma." Int J Gynecol Cancer **22**(8): 1310-1315.

Baert, T., T. Verschuere, A. Van Hoylandt, R. Gijsbers, I. Vergote and A. Coosemans (2015). "The dark side of ID8-Luc2: pitfalls for luciferase tagged murine models for ovarian cancer." J Immunother Cancer **3**: 57.

Bahassi, E. M., J. L. Ovesen, A. L. Riesenberg, W. Z. Bernstein, P. E. Hasty and P. J. Stambrook (2008). "The checkpoint kinases Chk1 and Chk2 regulate the functional associations between hBRCA2 and Rad51 in response to DNA damage." Oncogene **27**(28): 3977-3985.

Banerjee, A. K., C. A. Read, M. H. Griffiths, P. J. George and P. H. Rabbitts (2007). "Clonal divergence in lung cancer development is associated with allelic loss on chromosome 4." Genes Chromosomes Cancer **46**(9): 852-860.

Banerjee, S. and S. B. Kaye (2013). "New strategies in the treatment of ovarian cancer: current clinical perspectives and future potential." Clin Cancer Res **19**(5): 961-968.

Banerjee, S., J. Stewart, N. Porta, C. Toms, A. Leary, S. Lheureux, S. Khalique, J. Tai, A. Attygalle, K. Vroobel, C. J. Lord, R. Natrajan and J. Bliss (2021). "ATARI trial: ATR inhibitor in combination with olaparib in gynecological cancers with ARID1A loss or no loss (ENGOT/GYN1/NCRI)." Int J Gynecol Cancer **31**(11): 1471-1475.

Bao, Y. and X. Shen (2007). "SnapShot: chromatin remodeling complexes." Cell **129**(3): 632.

Barrangou, R., C. Fremaux, H. Deveau, M. Richards, P. Boyaval, S. Moineau, D. A. Romero and P. Horvath (2007). "CRISPR provides acquired resistance against viruses in prokaryotes." Science **315**(5819): 1709-1712.

Berger, A. C., A. Korkut, R. S. Kanchi, A. M. Hegde, W. Lenoir, W. Liu, Y. Liu, H. Fan, H. Shen, V. Ravikumar, A. Rao, A. Schultz, X. Li, P. Sumazin, C. Williams, P. Mestdagh, P. H. Gunaratne, C. Yau, R. Bowlby, A. G. Robertson, D. G. Tiezzi, C. Wang, A. D. Cherniack, A. K. Godwin, N. M. Kuderer, J. S. Rader, R. E. Zuna, A. K. Sood, A. J. Lazar, A. I. Ojesina, C. Adebamowo, S. N. Adebamowo, K. A. Baggerly, T. W. Chen, H. S. Chiu, S. Lefever, L. Liu, K. MacKenzie, S. Orsulic, J.

Roszik, C. S. Shelley, Q. Song, C. P. Vellano, N. Wentzensen, N. Cancer Genome Atlas Research, J. N. Weinstein, G. B. Mills, D. A. Levine and R. Akbani (2018). "A Comprehensive Pan-Cancer Molecular Study of Gynecologic and Breast Cancers." Cancer Cell **33**(4): 690-705 e699.

Bhardwaj, A., S. Singh, S. K. Srivastava, R. E. Honkanen, E. Reed and A. P. Singh (2011). "Modulation of protein phosphatase 2A activity alters androgen-independent growth of prostate cancer cells: therapeutic implications." Mol Cancer Ther **10**(5): 720-731.

Bhat, K. P. and D. Cortez (2018). "RPA and RAD51: fork reversal, fork protection, and genome stability." Nat Struct Mol Biol **25**(6): 446-453.

Bin, P., R. Huang and X. Zhou (2017). "Oxidation Resistance of the Sulfur Amino Acids: Methionine and Cysteine." Biomed Res Int **2017**: 9584932.

Birmingham, A., E. M. Anderson, A. Reynolds, D. Ilsley-Tyree, D. Leake, Y. Fedorov, S. Baskerville, E. Maksimova, K. Robinson, J. Karpilow, W. S. Marshall and A. Khvorova (2006). "3' UTR seed matches, but not overall identity, are associated with RNAi off-targets." Nat Methods **3**(3): 199-204.

Bitler, B. G., K. M. Aird, A. Garipov, H. Li, M. Amatangelo, A. V. Kossenkov, D. C. Schultz, Q. Liu, M. Shih Ie, J. R. Conejo-Garcia, D. W. Speicher and R. Zhang (2015). "Synthetic lethality by targeting EZH2 methyltransferase activity in ARID1A-mutated cancers." Nat Med **21**(3): 231-238.

Bitler, B. G., S. Wu, P. H. Park, Y. Hai, K. M. Aird, Y. Wang, Y. Zhai, A. V. Kossenkov, A. Vara-Ailor, F. J. Rauscher, III, W. Zou, D. W. Speicher, D. G. Huntsman, J. R. Conejo-Garcia, K. R. Cho, D. W. Christianson and R. Zhang (2017). "ARID1A-mutated ovarian cancers depend on HDAC6 activity." Nat Cell Biol **19**(8): 962-973.

Bonadona, V., B. Bonaiti, S. Olschwang, S. Grandjouan, L. Huiart, M. Longy, R. Guimbaud, B. Buecher, Y. J. Bignon, O. Caron, C. Colas, C. Nogues, S. Lejeune-Dumoulin, L. Olivier-Faivre, F. Polycarpe-Osaer, T. D. Nguyen, F. Desseigne, J. C. Saurin, P. Berthet, D. Leroux, J. Duffour, S. Manouvrier, T. Frebourg, H. Sobol, C. Lasset, C. Bonaiti-Pellie and N. French Cancer Genetics (2011). "Cancer risks associated with germline mutations in MLH1, MSH2, and MSH6 genes in Lynch syndrome." JAMA **305**(22): 2304-2310.

Boulos, J. C., M. R. Yousof Idres and T. Efferth (2020). "Investigation of cancer drug resistance mechanisms by phosphoproteomics." Pharmacol Res **160**: 105091.

Broderick, R. and H. P. Nasheuer (2009). "Regulation of Cdc45 in the cell cycle and after DNA damage." Biochem Soc Trans **37**(Pt 4): 926-930.

Brown, U., S. Bristol-Myers, H. Rhode Island, H. The Miriam, Women and I. Infants Hospital of Rhode. (2017, December). "BrUOG 354 Nivolumab +/- Ipilimumab for Ovarian and Extra-renal Clear Cell Carcinomas." from https://ClinicalTrials.gov/show/NCT03355976.

Buchbinder, E. I. and A. Desai (2016). "CTLA-4 and PD-1 Pathways: Similarities, Differences, and Implications of Their Inhibition." Am J Clin Oncol **39**(1): 98-106.

Bukhari, A. B., C. W. Lewis, J. J. Pearce, D. Luong, G. K. Chan and A. M. Gamper (2019). "Inhibiting Wee1 and ATR kinases produces tumor-selective synthetic lethality and suppresses metastasis." J Clin Invest **129**(3): 1329-1344.

Bultman, S. J., J. I. Herschkowitz, V. Godfrey, T. C. Gebuhr, M. Yaniv, C. M. Perou and T. Magnuson (2008). "Characterization of mammary tumors from Brg1 heterozygous mice." Oncogene **27**(4): 460-468.

Busino, L., M. Chiesa, G. F. Draetta and M. Donzelli (2004). "Cdc25A phosphatase: combinatorial phosphorylation, ubiquitylation and proteolysis." Oncogene **23**(11): 2050-2056.

Campbell, J. D., A. Alexandrov, J. Kim, J. Wala, A. H. Berger, C. S. Pedamallu, S. A. Shukla, G. Guo, A. N. Brooks, B. A. Murray, M. Imielinski, X. Hu, S. Ling, R. Akbani, M. Rosenberg, C. Cibulskis, A. Ramachandran, E. A. Collisson, D. J. Kwiatkowski, M. S. Lawrence, J. N. Weinstein, R. G. Verhaak, C. J. Wu, P. S. Hammerman, A. D. Cherniack, G. Getz, N. Cancer Genome Atlas Research, M. N. Artyomov, R. Schreiber, R. Govindan and M. Meyerson (2016). "Distinct patterns of somatic genome alterations in lung adenocarcinomas and squamous cell carcinomas." Nat Genet **48**(6): 607-616.

Cancer Genome Atlas Research, N. (2011). "Integrated genomic analyses of ovarian carcinoma." Nature **474**(7353): 609-615.

Cancer Genome Atlas Research, N., C. Kandoth, N. Schultz, A. D. Cherniack, R. Akbani, Y. Liu, H. Shen, A. G. Robertson, I. Pashtan, R. Shen, C. C. Benz, C. Yau, P. W. Laird, L. Ding, W. Zhang, G. B. Mills, R. Kucherlapati, E. R. Mardis

and D. A. Levine (2013). "Integrated genomic characterization of endometrial carcinoma." Nature **497**(7447): 67-73.

Cayla, X., C. Van Hoof, M. Bosch, E. Waelkens, J. Vandekerckhove, B. Peeters, W. Merlevede and J. Goris (1994). "Molecular cloning, expression, and characterization of PTPA, a protein that activates the tyrosyl phosphatase activity of protein phosphatase 2A." J Biol Chem **269**(22): 15668-15675.

Center, M. D. A. C. (2017, December 15). "Durvalumab and Tremelimumab in Treating Participants With Recurrent or Refractory Ovarian, Primary Peritoneal, or Fallopian Tube Cancer." from https://ClinicalTrials.gov/show/NCT03026062.

Cerami, E., J. Gao, U. Dogrusoz, B. E. Gross, S. O. Sumer, B. A. Aksoy, A. Jacobsen, C. J. Byrne, M. L. Heuer, E. Larsson, Y. Antipin, B. Reva, A. P. Goldberg, C. Sander and N. Schultz (2012). "The cBio cancer genomics portal: an open platform for exploring multidimensional cancer genomics data." Cancer Discov **2**(5): 401-404.

Chabanon, R. M., D. Morel and S. Postel-Vinay (2020). "Exploiting epigenetic vulnerabilities in solid tumors: Novel therapeutic opportunities in the treatment of SWI/SNF-defective cancers." Semin Cancer Biol **61**: 180-198.

Chan, J. K., D. Teoh, J. M. Hu, J. Y. Shin, K. Osann and D. S. Kapp (2008). "Do clear cell ovarian carcinomas have poorer prognosis compared to other epithelial cell types? A study of 1411 clear cell ovarian cancers." Gynecol Oncol **109**(3): 370-376.

Chandler, R. L., J. Brennan, J. C. Schisler, D. Serber, C. Patterson and T. Magnuson (2013). "ARID1a-DNA interactions are required for promoter occupancy by SWI/SNF." Mol Cell Biol **33**(2): 265-280.

Chandler, R. L., J. S. Damrauer, J. R. Raab, J. C. Schisler, M. D. Wilkerson, J. P. Didion, J. Starmer, D. Serber, D. Yee, J. Xiong, D. B. Darr, F. Pardo-Manuel de Villena, W. Y. Kim and T. Magnuson (2015). "Coexistent ARID1A-PIK3CA mutations promote ovarian clear-cell tumorigenesis through pro-tumorigenic inflammatory cytokine signalling." Nat Commun **6**: 6118.

Chavez, A., J. Scheiman, S. Vora, B. W. Pruitt, M. Tuttle, P. R. I. E, S. Lin, S. Kiani, C. D. Guzman, D. J. Wiegand, D. Ter-Ovanesyan, J. L. Braff, N. Davidsohn, B. E. Housden, N. Perrimon, R. Weiss, J. Aach, J. J. Collins and G. M. Church (2015). "Highly efficient Cas9-mediated transcriptional programming." Nat Methods **12**(4): 326-328.

Checkley, S., L. MacCallum, J. Yates, P. Jasper, H. Luo, J. Tolsma and C. Bendtsen (2015). "Bridging the gap between in vitro and in vivo: Dose and schedule predictions for the ATR inhibitor AZD6738." Sci Rep **5**: 13545.

Chen, P. J., J. A. Hussmann, J. Yan, F. Knipping, P. Ravisankar, P. F. Chen, C. Chen, J. W. Nelson, G. A. Newby, M. Sahin, M. J. Osborn, J. S. Weissman, B. Adamson and D. R. Liu (2021). "Enhanced prime editing systems by manipulating cellular determinants of editing outcomes." Cell **184**(22): 5635-5652 e5629.

Chen, W., M. Yazicioglu and M. H. Cobb (2004). "Characterization of OSR1, a member of the mammalian Ste20p/germinal center kinase subfamily." J Biol Chem **279**(12): 11129-11136.

Cheng, D. T., T. N. Mitchell, A. Zehir, R. H. Shah, R. Benayed, A. Syed, R. Chandramohan, Z. Y. Liu, H. H. Won, S. N. Scott, A. R. Brannon, C. O'Reilly, J. Sadowska, J. Casanova, A. Yannes, J. F. Hechtman, J. Yao, W. Song, D. S. Ross, A. Oultache, S. Dogan, L. Borsu, M. Hameed, K. Nafa, M. E. Arcila, M. Ladanyi and M. F. Berger (2015). "Memorial Sloan Kettering-Integrated Mutation Profiling of Actionable Cancer Targets (MSK-IMPACT): A Hybridization Capture-Based Next-Generation Sequencing Clinical Assay for Solid Tumor Molecular Oncology." J Mol Diagn **17**(3): 251-264.

Cheng, Y., W. Liu, S. T. Kim, J. Sun, L. Lu, J. Sun, S. L. Zheng, W. B. Isaacs and J. Xu (2011). "Evaluation of PPP2R2A as a prostate cancer susceptibility gene: a comprehensive germline and somatic study." Cancer Genet **204**(7): 375-381.

Cheung, H. W., G. S. Cowley, B. A. Weir, J. S. Boehm, S. Rusin, J. A. Scott, A. East, L. D. Ali, P. H. Lizotte, T. C. Wong, G. Jiang, J. Hsiao, C. H. Mermel, G. Getz, J. Barretina, S. Gopal, P. Tamayo, J. Gould, A. Tsherniak, N. Stransky, B. Luo, Y. Ren, R. Drapkin, S. N. Bhatia, J. P. Mesirov, L. A. Garraway, M. Meyerson, E. S. Lander, D. E. Root and W. C. Hahn (2011). "Systematic investigation of genetic vulnerabilities across cancer cell lines reveals lineage-specific dependencies in ovarian cancer." Proc Natl Acad Sci U S A **108**(30): 12372-12377.

Cho, H., J. S. Kim, H. Chung, C. Perry, H. Lee and J. H. Kim (2013). "Loss of ARID1A/BAF250a expression is linked to tumor progression and adverse prognosis in cervical cancer." Hum Pathol **44**(7): 1365-1374.

Cho, U. S. and W. Xu (2007). "Crystal structure of a protein phosphatase 2A heterotrimeric holoenzyme." Nature **445**(7123): 53-57.

Cimprich, K. A. and D. Cortez (2008). "ATR: an essential regulator of genome integrity." Nat Rev Mol Cell Biol **9**(8): 616-627.

Colic, M., G. Wang, M. Zimmermann, K. Mascall, M. McLaughlin, L. Bertolet, W. F. Lenoir, J. Moffat, S. Angers, D. Durocher and T. Hart (2019). "Identifying chemogenetic interactions from CRISPR screens with drugZ." Genome Med **11**(1): 52.

Colombo, N., C. Sessa, A. du Bois, J. Ledermann, W. G. McCluggage, I. McNeish, P. Morice, S. Pignata, I. Ray-Coquard, I. Vergote, T. Baert, I. Belaroussi, A. Dashora, S. Olbrecht, F. Planchamp, D. Querleu and E.-E. O. C. C. C. W. Group (2019). "ESMO-ESGO consensus conference recommendations on ovarian cancer: pathology and molecular biology, early and advanced stages, borderline tumours and recurrent diseasedagger." Ann Oncol **30**(5): 672-705.

Cong, K., M. Peng, A. N. Kousholt, W. T. C. Lee, S. Lee, S. Nayak, J. Krais, P. S. VanderVere-Carozza, K. S. Pawelczak, J. Calvo, N. J. Panzarino, J. J. Turchi, N. Johnson, J. Jonkers, E. Rothenberg and S. B. Cantor (2021). "Replication gaps are a key determinant of PARP inhibitor synthetic lethality with BRCA deficiency." Mol Cell **81**(15): 3227.

Cong, L., F. A. Ran, D. Cox, S. Lin, R. Barretto, N. Habib, P. D. Hsu, X. Wu, W. Jiang, L. A. Marraffini and F. Zhang (2013). "Multiplex genome engineering using CRISPR/Cas systems." Science **339**(6121): 819-823.

Cottini, F., T. Hideshima, R. Suzuki, Y. T. Tai, G. Bianchini, P. G. Richardson, K. C. Anderson and G. Tonon (2015). "Synthetic Lethal Approaches Exploiting DNA Damage in Aggressive Myeloma." Cancer Discov **5**(9): 972-987.

Couch, F. B., C. E. Bansbach, R. Driscoll, J. W. Luzwick, G. G. Glick, R. Betous, C. M. Carroll, S. Y. Jung, J. Qin, K. A. Cimprich and D. Cortez (2013). "ATR phosphorylates SMARCAL1 to prevent replication fork collapse." Genes Dev **27**(14): 1610-1623.

Cowley, G. S., B. A. Weir, F. Vazquez, P. Tamayo, J. A. Scott, S. Rusin, A. East-Seletsky, L. D. Ali, W. F. Gerath, S. E. Pantel, P. H. Lizotte, G. Jiang, J. Hsiao, A. Tsherniak, E. Dwinell, S. Aoyama, M. Okamoto, W. Harrington, E. Gelfand, T. M. Green, M. J. Tomko, S. Gopal, T. C. Wong, H. Li, S. Howell, N. Stransky, T. Liefeld, D. Jang, J. Bistline, B. Hill Meyers, S. A. Armstrong, K. C. Anderson, K. Stegmaier, M. Reich, D. Pellman, J. S. Boehm, J. P. Mesirov, T. R. Golub, D. E. Root and W. C. Hahn (2014). "Parallel genome-scale loss of function screens in 216 cancer cell lines for the identification of context-specific genetic dependencies." Sci Data **1**: 140035.

CRUK. (2018). "Ovarian Cancer Statistics." Retrieved 24th July, 2022, from https://www.cancerresearchuk.org/health-professional/cancer-statistics/statistics-by-cancer-type/ovarian-cancer#heading-Zero.

Csortos, C., S. Zolnierowicz, E. Bako, S. D. Durbin and A. A. DePaoli-Roach (1996). "High complexity in the expression of the B' subunit of protein phosphatase 2A0. Evidence for the existence of at least seven novel isoforms." J Biol Chem **271**(5): 2578-2588.

Dai, Y. and S. Grant (2010). "New insights into checkpoint kinase 1 in the DNA damage response signaling network." Clin Cancer Res **16**(2): 376-383.

De Kegel, B. and C. J. Ryan (2019). "Paralog buffering contributes to the variable essentiality of genes in cancer cell lines." PLoS Genet **15**(10): e1008466.

Deavers, M. T., D. M. Gershenson, G. Tortolero-Luna, A. Malpica, K. H. Lu and E. G. Silva (2002). "Micropapillary and cribriform patterns in ovarian serous tumors of low malignant potential: a study of 99 advanced stage cases." Am J Surg Pathol **26**(9): 1129-1141.

Deegan, T. D., J. T. Yeeles and J. F. Diffley (2016). "Phosphopeptide binding by Sld3 links Dbf4-dependent kinase to MCM replicative helicase activation." EMBO J **35**(9): 961-973.

Diamond, M. S., M. Kinder, H. Matsushita, M. Mashayekhi, G. P. Dunn, J. M. Archambault, H. Lee, C. D. Arthur, J. M. White, U. Kalinke, K. M. Murphy and R. D. Schreiber (2011). "Type I interferon is selectively required by dendritic cells for immune rejection of tumors." J Exp Med **208**(10): 1989-2003.

Dillon, M., J. Guevara, K. Mohammed, S. A. Smith, E. Dean, L. McLellan, Z. Boylan, J. Spicer, M. D. Forster and K. J. Harrington (2019). "450PD - A phase I study of ATR inhibitor, AZD6738, as monotherapy in advanced solid tumours (PATRIOT part A, B)." Annals of Oncology **30**: v165-v166.

Dillon, M. T., H. E. Barker, M. Pedersen, H. Hafsi, S. A. Bhide, K. L. Newbold, C. M. Nutting, M. McLaughlin and K. J. Harrington (2017). "Radiosensitization by the ATR Inhibitor AZD6738 through Generation of Acentric Micronuclei." Mol Cancer Ther **16**(1): 25-34.

Dillon, M. T., K. F. Bergerhoff, M. Pedersen, H. Whittock, E. Crespo-Rodriguez, E. C. Patin, A. Pearson, H. G. Smith, J. T. E. Paget, R. R. Patel, S. Foo, G. Bozhanova, C. Ragulan, E. Fontana, K. Desai, A. C. Wilkins, A. Sadanandam, A.

Melcher, M. McLaughlin and K. J. Harrington (2019). "ATR Inhibition Potentiates the Radiation-induced Inflammatory Tumor Microenvironment." Clin Cancer Res **25**(11): 3392-3403.

Disis, M. L., M. H. Taylor, K. Kelly, J. T. Beck, M. Gordon, K. M. Moore, M. R. Patel, J. Chaves, H. Park, A. C. Mita, E. P. Hamilton, C. M. Annunziata, H. J. Grote, A. von Heydebreck, J. Grewal, V. Chand and J. L. Gulley (2019). "Efficacy and Safety of Avelumab for Patients With Recurrent or Refractory Ovarian Cancer: Phase 1b Results From the JAVELIN Solid Tumor Trial." JAMA Oncol **5**(3): 393-401.

Doench, J. G., N. Fusi, M. Sullender, M. Hegde, E. W. Vaimberg, K. F. Donovan, I. Smith, Z. Tothova, C. Wilen, R. Orchard, H. W. Virgin, J. Listgarten and D. E. Root (2016). "Optimized sgRNA design to maximize activity and minimize off-target effects of CRISPR-Cas9." Nat Biotechnol **34**(2): 184-191.

Doench, J. G., E. Hartenian, D. B. Graham, Z. Tothova, M. Hegde, I. Smith, M. Sullender, B. L. Ebert, R. J. Xavier and D. E. Root (2014). "Rational design of highly active sgRNAs for CRISPR-Cas9-mediated gene inactivation." Nat Biotechnol **32**(12): 1262-1267.

Doench, J. G., C. P. Petersen and P. A. Sharp (2003). "siRNAs can function as miRNAs." Genes Dev **17**(4): 438-442.

Dominguez-Sola, D., C. Y. Ying, C. Grandori, L. Ruggiero, B. Chen, M. Li, D. A. Galloway, W. Gu, J. Gautier and R. Dalla-Favera (2007). "Non-transcriptional control of DNA replication by c-Myc." Nature **448**(7152): 445-451.

du Bois, A., M. Quinn, T. Thigpen, J. Vermorken, E. Avall-Lundqvist, M. Bookman, D. Bowtell, M. Brady, A. Casado, A. Cervantes, E. Eisenhauer, M. Friedlaender, K. Fujiwara, S. Grenman, J. P. Guastalla, P. Harper, T. Hogberg, S. Kaye, H. Kitchener, G. Kristensen, R. Mannel, W. Meier, B. Miller, J. P. Neijt, A. Oza, R. Ozols, M. Parmar, S. Pecorelli, J. Pfisterer, A. Poveda, D. Provencher, E. Pujade-Lauraine, M. Randall, J. Rochon, G. Rustin, S. Sagae, F. Stehman, G. Stuart, E. Trimble, P. Vasey, I. Vergote, R. Verheijen, U. Wagner, I. Gynecologic Cancer, O. Ago, Anzgog, Eortc, Geico, Gineco, Gog, Jgog, Mrc/Ncri, C. T. G. Ncic, U. S. Nci, Nsgo, Rtog, Sgctg, Igcs and O. Organizational team of the two prior International (2005). "2004 consensus statements on the management of ovarian cancer: final document of the 3rd International Gynecologic Cancer Intergroup Ovarian Cancer Consensus Conference (GCIG OCCC 2004)." Ann Oncol **16 Suppl 8**: viii7-viii12.

Dupont, W. D., J. P. Breyer, K. M. Bradley, P. A. Schuyler, W. D. Plummer, M. E. Sanders, D. L. Page and J. R. Smith (2010). "Protein phosphatase 2A subunit gene haplotypes and proliferative breast disease modify breast cancer risk." Cancer **116**(1): 8-19.

Duska, L. R., L. Garrett, M. Henretta, J. S. Ferriss, L. Lee and N. Horowitz (2010). "When 'never-events' occur despite adherence to clinical guidelines: the case of venous thromboembolism in clear cell cancer of the ovary compared with other epithelial histologic subtypes." Gynecol Oncol **116**(3): 374-377.

Dykhuizen, E. C., D. C. Hargreaves, E. L. Miller, K. Cui, A. Korshunov, M. Kool, S. Pfister, Y. J. Cho, K. Zhao and G. R. Crabtree (2013). "BAF complexes facilitate decatenation of DNA by topoisomerase IIalpha." Nature **497**(7451): 624-627.

Echeverri, C. J., P. A. Beachy, B. Baum, M. Boutros, F. Buchholz, S. K. Chanda, J. Downward, J. Ellenberg, A. G. Fraser, N. Hacohen, W. C. Hahn, A. L. Jackson, A. Kiger, P. S. Linsley, L. Lum, Y. Ma, B. Mathey-Prevot, D. E. Root, D. M. Sabatini, J. Taipale, N. Perrimon and R. Bernards (2006). "Minimizing the risk of reporting false positives in large-scale RNAi screens." Nat Methods **3**(10): 777-779.

EMA. (2022). "AVASTIN." Retrieved 26th July, 2022, from https://www.ema.europa.eu/en/medicines/human/EPAR/avastin#assessment-history-section.

Fadare, O., K. Gwin, M. M. Desouki, M. A. Crispens, H. W. Jones, 3rd, D. Khabele, S. X. Liang, W. Zheng, K. Mohammed, J. L. Hecht and V. Parkash (2013). "The clinicopathologic significance of p53 and BAF-250a (ARID1A) expression in clear cell carcinoma of the endometrium." Mod Pathol **26**(8): 1101-1110.

Fadare, O., I. L. Renshaw and S. X. Liang (2012). "Does the Loss of ARID1A (BAF-250a) Expression in Endometrial Clear Cell Carcinomas Have Any Clinicopathologic Significance? A Pilot Assessment." J Cancer **3**: 129-136.

Farmer, H., N. McCabe, C. J. Lord, A. N. Tutt, D. A. Johnson, T. B. Richardson, M. Santarosa, K. J. Dillon, I. Hickson, C. Knights, N. M. Martin, S. P. Jackson, G. C. Smith and A. Ashworth (2005). "Targeting the DNA repair defect in BRCA mutant cells as a therapeutic strategy." Nature **434**(7035): 917-921.

Farrington, C. C., E. Yuan, S. Mazhar, S. Izadmehr, L. Hurst, B. L. Allen-Petersen, M. Janghorban, E. Chung, G. Wolczanski, M. Galsky, R. Sears, J. Sangodkar

and G. Narla (2020). "Protein phosphatase 2A activation as a therapeutic strategy for managing MYC-driven cancers." J Biol Chem **295**(3): 757-770.

Fedorov, Y., E. M. Anderson, A. Birmingham, A. Reynolds, J. Karpilow, K. Robinson, D. Leake, W. S. Marshall and A. Khvorova (2006). "Off-target effects by siRNA can induce toxic phenotype." RNA **12**(7): 1188-1196.

Fife, B. T. and J. A. Bluestone (2008). "Control of peripheral T-cell tolerance and autoimmunity via the CTLA-4 and PD-1 pathways." Immunol Rev **224**: 166-182.

Fragkos, M., O. Ganier, P. Coulombe and M. Mechali (2015). "DNA replication origin activation in space and time." Nat Rev Mol Cell Biol **16**(6): 360-374.

Francia, G., R. Poulsom, A. M. Hanby, S. D. Mitchell, G. Williams, P. McKee and I. R. Hart (1999). "Identification by differential display of a protein phosphatase-2A regulatory subunit preferentially expressed in malignant melanoma cells." Int J Cancer **82**(5): 709-713.

Gao, J., B. A. Aksoy, U. Dogrusoz, G. Dresdner, B. Gross, S. O. Sumer, Y. Sun, A. Jacobsen, R. Sinha, E. Larsson, E. Cerami, C. Sander and N. Schultz (2013). "Integrative analysis of complex cancer genomics and clinical profiles using the cBioPortal." Sci Signal **6**(269): pl1.

Gao, X., P. Tate, P. Hu, R. Tjian, W. C. Skarnes and Z. Wang (2008). "ES cell pluripotency and germ-layer formation require the SWI/SNF chromatin remodeling component BAF250a." Proc Natl Acad Sci U S A **105**(18): 6656-6661.

Gershenson, D. M. (2016). "Low-grade serous carcinoma of the ovary or peritoneum." Ann Oncol **27 Suppl 1**: i45-i49.

Gier, R. A., K. A. Budinich, N. H. Evitt, Z. Cao, E. S. Freilich, Q. Chen, J. Qi, Y. Lan, R. M. Kohli and J. Shi (2020). "High-performance CRISPR-Cas12a genome editing for combinatorial genetic screening." Nat Commun **11**(1): 3455.

Gilbert, L. A., M. H. Larson, L. Morsut, Z. Liu, G. A. Brar, S. E. Torres, N. Stern-Ginossar, O. Brandman, E. H. Whitehead, J. A. Doudna, W. A. Lim, J. S. Weissman and L. S. Qi (2013). "CRISPR-mediated modular RNA-guided regulation of transcription in eukaryotes." Cell **154**(2): 442-451.

Glasspool, R., I. Mcneish, A. Westermann, S. Hinsley, J. Ledermann, I. Ray-Coquard, C. Lawless, N. Ottevanger, M. R. Mirza and J. Alexandre (2020). "596

A randomised phase II study of nintedanib (BIBF1120) compared to chemotherapy in patients with recurrent clear cell carcinoma of the ovary or endometrium. (NICCC/ENGOT-OV36)." International Journal of Gynecologic Cancer **30**: A127-A128.

Golan, T., P. Hammel, M. Reni, E. Van Cutsem, T. Macarulla, M. J. Hall, J. O. Park, D. Hochhauser, D. Arnold, D. Y. Oh, A. Reinacher-Schick, G. Tortora, H. Algul, E. M. O'Reilly, D. McGuinness, K. Y. Cui, K. Schlienger, G. Y. Locker and H. L. Kindler (2019). "Maintenance Olaparib for Germline BRCA-Mutated Metastatic Pancreatic Cancer." N Engl J Med **381**(4): 317-327.

Gonzalez-Martin, A., B. Pothuri, I. Vergote, R. DePont Christensen, W. Graybill, M. R. Mirza, C. McCormick, D. Lorusso, P. Hoskins, G. Freyer, K. Baumann, K. Jardon, A. Redondo, R. G. Moore, C. Vulsteke, R. E. O'Cearbhaill, B. Lund, F. Backes, P. Barretina-Ginesta, A. F. Haggerty, M. J. Rubio-Perez, M. S. Shahin, G. Mangili, W. H. Bradley, I. Bruchim, K. Sun, I. A. Malinowska, Y. Li, D. Gupta, B. J. Monk and P. E.-O. G.-. Investigators (2019). "Niraparib in Patients with Newly Diagnosed Advanced Ovarian Cancer." N Engl J Med **381**(25): 2391-2402.

Gorrini, C., I. S. Harris and T. W. Mak (2013). "Modulation of oxidative stress as an anticancer strategy." Nat Rev Drug Discov **12**(12): 931-947.

Gottschalk, A. J., R. D. Trivedi, J. W. Conaway and R. C. Conaway (2012). "Activation of the SNF2 family ATPase ALC1 by poly(ADP-ribose) in a stable ALC1.PARP1.nucleosome intermediate." J Biol Chem **287**(52): 43527-43532.

Grisham, R. N., B. E. Sylvester, H. Won, G. McDermott, D. DeLair, R. Ramirez, Z. Yao, R. Shen, F. Dao, F. Bogomolniy, V. Makker, E. Sala, T. E. Soumerai, D. M. Hyman, N. D. Socci, A. Viale, D. M. Gershenson, J. Farley, D. A. Levine, N. Rosen, M. F. Berger, D. R. Spriggs, C. A. Aghajanian, D. B. Solit and G. Iyer (2015). "Extreme Outlier Analysis Identifies Occult Mitogen-Activated Protein Kinase Pathway Mutations in Patients With Low-Grade Serous Ovarian Cancer." J Clin Oncol **33**(34): 4099-4105.

Gu, Y. F., S. Cohn, A. Christie, T. McKenzie, N. Wolff, Q. N. Do, A. J. Madhuranthakam, I. Pedrosa, T. Wang, A. Dey, M. Busslinger, X. J. Xie, R. E. Hammer, R. M. McKay, P. Kapur and J. Brugarolas (2017). "Modeling Renal Cell Carcinoma in Mice: Bap1 and Pbrm1 Inactivation Drive Tumor Grade." Cancer Discov **7**(8): 900-917.

Guan, B., T. L. Mao, P. K. Panuganti, E. Kuhn, R. J. Kurman, D. Maeda, E. Chen, Y. M. Jeng, T. L. Wang and M. Shih Ie (2011). "Mutation and loss of expression

of ARID1A in uterine low-grade endometrioid carcinoma." Am J Surg Pathol **35**(5): 625-632.

Guerrero Llobet, S., B. van der Vegt, E. Jongeneel, R. D. Bense, M. C. Zwager, C. P. Schroder, M. Everts, R. S. N. Fehrmann, G. H. de Bock and M. van Vugt (2020). "Cyclin E expression is associated with high levels of replication stress in triple-negative breast cancer." NPJ Breast Cancer **6**: 40.

Haesen, D., L. Abbasi Asbagh, R. Derua, A. Hubert, S. Schrauwen, Y. Hoorne, F. Amant, E. Waelkens, A. Sablina and V. Janssens (2016). "Recurrent PPP2R1A Mutations in Uterine Cancer Act through a Dominant-Negative Mechanism to Promote Malignant Cell Growth." Cancer Res **76**(19): 5719-5731.

Hamanishi, J., M. Mandai, T. Ikeda, M. Minami, A. Kawaguchi, T. Murayama, M. Kanai, Y. Mori, S. Matsumoto, S. Chikuma, N. Matsumura, K. Abiko, T. Baba, K. Yamaguchi, A. Ueda, Y. Hosoe, S. Morita, M. Yokode, A. Shimizu, T. Honjo and I. Konishi (2015). "Safety and Antitumor Activity of Anti-PD-1 Antibody, Nivolumab, in Patients With Platinum-Resistant Ovarian Cancer." J Clin Oncol **33**(34): 4015-4022.

Hamperl, S., M. J. Bocek, J. C. Saldivar, T. Swigut and K. A. Cimprich (2017). "Transcription-Replication Conflict Orientation Modulates R-Loop Levels and Activates Distinct DNA Damage Responses." Cell **170**(4): 774-786 e719.

Hanahan, D. and R. A. Weinberg (2000). "The hallmarks of cancer." Cell **100**(1): 57-70.

Harding, S. M., J. L. Benci, J. Irianto, D. E. Discher, A. J. Minn and R. A. Greenberg (2017). "Mitotic progression following DNA damage enables pattern recognition within micronuclei." Nature **548**(7668): 466-470.

Harlin, H., Y. Meng, A. C. Peterson, Y. Zha, M. Tretiakova, C. Slingluff, M. McKee and T. F. Gajewski (2009). "Chemokine expression in melanoma metastases associated with CD8+ T-cell recruitment." Cancer Res **69**(7): 3077-3085.

Harsha, H. C. and A. Pandey (2010). "Phosphoproteomics in cancer." Mol Oncol **4**(6): 482-495.

Hart, T., M. Chandrashekhar, M. Aregger, Z. Steinhart, K. R. Brown, G. MacLeod, M. Mis, M. Zimmermann, A. Fradet-Turcotte, S. Sun, P. Mero, P. Dirks, S. Sidhu, F. P. Roth, O. S. Rissland, D. Durocher, S. Angers and J. Moffat (2015). "High-

Resolution CRISPR Screens Reveal Fitness Genes and Genotype-Specific Cancer Liabilities." Cell **163**(6): 1515-1526.

Heffernan, T. P., K. Unsal-Kacmaz, A. N. Heinloth, D. A. Simpson, R. S. Paules, A. Sancar, M. Cordeiro-Stone and W. K. Kaufmann (2007). "Cdc7-Dbf4 and the human S checkpoint response to UVC." J Biol Chem **282**(13): 9458-9468.

Helming, K. C., X. Wang and C. W. M. Roberts (2014). "Vulnerabilities of mutant SWI/SNF complexes in cancer." Cancer Cell **26**(3): 309-317.

Helming, K. C., X. Wang, B. G. Wilson, F. Vazquez, J. R. Haswell, H. E. Manchester, Y. Kim, G. V. Kryukov, M. Ghandi, A. J. Aguirre, Z. Jagani, Z. Wang, L. A. Garraway, W. C. Hahn and C. W. Roberts (2014). "ARID1B is a specific vulnerability in ARID1A-mutant cancers." Nat Med **20**(3): 251-254.

Hemmings, B. A., C. Adams-Pearson, F. Maurer, P. Muller, J. Goris, W. Merlevede, J. Hofsteenge and S. R. Stone (1990). "alpha- and beta-forms of the 65-kDa subunit of protein phosphatase 2A have a similar 39 amino acid repeating structure." Biochemistry **29**(13): 3166-3173.

Hilberg, F., G. J. Roth, M. Krssak, S. Kautschitsch, W. Sommergruber, U. Tontsch-Grunt, P. Garin-Chesa, G. Bader, A. Zoephel, J. Quant, A. Heckel and W. J. Rettig (2008). "BIBF 1120: triple angiokinase inhibitor with sustained receptor blockade and good antitumor efficacy." Cancer Res **68**(12): 4774-4782.

Hopkins, T. A., W. B. Ainsworth, P. A. Ellis, C. K. Donawho, E. L. DiGiammarino, S. C. Panchal, V. C. Abraham, M. A. Algire, Y. Shi, A. M. Olson, E. F. Johnson, J. L. Wilsbacher and D. Maag (2019). "PARP1 Trapping by PARP Inhibitors Drives Cytotoxicity in Both Cancer Cells and Healthy Bone Marrow." Mol Cancer Res **17**(2): 409-419.

Horton, J. K., D. F. Stefanick, P. S. Kedar and S. H. Wilson (2007). "ATR signaling mediates an S-phase checkpoint after inhibition of poly(ADP-ribose) polymerase activity." DNA Repair (Amst) **6**(6): 742-750.

Hsu, P. D., D. A. Scott, J. A. Weinstein, F. A. Ran, S. Konermann, V. Agarwala, Y. Li, E. J. Fine, X. Wu, O. Shalem, T. J. Cradick, L. A. Marraffini, G. Bao and F. Zhang (2013). "DNA targeting specificity of RNA-guided Cas9 nucleases." Nat Biotechnol **31**(9): 827-832.

Hunter, S. M., M. S. Anglesio, G. L. Ryland, R. Sharma, Y. E. Chiew, S. M. Rowley, M. A. Doyle, J. Li, C. B. Gilks, P. Moss, P. E. Allan, A. N. Stephens, D.

G. Huntsman, A. deFazio, D. D. Bowtell, G. Australian Ovarian Cancer Study, K. L. Gorringe and I. G. Campbell (2015). "Molecular profiling of low grade serous ovarian tumours identifies novel candidate driver genes." Oncotarget **6**(35): 37663-37677.

Hustedt, N., A. Alvarez-Quilon, A. McEwan, J. Y. Yuan, T. Cho, L. Koob, T. Hart and D. Durocher (2019). "A consensus set of genetic vulnerabilities to ATR inhibition." Open Biol **9**(9): 190156.

ICGC/TCGA (2020). "Icgc Tcga Pan-Cancer Analysis of Whole Genomes Consortium. Pan-cancer analysis of whole genomes." Nature **578**(7793): 82-93.

Illuzzi, G., A. D. Staniszewska, S. J. Gill, A. Pike, L. McWilliams, S. E. Critchlow, A. Cronin, S. Fawell, G. Hawthorne, K. Jamal, J. Johannes, E. Leonard, R. Macdonald, G. Maglennon, J. Nikkil, M. J. O'Connor, A. Smith, H. Southgate, J. Wilson, J. Yates, S. Cosulich and E. Leo (2022). "Preclinical characterization of AZD5305, a next generation, highly selective PARP1 inhibitor and trapper." Clin Cancer Res.

Itamochi, H., T. Oishi, N. Oumi, S. Takeuchi, K. Yoshihara, M. Mikami, N. Yaegashi, Y. Terao, K. Takehara, K. Ushijima, H. Watari, D. Aoki, T. Kimura, T. Nakamura, Y. Yokoyama, J. Kigawa and T. Sugiyama (2017). "Whole-genome sequencing revealed novel prognostic biomarkers and promising targets for therapy of ovarian clear cell carcinoma." Br J Cancer **117**(5): 717-724.

Jansen, R., J. D. Embden, W. Gaastra and L. M. Schouls (2002). "Identification of genes that are associated with DNA repeats in prokaryotes." Mol Microbiol **43**(6): 1565-1575.

Janssens, V. and J. Goris (2001). "Protein phosphatase 2A: a highly regulated family of serine/threonine phosphatases implicated in cell growth and signalling." Biochem J **353**(Pt 3): 417-439.

Jaspers, J. E., A. Kersbergen, U. Boon, W. Sol, L. van Deemter, S. A. Zander, R. Drost, E. Wientjens, J. Ji, A. Aly, J. H. Doroshow, A. Cranston, N. M. Martin, A. Lau, M. J. O'Connor, S. Ganesan, P. Borst, J. Jonkers and S. Rottenberg (2013). "Loss of 53BP1 causes PARP inhibitor resistance in Brca1-mutated mouse mammary tumors." Cancer Discov **3**(1): 68-81.

Jaykumar, A. B., J. U. Jung, P. K. Parida, T. T. Dang, C. Wichaidit, A. R. Kannangara, S. Earnest, E. J. Goldsmith, G. W. Pearson, S. Malladi and M. H.

Cobb (2021). "WNK1 Enhances Migration and Invasion in Breast Cancer Models." Mol Cancer Ther **20**(10): 1800-1808.

Jayson, G. C., E. C. Kohn, H. C. Kitchener and J. A. Ledermann (2014). "Ovarian cancer." Lancet **384**(9951): 1376-1388.

Jiang, Z. Y., Q. L. Zhou, J. Holik, S. Patel, J. Leszyk, K. Coleman, M. Chouinard and M. P. Czech (2005). "Identification of WNK1 as a substrate of Akt/protein kinase B and a negative regulator of insulin-stimulated mitogenesis in 3T3-L1 cells." J Biol Chem **280**(22): 21622-21628.

Jinek, M., K. Chylinski, I. Fonfara, M. Hauer, J. A. Doudna and E. Charpentier (2012). "A programmable dual-RNA-guided DNA endonuclease in adaptive bacterial immunity." Science **337**(6096): 816-821.

Jones, S., T. L. Wang, R. J. Kurman, K. Nakayama, V. E. Velculescu, B. Vogelstein, K. W. Kinzler, N. Papadopoulos and M. Shih Ie (2012). "Low-grade serous carcinomas of the ovary contain very few point mutations." J Pathol **226**(3): 413-420.

Jones, S., T. L. Wang, M. Shih Ie, T. L. Mao, K. Nakayama, R. Roden, R. Glas, D. Slamon, L. A. Diaz, Jr., B. Vogelstein, K. W. Kinzler, V. E. Velculescu and N. Papadopoulos (2010). "Frequent mutations of chromatin remodeling gene ARID1A in ovarian clear cell carcinoma." Science **330**(6001): 228-231.

Kadoch, C., D. C. Hargreaves, C. Hodges, L. Elias, L. Ho, J. Ranish and G. R. Crabtree (2013). "Proteomic and bioinformatic analysis of mammalian SWI/SNF complexes identifies extensive roles in human malignancy." Nat Genet **45**(6): 592-601.

Kalev, P., M. Simicek, I. Vazquez, S. Munck, L. Chen, T. Soin, N. Danda, W. Chen and A. Sablina (2012). "Loss of PPP2R2A inhibits homologous recombination DNA repair and predicts tumor sensitivity to PARP inhibition." Cancer Res **72**(24): 6414-6424.

Kamenz, J., L. Gelens and J. E. Ferrell, Jr. (2021). "Bistable, Biphasic Regulation of PP2A-B55 Accounts for the Dynamics of Mitotic Substrate Phosphorylation." Curr Biol **31**(4): 794-808 e796.

Kamnasaran, D., C. P. Chen, K. Devriendt, L. Mehta and D. W. Cox (2005). "Defining a holoprosencephaly locus on human chromosome 14q13 and characterization of potential candidate genes." Genomics **85**(5): 608-621.

Kang, J. G., J. S. Park, J. H. Ko and Y. S. Kim (2019). "Regulation of gene expression by altered promoter methylation using a CRISPR/Cas9-mediated epigenetic editing system." Sci Rep **9**(1): 11960.

Kanska, J., M. Zakhour, B. Taylor-Harding, B. Y. Karlan and W. R. Wiedemeyer (2016). "Cyclin E as a potential therapeutic target in high grade serous ovarian cancer." Gynecol Oncol **143**(1): 152-158.

Kastrinos, F., E. M. Stoffel, J. Balmana, E. W. Steyerberg, R. Mercado and S. Syngal (2008). "Phenotype comparison of MLH1 and MSH2 mutation carriers in a cohort of 1,914 individuals undergoing clinical genetic testing in the United States." Cancer Epidemiol Biomarkers Prev **17**(8): 2044-2051.

Katagiri, A., K. Nakayama, M. T. Rahman, M. Rahman, H. Katagiri, M. Ishikawa, T. Ishibashi, K. Iida, Y. Otsuki, S. Nakayama and K. Miyazaki (2012). "Frequent loss of tumor suppressor ARID1A protein expression in adenocarcinomas/adenosquamous carcinomas of the uterine cervix." Int J Gynecol Cancer **22**(2): 208-212.

Keir, M. E., M. J. Butte, G. J. Freeman and A. H. Sharpe (2008). "PD-1 and its ligands in tolerance and immunity." Annu Rev Immunol **26**: 677-704.

Khalique, S., K. Naidoo, A. D. Attygalle, D. Kriplani, F. Daley, A. Lowe, J. Campbell, T. Jones, M. Hubank, K. Fenwick, N. Matthews, A. G. Rust, C. J. Lord, S. Banerjee and R. Natrajan (2018). "Optimised ARID1A immunohistochemistry is an accurate predictor of ARID1A mutational status in gynaecological cancers." J Pathol Clin Res **4**(3): 154-166.

Khalique, S., S. Nash, D. Mansfield, J. Wampfler, A. Attygale, K. Vroobel, H. Kemp, R. Buus, H. Cottom, I. Roxanis, T. Jones, K. von Loga, D. Begum, N. Guppy, P. Ramagiri, K. Fenwick, N. Matthews, M. J. F. Hubank, C. J. Lord, S. Haider, A. Melcher, S. Banerjee and R. Natrajan (2021). "Quantitative Assessment and Prognostic Associations of the Immune Landscape in Ovarian Clear Cell Carcinoma." Cancers (Basel) **13**(15).

Khew-Goodall, Y. and B. A. Hemmings (1988). "Tissue-specific expression of mRNAs encoding alpha- and beta-catalytic subunits of protein phosphatase 2A." FEBS Lett **238**(2): 265-268.

Kilgour, E., D. G. Rothwell, G. Brady and C. Dive (2020). "Liquid Biopsy-Based Biomarkers of Treatment Response and Resistance." Cancer Cell **37**(4): 485-495.

Kim, J. E., S. A. McAvoy, D. I. Smith and J. Chen (2005). "Human TopBP1 ensures genome integrity during normal S phase." Mol Cell Biol **25**(24): 10907-10915.

Kim, K. H., W. Kim, T. P. Howard, F. Vazquez, A. Tsherniak, J. N. Wu, W. Wang, J. R. Haswell, L. D. Walensky, W. C. Hahn, S. H. Orkin and C. W. Roberts (2015). "SWI/SNF-mutant cancers depend on catalytic and non-catalytic activity of EZH2." Nat Med **21**(12): 1491-1496.

Kim, S. I., J. W. Lee, M. Lee, H. S. Kim, H. H. Chung, J. W. Kim, N. H. Park, Y. S. Song and J. S. Seo (2018). "Genomic landscape of ovarian clear cell carcinoma via whole exome sequencing." Gynecol Oncol **148**(2): 375-382.

Kim, S. I., M. C. Lim, J. Lim, Y. J. Won, S. S. Seo, S. Kang and S. Y. Park (2016). "Incidence of epithelial ovarian cancer according to histologic subtypes in Korea, 1999 to 2012." J Gynecol Oncol **27**(1): e5.

King, D., H. E. D. Southgate, S. Roetschke, P. Gravells, L. Fields, J. B. Watson, L. Chen, D. Chapman, D. Harrison, D. Yeomanson, N. J. Curtin, D. A. Tweddle and H. E. Bryant (2021). "Increased Replication Stress Determines ATR Inhibitor Sensitivity in Neuroblastoma Cells." Cancers (Basel) **13**(24).

Kobel, M., S. E. Kalloger, N. Boyd, S. McKinney, E. Mehl, C. Palmer, S. Leung, N. J. Bowen, D. N. Ionescu, A. Rajput, L. M. Prentice, D. Miller, J. Santos, K. Swenerton, C. B. Gilks and D. Huntsman (2008). "Ovarian carcinoma subtypes are different diseases: implications for biomarker studies." PLoS Med **5**(12): e232.

Kobel, M., S. E. Kalloger, D. G. Huntsman, J. L. Santos, K. D. Swenerton, J. D. Seidman, C. B. Gilks and V. B. C. Cheryl Brown Ovarian Cancer Outcomes Unit of the British Columbia Cancer Agency (2010). "Differences in tumor type in low-stage versus high-stage ovarian carcinomas." Int J Gynecol Pathol **29**(3): 203-211.

Kobel, M., A. M. Piskorz, S. Lee, S. Lui, C. LePage, F. Marass, N. Rosenfeld, A. M. Mes Masson and J. D. Brenton (2016). "Optimized p53 immunohistochemistry is an accurate predictor of TP53 mutation in ovarian carcinoma." J Pathol Clin Res **2**(4): 247-258.

Koike-Yusa, H., Y. Li, E. P. Tan, C. Velasco-Herrera Mdel and K. Yusa (2014). "Genome-wide recessive genetic screening in mammalian cells with a lentiviral CRISPR-guide RNA library." Nat Biotechnol **32**(3): 267-273.

Koppenhafer, S. L., K. L. Goss, W. W. Terry and D. J. Gordon (2020). "Inhibition of the ATR-CHK1 Pathway in Ewing Sarcoma Cells Causes DNA Damage and Apoptosis via the CDK2-Mediated Degradation of RRM2." Mol Cancer Res **18**(1): 91-104.

Krasinska, L., M. R. Domingo-Sananes, O. Kapuy, N. Parisis, B. Harker, G. Moorhead, M. Rossignol, B. Novak and D. Fisher (2011). "Protein phosphatase 2A controls the order and dynamics of cell-cycle transitions." Mol Cell **44**(3): 437-450.

Kumagai, A., J. Lee, H. Y. Yoo and W. G. Dunphy (2006). "TopBP1 activates the ATR-ATRIP complex." Cell **124**(5): 943-955.

Kuo, K. T., T. L. Mao, X. Chen, Y. Feng, K. Nakayama, Y. Wang, R. Glas, M. J. Ma, R. J. Kurman, M. Shih Ie and T. L. Wang (2010). "DNA copy numbers profiles in affinity-purified ovarian clear cell carcinoma." Clin Cancer Res **16**(7): 1997-2008.

Kuo, K. T., T. L. Mao, S. Jones, E. Veras, A. Ayhan, T. L. Wang, R. Glas, D. Slamon, V. E. Velculescu, R. J. Kuman and M. Shih Ie (2009). "Frequent activating mutations of PIK3CA in ovarian clear cell carcinoma." Am J Pathol **174**(5): 1597-1601.

Kurashima, K., H. Kashiwagi, I. Shimomura, A. Suzuki, F. Takeshita, M. Mazevet, M. Harata, T. Yamashita, Y. Yamamoto, T. Kohno and B. Shiotani (2020). "SMARCA4 deficiency-associated heterochromatin induces intrinsic DNA replication stress and susceptibility to ATR inhibition in lung adenocarcinoma." NAR Cancer **2**(2): zcaa005.

Kurian, A. W., R. R. Balise, V. McGuire and A. S. Whittemore (2005). "Histologic types of epithelial ovarian cancer: have they different risk factors?" Gynecol Oncol **96**(2): 520-530.

Kurz, L., A. Miklyaeva, M. A. Skowron, N. Overbeck, G. Poschmann, T. Becker, K. Eul, T. Kurz, S. Schonberger, G. Calaminus, K. Stuhler, E. Dykhuizen, P. Albers and D. Nettersheim (2020). "ARID1A Regulates Transcription and the Epigenetic Landscape via POLE and DMAP1 while ARID1A Deficiency or Pharmacological Inhibition Sensitizes Germ Cell Tumor Cells to ATR Inhibition." Cancers (Basel) **12**(4).

Le, T. M., S. Poddar, J. R. Capri, E. R. Abt, W. Kim, L. Wei, N. T. Uong, C. M. Cheng, D. Braas, M. Nikanjam, P. Rix, D. Merkurjev, J. Zaretsky, H. I. Kornblum,

A. Ribas, H. R. Herschman, J. Whitelegge, K. F. Faull, T. R. Donahue, J. Czernin and C. G. Radu (2017). "ATR inhibition facilitates targeting of leukemia dependence on convergent nucleotide biosynthetic pathways." Nat Commun **8**(1): 241.

Ledermann, J. A., F. A. Raja, C. Fotopoulou, A. Gonzalez-Martin, N. Colombo, C. Sessa and E. G. W. Group (2013). "Newly diagnosed and relapsed epithelial ovarian carcinoma: ESMO Clinical Practice Guidelines for diagnosis, treatment and follow-up." Ann Oncol **24 Suppl 6**: vi24-32.

Lee, B. H., W. Chen, S. Stippec and M. H. Cobb (2007). "Biological cross-talk between WNK1 and the transforming growth factor beta-Smad signaling pathway." J Biol Chem **282**(25): 17985-17996.

Lee, Y. C., Q. Zhou, J. Chen and J. Yuan (2016). "RPA-Binding Protein ETAA1 Is an ATR Activator Involved in DNA Replication Stress Response." Curr Biol **26**(24): 3257-3268.

Lee, Y. Y., T. J. Kim, M. J. Kim, H. J. Kim, T. Song, M. K. Kim, C. H. Choi, J. W. Lee, D. S. Bae and B. G. Kim (2011). "Prognosis of ovarian clear cell carcinoma compared to other histological subtypes: a meta-analysis." Gynecol Oncol **122**(3): 541-547.

Lempiainen, H. and T. D. Halazonetis (2009). "Emerging common themes in regulation of PIKKs and PI3Ks." EMBO J **28**(20): 3067-3073.

Lenaerts, L., S. Reynhout, I. Verbinnen, F. Laumonnier, A. Toutain, F. Bonnet-Brilhault, Y. Hoorne, S. Joss, A. K. Chassevent, C. Smith-Hicks, B. Loeys, P. Joset, K. Steindl, A. Rauch, S. G. Mehta, W. K. Chung, K. Devriendt, S. E. Holder, T. Jewett, L. M. Baldwin, W. G. Wilson, S. Towner, S. Srivastava, H. F. Johnson, C. Daumer-Haas, M. Baethmann, A. Ruiz, E. Gabau, V. Jain, V. Varghese, A. Al-Beshri, S. Fulton, O. Wechsberg, N. Orenstein, K. Prescott, A. M. Childs, L. Faivre, S. Moutton, J. A. Sullivan, V. Shashi, S. M. Koudijs, M. Heijligers, E. Kivuva, A. McTague, A. Male, Y. van Ierland, B. Plecko, I. Maystadt, R. Hamid, V. L. Hannig, G. Houge and V. Janssens (2021). "The broad phenotypic spectrum of PPP2R1A-related neurodevelopmental disorders correlates with the degree of biochemical dysfunction." Genet Med **23**(2): 352-362.

Lheureux, S., A. Tinker, B. Clarke, P. Ghatage, S. Welch, J. I. Weberpals, N. C. Dhani, M. O. Butler, K. Tonkin, Q. Tan, D. S. P. Tan, K. Brooks, J. Ramsahai, L. Wang, N. A. Pham, P. A. Shaw, M. S. Tsao, S. Garg, T. Stockley and A. M. Oza (2018). "A Clinical and Molecular Phase II Trial of Oral ENMD-2076 in Ovarian

Clear Cell Carcinoma (OCCC): A Study of the Princess Margaret Phase II Consortium." Clin Cancer Res **24**(24): 6168-6174.

Li, F., D. Kozono, P. Deraska, T. Branigan, C. Dunn, X. F. Zheng, K. Parmar, H. Nguyen, J. DeCaprio, G. I. Shapiro, D. Chowdhury and A. D. D'Andrea (2020). "CHK1 Inhibitor Blocks Phosphorylation of FAM122A and Promotes Replication Stress." Mol Cell **80**(3): 410-422 e416.

Li, L., M. Li, Z. Jiang and X. Wang (2019). "ARID1A Mutations Are Associated with Increased Immune Activity in Gastrointestinal Cancer." Cells **8**(7).

Li, Y., L. Li, J. Qin, J. Wu, X. Dai and J. Xu (2021). "OSR1 phosphorylates the Smad2/3 linker region and induces TGF-beta1 autocrine to promote EMT and metastasis in breast cancer." Oncogene **40**(1): 68-84.

Liang, H., L. W. Cheung, J. Li, Z. Ju, S. Yu, K. Stemke-Hale, T. Dogruluk, Y. Lu, X. Liu, C. Gu, W. Guo, S. E. Scherer, H. Carter, S. N. Westin, M. D. Dyer, R. G. Verhaak, F. Zhang, R. Karchin, C. G. Liu, K. H. Lu, R. R. Broaddus, K. L. Scott, B. T. Hennessy and G. B. Mills (2012). "Whole-exome sequencing combined with functional genomics reveals novel candidate driver cancer genes in endometrial cancer." Genome Res **22**(11): 2120-2129.

Lin-Hurtubise, K. M., C. G. Yheulon, R. A. Gagliano, Jr. and H. T. Lynch (2013). "Excess of extracolonic non-endometrial multiple primary cancers in MSH2 germline mutation carriers over MLH1." J Surg Oncol **108**(7): 433-437.

Litton, J. K., S. A. Hurvitz, L. A. Mina, H. S. Rugo, K. H. Lee, A. Goncalves, S. Diab, N. Woodward, A. Goodwin, R. Yerushalmi, H. Roche, Y. H. Im, W. Eiermann, R. G. W. Quek, T. Usari, S. Lanzalone, A. Czibere, J. L. Blum, M. Martin and J. Ettl (2020). "Talazoparib versus chemotherapy in patients with germline BRCA1/2-mutated HER2-negative advanced breast cancer: final overall survival results from the EMBRACA trial." Ann Oncol **31**(11): 1526-1535.

Liu, Q., S. Guntuku, X. S. Cui, S. Matsuoka, D. Cortez, K. Tamai, G. Luo, S. Carattini-Rivera, F. DeMayo, A. Bradley, L. A. Donehower and S. J. Elledge (2000). "Chk1 is an essential kinase that is regulated by Atr and required for the G(2)/M DNA damage checkpoint." Genes Dev **14**(12): 1448-1459.

Liu, S., X. Cai, J. Wu, Q. Cong, X. Chen, T. Li, F. Du, J. Ren, Y. T. Wu, N. V. Grishin and Z. J. Chen (2015). "Phosphorylation of innate immune adaptor proteins MAVS, STING, and TRIF induces IRF3 activation." Science **347**(6227): aaa2630.

Lord, C. J. and A. Ashworth (2016). "BRCAness revisited." Nat Rev Cancer **16**(2): 110-120.

Lord, C. J. and A. Ashworth (2017). "PARP inhibitors: Synthetic lethality in the clinic." Science **355**(6330): 1152-1158.

Lord, C. J., A. N. Tutt and A. Ashworth (2015). "Synthetic lethality and cancer therapy: lessons learned from the development of PARP inhibitors." Annu Rev Med **66**: 455-470.

Lossaint, G., M. Larroque, C. Ribeyre, N. Bec, C. Larroque, C. Decaillet, K. Gari and A. Constantinou (2013). "FANCD2 binds MCM proteins and controls replisome function upon activation of s phase checkpoint signaling." Mol Cell **51**(5): 678-690.

Loveday, C., C. Turnbull, E. Ramsay, D. Hughes, E. Ruark, J. R. Frankum, G. Bowden, B. Kalmyrzaev, M. Warren-Perry, K. Snape, J. W. Adlard, J. Barwell, J. Berg, A. F. Brady, C. Brewer, G. Brice, C. Chapman, J. Cook, R. Davidson, A. Donaldson, F. Douglas, L. Greenhalgh, A. Henderson, L. Izatt, A. Kumar, F. Lalloo, Z. Miedzybrodzka, P. J. Morrison, J. Paterson, M. Porteous, M. T. Rogers, S. Shanley, L. Walker, C. Breast Cancer Susceptibility, D. Eccles, D. G. Evans, A. Renwick, S. Seal, C. J. Lord, A. Ashworth, J. S. Reis-Filho, A. C. Antoniou and N. Rahman (2011). "Germline mutations in RAD51D confer susceptibility to ovarian cancer." Nat Genet **43**(9): 879-882.

Loveday, C., C. Turnbull, E. Ruark, R. M. Xicola, E. Ramsay, D. Hughes, M. Warren-Perry, K. Snape, C. Breast Cancer Susceptibility, D. Eccles, D. G. Evans, M. Gore, A. Renwick, S. Seal, A. C. Antoniou and N. Rahman (2012). "Germline RAD51C mutations confer susceptibility to ovarian cancer." Nat Genet **44**(5): 475-476; author reply 476.

Lowery, W. J., J. M. Schildkraut, L. Akushevich, R. Bentley, J. R. Marks, D. Huntsman and A. Berchuck (2012). "Loss of ARID1A-associated protein expression is a frequent event in clear cell and endometrioid ovarian cancers." Int J Gynecol Cancer **22**(1): 9-14.

Lujan, S. A., J. S. Williams and T. A. Kunkel (2016). "DNA Polymerases Divide the Labor of Genome Replication." Trends Cell Biol **26**(9): 640-654.

Lukas, C., V. Savic, S. Bekker-Jensen, C. Doil, B. Neumann, R. S. Pedersen, M. Grofte, K. L. Chan, I. D. Hickson, J. Bartek and J. Lukas (2011). "53BP1 nuclear

bodies form around DNA lesions generated by mitotic transmission of chromosomes under replication stress." Nat Cell Biol **13**(3): 243-253.

Ma, C. X., J. W. Janetka and H. Piwnica-Worms (2011). "Death by releasing the breaks: CHK1 inhibitors as cancer therapeutics." Trends Mol Med **17**(2): 88-96.

Mabuchi, S., C. Kawase, D. A. Altomare, K. Morishige, M. Hayashi, K. Sawada, K. Ito, Y. Terai, Y. Nishio, A. J. Klein-Szanto, R. A. Burger, M. Ohmichi, J. R. Testa and T. Kimura (2010). "Vascular endothelial growth factor is a promising therapeutic target for the treatment of clear cell carcinoma of the ovary." Mol Cancer Ther **9**(8): 2411-2422.

Mackay, H. J., M. F. Brady, A. M. Oza, A. Reuss, E. Pujade-Lauraine, A. M. Swart, N. Siddiqui, N. Colombo, M. A. Bookman, J. Pfisterer, A. du Bois and I. Gynecologic Cancer (2010). "Prognostic relevance of uncommon ovarian histology in women with stage III/IV epithelial ovarian cancer." Int J Gynecol Cancer **20**(6): 945-952.

Mackenzie, K. J., P. Carroll, C. A. Martin, O. Murina, A. Fluteau, D. J. Simpson, N. Olova, H. Sutcliffe, J. K. Rainger, A. Leitch, R. T. Osborn, A. P. Wheeler, M. Nowotny, N. Gilbert, T. Chandra, M. A. M. Reijns and A. P. Jackson (2017). "cGAS surveillance of micronuclei links genome instability to innate immunity." Nature **548**(7668): 461-465.

Mackenzie, R., S. Kommoss, B. J. Winterhoff, B. R. Kipp, J. J. Garcia, J. Voss, K. Halling, A. Karnezis, J. Senz, W. Yang, E. S. Prigge, M. Reuschenbach, M. V. Doeberitz, B. C. Gilks, D. G. Huntsman, J. Bakkum-Gamez, J. N. McAlpine and M. S. Anglesio (2015). "Targeted deep sequencing of mucinous ovarian tumors reveals multiple overlapping RAS-pathway activating mutations in borderline and cancerous neoplasms." BMC Cancer **15**: 415.

Maeda, D., T. L. Mao, M. Fukayama, S. Nakagawa, T. Yano, Y. Taketani and M. Shih Ie (2010). "Clinicopathological significance of loss of ARID1A immunoreactivity in ovarian clear cell carcinoma." Int J Mol Sci **11**(12): 5120-5128.

Mailand, N., J. Falck, C. Lukas, R. G. Syljuasen, M. Welcker, J. Bartek and J. Lukas (2000). "Rapid destruction of human Cdc25A in response to DNA damage." Science **288**(5470): 1425-1429.

Mali, P., J. Aach, P. B. Stranges, K. M. Esvelt, M. Moosburner, S. Kosuri, L. Yang and G. M. Church (2013). "CAS9 transcriptional activators for target specificity

screening and paired nickases for cooperative genome engineering." Nat Biotechnol **31**(9): 833-838.

Mali, P., L. Yang, K. M. Esvelt, J. Aach, M. Guell, J. E. DiCarlo, J. E. Norville and G. M. Church (2013). "RNA-guided human genome engineering via Cas9." Science **339**(6121): 823-826.

Martens, E., I. Stevens, V. Janssens, J. Vermeesch, J. Gotz, J. Goris and C. Van Hoof (2004). "Genomic organisation, chromosomal localisation tissue distribution and developmental regulation of the PR61/B' regulatory subunits of protein phosphatase 2A in mice." J Mol Biol **336**(4): 971-986.

Mashtalir, N., A. R. D'Avino, B. C. Michel, J. Luo, J. Pan, J. E. Otto, H. J. Zullow, Z. M. McKenzie, R. L. Kubiak, R. St Pierre, A. M. Valencia, S. J. Poynter, S. H. Cassel, J. A. Ranish and C. Kadoch (2018). "Modular Organization and Assembly of SWI/SNF Family Chromatin Remodeling Complexes." Cell **175**(5): 1272-1288 e1220.

Mateo, J., N. Porta, D. Bianchini, U. McGovern, T. Elliott, R. Jones, I. Syndikus, C. Ralph, S. Jain, M. Varughese, O. Parikh, S. Crabb, A. Robinson, D. McLaren, A. Birtle, J. Tanguay, S. Miranda, I. Figueiredo, G. Seed, C. Bertan, P. Flohr, B. Ebbs, P. Rescigno, G. Fowler, A. Ferreira, R. Riisnaes, R. Pereira, A. Curcean, R. Chandler, M. Clarke, B. Gurel, M. Crespo, D. Nava Rodrigues, S. Sandhu, A. Espinasse, P. Chatfield, N. Tunariu, W. Yuan, E. Hall, S. Carreira and J. S. de Bono (2020). "Olaparib in patients with metastatic castration-resistant prostate cancer with DNA repair gene aberrations (TOPARP-B): a multicentre, open-label, randomised, phase 2 trial." Lancet Oncol **21**(1): 162-174.

Mathur, R., B. H. Alver, A. K. San Roman, B. G. Wilson, X. Wang, A. T. Agoston, P. J. Park, R. A. Shivdasani and C. W. Roberts (2017). "ARID1A loss impairs enhancer-mediated gene regulation and drives colon cancer in mice." Nat Genet **49**(2): 296-302.

Matsuo, K., K. Hasegawa, K. Yoshino, R. Murakami, T. Hisamatsu, R. L. Stone, R. A. Previs, J. M. Hansen, Y. Ikeda, A. Miyara, K. Hiramatsu, T. Enomoto, K. Fujiwara, N. Matsumura, I. Konishi, L. D. Roman, H. Gabra, C. Fotopoulou and A. K. Sood (2015). "Venous thromboembolism, interleukin-6 and survival outcomes in patients with advanced ovarian clear cell carcinoma." Eur J Cancer **51**(14): 1978-1988.

Matulonis, U. A., R. Shapira-Frommer, A. D. Santin, A. S. Lisyanskaya, S. Pignata, I. Vergote, F. Raspagliesi, G. S. Sonke, M. Birrer, D. M. Provencher, J. Sehouli, N. Colombo, A. Gonzalez-Martin, A. Oaknin, P. B. Ottevanger, V.

Rudaitis, K. Katchar, H. Wu, S. Keefe, J. Ruman and J. A. Ledermann (2019). "Antitumor activity and safety of pembrolizumab in patients with advanced recurrent ovarian cancer: results from the phase II KEYNOTE-100 study." Ann Oncol **30**(7): 1080-1087.

Mayer-Jaekel, R. E. and B. A. Hemmings (1994). "Protein phosphatase 2A--a 'menage a trois'." Trends Cell Biol **4**(8): 287-291.

McCabe, N., N. C. Turner, C. J. Lord, K. Kluzek, A. Bialkowska, S. Swift, S. Giavara, M. J. O'Connor, A. N. Tutt, M. Z. Zdzienicka, G. C. Smith and A. Ashworth (2006). "Deficiency in the repair of DNA damage by homologous recombination and sensitivity to poly(ADP-ribose) polymerase inhibition." Cancer Res **66**(16): 8109-8115.

McClinch, K., R. A. Avelar, D. Callejas, S. Izadmehr, D. Wiredja, A. Perl, J. Sangodkar, D. B. Kastrinsky, D. Schlatzer, M. Cooper, J. Kiselar, A. Stachnik, S. Yao, D. Hoon, D. McQuaid, N. Zaware, Y. Gong, D. L. Brautigan, S. R. Plymate, C. C. T. Sprenger, W. K. Oh, A. C. Levine, A. Kirschenbaum, J. P. Sfakianos, R. Sears, A. DiFeo, Y. Ioannou, M. Ohlmeyer, G. Narla and M. D. Galsky (2018). "Small-Molecule Activators of Protein Phosphatase 2A for the Treatment of Castration-Resistant Prostate Cancer." Cancer Res **78**(8): 2065-2080.

McCluggage, W. G. (2011). "Morphological subtypes of ovarian carcinoma: a review with emphasis on new developments and pathogenesis." Pathology **43**(5): 420-432.

McConechy, M. C., V.; Morin, G.; Brenton, J.; Huntsman, D. (2013). "PPP2R1A mutations affect PP2A complex formation, and novel protein interactions in gynecological carcinoma cell lines. [abstract]In: Proceedings of the AACR Special Conference on Advances in Ovarian Cancer Research: From Concept to Clinic; Sep 18-21, 2013; Miami, FL." Clin Cancer Res **19**.

McConechy, M. K., M. S. Anglesio, S. E. Kalloger, W. Yang, J. Senz, C. Chow, A. Heravi-Moussavi, G. B. Morin, A. M. Mes-Masson, G. Australian Ovarian Cancer Study, M. S. Carey, J. N. McAlpine, J. S. Kwon, L. M. Prentice, N. Boyd, S. P. Shah, C. B. Gilks and D. G. Huntsman (2011). "Subtype-specific mutation of PPP2R1A in endometrial and ovarian carcinomas." J Pathol **223**(5): 567-573.

McCright, B., A. M. Rivers, S. Audlin and D. M. Virshup (1996). "The B56 family of protein phosphatase 2A (PP2A) regulatory subunits encodes differentiation-induced phosphoproteins that target PP2A to both nucleus and cytoplasm." J Biol Chem **271**(36): 22081-22089.

McGlynn, P. and R. G. Lloyd (2002). "Recombinational repair and restart of damaged replication forks." Nat Rev Mol Cell Biol **3**(11): 859-870.

Mei, L., J. Zhang, K. He and J. Zhang (2019). "Ataxia telangiectasia and Rad3-related inhibitors and cancer therapy: where we stand." J Hematol Oncol **12**(1): 43.

Meister, G., M. Landthaler, Y. Dorsett and T. Tuschl (2004). "Sequence-specific inhibition of microRNA- and siRNA-induced RNA silencing." RNA **10**(3): 544-550.

Michel, B. C., A. R. D'Avino, S. H. Cassel, N. Mashtalir, Z. M. McKenzie, M. J. McBride, A. M. Valencia, Q. Zhou, M. Bocker, L. M. M. Soares, J. Pan, D. I. Remillard, C. A. Lareau, H. J. Zullow, N. Fortoul, N. S. Gray, J. E. Bradner, H. M. Chan and C. Kadoch (2018). "A non-canonical SWI/SNF complex is a synthetic lethal target in cancers driven by BAF complex perturbation." Nat Cell Biol **20**(12): 1410-1420.

Miller, R. E., R. Brough, I. Bajrami, C. T. Williamson, S. McDade, J. Campbell, A. Kigozi, R. Rafiq, H. Pemberton, R. Natrajan, J. Joel, H. Astley, C. Mahoney, J. D. Moore, C. Torrance, J. D. Gordan, J. T. Webber, R. S. Levin, K. M. Shokat, S. Bandyopadhyay, C. J. Lord and A. Ashworth (2016). "Synthetic Lethal Targeting of ARID1A-Mutant Ovarian Clear Cell Tumors with Dasatinib." Mol Cancer Ther **15**(7): 1472-1484.

Mizuno, M., H. Kajiyama, K. Shibata, K. Mizuno, O. Yamamuro, M. Kawai, T. Nakanishi, T. Nagasaka and F. Kikkawa (2012). "Adjuvant chemotherapy for stage i ovarian clear cell carcinoma: is it necessary for stage IA?" Int J Gynecol Cancer **22**(7): 1143-1149.

Mogensen, J. B., S. K. Kjaer, L. Mellemkjaer and A. Jensen (2016). "Endometriosis and risks for ovarian, endometrial and breast cancers: A nationwide cohort study." Gynecol Oncol **143**(1): 87-92.

Moiseeva, T., B. Hood, S. Schamus, M. J. O'Connor, T. P. Conrads and C. J. Bakkenist (2017). "ATR kinase inhibition induces unscheduled origin firing through a Cdc7-dependent association between GINS and And-1." Nat Commun **8**(1): 1392.

Moiseeva, T. N., Y. Yin, M. J. Calderon, C. Qian, S. Schamus-Haynes, N. Sugitani, H. U. Osmanbeyoglu, E. Rothenberg, S. C. Watkins and C. J. Bakkenist (2019). "An ATR and CHK1 kinase signaling mechanism that limits origin firing

during unperturbed DNA replication." Proc Natl Acad Sci U S A **116**(27): 13374-13383.

Mojica, F. J., C. Diez-Villasenor, J. Garcia-Martinez and E. Soria (2005). "Intervening sequences of regularly spaced prokaryotic repeats derive from foreign genetic elements." J Mol Evol **60**(2): 174-182.

Moreno, A., J. T. Carrington, L. Albergante, M. Al Mamun, E. J. Haagensen, E. S. Komseli, V. G. Gorgoulis, T. J. Newman and J. J. Blow (2016). "Unreplicated DNA remaining from unperturbed S phases passes through mitosis for resolution in daughter cells." Proc Natl Acad Sci U S A **113**(39): E5757-5764.

Moreno, C. S., S. Park, K. Nelson, D. Ashby, F. Hubalek, W. S. Lane and D. C. Pallas (2000). "WD40 repeat proteins striatin and S/G(2) nuclear autoantigen are members of a novel family of calmodulin-binding proteins that associate with protein phosphatase 2A." J Biol Chem **275**(8): 5257-5263.

Murai, J., S. Y. Huang, B. B. Das, A. Renaud, Y. Zhang, J. H. Doroshow, J. Ji, S. Takeda and Y. Pommier (2012). "Trapping of PARP1 and PARP2 by Clinical PARP Inhibitors." Cancer Res **72**(21): 5588-5599.

Murai, J., S. Y. Huang, A. Renaud, Y. Zhang, J. Ji, S. Takeda, J. Morris, B. Teicher, J. H. Doroshow and Y. Pommier (2014). "Stereospecific PARP trapping by BMN 673 and comparison with olaparib and rucaparib." Mol Cancer Ther **13**(2): 433-443.

Murali, R., R. A. Soslow and B. Weigelt (2014). "Classification of endometrial carcinoma: more than two types." Lancet Oncol **15**(7): e268-278.

Nagl, N. G., Jr., A. Patsialou, D. S. Haines, P. B. Dallas, G. R. Beck, Jr. and E. Moran (2005). "The p270 (ARID1A/SMARCF1) subunit of mammalian SWI/SNF-related complexes is essential for normal cell cycle arrest." Cancer Res **65**(20): 9236-9244.

Narushima, Y., H. Kozuka-Hata, K. Tsumoto, J. Inoue and M. Oyama (2016). "Quantitative phosphoproteomics-based molecular network description for high-resolution kinase-substrate interactome analysis." Bioinformatics **32**(14): 2083-2088.

National Cancer, I. and N. Oncology. (2016, November 11). "Dasatinib in Treating Patients With Recurrent or Persistent Ovarian, Fallopian Tube, Endometrial or

Peritoneal Cancer." Retrieved 29th July, 2022, from https://ClinicalTrials.gov/show/NCT02059265.

National Cancer, I. and N. R. G. Oncology. (2017, January 31). "Tazemetostat in Treating Patients With Recurrent Ovarian or Endometrial Cancer." Retrieved 28th July, 2022, from https://ClinicalTrials.gov/show/NCT03348631.

NICE. (2013). "Bevacizumab in combination with paclitaxel and carboplatin for first-line treatment of advanced ovarian cancer
." Retrieved 26th July, 2022, from https://www.nice.org.uk/guidance/ta284.

NICE. (2019). "Olaparib for maintenance treatment of BRCA mutation-positive advanced ovarian, fallopian tube or peritoneal cancer after response to first-line platinum-based chemotherapy." Retrieved 26th July, 2022, from https://www.nice.org.uk/guidance/ta598/chapter/1-Recommendations.

NICE. (2019). "Rucaparib for maintenance treatment of relapsed platinum-sensitive ovarian, fallopian tube or peritoneal cancer." Retrieved 26th July, 2022, from https://www.nice.org.uk/guidance/ta611.

NICE. (2021). "Niraparib for maintenance treatment of advanced ovarian, fallopian tube and peritoneal cancer after response to first-line platinum-based chemotherapy." Retrieved 26th July, 2022, from https://www.nice.org.uk/guidance/ta673/documents/final-appraisal-determination-document.

NICE. (2021). "Olaparib plus bevacizumab for maintenance treatment of advanced ovarian, fallopian tube or primary peritoneal cancer " Retrieved 26th July, 2022 from https://www.nice.org.uk/guidance/ta693/resources/olaparib-plus-bevacizumab-for-maintenance-treatment-of-advanced-ovarian-fallopian-tube-or-primary-peritoneal-cancer-pdf-82609438840261.

NICE. (2022). "Niraparib for maintenance treatment of relapsed, platinum-sensitive ovarian, fallopian tube and peritoneal cancer." Retrieved 26th July, 2022, from https://www.nice.org.uk/guidance/ta784/chapter/1-Recommendations.

O'Connell, J. D., J. A. Paulo, J. J. O'Brien and S. P. Gygi (2018). "Proteome-Wide Evaluation of Two Common Protein Quantification Methods." J Proteome Res **17**(5): 1934-1942.

O'Connor, C. M., D. Leonard, D. Wiredja, R. A. Avelar, Z. Wang, D. Schlatzer, B. Bryson, E. Tokala, S. E. Taylor, A. Upadhyay, J. Sangodkar, A. C. Gingras, J. Westermarck, W. Xu, A. DiFeo, D. L. Brautigan, S. Haider, M. Jackson and G. Narla (2020). "Inactivation of PP2A by a recurrent mutation drives resistance to MEK inhibitors." Oncogene **39**(3): 703-717.

O'Connor, C. M., S. E. Taylor, K. M. Miller, L. Hurst, T. J. Haanen, T. K. Suhan, K. P. Zawacki, F. K. Noto, J. Trako, A. Mohan, J. Sangodkar, D. Zamarin, A. DiFeo and G. Narla (2022). "Targeting Ribonucleotide Reductase Induces Synthetic Lethality in PP2A-Deficient Uterine Serous Carcinoma." Cancer Res **82**(4): 721-733.

Ogiwara, H., K. Takahashi, M. Sasaki, T. Kuroda, H. Yoshida, R. Watanabe, A. Maruyama, H. Makinoshima, F. Chiwaki, H. Sasaki, T. Kato, A. Okamoto and T. Kohno (2019). "Targeting the Vulnerability of Glutathione Metabolism in ARID1A-Deficient Cancers." Cancer Cell **35**(2): 177-190 e178.

Okamoto, A., R. M. Glasspool, S. Mabuchi, N. Matsumura, H. Nomura, H. Itamochi, M. Takano, T. Takano, N. Susumu, D. Aoki, I. Konishi, A. Covens, J. Ledermann, D. Mezzanzanica, C. Steer, D. Millan, I. A. McNeish, J. Pfisterer, S. Kang, L. Gladieff, J. Bryce and A. Oza (2014). "Gynecologic Cancer InterGroup (GCIG) consensus review for clear cell carcinoma of the ovary." Int J Gynecol Cancer **24**(9 Suppl 3): S20-25.

Okazaki, T. (2017). "Days weaving the lagging strand synthesis of DNA - A personal recollection of the discovery of Okazaki fragments and studies on discontinuous replication mechanism." Proc Jpn Acad Ser B Phys Biol Sci **93**(5): 322-338.

Oliver, K. E., W. E. Brady, M. Birrer, D. M. Gershenson, G. Fleming, L. J. Copeland, K. Tewari, P. A. Argenta, R. S. Mannel, A. A. Secord, J. M. Stephan, D. G. Mutch, F. B. Stehman, F. M. Muggia, P. G. Rose, D. K. Armstrong, M. A. Bookman, R. A. Burger and J. H. Farley (2017). "An evaluation of progression free survival and overall survival of ovarian cancer patients with clear cell carcinoma versus serous carcinoma treated with platinum therapy: An NRG Oncology/Gynecologic Oncology Group experience." Gynecol Oncol **147**(2): 243-249.

Ordi, J., C. Romagosa, F. A. Tavassoli, F. Nogales, A. Palacin, E. Condom, A. Torne and A. Cardesa (2003). "CD10 expression in epithelial tissues and tumors of the gynecologic tract: a useful marker in the diagnosis of mesonephric, trophoblastic, and clear cell tumors." Am J Surg Pathol **27**(2): 178-186.

Oza, A. M., F. Selle, I. Davidenko, J. Korach, C. Mendiola, P. Pautier, E. Chmielowska, A. Bamias, A. DeCensi, Z. Zvirbule, A. Gonzalez-Martin, R. Hegg, F. Joly, C. Zamagni, A. Gadducci, N. Martin, S. Robb and N. Colombo (2017). "Efficacy and Safety of Bevacizumab-Containing Therapy in Newly Diagnosed Ovarian Cancer: ROSiA Single-Arm Phase 3B Study." Int J Gynecol Cancer **27**(1): 50-58.

Pantel, K. and C. Alix-Panabieres (2010). "Circulating tumour cells in cancer patients: challenges and perspectives." Trends Mol Med **16**(9): 398-406.

Panzarino, N. J., J. J. Krais, K. Cong, M. Peng, M. Mosqueda, S. U. Nayak, S. M. Bond, J. A. Calvo, M. B. Doshi, M. Bere, J. Ou, B. Deng, L. J. Zhu, N. Johnson and S. B. Cantor (2021). "Replication Gaps Underlie BRCA Deficiency and Therapy Response." Cancer Res **81**(5): 1388-1397.

Pardoll, D. M. (2012). "The blockade of immune checkpoints in cancer immunotherapy." Nat Rev Cancer **12**(4): 252-264.

Pather, S. and M. A. Quinn (2005). "Clear-cell cancer of the ovary-is it chemosensitive?" Int J Gynecol Cancer **15**(3): 432-437.

Pearce, C. L., C. Templeman, M. A. Rossing, A. Lee, A. M. Near, P. M. Webb, C. M. Nagle, J. A. Doherty, K. L. Cushing-Haugen, K. G. Wicklund, J. Chang-Claude, R. Hein, G. Lurie, L. R. Wilkens, M. E. Carney, M. T. Goodman, K. Moysich, S. K. Kjaer, E. Hogdall, A. Jensen, E. L. Goode, B. L. Fridley, M. C. Larson, J. M. Schildkraut, R. T. Palmieri, D. W. Cramer, K. L. Terry, A. F. Vitonis, L. J. Titus, A. Ziogas, W. Brewster, H. Anton-Culver, A. Gentry-Maharaj, S. J. Ramus, A. R. Anderson, D. Brueggmann, P. A. Fasching, S. A. Gayther, D. G. Huntsman, U. Menon, R. B. Ness, M. C. Pike, H. Risch, A. H. Wu, A. Berchuck and C. Ovarian Cancer Association (2012). "Association between endometriosis and risk of histological subtypes of ovarian cancer: a pooled analysis of case-control studies." Lancet Oncol **13**(4): 385-394.

Perl, A. L., C. M. O'Connor, P. Fa, F. Mayca Pozo, J. Zhang, Y. Zhang and G. Narla (2019). "Protein phosphatase 2A controls ongoing DNA replication by binding to and regulating cell division cycle 45 (CDC45)." J Biol Chem **294**(45): 17043-17059.

Perry, J. A. and S. Kornbluth (2007). "Cdc25 and Wee1: analogous opposites?" Cell Div **2**: 12.

Petermann, E., M. Woodcock and T. Helleday (2010). "Chk1 promotes replication fork progression by controlling replication initiation." Proc Natl Acad Sci U S A **107**(37): 16090-16095.

Pettitt, S. J., F. L. Rehman, I. Bajrami, R. Brough, F. Wallberg, I. Kozarewa, K. Fenwick, I. Assiotis, L. Chen, J. Campbell, C. J. Lord and A. Ashworth (2013). "A genetic screen using the PiggyBac transposon in haploid cells identifies Parp1 as a mediator of olaparib toxicity." PLoS One **8**(4): e61520.

Pommier, Y., E. Leo, H. Zhang and C. Marchand (2010). "DNA topoisomerases and their poisoning by anticancer and antibacterial drugs." Chem Biol **17**(5): 421-433.

Prat, J. and F. C. o. G. Oncology (2014). "Staging classification for cancer of the ovary, fallopian tube, and peritoneum." Int J Gynaecol Obstet **124**(1): 1-5.

Prat, J. and F. C. o. G. Oncology (2015). "FIGO's staging classification for cancer of the ovary, fallopian tube, and peritoneum: abridged republication." J Gynecol Oncol **26**(2): 87-89.

Prisma, H.-U. and I. Epizyme. (2021, January). "Phase II Study of Tazemetostat in Solid Tumors Harboring an ARID1A Mutation." Retrieved 28th July, 2022, from https://ClinicalTrials.gov/show/NCT05023655.

Pursell, Z. F., I. Isoz, E. B. Lundstrom, E. Johansson and T. A. Kunkel (2007). "Yeast DNA polymerase epsilon participates in leading-strand DNA replication." Science **317**(5834): 127-130.

Qiu, Z., P. Fa, T. Liu, C. B. Prasad, S. Ma, Z. Hong, E. R. Chan, H. Wang, Z. Li, K. He, Q. E. Wang, T. M. Williams, C. Yan, S. T. Sizemore, G. Narla and J. Zhang (2020). "A genome-wide pooled shRNA screen identifies PPP2R2A as a predictive biomarker for the response to ATR and CHK1 inhibitors." Cancer Res.

Rafnar, T., D. F. Gudbjartsson, P. Sulem, A. Jonasdottir, A. Sigurdsson, A. Jonasdottir, S. Besenbacher, P. Lundin, S. N. Stacey, J. Gudmundsson, O. T. Magnusson, L. le Roux, G. Orlygsdottir, H. T. Helgadottir, H. Johannsdottir, A. Gylfason, L. Tryggvadottir, J. G. Jonasson, A. de Juan, E. Ortega, J. M. Ramon-Cajal, M. D. Garcia-Prats, C. Mayordomo, A. Panadero, F. Rivera, K. K. Aben, A. M. van Altena, L. F. Massuger, M. Aavikko, P. M. Kujala, S. Staff, L. A. Aaltonen, K. Olafsdottir, J. Bjornsson, A. Kong, A. Salvarsdottir, H. Saemundsson, K. Olafsson, K. R. Benediktsdottir, J. Gulcher, G. Masson, L. A. Kiemeney, J. I.

Mayordomo, U. Thorsteinsdottir and K. Stefansson (2011). "Mutations in BRIP1 confer high risk of ovarian cancer." Nat Genet **43**(11): 1104-1107.

Ragland, R. L., S. Patel, R. S. Rivard, K. Smith, A. A. Peters, A. K. Bielinsky and E. J. Brown (2013). "RNF4 and PLK1 are required for replication fork collapse in ATR-deficient cells." Genes Dev **27**(20): 2259-2273.

Rahman, M., K. Nakayama, M. T. Rahman, H. Katagiri, A. Katagiri, T. Ishibashi, M. Ishikawa, K. Iida and K. Miyazaki (2013). "Clinicopathologic analysis of loss of AT-rich interactive domain 1A expression in endometrial cancer." Hum Pathol **44**(1): 103-109.

Rahman, M. T., K. Nakayama, M. Rahman, N. Nakayama, M. Ishikawa, A. Katagiri, K. Iida, S. Nakayama, Y. Otsuki, M. Shih Ie and K. Miyazaki (2012). "Prognostic and therapeutic impact of the chromosome 20q13.2 ZNF217 locus amplification in ovarian clear cell carcinoma." Cancer **118**(11): 2846-2857.

Ray-Coquard, I., P. Morice, D. Lorusso, J. Prat, A. Oaknin, P. Pautier, N. Colombo and E. G. C. E. a. clinicalguidelines@esmo.org (2018). "Non-epithelial ovarian cancer: ESMO Clinical Practice Guidelines for diagnosis, treatment and follow-up." Ann Oncol **29 Suppl 4**: iv1-iv18.

Ray-Coquard, I., P. Pautier, S. Pignata, D. Perol, A. Gonzalez-Martin, R. Berger, K. Fujiwara, I. Vergote, N. Colombo, J. Maenpaa, F. Selle, J. Sehouli, D. Lorusso, E. M. Guerra Alia, A. Reinthaller, S. Nagao, C. Lefeuvre-Plesse, U. Canzler, G. Scambia, A. Lortholary, F. Marme, P. Combe, N. de Gregorio, M. Rodrigues, P. Buderath, C. Dubot, A. Burges, B. You, E. Pujade-Lauraine, P. Harter and P.-. Investigators (2019). "Olaparib plus Bevacizumab as First-Line Maintenance in Ovarian Cancer." N Engl J Med **381**(25): 2416-2428.

Rehman, F. L., C. J. Lord and A. Ashworth (2010). "Synthetic lethal approaches to breast cancer therapy." Nat Rev Clin Oncol **7**(12): 718-724.

Reid, B. M., J. B. Permuth and T. A. Sellers (2017). "Epidemiology of ovarian cancer: a review." Cancer Biol Med **14**(1): 9-32.

Risch, H. A., J. R. McLaughlin, D. E. Cole, B. Rosen, L. Bradley, E. Kwan, E. Jack, D. J. Vesprini, G. Kuperstein, J. L. Abrahamson, I. Fan, B. Wong and S. A. Narod (2001). "Prevalence and penetrance of germline BRCA1 and BRCA2 mutations in a population series of 649 women with ovarian cancer." Am J Hum Genet **68**(3): 700-710.

Robson, M., C. Goessl and S. Domchek (2017). "Olaparib for Metastatic Germline BRCA-Mutated Breast Cancer." N Engl J Med **377**(18): 1792-1793.

Ruiz, S., C. Mayor-Ruiz, V. Lafarga, M. Murga, M. Vega-Sendino, S. Ortega and O. Fernandez-Capetillo (2016). "A Genome-wide CRISPR Screen Identifies CDC25A as a Determinant of Sensitivity to ATR Inhibitors." Mol Cell **62**(2): 307-313.

Ruvolo, P. P., V. R. Ruvolo, R. Jacamo, J. K. Burks, Z. Zeng, S. R. Duvvuri, L. Zhou, Y. Qiu, K. R. Coombes, N. Zhang, S. Y. Yoo, R. Pan, N. Hail, Jr., M. Konopleva, G. Calin, S. M. Kornblau and M. Andreeff (2014). "The protein phosphatase 2A regulatory subunit B55alpha is a modulator of signaling and microRNA expression in acute myeloid leukemia cells." Biochim Biophys Acta **1843**(9): 1969-1977.

Ryan, C. J., I. Bajrami and C. J. Lord (2018). "Synthetic Lethality and Cancer - Penetrance as the Major Barrier." Trends Cancer **4**(10): 671-683.

Saldivar, J. C., D. Cortez and K. A. Cimprich (2017). "The essential kinase ATR: ensuring faithful duplication of a challenging genome." Nat Rev Mol Cell Biol **18**(10): 622-636.

Saldivar, J. C., S. Hamperl, M. J. Bocek, M. Chung, T. E. Bass, F. Cisneros-Soberanis, K. Samejima, L. Xie, J. R. Paulson, W. C. Earnshaw, D. Cortez, T. Meyer and K. A. Cimprich (2018). "An intrinsic S/G2 checkpoint enforced by ATR." Science **361**(6404): 806-810.

Samartzis, E. P., K. Gutsche, K. J. Dedes, D. Fink, M. Stucki and P. Imesch (2014). "Loss of ARID1A expression sensitizes cancer cells to PI3K- and AKT-inhibition." Oncotarget **5**(14): 5295-5303.

Sancar, A., L. A. Lindsey-Boltz, K. Unsal-Kacmaz and S. Linn (2004). "Molecular mechanisms of mammalian DNA repair and the DNA damage checkpoints." Annu Rev Biochem **73**: 39-85.

Sasaki, H., H. Sato, K. Kuriyama-Matsumura, K. Sato, K. Maebara, H. Wang, M. Tamba, K. Itoh, M. Yamamoto and S. Bannai (2002). "Electrophile response element-mediated induction of the cystine/glutamate exchange transporter gene expression." J Biol Chem **277**(47): 44765-44771.

Schoonen, P. M., Y. P. Kok, E. Wierenga, B. Bakker, F. Foijer, D. C. J. Spierings and M. van Vugt (2019). "Premature mitotic entry induced by ATR inhibition

potentiates olaparib inhibition-mediated genomic instability, inflammatory signaling, and cytotoxicity in BRCA2-deficient cancer cells." Mol Oncol **13**(11): 2422-2440.

Senter, L., M. Clendenning, K. Sotamaa, H. Hampel, J. Green, J. D. Potter, A. Lindblom, K. Lagerstedt, S. N. Thibodeau, N. M. Lindor, J. Young, I. Winship, J. G. Dowty, D. M. White, J. L. Hopper, L. Baglietto, M. A. Jenkins and A. de la Chapelle (2008). "The clinical phenotype of Lynch syndrome due to germ-line PMS2 mutations." Gastroenterology **135**(2): 419-428.

Serebrenik, A. A., P. P. Argyris, M. C. Jarvis, W. L. Brown, M. Bazzaro, R. I. Vogel, B. K. Erickson, S. H. Lee, K. M. Goergen, M. J. Maurer, E. P. Heinzen, A. L. Oberg, Y. Huang, X. Hou, S. J. Weroha, S. H. Kaufmann and R. S. Harris (2020). "The DNA Cytosine Deaminase APOBEC3B is a Molecular Determinant of Platinum Responsiveness in Clear Cell Ovarian Cancer." Clin Cancer Res **26**(13): 3397-3407.

Serov, S. F., Scully, R.E., Sobin, L.H. (1973). Histological typing of ovarian tumours / S. F. Serov, R. E. Scully, in collaboration with L. H. Sobin and pathologists in ten countries.

Shain, A. H. and J. R. Pollack (2013). "The spectrum of SWI/SNF mutations, ubiquitous in human cancers." PLoS One **8**(1): e55119.

Shekarabi, M., J. Zhang, A. R. Khanna, D. H. Ellison, E. Delpire and K. T. Kahle (2017). "WNK Kinase Signaling in Ion Homeostasis and Human Disease." Cell Metab **25**(2): 285-299.

Shen, J., Z. Ju, W. Zhao, L. Wang, Y. Peng, Z. Ge, Z. D. Nagel, J. Zou, C. Wang, P. Kapoor, X. Ma, D. Ma, J. Liang, S. Song, J. Liu, L. D. Samson, J. A. Ajani, G. M. Li, H. Liang, X. Shen, G. B. Mills and G. Peng (2018). "ARID1A deficiency promotes mutability and potentiates therapeutic antitumor immunity unleashed by immune checkpoint blockade." Nat Med **24**(5): 556-562.

Shen, J., Y. Peng, L. Wei, W. Zhang, L. Yang, L. Lan, P. Kapoor, Z. Ju, Q. Mo, M. Shih Ie, I. P. Uray, X. Wu, P. H. Brown, X. Shen, G. B. Mills and G. Peng (2015). "ARID1A Deficiency Impairs the DNA Damage Checkpoint and Sensitizes Cells to PARP Inhibitors." Cancer Discov **5**(7): 752-767.

Shen, T. and S. Huang (2012). "The role of Cdc25A in the regulation of cell proliferation and apoptosis." Anticancer Agents Med Chem **12**(6): 631-639.

Sheng, H., Y. Huang, Y. Xiao, Z. Zhu, M. Shen, P. Zhou, Z. Guo, J. Wang, H. Wang, W. Dai, W. Zhang, J. Sun and C. Cao (2020). "ATR inhibitor AZD6738 enhances the antitumor activity of radiotherapy and immune checkpoint inhibitors by potentiating the tumor immune microenvironment in hepatocellular carcinoma." J Immunother Cancer **8**(1).

Shibuya, Y., H. Tokunaga, S. Saito, K. Shimokawa, F. Katsuoka, L. Bin, K. Kojima, M. Nagasaki, M. Yamamoto, N. Yaegashi and J. Yasuda (2018). "Identification of somatic genetic alterations in ovarian clear cell carcinoma with next generation sequencing." Genes Chromosomes Cancer **57**(2): 51-60.

Shih Ie, M., P. K. Panuganti, K. T. Kuo, T. L. Mao, E. Kuhn, S. Jones, V. E. Velculescu, R. J. Kurman and T. L. Wang (2011). "Somatic mutations of PPP2R1A in ovarian and uterine carcinomas." Am J Pathol **178**(4): 1442-1447.

Sie, Z. L., R. Y. Li, B. P. Sampurna, P. J. Hsu, S. C. Liu, H. D. Wang, C. L. Huang and C. H. Yuh (2020). "WNK1 Kinase Stimulates Angiogenesis to Promote Tumor Growth and Metastasis." Cancers (Basel) **12**(3).

Sondka, Z., S. Bamford, C. G. Cole, S. A. Ward, I. Dunham and S. A. Forbes (2018). "The COSMIC Cancer Gene Census: describing genetic dysfunction across all human cancers." Nat Rev Cancer **18**(11): 696-705.

Sontag, E. (2001). "Protein phosphatase 2A: the Trojan Horse of cellular signaling." Cell Signal **13**(1): 7-16.

Stewart, J., S. Banerjee, S. J. Pettitt and C. J. Lord (2020). "Modelling the Cancer Phenotype in the Era of CRISPR-Cas9 Gene Editing." Clin Oncol (R Coll Radiol) **32**(2): 69-74.

Strack, S., D. Chang, J. A. Zaucha, R. J. Colbran and B. E. Wadzinski (1999). "Cloning and characterization of B delta, a novel regulatory subunit of protein phosphatase 2A." FEBS Lett **460**(3): 462-466.

Stratton, J. F., S. A. Gayther, P. Russell, J. Dearden, M. Gore, P. Blake, D. Easton and B. A. Ponder (1997). "Contribution of BRCA1 mutations to ovarian cancer." N Engl J Med **336**(16): 1125-1130.

Sugitani, N., F. P. Vendetti, A. J. Cipriano, J. J. Deppas, T. N. Moiseeva, S. Schamus-Haynes, Y. Wang, D. Palmer, H. U. Osmanbeyoglu, A. Bostwick, N. W. Snyder, Y.-N. Gong, K. M. Aird, G. M. Delgoffe, J. H. Beumer and C. J. Bakkenist

(2022). "ATR kinase inhibition induces thymineless death in proliferating CD8⁺ T cells." bioRxiv.

Sun, L., J. Wu, F. Du, X. Chen and Z. J. Chen (2013). "Cyclic GMP-AMP synthase is a cytosolic DNA sensor that activates the type I interferon pathway." Science **339**(6121): 786-791.

Sun, L. L., R. Y. Yang, C. W. Li, M. K. Chen, B. Shao, J. M. Hsu, L. C. Chan, Y. Yang, J. L. Hsu, Y. J. Lai and M. C. Hung (2018). "Inhibition of ATR downregulates PD-L1 and sensitizes tumor cells to T cell-mediated killing." Am J Cancer Res **8**(7): 1307-1316.

Susa, K., E. Sohara, T. Rai, M. Zeniya, Y. Mori, T. Mori, M. Chiga, N. Nomura, H. Nishida, D. Takahashi, K. Isobe, Y. Inoue, K. Takeishi, N. Takeda, S. Sasaki and S. Uchida (2014). "Impaired degradation of WNK1 and WNK4 kinases causes PHAII in mutant KLHL3 knock-in mice." Hum Mol Genet **23**(19): 5052-5060.

Syljuasen, R. G., C. S. Sorensen, L. T. Hansen, K. Fugger, C. Lundin, F. Johansson, T. Helleday, M. Sehested, J. Lukas and J. Bartek (2005). "Inhibition of human Chk1 causes increased initiation of DNA replication, phosphorylation of ATR targets, and DNA breakage." Mol Cell Biol **25**(9): 3553-3562.

Takada, T., H. Iwase, C. Iitsuka, H. Nomura, K. Sakamoto, K. Omatsu, N. Takeshima and K. Takizawa (2012). "Adjuvant chemotherapy for stage I clear cell carcinoma of the ovary: an analysis of fully staged patients." Int J Gynecol Cancer **22**(4): 573-578.

Takano, M., Y. Kikuchi, N. Yaegashi, K. Kuzuya, M. Ueki, H. Tsuda, M. Suzuki, J. Kigawa, S. Takeuchi, H. Tsuda, T. Moriya and T. Sugiyama (2006). "Clear cell carcinoma of the ovary: a retrospective multicentre experience of 254 patients with complete surgical staging." Br J Cancer **94**(10): 1369-1374.

Takano, M., T. Sugiyama, N. Yaegashi, M. Sakuma, M. Suzuki, Y. Saga, K. Kuzuya, J. Kigawa, M. Shimada, H. Tsuda, T. Moriya, A. Yoshizaki, T. Kita and Y. Kikuchi (2008). "Low response rate of second-line chemotherapy for recurrent or refractory clear cell carcinoma of the ovary: a retrospective Japan Clear Cell Carcinoma Study." Int J Gynecol Cancer **18**(5): 937-942.

Tan, D. S., M. Iravani, W. G. McCluggage, M. B. Lambros, F. Milanezi, A. Mackay, C. Gourley, F. C. Geyer, R. Vatcheva, J. Millar, K. Thomas, R. Natrajan, K. Savage, K. Fenwick, A. Williams, C. Jameson, M. El-Bahrawy, M. E. Gore, H. Gabra, S. B. Kaye, A. Ashworth and J. S. Reis-Filho (2011). "Genomic analysis

reveals the molecular heterogeneity of ovarian clear cell carcinomas." Clin Cancer Res **17**(6): 1521-1534.

Tan, D. S. P., C. H. Choi, N. Ngoi, H. Sun, V. Heong, S. G. W. Ow, W. Y. Chay, H. S. Kim, Y. W. Lim, G. Goss, J. C. Goh, V. Luo, B. C. Tai, D. Lim, N. Kaliaperumal, V. B. AU, J. Connolly, J.-W. Kim, M. Friedlander and K. Kim (2022). "A multicenter phase II randomized trial of durvalumab (D) versus physician's choice chemotherapy (PCC) in patients (pts) with recurrent ovarian clear cell adenocarcinoma (MOCCA/APGOT-OV2/GCGS-OV3)." Journal of Clinical Oncology **40**(16_suppl): 5565-5565.

Tanabe, O., T. Nagase, T. Murakami, H. Nozaki, H. Usui, Y. Nishito, H. Hayashi, H. Kagamiyama and M. Takeda (1996). "Molecular cloning of a 74-kDa regulatory subunit (B" or delta) of human protein phosphatase 2A." FEBS Lett **379**(1): 107-111.

Taylor, S. E., C. M. O'Connor, Z. Wang, G. Shen, H. Song, D. Leonard, J. Sangodkar, C. LaVasseur, S. Avril, S. Waggoner, K. Zanotti, A. J. Armstrong, C. Nagel, K. Resnick, S. Singh, M. W. Jackson, W. Xu, S. Haider, A. DiFeo and G. Narla (2019). "The Highly Recurrent PP2A Aalpha-Subunit Mutation P179R Alters Protein Structure and Impairs PP2A Enzyme Function to Promote Endometrial Tumorigenesis." Cancer Res **79**(16): 4242-4257.

Thomas, P. and T. G. Smart (2005). "HEK293 cell line: a vehicle for the expression of recombinant proteins." J Pharmacol Toxicol Methods **51**(3): 187-200.

Timmers, P. J., A. H. Zwinderman, I. Teodorovic, I. Vergote and J. B. Trimbos (2009). "Clear cell carcinoma compared to serous carcinoma in early ovarian cancer: same prognosis in a large randomized trial." Int J Gynecol Cancer **19**(1): 88-93.

Toda-Ishii, M., K. Akaike, Y. Suehara, K. Mukaihara, D. Kubota, S. Kohsaka, T. Okubo, K. Mitani, K. Mogushi, T. Takagi, K. Kaneko, T. Yao and T. Saito (2016). "Clinicopathological effects of protein phosphatase 2, regulatory subunit A, alpha mutations in gastrointestinal stromal tumors." Mod Pathol **29**(11): 1424-1432.

Toledo, L. I., M. Altmeyer, M. B. Rask, C. Lukas, D. H. Larsen, L. K. Povlsen, S. Bekker-Jensen, N. Mailand, J. Bartek and J. Lukas (2013). "ATR prohibits replication catastrophe by preventing global exhaustion of RPA." Cell **155**(5): 1088-1103.

Tsherniak, A., F. Vazquez, P. G. Montgomery, B. A. Weir, G. Kryukov, G. S. Cowley, S. Gill, W. F. Harrington, S. Pantel, J. M. Krill-Burger, R. M. Meyers, L. Ali, A. Goodale, Y. Lee, G. Jiang, J. Hsiao, W. F. J. Gerath, S. Howell, E. Merkel, M. Ghandi, L. A. Garraway, D. E. Root, T. R. Golub, J. S. Boehm and W. C. Hahn (2017). "Defining a Cancer Dependency Map." Cell **170**(3): 564-576 e516.

Tsuchiya, A., M. Sakamoto, J. Yasuda, M. Chuma, T. Ohta, M. Ohki, T. Yasugi, Y. Taketani and S. Hirohashi (2003). "Expression profiling in ovarian clear cell carcinoma: identification of hepatocyte nuclear factor-1 beta as a molecular marker and a possible molecular target for therapy of ovarian clear cell carcinoma." Am J Pathol **163**(6): 2503-2512.

Tu, S. W., A. Bugde, K. Luby-Phelps and M. H. Cobb (2011). "WNK1 is required for mitosis and abscission." Proc Natl Acad Sci U S A **108**(4): 1385-1390.

Tutt, A. N. J., J. E. Garber, B. Kaufman, G. Viale, D. Fumagalli, P. Rastogi, R. D. Gelber, E. de Azambuja, A. Fielding, J. Balmana, S. M. Domchek, K. A. Gelmon, S. J. Hollingsworth, L. A. Korde, B. Linderholm, H. Bandos, E. Senkus, J. M. Suga, Z. Shao, A. W. Pippas, Z. Nowecki, T. Huzarski, P. A. Ganz, P. C. Lucas, N. Baker, S. Loibl, R. McConnell, M. Piccart, R. Schmutzler, G. G. Steger, J. P. Costantino, A. Arahmani, N. Wolmark, E. McFadden, V. Karantza, S. R. Lakhani, G. Yothers, C. Campbell, C. E. Geyer, Jr., A. C. T. S. C. Olympi and Investigators (2021). "Adjuvant Olaparib for Patients with BRCA1- or BRCA2-Mutated Breast Cancer." N Engl J Med **384**(25): 2394-2405.

Uehara, Y., K. Oda, Y. Ikeda, T. Koso, S. Tsuji, S. Yamamoto, K. Asada, K. Sone, R. Kurikawa, C. Makii, O. Hagiwara, M. Tanikawa, D. Maeda, K. Hasegawa, S. Nakagawa, O. Wada-Hiraike, K. Kawana, M. Fukayama, K. Fujiwara, T. Yano, Y. Osuga, T. Fujii and H. Aburatani (2015). "Integrated copy number and expression analysis identifies profiles of whole-arm chromosomal alterations and subgroups with favorable outcome in ovarian clear cell carcinomas." PLoS One **10**(6): e0128066.

University College, L. (2018, September). "A Study of Pembrolizumab in Patients With Advanced Gynaecological Clear Cell Cancer." from https://ClinicalTrials.gov/show/NCT03425565.

University of, U. and I. National Cancer. (2021, November 30). "Tremelimumab, Durvalumab, and Belinostat for the Treatment of ARID1A Mutated Metastatic or Unresectable, Locally Advanced Urothelial Carcinoma." Retrieved 26th July, 2022, from https://ClinicalTrials.gov/show/NCT05154994.

Vaitsiankova, A., K. Burdova, M. Sobol, A. Gautam, O. Benada, H. Hanzlikova and K. W. Caldecott (2022). "PARP inhibition impedes the maturation of nascent DNA strands during DNA replication." Nat Struct Mol Biol **29**(4): 329-338.

Vendetti, F. P., P. Karukonda, D. A. Clump, T. Teo, R. Lalonde, K. Nugent, M. Ballew, B. F. Kiesel, J. H. Beumer, S. N. Sarkar, T. P. Conrads, M. J. O'Connor, R. L. Ferris, P. T. Tran, G. M. Delgoffe and C. J. Bakkenist (2018). "ATR kinase inhibitor AZD6738 potentiates CD8+ T cell-dependent antitumor activity following radiation." J Clin Invest **128**(9): 3926-3940.

Vendetti, F. P., A. Lau, S. Schamus, T. P. Conrads, M. J. O'Connor and C. J. Bakkenist (2015). "The orally active and bioavailable ATR kinase inhibitor AZD6738 potentiates the anti-tumor effects of cisplatin to resolve ATM-deficient non-small cell lung cancer in vivo." Oncotarget **6**(42): 44289-44305.

Vitari, A. C., J. Thastrup, F. H. Rafiqi, M. Deak, N. A. Morrice, H. K. Karlsson and D. R. Alessi (2006). "Functional interactions of the SPAK/OSR1 kinases with their upstream activator WNK1 and downstream substrate NKCC1." Biochem J **397**(1): 223-231.

Voorhoeve, P. M., R. J. Watson, P. G. Farlie, R. Bernards and E. W. Lam (1999). "Rapid dephosphorylation of p107 following UV irradiation." Oncogene **18**(3): 679-688.

Wallez, Y., C. R. Dunlop, T. I. Johnson, S. B. Koh, C. Fornari, J. W. T. Yates, S. Bernaldo de Quiros Fernandez, A. Lau, F. M. Richards and D. I. Jodrell (2018). "The ATR Inhibitor AZD6738 Synergizes with Gemcitabine In Vitro and In Vivo to Induce Pancreatic Ductal Adenocarcinoma Regression." Mol Cancer Ther **17**(8): 1670-1682.

Wang, F., S. Zhu, L. A. Fisher, W. Wang, G. G. Oakley, C. Li and A. Peng (2018). "Protein interactomes of protein phosphatase 2A B55 regulatory subunits reveal B55-mediated regulation of replication protein A under replication stress." Sci Rep **8**(1): 2683.

Wang, H., S. Hu, X. Chen, H. Shi, C. Chen, L. Sun and Z. J. Chen (2017). "cGAS is essential for the antitumor effect of immune checkpoint blockade." Proc Natl Acad Sci U S A **114**(7): 1637-1642.

Wang, L., L. Yang, C. Wang, W. Zhao, Z. Ju, W. Zhang, J. Shen, Y. Peng, C. An, Y. T. Luu, S. Song, T. A. Yap, J. A. Ajani, G. B. Mills, X. Shen and G. Peng (2020).

"Inhibition of the ATM/Chk2 axis promotes cGAS/STING signaling in ARID1A-deficient tumors." J Clin Invest **130**(11): 5951-5966.

Wang, S. S., E. D. Esplin, J. L. Li, L. Huang, A. Gazdar, J. Minna and G. A. Evans (1998). "Alterations of the PPP2R1B gene in human lung and colon cancer." Science **282**(5387): 284-287.

Wang, Y. K., A. Bashashati, M. S. Anglesio, D. R. Cochrane, D. S. Grewal, G. Ha, A. McPherson, H. M. Horlings, J. Senz, L. M. Prentice, A. N. Karnezis, D. Lai, M. R. Aniba, A. W. Zhang, K. Shumansky, C. Siu, A. Wan, M. K. McConechy, H. Li-Chang, A. Tone, D. Provencher, M. de Ladurantaye, H. Fleury, A. Okamoto, S. Yanagida, N. Yanaihara, M. Saito, A. J. Mungall, R. Moore, M. A. Marra, C. B. Gilks, A. M. Mes-Masson, J. N. McAlpine, S. Aparicio, D. G. Huntsman and S. P. Shah (2017). "Genomic consequences of aberrant DNA repair mechanisms stratify ovarian cancer histotypes." Nat Genet **49**(6): 856-865.

Watanabe, R., A. Ui, S. Kanno, H. Ogiwara, T. Nagase, T. Kohno and A. Yasui (2014). "SWI/SNF factors required for cellular resistance to DNA damage include ARID1A and ARID1B and show interdependent protein stability." Cancer Res **74**(9): 2465-2475.

Weinstein, I. B. and A. K. Joe (2006). "Mechanisms of disease: Oncogene addiction--a rationale for molecular targeting in cancer therapy." Nat Clin Pract Oncol **3**(8): 448-457.

Wentzensen, N., E. M. Poole, B. Trabert, E. White, A. A. Arslan, A. V. Patel, V. W. Setiawan, K. Visvanathan, E. Weiderpass, H. O. Adami, A. Black, L. Bernstein, L. A. Brinton, J. Buring, L. M. Butler, S. Chamosa, T. V. Clendenen, L. Dossus, R. Fortner, S. M. Gapstur, M. M. Gaudet, I. T. Gram, P. Hartge, J. Hoffman-Bolton, A. Idahl, M. Jones, R. Kaaks, V. Kirsh, W. P. Koh, J. V. Lacey, Jr., I. M. Lee, E. Lundin, M. A. Merritt, N. C. Onland-Moret, U. Peters, J. N. Poynter, S. Rinaldi, K. Robien, T. Rohan, D. P. Sandler, C. Schairer, L. J. Schouten, L. K. Sjoholm, S. Sieri, A. Swerdlow, A. Tjonneland, R. Travis, A. Trichopoulou, P. A. van den Brandt, L. Wilkens, A. Wolk, H. P. Yang, A. Zeleniuch-Jacquotte and S. S. Tworoger (2016). "Ovarian Cancer Risk Factors by Histologic Subtype: An Analysis From the Ovarian Cancer Cohort Consortium." J Clin Oncol **34**(24): 2888-2898.

Werner, H. M., A. Berg, E. Wik, E. Birkeland, C. Krakstad, K. Kusonmano, K. Petersen, K. H. Kalland, A. M. Oyan, L. A. Akslen, J. Trovik and H. B. Salvesen (2013). "ARID1A loss is prevalent in endometrial hyperplasia with atypia and low-grade endometrioid carcinomas." Mod Pathol **26**(3): 428-434.

WHO (2020). GLOBOCAN.

Wiegand, K. C., A. F. Lee, O. M. Al-Agha, C. Chow, S. E. Kalloger, D. W. Scott, C. Steidl, S. M. Wiseman, R. D. Gascoyne, B. Gilks and D. G. Huntsman (2011). "Loss of BAF250a (ARID1A) is frequent in high-grade endometrial carcinomas." J Pathol **224**(3): 328-333.

Wiegand, K. C., S. P. Shah, O. M. Al-Agha, Y. Zhao, K. Tse, T. Zeng, J. Senz, M. K. McConechy, M. S. Anglesio, S. E. Kalloger, W. Yang, A. Heravi-Moussavi, R. Giuliany, C. Chow, J. Fee, A. Zayed, L. Prentice, N. Melnyk, G. Turashvili, A. D. Delaney, J. Madore, S. Yip, A. W. McPherson, G. Ha, L. Bell, S. Fereday, A. Tam, L. Galletta, P. N. Tonin, D. Provencher, D. Miller, S. J. Jones, R. A. Moore, G. B. Morin, A. Oloumi, N. Boyd, S. A. Aparicio, M. Shih Ie, A. M. Mes-Masson, D. D. Bowtell, M. Hirst, B. Gilks, M. A. Marra and D. G. Huntsman (2010). "ARID1A mutations in endometriosis-associated ovarian carcinomas." N Engl J Med **363**(16): 1532-1543.

Williamson, C. T., R. Miller, H. N. Pemberton, S. E. Jones, J. Campbell, A. Konde, N. Badham, R. Rafiq, R. Brough, A. Gulati, C. J. Ryan, J. Francis, P. B. Vermulen, A. R. Reynolds, P. M. Reaper, J. R. Pollard, A. Ashworth and C. J. Lord (2016). "ATR inhibitors as a synthetic lethal therapy for tumours deficient in ARID1A." Nat Commun **7**: 13837.

Wilson, F. H., S. Disse-Nicodeme, K. A. Choate, K. Ishikawa, C. Nelson-Williams, I. Desitter, M. Gunel, D. V. Milford, G. W. Lipkin, J. M. Achard, M. P. Feely, B. Dussol, Y. Berland, R. J. Unwin, H. Mayan, D. B. Simon, Z. Farfel, X. Jeunemaitre and R. P. Lifton (2001). "Human hypertension caused by mutations in WNK kinases." Science **293**(5532): 1107-1112.

Wlodarchak, N. and Y. Xing (2016). "PP2A as a master regulator of the cell cycle." Crit Rev Biochem Mol Biol **51**(3): 162-184.

Wu, C., J. Lyu, E. J. Yang, Y. Liu, B. Zhang and J. S. Shim (2018). "Targeting AURKA-CDC25C axis to induce synthetic lethality in ARID1A-deficient colorectal cancer cells." Nat Commun **9**(1): 3212.

Wu, J. N. and C. W. Roberts (2013). "ARID1A mutations in cancer: another epigenetic tumor suppressor?" Cancer Discov **3**(1): 35-43.

Xing, M., F. Zhang, H. Liao, S. Chen, L. Che, X. Wang, Z. Bao, F. Ji, G. Chen, H. Zhang, W. Li, Z. Chen, Y. Liu, I. D. Hickson, H. Shen and S. Ying (2020).

"Replication Stress Induces ATR/CHK1-Dependent Nonrandom Segregation of Damaged Chromosomes." Mol Cell **78**(4): 714-724 e715.

Xu, B. E., S. Stippec, A. Lazrak, C. L. Huang and M. H. Cobb (2005). "WNK1 activates SGK1 by a phosphatidylinositol 3-kinase-dependent and non-catalytic mechanism." J Biol Chem **280**(40): 34218-34223.

Xu, H., E. George, Y. Kinose, H. Kim, J. B. Shah, J. D. Peake, B. Ferman, S. Medvedev, T. Murtha, C. J. Barger, K. M. Devins, K. D'Andrea, B. Wubbenhorst, L. E. Schwartz, W. T. Hwang, G. B. Mills, K. L. Nathanson, A. R. Karpf, R. Drapkin, E. J. Brown and F. Simpkins (2021). "CCNE1 copy number is a biomarker for response to combination WEE1-ATR inhibition in ovarian and endometrial cancer models." Cell Rep Med **2**(9): 100394.

Yaeger, R., W. K. Chatila, M. D. Lipsyc, J. F. Hechtman, A. Cercek, F. Sanchez-Vega, G. Jayakumaran, S. Middha, A. Zehir, M. T. A. Donoghue, D. You, A. Viale, N. Kemeny, N. H. Segal, Z. K. Stadler, A. M. Varghese, R. Kundra, J. Gao, A. Syed, D. M. Hyman, E. Vakiani, N. Rosen, B. S. Taylor, M. Ladanyi, M. F. Berger, D. B. Solit, J. Shia, L. Saltz and N. Schultz (2018). "Clinical Sequencing Defines the Genomic Landscape of Metastatic Colorectal Cancer." Cancer Cell **33**(1): 125-136 e123.

Yamada, K., J. Levell, T. Yoon, D. Kohls, D. Yowe, D. F. Rigel, H. Imase, J. Yuan, K. Yasoshima, K. DiPetrillo, L. Monovich, L. Xu, M. Zhu, M. Kato, M. Jain, N. Idamakanti, P. Taslimi, T. Kawanami, U. A. Argikar, V. Kunjathoor, X. Xie, Y. I. Yagi, Y. Iwaki, Z. Robinson and H. M. Park (2017). "Optimization of Allosteric With-No-Lysine (WNK) Kinase Inhibitors and Efficacy in Rodent Hypertension Models." J Med Chem **60**(16): 7099-7107.

Yamada, Y., H. Shigetomi, A. Onogi, S. Haruta, R. Kawaguchi, S. Yoshida, N. Furukawa, A. Nagai, Y. Tanase, T. Tsunemi, H. Oi and H. Kobayashi (2011). "Redox-active iron-induced oxidative stress in the pathogenesis of clear cell carcinoma of the ovary." Int J Gynecol Cancer **21**(7): 1200-1207.

Yamaguchi, K., M. Mandai, S. Toyokuni, J. Hamanishi, T. Higuchi, K. Takakura and S. Fujii (2008). "Contents of endometriotic cysts, especially the high concentration of free iron, are a possible cause of carcinogenesis in the cysts through the iron-induced persistent oxidative stress." Clin Cancer Res **14**(1): 32-40.

Yamamoto, S., H. Tsuda, M. Takano, S. Tamai and O. Matsubara (2012). "Loss of ARID1A protein expression occurs as an early event in ovarian clear-cell

carcinoma development and frequently coexists with PIK3CA mutations." Mod Pathol **25**(4): 615-624.

Yan, Z., S. A. Fedorov, M. C. Mumby and R. S. Williams (2000). "PR48, a novel regulatory subunit of protein phosphatase 2A, interacts with Cdc6 and modulates DNA replication in human cells." Mol Cell Biol **20**(3): 1021-1029.

Yang, X., J. S. Boehm, X. Yang, K. Salehi-Ashtiani, T. Hao, Y. Shen, R. Lubonja, S. R. Thomas, O. Alkan, T. Bhimdi, T. M. Green, C. M. Johannessen, S. J. Silver, C. Nguyen, R. R. Murray, H. Hieronymus, D. Balcha, C. Fan, C. Lin, L. Ghamsari, M. Vidal, W. C. Hahn, D. E. Hill and D. E. Root (2011). "A public genome-scale lentiviral expression library of human ORFs." Nat Methods **8**(8): 659-661.

Yap, T. A., S.-A. Im, A. M. Schram, A. Sharp, J. Balmana, R. D. Baird, J. S. Brown, M. Schwaederle, E. A. Pilling, G. Moorthy, S. Linardopoulos, A. Dowson, C. Pound, E. Lukacs, S. Cosulich and S. J. Luen (2022). "Abstract CT007: PETRA: First in class, first in human trial of the next generation PARP1-selective inhibitor AZD5305 in patients (pts) with BRCA1/2, PALB2 or RAD51C/D mutations." Cancer Research **82**(12_Supplement): CT007-CT007.

Yap, T. A., B. O'Carrigan, M. S. Penney, J. S. Lim, J. S. Brown, M. J. de Miguel Luken, N. Tunariu, R. Perez-Lopez, D. N. Rodrigues, R. Riisnaes, I. Figueiredo, S. Carreira, B. Hare, K. McDermott, S. Khalique, C. T. Williamson, R. Natrajan, S. J. Pettitt, C. J. Lord, U. Banerji, J. Pollard, J. Lopez and J. S. de Bono (2020). "Phase I Trial of First-in-Class ATR Inhibitor M6620 (VX-970) as Monotherapy or in Combination With Carboplatin in Patients With Advanced Solid Tumors." J Clin Oncol **38**(27): 3195-3204.

Yap, T. A., B. O'Carrigan, M. S. Penney, J. S. Lim, J. S. Brown, M. J. d. M. Luken, N. Tunariu, R. Perez-Lopez, D. N. Rodrigues, R. Riisnaes, I. Figueiredo, S. Carreira, B. Hare, K. McDermott, S. Khalique, C. T. Williamson, R. Natrajan, S. J. Pettitt, C. J. Lord, U. Banerji, J. Pollard, J. Lopez and J. S. d. Bono (2020). "Phase I Trial of First-in-Class ATR Inhibitor M6620 (VX-970) as Monotherapy or in Combination With Carboplatin in Patients With Advanced Solid Tumors." Journal of Clinical Oncology **38**(27): 3195-3204.

Yazinski, S. A., V. Comaills, R. Buisson, M. M. Genois, H. D. Nguyen, C. K. Ho, T. Todorova Kwan, R. Morris, S. Lauffer, A. Nussenzweig, S. Ramaswamy, C. H. Benes, D. A. Haber, S. Maheswaran, M. J. Birrer and L. Zou (2017). "ATR inhibition disrupts rewired homologous recombination and fork protection pathways in PARP inhibitor-resistant BRCA-deficient cancer cells." Genes Dev **31**(3): 318-332.

Yekezare, M., B. Gomez-Gonzalez and J. F. Diffley (2013). "Controlling DNA replication origins in response to DNA damage - inhibit globally, activate locally." J Cell Sci **126**(Pt 6): 1297-1306.

Yin, Y., W. T. C. Lee, D. Gupta, H. Xue, P. Tonzi, J. A. Borowiec, T. T. Huang, M. Modesti and E. Rothenberg (2021). "A basal-level activity of ATR links replication fork surveillance and stress response." Mol Cell **81**(20): 4243-4257 e4246.

Ying, S., F. C. Hamdy and T. Helleday (2012). "Mre11-dependent degradation of stalled DNA replication forks is prevented by BRCA2 and PARP1." Cancer Res **72**(11): 2814-2821.

Young, L. A., L. O. O'Connor, C. de Renty, M. H. Veldman-Jones, T. Dorval, Z. Wilson, D. R. Jones, D. Lawson, R. Odedra, A. Maya-Mendoza, C. Reimer, J. Bartek, A. Lau and M. J. O'Connor (2019). "Differential Activity of ATR and WEE1 Inhibitors in a Highly Sensitive Subpopulation of DLBCL Linked to Replication Stress." Cancer Res **79**(14): 3762-3775.

Yu, H. A., M. E. Arcila, N. Rekhtman, C. S. Sima, M. F. Zakowski, W. Pao, M. G. Kris, V. A. Miller, M. Ladanyi and G. J. Riely (2013). "Analysis of tumor specimens at the time of acquired resistance to EGFR-TKI therapy in 155 patients with EGFR-mutant lung cancers." Clin Cancer Res **19**(8): 2240-2247.

Yu, S., X. Xiao, J. Lu, X. Qian, B. Liu and J. Feng (2013). "Colorectal cancer patients with low abundance of KRAS mutation may benefit from EGFR antibody therapy." PLoS One **8**(7): e68022.

Zamarin, D., R. A. Burger, M. W. Sill, D. J. Powell, Jr., H. A. Lankes, M. D. Feldman, O. Zivanovic, C. Gunderson, E. Ko, C. Mathews, S. Sharma, A. R. Hagemann, S. Khleif and C. Aghajanian (2020). "Randomized Phase II Trial of Nivolumab Versus Nivolumab and Ipilimumab for Recurrent or Persistent Ovarian Cancer: An NRG Oncology Study." J Clin Oncol **38**(16): 1814-1823.

Zatreanu, D., H. M. R. Robinson, O. Alkhatib, M. Boursier, H. Finch, L. Geo, D. Grande, V. Grinkevich, R. A. Heald, S. Langdon, J. Majithiya, C. McWhirter, N. M. B. Martin, S. Moore, J. Neves, E. Rajendra, M. Ranzani, T. Schaedler, M. Stockley, K. Wiggins, R. Brough, S. Sridhar, A. Gulati, N. Shao, L. M. Badder, D. Novo, E. G. Knight, R. Marlow, S. Haider, E. Callen, G. Hewitt, J. Schimmel, R. Prevo, C. Alli, A. Ferdinand, C. Bell, P. Blencowe, C. Bot, M. Calder, M. Charles, J. Curry, T. Ekwuru, K. Ewings, W. Krajewski, E. MacDonald, H. McCarron, L. Pang, C. Pedder, L. Rigoreau, M. Swarbrick, E. Wheatley, S. Willis, A. C. Wong, A. Nussenzweig, M. Tijsterman, A. Tutt, S. J. Boulton, G. S. Higgins, S. J. Pettitt,

G. C. M. Smith and C. J. Lord (2021). "Poltheta inhibitors elicit BRCA-gene synthetic lethality and target PARP inhibitor resistance." Nat Commun **12**(1): 3636.

Zehir, A., R. Benayed, R. H. Shah, A. Syed, S. Middha, H. R. Kim, P. Srinivasan, J. Gao, D. Chakravarty, S. M. Devlin, M. D. Hellmann, D. A. Barron, A. M. Schram, M. Hameed, S. Dogan, D. S. Ross, J. F. Hechtman, D. F. DeLair, J. Yao, D. L. Mandelker, D. T. Cheng, R. Chandramohan, A. S. Mohanty, R. N. Ptashkin, G. Jayakumaran, M. Prasad, M. H. Syed, A. B. Rema, Z. Y. Liu, K. Nafa, L. Borsu, J. Sadowska, J. Casanova, R. Bacares, I. J. Kiecka, A. Razumova, J. B. Son, L. Stewart, T. Baldi, K. A. Mullaney, H. Al-Ahmadie, E. Vakiani, A. A. Abeshouse, A. V. Penson, P. Jonsson, N. Camacho, M. T. Chang, H. H. Won, B. E. Gross, R. Kundra, Z. J. Heins, H. W. Chen, S. Phillips, H. Zhang, J. Wang, A. Ochoa, J. Wills, M. Eubank, S. B. Thomas, S. M. Gardos, D. N. Reales, J. Galle, R. Durany, R. Cambria, W. Abida, A. Cercek, D. R. Feldman, M. M. Gounder, A. A. Hakimi, J. J. Harding, G. Iyer, Y. Y. Janjigian, E. J. Jordan, C. M. Kelly, M. A. Lowery, L. G. T. Morris, A. M. Omuro, N. Raj, P. Razavi, A. N. Shoushtari, N. Shukla, T. E. Soumerai, A. M. Varghese, R. Yaeger, J. Coleman, B. Bochner, G. J. Riely, L. B. Saltz, H. I. Scher, P. J. Sabbatini, M. E. Robson, D. S. Klimstra, B. S. Taylor, J. Baselga, N. Schultz, D. M. Hyman, M. E. Arcila, D. B. Solit, M. Ladanyi and M. F. Berger (2017). "Mutational landscape of metastatic cancer revealed from prospective clinical sequencing of 10,000 patients." Nat Med **23**(6): 703-713.

Zeman, M. K. and K. A. Cimprich (2014). "Causes and consequences of replication stress." Nat Cell Biol **16**(1): 2-9.

Zhang, J., K. Siew, T. Macartney, K. M. O'Shaughnessy and D. R. Alessi (2015). "Critical role of the SPAK protein kinase CCT domain in controlling blood pressure." Hum Mol Genet **24**(16): 4545-4558.

Zhang, Q., H. B. Yan, J. Wang, S. J. Cui, X. Q. Wang, Y. H. Jiang, L. Feng, P. Y. Yang and F. Liu (2016). "Chromatin remodeling gene AT-rich interactive domain-containing protein 1A suppresses gastric cancer cell proliferation by targeting PIK3CA and PDK1." Oncotarget **7**(29): 46127-46141.

Zhang, X., T. Mao, B. Zhang, H. Xu, J. Cui, F. Jiao, D. Chen, Y. Wang, J. Hu, Q. Xia, W. Ge, S. Li, M. Yue, J. Ma, J. Yao, Y. Wang, Y. Wang, D. Shentu, X. Zhang, S. Chen, Y. Bai, Y. Wang, X. Zhang, Q. Liu, Y. Sun, D. Fu, Y. Liu, L. Xiong and L. Wang (2022). "Characterization of the genomic landscape in large-scale Chinese patients with pancreatic cancer." EBioMedicine **77**: 103897.

Zhang, X. H., L. Y. Tee, X. G. Wang, Q. S. Huang and S. H. Yang (2015). "Off-target Effects in CRISPR/Cas9-mediated Genome Engineering." Mol Ther Nucleic Acids **4**: e264.

Zhao, B., F. Du, P. Xu, C. Shu, B. Sankaran, S. L. Bell, M. Liu, Y. Lei, X. Gao, X. Fu, F. Zhu, Y. Liu, A. Laganowsky, X. Zheng, J. Y. Ji, A. P. West, R. O. Watson and P. Li (2019). "A conserved PLPLRT/SD motif of STING mediates the recruitment and activation of TBK1." Nature **569**(7758): 718-722.

Zhou, J., S. G. Wu, J. Wang, J. Y. Sun, Z. Y. He, X. Jin and W. W. Zhang (2018). "The Effect of Histological Subtypes on Outcomes of Stage IV Epithelial Ovarian Cancer." Front Oncol **8**: 577.

Zolnierowicz, S., C. Csortos, J. Bondor, A. Verin, M. C. Mumby and A. A. DePaoli-Roach (1994). "Diversity in the regulatory B-subunits of protein phosphatase 2A: identification of a novel isoform highly expressed in brain." Biochemistry **33**(39): 11858-11867.

Zou, L. and S. J. Elledge (2003). "Sensing DNA damage through ATRIP recognition of RPA-ssDNA complexes." Science **300**(5625): 1542-1548.

Zou, Y., J. Y. Zhou, J. B. Guo, L. Q. Wang, Y. Luo, Z. Y. Zhang, F. Y. Liu, J. Tan, F. Wang and O. P. Huang (2018). "The presence of KRAS, PPP2R1A and ARID1A mutations in 101 Chinese samples with ovarian endometriosis." Mutat Res **809**: 1-5.

Chapter 9. Appendix

9.1 TOV21G PPP2R1A WT/WT DE scores from siRNA screen

Gene Name	DE_Zscore	Gene Name	DE_Zscore	Gene Name	DE_Zscore
AAK1	-1.0928616	JAK3	-0.1445779	RPS6KA6	1.30875403
AATK	0.8374957	KCNH2	0.32919919	RPS6KB1	-0.067259
ABL1	0.58501423	KCNH8	0.46709739	RPS6KB2	-1.6526832
ABL2	0.45092069	KDR	-0.7764106	RPS6KC1	-0.4615545
ACVR1	1.07545884	KHK	-1.7145777	RPS6KL1	-0.3330305
ACVR1B	-2.0905429	KIAA1804	-0.969461	RRM2B	-0.573342
ACVR1C	0.70006893	KIT	0.15297268	RYK	0.59044701
ACVR2A	-0.2753942	KLF6	0.01882933	SBDS	0.16961653
ACVR2B	-1.5420408	KSR1	0.24106383	SBK1	-0.1945456
ACVRL1	0.42866039	KSR2	2.0253637	SCYL1	0.80030282
ADCK1	-0.0572791	LATS1	-0.0273667	SCYL3	1.55701962
ADCK2	-2.1166076	LATS2	-1.3061229	SDHB	1.05669883
ADCK4	1.46939823	LCK	0.12868475	SDHC	1.004977
ADCK5	1.08307158	LIG1	-0.3558221	SDHD	0.18480514
ADK	0.62460158	LIG3	-0.2839735	SETMAR	-0.4280142
ADPGK	-0.727684	LIG4	0.30526249	SGK1	-1.2414369
ADRBK1	0.27803953	LIMK1	0.70954401	SGK2	-1.6768132
ADRBK2	-0.081522	LIMK2	-2.2903212	SGK223	0.35103786
AGK	0.60935094	LMBR1	-1.0118881	SGK3	1.51897435
AK1	-0.4197581	LMTK2	-0.2370184	SGK494	-0.7709586
AK2	-0.0488168	LMTK3	-0.3466471	SHFM1	0.01022411
AK3	0.39066008	LRRK1	1.49353533	SHPK	-2.1659947
AK4	-0.4942048	LRRK2	0.49000142	SIK1	-0.4261036
AK5	0.8186716	LTK	1.66036966	SIK2	0.56477567
AK7	0.16086674	LYN	1.35474533	SIK3	0.19787383
AKT1	-1.1830306	MAD2L2	-0.4423444	SKAP1	-1.2636616
AKT2	-1.1162545	MAGI1	-0.5452329	SLK	0.73044328
AKT3	-0.4442703	MAGI2	1.11267439	SLX1A	-0.2138461
ALDH18A1	2.27899884	MAGI3	5.10547374	SLX4	0.31683632
ALK	-1.2832971	MAK	1.08818328	SMAD4	0.06128923
ALKBH2	0.31385162	MAP2K1	-0.911992	SMARCB1	-0.2101376
ALKBH3	-0.2283818	MAP2K2	-0.025858	SMG1	-0.1311935
ALPK1	0.31985348	MAP2K3	-2.0712455	SMUG1	0.14991906
ALPK2	0.94802938	MAP2K4	0.32679293	SNRK	0.30167625
ALPK3	-0.042661	MAP2K4	1.0678558	SOCS1	-0.5467374
AMER1	1.28036653	MAP2K5	-0.9930403	SPEG	-0.0980675
AMHR2	0.91738965	MAP2K6	0.04241699	SPHK1	0.95953468
ANKK1	-1.0093449	MAP2K7	-0.392829	SPHK2	0.86208618
APC	-0.4364905	MAP3K1	-0.2505643	SPO11	0.09158252
APEX1	0.89974556	MAP3K10	1.57377909	SRC	-1.6557471
APEX2	-0.1307553	MAP3K11	1.8855249	SRMS	-0.0946261
APTX	-0.128423	MAP3K12	1.32589602	SRP72	-0.1183902
ARAF	-0.0686547	MAP3K13	-0.5353868	SRPK1	0.49516516
ATM	-1.1632577	MAP3K14	1.06810277	SRPK2	0.45496615

ATM	-0.1396253	MAP3K15	-0.8729472	SRPK3	-0.3038238
ATM	-0.0463428	MAP3K19	-1.4499835	STK10	0.6902956
ATR	-2.1310048	MAP3K2	-0.7609146	STK11	-0.9901351
ATR	-0.3997079	MAP3K3	-0.335051	STK11	1.09497203
ATRIP	-0.6744908	MAP3K4	0.39803386	STK16	0.28305243
AURKA	0.6468128	MAP3K5	-0.3432971	STK17A	-1.7477651
AURKB	1.74888501	MAP3K6	0.3750623	STK17B	-1.0367453
AURKC	1.41387576	MAP3K7	2.57713772	STK19	-0.6949693
AXL	1.03729982	MAP3K8	1.24510112	STK24	0.07721306
BCKDK	-0.2206923	MAP3K9	0.28672691	STK25	-0.6903408
BCR	-0.8291962	MAP4K1	-0.3385015	STK26	-0.1400359
BLK	-0.4640955	MAP4K2	-0.8036964	STK3	-0.8904899
BLM	-2.9920908	MAP4K3	0.51300929	STK31	-0.1158165
BLM	0.43480207	MAP4K4	-0.6384717	STK32A	0.51794766
BMP2K	-0.341166	MAP4K5	-0.1581508	STK32B	1.06794457
BMPR1A	0.83783961	MAPK1	0.08817595	STK32C	0.42546775
BMPR1A	0.96769564	MAPK10	1.91011363	STK33	-0.2842621
BMPR1B	-0.0199773	MAPK11	-1.3090491	STK35	-0.6934393
BMPR2	1.46173129	MAPK12	0.62646604	STK36	-0.7453167
BMX	0.47249653	MAPK13	-1.1941833	STK38	1.94445165
BRAF	-0.2520103	MAPK14	-0.3482212	STK38L	4.05534871
BRCA1	-0.5090234	MAPK15	1.26002869	STK39	2.6584701
BRCA1	-0.1939366	MAPK3	-2.8559004	STK4	-0.5397373
BRCA2	-1.5591489	MAPK4	1.01296268	STK40	-0.3716006
BRCA2	-0.378732	MAPK6	0.18762455	STKLD1	0.00399866
BRD2	0.07339315	MAPK7	-1.2322788	STRADA	0.47229398
BRD3	-0.2879429	MAPK8	1.69064492	STRADB	0.28713136
BRD4	-0.8646321	MAPK9	0.7117606	STYK1	-1.2495034
BRDT	-0.0805545	MAPKAPK2	0.20829094	SUFU	0.68390371
BRIP1	-0.8456785	MAPKAPK3	-1.881001	SYK	-1.3652032
BRIP1	0.02133416	MAPKAPK5	0.14909621	TAB1	1.20840563
BRSK1	-1.5934284	MARK1	-0.169912	TAF1	1.41117903
BRSK2	-0.7138554	MARK2	0.48448432	TAF1L	-1.5361819
BTK	-0.5880514	MARK3	-0.9937819	TAOK1	-0.8775121
BUB1	-0.8988849	MARK4	2.55209848	TAOK2	2.38528638
BUB1B	-0.1042949	MAST1	0.63029201	TAOK3	-0.6673334
BUB1B	1.28721439	MAST2	1.0998836	TBCK	-1.9276616
CALM1	-0.6627144	MAST3	-0.7131925	TBK1	0.8896111
CALM2	-1.3085794	MAST4	0.74112116	TDG	0.8012369
CALM3	0.53615688	MASTL	1.00718738	TDP1	-0.0523097
CAMK1	-0.774767	MATK	0.17617938	TDP2	-0.0450141
CAMK1D	0.69070733	MBD4	-0.1835462	TEC	-1.2212602
CAMK1G	-0.2817003	MDC1	0.33066706	TEK	-0.3340367
CAMK2A	-0.11823	MELK	1.50136314	TESK1	-0.7933284
CAMK2B	0.06313739	MEN1	0.62599177	TESK2	0.453181
CAMK2D	0.32395327	MERTK	-0.3605155	TEX14	0.01958529
CAMK2G	-0.9385635	MET	-0.0723289	TGFBR1	2.08197629
CAMK2N1	0.20242837	MGMT	0.06032407	TGFBR2	2.41333224
CAMK4	-0.7038137	MINK1	0.34657332	TGFBR3	-0.3498653
CAMKK1	1.56011859	MKNK1	1.23421807	THNSL1	-1.4081833
CAMKK2	-1.7045933	MKNK2	1.21470897	TJP2	0.49116787
CAMKV	0.9710485	MLH1	-0.8143212	TK2	-0.4168793

CASK	1.68646301	MLH1	-0.7325908	TLK1	0.31698342
CCNH	0.37572168	MLH3	-0.1733398	TLK2	-2.5724086
CDADC1	-0.6640956	MLKL	-0.280302	TNIK	-1.3808797
CDC42BPA	1.63894551	MMS19	-0.6394649	TNK1	-0.1530366
CDC42BPB	1.87287759	MNAT1	-0.5099836	TNK2	2.18564717
CDC42BPG	0.28848362	MOK	1.32549576	TNKS	-0.2838038
CDC7	-2.0660088	MOS	-0.2674403	TNKS2	-0.6767232
CDC73	-0.2111256	MPG	-0.6108701	TNNI3K	0.42075758
CDH1	1.50973191	MPLKIP	0.52118232	TOPBP1	-0.7108991
CDK1	0.52168638	MPP1	1.11517419	TP53	-1.4460606
CDK10	0.63478366	MPP2	-0.057942	TP53	-0.0478003
CDK11A	-0.6932658	MPP3	0.83835057	TP53BP1	-0.2582834
CDK11B	-0.5415879	MRE11A	-0.2773157	TP53RK	1.33824401
CDK12	-0.8173158	MSH2	-0.194119	TPD52L3	-1.0462717
CDK13	-0.9855181	MSH2	0.34309937	TPK1	-1.2416515
CDK14	-2.185809	MSH3	-0.2675158	TREX1	0.00514735
CDK15	-0.0994158	MSH4	-0.3115939	TREX2	-0.0545884
CDK16	2.05796768	MSH5	-1.0248422	TRIB1	0.08761434
CDK17	-0.2375134	MSH6	0.71162396	TRIB2	-0.4926933
CDK18	-0.0825174	MSH6	0.77394851	TRIB3	-0.3310327
CDK19	0.9790789	MST1R	-0.4560508	TRIM27	-0.3055024
CDK2	-0.3014183	MTOR	-1.2588493	TRIO	-0.3557359
CDK20	-0.6288898	MUS81	0.30481343	TRPM6	1.02466391
CDK3	0.58268531	MUSK	-0.9535636	TRPM7	1.53433744
CDK4	0.71861734	MUTYH	0.39103609	TSC1	0.88061497
CDK5	-3.6306041	MUTYH	1.66930817	TSC2	0.67063157
CDK5	-2.5770614	MVK	-2.3347011	TSKS	-0.7936257
CDK5R1	1.06795341	MYLK	-0.3047098	TSSK1B	-0.4573888
CDK5R2	1.90762038	MYLK2	-1.2547084	TSSK2	0.70508356
CDK6	0.61362542	MYLK3	0.60597269	TSSK3	-1.2777569
CDK7	-2.7316468	MYLK4	-1.7337572	TSSK4	-0.1593625
CDK7	-0.0696292	MYO3A	-0.257176	TSSK6	0.50097802
CDK8	0.46835574	MYO3B	-0.11999	TTBK1	0.63812358
CDK9	1.01407053	N4BP2	1.3005385	TTBK2	2.38554975
CDKL1	-1.0508092	NABP2	-0.0210635	TTK	0.716125
CDKL2	0.96313427	NADK	-0.8922146	TWF1	-0.0375971
CDKL3	0.27205042	NAGK	0.36176932	TWF2	-1.0442428
CDKL4	-0.5272207	NBN	0.46919784	TYK2	-0.0055956
CDKL5	-0.6567412	NBN	0.52869586	TYRO3	0.11025743
CDKN1A	1.4148145	NEIL1	-0.1912332	UBE2A	-0.227257
CDKN1B	0.53868284	NEIL2	0.20906878	UBE2B	0.20666597
CDKN1C	-0.0853251	NEIL3	0.43461717	UBE2N	0.43548665
CDKN2A	-0.320699	NEK1	1.69565455	UBE2V2	-0.4859236
CDKN2B	0.35081362	NEK10	0.00352515	UCK1	1.45284803
CDKN2C	-0.4954232	NEK11	-0.9849425	UCK2	1.65876802
CDKN2D	0.03608155	NEK2	0.82542013	UCKL1	-0.1931638
CERK	-1.5241998	NEK3	0.13462316	UHMK1	0.07540051
CETN2	-0.3029728	NEK4	-1.727508	ULK1	0.64817537
CHAF1A	-0.343855	NEK5	1.89161643	ULK2	-0.8787193
CHEK1	-1.6816834	NEK6	-1.4956925	ULK3	1.11427364
CHEK1	0.14773407	NEK7	0.15698563	ULK4	0.40729229
CHEK2	-0.8378396	NEK8	-0.6101534	UNG	0.15142531

CHEK2	0.66747042	NEK9	-0.4171304	VHL	0.37590348
CHEK2	1.28705864	NF1	0.15591411	VRK1	1.5024125
CHKA	1.53414841	NF2	-0.3496817	VRK2	1.66946466
CHKB	0.37127409	NHEJ1	0.41566793	VRK3	1.11370604
CHUK	1.72225347	NIM1K	-0.5676313	WAS	-0.4896856
CIB2	-0.6237243	NLK	-1.4175067	WEE1	-1.0215465
CIT	-0.2689251	NME1	1.04244111	WNK1	-0.211372
CKB	0.36498731	NME2	0.40127191	WNK2	-0.6800782
CKM	0.40606954	NME3	0.33977888	WNK3	-0.4919756
CKMT1B	-1.5013632	NME4	0.42351051	WNK4	0.23710779
CKMT2	-0.224776	NME5	-0.2482391	WRN	-0.3555084
CKS1B	-0.1710904	NME6	1.39356083	WRN	-0.1422586
CKS2	-0.7579731	NME7	0.84680216	WT1	-0.2388482
CLK1	-0.8027403	NPR2	-1.1233226	XAB2	0.05399273
CLK2	-0.3519998	NRBP1	1.13451997	XPA	0.13997835
CLK2	1.23313184	NRBP2	0.86818477	XPA	0.91874138
CLK3	-0.2761758	NRK	-0.3942383	XPC	-0.4432245
CLK4	0.67677893	NTHL1	0.24482071	XPC	0.30033687
CMPK1	1.9254893	NTRK1	0.33661293	XRCC1	0.17058063
COASY	-0.3718787	NTRK2	1.94673273	XRCC2	0.66264044
COL4A3BP	-0.2168409	NTRK3	-1.3535613	XRCC3	-0.0474507
COMMD3	0.75331583	NUAK1	0.46435787	XRCC4	-0.4110797
CPNE3	0.47524842	NUAK2	0.00934604	XRCC5	-0.0602115
CRIM1	0.3295459	NUCKS1	-1.2768787	XRCC6	0.27206579
CRKL	0.25642828	NUDT1	0.37410981	XRCC6BP1	0.9654604
CSF1R	0.53970555	NUP62	0.85947958	XYLB	1.51388929
CSK	0.70095462	OGG1	0.36703862	YES1	0.60104798
CSNK1A1	0.41874994	OXSR1	1.72462556	ZAK	0.08355226
CSNK1A1L	-0.3420614	PACSIN1	-1.1681897	ZAP70	0.32967978
CSNK1D	0.34190426	PAK1	2.02279628	RPS6KA6	1.30875403
CSNK1E	-0.2022904	PAK2	0.32188265	RPS6KB1	-0.067259
CSNK1G1	-0.0673336	PAK3	2.04895149	RPS6KB2	-1.6526832
CSNK1G2	-0.4122958	PAK4	-0.9911838	RPS6KC1	-0.4615545
CSNK1G3	1.14519811	PAK6	-0.7071696	RPS6KL1	-0.3330305
CSNK2A1	-1.2219498	PAK7	0.31968739	RRM2B	-0.573342
CSNK2A2	-2.3101143	PALB2	-0.2940568	RYK	0.59044701
CSNK2B	-0.1994384	PALB2	0.18217507	SBDS	0.16961653
CYLD	0.99629499	PANK1	0.52208464	SBK1	-0.1945456
DAPK1	-0.8321932	PANK2	-0.1090363	SCYL1	0.80030282
DAPK2	-1.271952	PANK3	0.13622464	SCYL3	1.55701962
DAPK3	-0.4347999	PANK4	0.84879317	SDHB	1.05669883
DBF4	0.31139354	PAPSS1	-0.4746284	SDHC	1.004977
DCK	-1.1542884	PAPSS2	-1.3630272	SDHD	0.18480514
DCLK1	-0.2851888	PARP1	-0.3680899	SETMAR	-0.4280142
DCLK2	-1.0914172	PARP2	0.64009083	SGK1	-1.2414369
DCLK3	-0.799511	PASK	0.13061179	SGK2	-1.6768132
DCLRE1A	-0.5833882	PBK	-0.4775367	SGK223	0.35103786
DCLRE1B	0.06363085	PCK1	1.26961179	SGK3	1.51897435
DCLRE1C	-0.4537329	PCK2	-0.1985971	SGK494	-0.7709586
DDB1	0.22916346	PCNA	-0.3687739	SHFM1	0.01022411
DDB2	0.10646155	PDGFRA	-1.6813943	SHPK	-2.1659947
DDB2	0.70328372	PDGFRB	-0.8624166	SIK1	-0.4261036

DDR1	-1.1588154	PDGFRL	-1.5438063	SIK2	0.56477567
DDR2	-3.5849738	PDIK1L	-0.2221848	SIK3	0.19787383
DGKA	1.03068784	PDK1	-1.0563865	SKAP1	-1.2636616
DGKB	-0.7087605	PDK2	-0.8623195	SLK	0.73044328
DGKD	0.73444609	PDK3	4.43662926	SLX1A	-0.2138461
DGKG	-0.0530522	PDK4	0.02901842	SLX4	0.31683632
DGKH	1.14125846	PDPK1	0.86152128	SMAD4	0.06128923
DGKI	1.12897946	PDXK	0.65714154	SMARCB1	-0.2101376
DGKK	1.21075688	PEAK1	1.05898699	SMG1	-0.1311935
DGKQ	-0.1137151	PER1	2.57706142	SMUG1	0.14991906
DGUOK	0.60317608	PFKFB1	0.0725897	SNRK	0.30167625
DLG1	-0.2523676	PFKFB2	1.38956039	SOCS1	-0.5467374
DLG2	-2.1394816	PFKFB3	1.34871412	SPEG	-0.0980675
DLG3	-0.1080102	PFKFB4	0.23517221	SPHK1	0.95953468
DLG4	-0.7299811	PFKL	-2.0134506	SPHK2	0.86208618
DMC1	-0.1746538	PFKM	1.01075354	SPO11	0.09158252
DMPK	0.40885443	PFKP	-0.6101662	SRC	-1.6557471
DSTYK	-1.0065338	PGK1	0.27445417	SRMS	-0.0946261
DTYMK	1.56551547	PGK2	0.71051531	SRP72	-0.1183902
DUSP21	0.51987989	PHKA1	1.12804868	SRPK1	0.49516516
DUT	0.02309511	PHKA2	0.46367245	SRPK2	0.45496615
DYRK1A	-1.4792983	PHKB	1.91801563	SRPK3	-0.3038238
DYRK1B	-1.8390185	PHKG1	-3.0262053	STK10	0.6902956
DYRK2	-0.0231849	PHKG2	-0.8286224	STK11	-0.9901351
DYRK3	-0.086974	PHOX2B	-0.5597392	STK11	1.09497203
DYRK4	0.75566686	PI4K2A	0.64553299	STK16	0.28305243
EEF2K	-1.980063	PI4K2B	-0.1083037	STK17A	-1.7477651
EFNA3	-0.0766678	PI4KA	0.79899255	STK17B	-1.0367453
EFNA4	-1.0518948	PI4KB	-0.1343865	STK19	-0.6949693
EFNA5	0.46850928	PIK3C2A	1.00675379	STK24	0.07721306
EFNB3	0.39610959	PIK3C2B	1.69404249	STK25	-0.6903408
EGFR	0.01482661	PIK3C2G	-0.1197777	STK26	-0.1400359
EIF2AK1	-1.4165806	PIK3C3	2.56822696	STK3	-0.8904899
EIF2AK2	-0.456293	PIK3CA	0.34895257	STK31	-0.1158165
EIF2AK3	0.11154899	PIK3CB	0.23656588	STK32A	0.51794766
EIF2AK4	-0.034635	PIK3CD	0.66796792	STK32B	1.06794457
EME1	0.0160877	PIK3CG	0.33890277	STK32C	0.42546775
EME2	0.08815857	PIK3R1	-0.5812513	STK33	-0.2842621
ENDOV	-0.1560648	PIK3R1	-0.4268681	STK35	-0.6934393
EP300	0.74145818	PIK3R2	-1.0541787	STK36	-0.7453167
EPHA1	0.34348591	PIK3R3	-1.1893095	STK38	1.94445165
EPHA10	-0.0983831	PIK3R4	-1.2711412	STK38L	4.05534871
EPHA2	-0.8073007	PIK3R5	-0.4623735	STK39	2.6584701
EPHA3	-0.1133814	PIKFYVE	-0.8850404	STK4	-0.5397373
EPHA4	-0.8200116	PIM1	-0.0105669	STK40	-0.3716006
EPHA5	0.18728152	PIM2	-0.4189618	STKLD1	0.00399866
EPHA6	0.85679066	PIM3	0.51251784	STRADA	0.47229398
EPHA7	-0.153087	PINK1	0.61915353	STRADB	0.28713136
EPHA8	1.47603349	PIP4K2A	-0.9222885	STYK1	-1.2495034
EPHB1	3.01259158	PIP4K2B	-0.4403879	SUFU	0.68390371
EPHB2	0.03709069	PIP4K2C	1.5292526	SYK	-1.3652032
EPHB3	-2.6844575	PIP5K1A	0.61913677	TAB1	1.20840563

EPHB4	-0.4800125	PIP5K1B	-0.2925544	TAF1	1.41117903
EPHB6	-0.4265595	PIP5K1C	-0.943881	TAF1L	-1.5361819
ERBB2	0.52081548	PIP5KL1	-0.699746	TAOK1	-0.8775121
ERBB3	1.15020851	PKDCC	-0.628156	TAOK2	2.38528638
ERBB4	1.13167384	PKIA	-0.3963436	TAOK3	-0.6673334
ERCC1	-0.9761225	PKIB	-2.7892025	TBCK	-1.9276616
ERCC2	-0.4704922	PKLR	0.54126153	TBK1	0.8896111
ERCC2	0.63366729	PKM	-0.6039265	TDG	0.8012369
ERCC3	0.31053539	PKMYT1	1.32152497	TDP1	-0.0523097
ERCC3	1.4022019	PKN1	-0.3409954	TDP2	-0.0450141
ERCC4	0.05208934	PKN2	1.05530619	TEC	-1.2212602
ERCC4	0.37581011	PKN3	1.57056393	TEK	-0.3340367
ERCC5	-0.9411214	PLK1	-0.1478353	TESK1	-0.7933284
ERCC5	-0.0729591	PLK1	-0.0070212	TESK2	0.453181
ERCC6	-0.3290594	PLK1	0.46756212	TEX14	0.01958529
ERCC8	-0.0024509	PLK2	-0.1044169	TGFBR1	2.08197629
ERN1	0.03232155	PLK3	0.1710685	TGFBR2	2.41333224
ERN2	-1.5771066	PLK4	-0.0253188	TGFBR3	-0.3498653
ETNK1	-0.2534426	PMS1	-3.9126956	THNSL1	-1.4081833
ETNK2	-0.0007886	PMS1	0.48744479	TJP2	0.49116787
EXO1	0.35310918	PMS2	-0.1879189	TK2	-0.4168793
EXOSC10	-0.291003	PMS2	1.11499972	TLK1	0.31698342
EXT1	1.16072378	PMVK	0.7405112	TLK2	-2.5724086
EXT2	-0.7499896	PNCK	-0.5246617	TNIK	-1.3808797
FAAP24	0.2769899	PNKP	0.07925242	TNK1	-0.1530366
FAN1	0.50115345	PNKP	0.16110385	TNK2	2.18564717
FANCA	-0.4640128	POLB	0.09940052	TNKS	-0.2838038
FANCA	-0.3246251	POLD1	-0.6628415	TNKS2	-0.6767232
FANCB	0.3625315	POLE	-0.3403683	TNNI3K	0.42075758
FANCC	0.15917522	POLG	-0.0342504	TOPBP1	-0.7108991
FANCC	0.50697289	POLH	0.22614492	TP53	-1.4460606
FANCD2	-0.421573	POLI	-0.0749873	TP53	-0.0478003
FANCD2	-0.0257009	POLK	-0.5551221	TP53BP1	-0.2582834
FANCE	-0.6677585	POLL	0.56984155	TP53RK	1.33824401
FANCE	0.23558952	POLM	0.07188977	TPD52L3	-1.0462717
FANCF	0.09110815	POLN	-0.2786032	TPK1	-1.2416515
FANCF	0.31851799	POLQ	0.15407473	TREX1	0.00514735
FANCG	0.01745168	POMK	-0.0004967	TREX2	-0.0545884
FANCG	0.6185555	PRKAA1	-0.7254537	TRIB1	0.08761434
FANCI	0.32069522	PRKAA2	-0.2291103	TRIB2	-0.4926933
FANCL	-0.2455096	PRKAB1	0.02048023	TRIB3	-0.3310327
FANCM	0.17615931	PRKAB2	-0.5728407	TRIM27	-0.3055024
FAS	-0.489644	PRKACA	0.07713121	TRIO	-0.3557359
FASTK	-2.1143854	PRKACB	2.1887192	TRPM6	1.02466391
FBXW7	1.59576613	PRKACG	-0.6036684	TRPM7	1.53433744
FEN1	-0.207288	PRKAG1	-0.2003936	TSC1	0.88061497
FER	-0.4976234	PRKAG2	-0.4510177	TSC2	0.67063157
FES	-1.7752546	PRKAG3	-0.5809101	TSKS	-0.7936257
FGFR1	-0.8906191	PRKAR1A	0.94711011	TSSK1B	-0.4573888
FGFR2	0.55078631	PRKAR1A	0.99013512	TSSK2	0.70508356
FGFR3	0.07392802	PRKAR1B	-3.2632151	TSSK3	-1.2777569
FGFR4	-0.9604286	PRKAR2A	-1.2409424	TSSK4	-0.1593625

FGFRL1	-0.8801865	PRKAR2B	1.25937592	TSSK6	0.50097802
FGR	-1.2247449	PRKCA	-0.1138203	TTBK1	0.63812358
FH	0.63663016	PRKCB	0.13239516	TTBK2	2.38554975
FLCN	-0.5259104	PRKCD	0.83229342	TTK	0.716125
FLT1	-0.1886822	PRKCE	-0.9060483	TWF1	-0.0375971
FLT3	0.86101691	PRKCG	0.42893741	TWF2	-1.0442428
FLT4	-1.0967129	PRKCH	-0.6168841	TYK2	-0.0055956
FN3K	0.42094331	PRKCI	-0.7576271	TYRO3	0.11025743
FN3KRP	-0.4921601	PRKCQ	-1.324897	UBE2A	-0.227257
FRK	-0.2590481	PRKCSH	0.71869531	UBE2B	0.20666597
FUK	-0.2772298	PRKCZ	0.84684672	UBE2N	0.43548665
FXN	0.44581152	PRKD1	-0.350057	UBE2V2	-0.4859236
FYN	-1.555185	PRKD2	-0.4637407	UCK1	1.45284803

9.2 TOV21G PPP2R1A R183P/WT DE scores from siRNA screen

Gene Name	DE_Zscore	Gene Name	DE_Zscore	Gene Name	DE_Zscore
AAK1	-1.1795768	JAK3	1.40783573	RPS6KA6	-0.2458142
AATK	-0.7204259	KCNH2	3.17134316	RPS6KB1	1.93748838
ABL1	-3.1679518	KCNH8	-0.6104742	RPS6KB2	1.45729173
ABL2	2.0566962	KDR	-2.6259561	RPS6KC1	-0.3444728
ACVR1	-0.2848598	KHK	-0.3724599	RPS6KL1	-0.1403554
ACVR1B	0.80176171	KIAA1804	0.39210101	RRM2B	-0.2050529
ACVR1C	-0.7772521	KIT	-1.5938064	RYK	-0.3267681
ACVR2A	0.26327926	KLF6	-0.7013985	SBDS	-0.3360723
ACVR2B	1.52020664	KSR1	-0.1061598	SBK1	-1.139953
ACVRL1	-0.0686261	KSR2	1.40574158	SCYL1	0.82143399
ADCK1	-0.619008	LATS1	-0.9328694	SCYL3	0.96124865
ADCK2	0.2988514	LATS2	1.14581055	SDHB	-0.0909775
ADCK4	-1.8876855	LCK	-0.3576854	SDHC	0.25380961
ADCK5	-1.3308031	LIG1	-1.4157982	SDHD	-0.8651272
ADK	1.63192949	LIG3	0.65723277	SETMAR	-0.6706376
ADPGK	0.83212804	LIG4	0.7338707	SGK1	-1.0422318
ADRBK1	-0.1155917	LIMK1	-0.8916782	SGK2	-0.7797197
ADRBK2	1.95225708	LIMK2	1.19865815	SGK223	1.56598331
AGK	2.06585108	LMBR1	1.2365801	SGK3	1.07154401
AK1	0.059769	LMTK2	-1.3871445	SGK494	0.83233107
AK2	-0.0399758	LMTK3	-0.2586654	SHFM1	-0.8954845
AK3	-0.2549294	LRRK1	0.59825322	SHPK	-0.6471847
AK4	1.73338367	LRRK2	0.13257032	SIK1	0.75101721
AK5	-0.91432	LTK	0.82678122	SIK2	-0.1293431
AK7	-1.476206	LYN	0.66854588	SIK3	1.01133185
AKT1	0.0118356	MAD2L2	-1.7715318	SKAP1	1.40027075
AKT2	0.41396424	MAGI1	0.66456659	SLK	-1.1126582
AKT3	1.98806479	MAGI2	0.1673257	SLX1A	-1.3215624
ALDH18A1	0.02529944	MAGI3	-1.116556	SLX4	-0.9815001
ALK	-0.3058776	MAK	-1.1620382	SMAD4	0.83963268
ALKBH2	0.42651037	MAP2K1	0.02056858	SMARCB1	-0.271087
ALKBH3	0.34857921	MAP2K2	-0.176167	SMG1	-0.6136075
ALPK1	0.92712617	MAP2K3	0.88977986	SMUG1	-1.0070453
ALPK2	0.90854207	MAP2K4	-0.0132111	SNRK	0.99716437
ALPK3	-1.3643727	MAP2K4	1.21460775	SOCS1	-0.3435363
AMER1	1.17061087	MAP2K5	1.54335424	SPEG	-1.5737419
AMHR2	1.68360783	MAP2K6	-0.7308556	SPHK1	0.84740383

ANKK1	-1.1793589	MAP2K7	-0.5649734	SPHK2	-1.5196128
APC	0.23342696	MAP3K1	0.05793848	SPO11	0.51292911
APEX1	0.24658443	MAP3K10	0.25645084	SRC	-0.5209873
APEX2	1.66393097	MAP3K11	0.40548169	SRMS	-2.8998915
APTX	-0.7044801	MAP3K12	0.58198388	SRP72	0.10342098
ARAF	1.38063234	MAP3K13	-2.1185463	SRPK1	-0.7543575
ATM	-1.158918	MAP3K14	-0.9814455	SRPK2	-0.3760319
ATM	0.13551933	MAP3K15	-0.6057335	SRPK3	0.90466969
ATM	0.31206844	MAP3K19	-0.0041674	STK10	0.75891049
ATR	-2.8877528	MAP3K2	-1.089393	STK11	-1.7172641
ATR	-1.2935855	MAP3K3	1.50484854	STK11	-1.2963848
ATRIP	-0.9146579	MAP3K4	-1.2785966	STK16	0.01874368
AURKA	0.27879107	MAP3K5	-1.1624862	STK17A	0.66762472
AURKB	-0.9813897	MAP3K6	-1.4990561	STK17B	-2.1162229
AURKC	-0.7737339	MAP3K7	0.06056959	STK19	4.87E-05
AXL	0.29367849	MAP3K8	-0.3352502	STK24	-1.3080113
BCKDK	-1.3393866	MAP3K9	-0.2522778	STK25	1.18153501
BCR	1.01753515	MAP4K1	0.89399064	STK26	-0.4377305
BLK	0.54123325	MAP4K2	-0.7181201	STK3	-0.3268349
BLM	1.49213227	MAP4K3	-0.2845249	STK31	0.49182643
BLM	1.82673765	MAP4K4	-0.8066427	STK32A	-1.6199704
BMP2K	-2.4171889	MAP4K5	-0.9195591	STK32B	0.80895756
BMPR1A	-0.4393613	MAPK1	-0.7789671	STK32C	-1.302827
BMPR1A	0.79896655	MAPK10	-0.407311	STK33	0.19858387
BMPR1B	-1.1142051	MAPK11	-0.8282626	STK35	0.03982179
BMPR2	0.96433359	MAPK12	0.32705481	STK36	-0.8398323
BMX	-2.44077	MAPK13	-0.9693607	STK38	-0.7594389
BRAF	-0.5884347	MAPK14	-2.0506545	STK38L	-0.7400468
BRCA1	-0.3779116	MAPK15	0.22628347	STK39	1.65021264
BRCA1	0.8435548	MAPK3	-1.3113125	STK4	-1.9106641
BRCA2	-0.3821404	MAPK4	-2.0254271	STK40	-0.2509899
BRCA2	0.70603002	MAPK6	0.71551976	STKLD1	-0.4888016
BRD2	-0.5199158	MAPK7	-1.1821191	STRADA	-0.7719982
BRD3	-1.3039487	MAPK8	-1.1619833	STRADB	-0.0128516
BRD4	-0.7383832	MAPK9	-0.2415771	STYK1	0.15137077
BRDT	-0.7689755	MAPKAPK2	0.05328858	SUFU	-2.3121254
BRIP1	0.17292203	MAPKAPK3	0.19044808	SYK	2.00209669
BRIP1	0.5685425	MAPKAPK5	-1.134684	TAB1	-1.0238607
BRSK1	1.30842801	MARK1	2.22938821	TAF1	-1.4197128
BRSK2	1.67332114	MARK2	0.01830946	TAF1L	0.38579305
BTK	-0.241021	MARK3	1.6820469	TAOK1	-1.0862889
BUB1	-0.4568155	MARK4	-1.0911673	TAOK2	-0.287755
BUB1B	-0.5547943	MAST1	-1.0760267	TAOK3	-0.6588305

BUB1B	0.55222068	MAST2	-0.8508374	TBCK	0.72035932
CALM1	0.55457308	MAST3	0.85791792	TBK1	0.90437243
CALM2	-1.4749004	MAST4	-1.8159649	TDG	-0.0586246
CALM3	0.37352147	MASTL	-0.8003261	TDP1	1.55336314
CAMK1	-0.0815061	MATK	1.83134758	TDP2	0.97203047
CAMK1D	-1.5573348	MBD4	-0.0435506	TEC	1.1115753
CAMK1G	-1.6103071	MDC1	-1.5050965	TEK	0.21289197
CAMK2A	1.4144369	MELK	0.73356515	TESK1	-0.4306226
CAMK2B	0.37871202	MEN1	0.49042962	TESK2	-0.3735788
CAMK2D	-0.0128442	MERTK	0.2080053	TEX14	-0.2606861
CAMK2G	0.27761492	MET	-0.3503517	TGFBR1	-1.560595
CAMK2N1	-1.6030482	MGMT	-0.9936079	TGFBR2	-0.0358803
CAMK4	-0.7598584	MINK1	1.68762361	TGFBR3	-2.0835855
CAMKK1	0.21991352	MKNK1	-0.3766407	THNSL1	-0.485866
CAMKK2	-0.3008164	MKNK2	-0.2232774	TJP2	-0.0630873
CAMKV	0.10401356	MLH1	-0.0811474	TK2	-1.3640389
CASK	-0.4915669	MLH1	1.42422405	TLK1	-0.503356
CCNH	1.02163902	MLH3	0.05974722	TLK2	-1.2588615
CDADC1	-1.1219743	MLKL	0.06925368	TNIK	0.2238411
CDC42BPA	0.92507256	MMS19	-2.6501402	TNK1	0.53455373
CDC42BPB	0.73879575	MNAT1	-0.8819536	TNK2	0.08311964
CDC42BPG	-0.5378688	MOK	0.68893767	TNKS	-0.4735161
CDC7	0.88763742	MOS	-1.0134234	TNKS2	4.54526341
CDC73	0.54899195	MPG	1.12448711	TNNI3K	1.61254052
CDH1	-0.3622491	MPLKIP	0.30130512	TOPBP1	2.32169621
CDK1	0.77809762	MPP1	1.03168631	TP53	-0.9758979
CDK10	0.67936713	MPP2	0.25531465	TP53	0.64379391
CDK11A	-0.5188951	MPP3	-1.394994	TP53BP1	0.68696209
CDK11B	-0.0251885	MRE11A	-0.4821189	TP53RK	-1.7528525
CDK12	0.63135092	MSH2	-0.7504526	TPD52L3	-0.2529661
CDK13	0.49569465	MSH2	-0.7261939	TPK1	-1.4331867
CDK14	2.37063903	MSH3	-0.7099643	TREX1	0.13662241
CDK15	-1.2193117	MSH4	-0.5384215	TREX2	0.20938989
CDK16	1.70200049	MSH5	0.36645694	TRIB1	-0.4371239
CDK17	-0.7385376	MSH6	-0.0809375	TRIB2	0.48966956
CDK18	-0.2193994	MSH6	0.1660413	TRIB3	-0.0573887
CDK19	-0.6601839	MST1R	-0.8865243	TRIM27	0.31936547
CDK2	-0.1096343	MTOR	2.21516305	TRIO	-0.7265997
CDK20	-0.4582187	MUS81	-1.2711947	TRPM6	-0.3003378
CDK3	-0.6135968	MUSK	-0.621215	TRPM7	-0.1709275
CDK4	-1.0570619	MUTYH	0.33909439	TSC1	0.03299539
CDK5	-0.6744908	MUTYH	1.01707677	TSC2	-1.0024844
CDK5	0.24763716	MVK	0.07468088	TSKS	1.48077641

CDK5R1	-0.5747927	MYLK	0.00110146	TSSK1B	-0.7391901
CDK5R2	1.14948467	MYLK2	1.30560601	TSSK2	-0.0871459
CDK6	-0.1731936	MYLK3	0.33364847	TSSK3	0.32825623
CDK7	-1.6397342	MYLK4	0.03098029	TSSK4	1.44507669
CDK7	0.29538424	MYO3A	0.02344858	TSSK6	0.45037894
CDK8	-0.1178181	MYO3B	0.80050987	TTBK1	0.80441271
CDK9	-0.1375595	N4BP2	-0.2007437	TTBK2	2.64979124
CDKL1	-0.9295676	NABP2	-0.3532285	TTK	0.01745506
CDKL2	1.01344785	NADK	1.0296285	TWF1	1.27633408
CDKL3	0.20315663	NAGK	1.01472373	TWF2	-0.7918855
CDKL4	-0.7647986	NBN	-2.3434823	TYK2	1.98718818
CDKL5	0.60478164	NBN	-0.0188229	TYRO3	-2.6778926
CDKN1A	-0.4037556	NEIL1	0.75312382	UBE2A	-0.8714809
CDKN1B	0.96674434	NEIL2	0.0603113	UBE2B	-1.3135755
CDKN1C	-1.0450088	NEIL3	-0.605806	UBE2N	-0.3684381
CDKN2A	0.29039197	NEK1	-0.8741956	UBE2V2	-0.9626682
CDKN2B	-0.1646833	NEK10	1.27393192	UCK1	-1.0831424
CDKN2C	-0.1078573	NEK11	-0.0527008	UCK2	0.51217481
CDKN2D	0.40982198	NEK2	-1.456468	UCKL1	-0.3847967
CERK	1.27594548	NEK3	0.57950271	UHMK1	-0.3008695
CETN2	-1.5448229	NEK4	-2.0094654	ULK1	0.31090234
CHAF1A	0.01138232	NEK5	0.56707745	ULK2	-0.7338941
CHEK1	-1.395009	NEK6	1.13130714	ULK3	1.08651024
CHEK1	1.00805561	NEK7	0.2593347	ULK4	-1.5159907
CHEK2	-1.2029678	NEK8	1.97068056	UNG	-1.3557052
CHEK2	-0.2175794	NEK9	-1.716515	VHL	0.90089018
CHEK2	0.43936127	NF1	-0.563728	VRK1	-0.4657898
CHKA	-0.469215	NF2	0.72969427	VRK2	0.88924959
CHKB	-0.0883875	NHEJ1	-0.095643	VRK3	-1.1914663
CHUK	-3.0677907	NIM1K	1.03529072	WAS	-0.9239317
CIB2	-0.8770054	NLK	0.4646854	WEE1	0.15093079
CIT	-0.6051533	NME1	1.20992719	WNK1	1.77920284
CKB	-0.2450813	NME2	-0.4671459	WNK2	-0.9373722
CKM	-0.6328563	NME3	0.23078806	WNK3	2.23168901
CKMT1B	0.42020005	NME4	-0.1138885	WNK4	0.62618155
CKMT2	-0.5959807	NME5	0.54108864	WRN	0.32936327
CKS1B	-0.7961795	NME6	-3.3533817	WRN	0.78350481
CKS2	0.13482981	NME7	-0.4528889	WT1	1.10750736
CLK1	0.22987115	NPR2	-1.236547	XAB2	-1.3360052
CLK2	-1.7223261	NRBP1	-0.8012283	XPA	-0.6313959
CLK2	-0.1085041	NRBP2	0.10877837	XPA	0.41018116
CLK3	0.84202397	NRK	-1.7524468	XPC	-0.6393036
CLK4	-1.942739	NTHL1	1.54525028	XPC	1.84787187

CMPK1	0.77490157	NTRK1	-0.700545	XRCC1	0.18568917
COASY	-0.1149132	NTRK2	-0.1944109	XRCC2	0.76791117
COL4A3BP	0.92379303	NTRK3	-1.9267719	XRCC3	1.68628014
COMMD3	-0.4655028	NUAK1	0.02343497	XRCC4	0.97081162
CPNE3	1.14095551	NUAK2	-0.5751452	XRCC5	0.86995047
CRIM1	-0.7435426	NUCKS1	-0.10246	XRCC6	0.05556921
CRKL	-0.1757622	NUDT1	1.43754365	XRCC6BP1	-0.0537942
CSF1R	0.28019373	NUP62	0.08693898	XYLB	0.10683095
CSK	1.59632684	OGG1	0.03268438	YES1	-1.5157646
CSNK1A1	1.21499705	OXSR1	0.65070161	ZAK	-1.6636376
CSNK1A1L	2.17992144	PACSIN1	2.22611559	ZAP70	-1.3778234
CSNK1D	0.20537038	PAK1	-1.1340341	RPS6KA6	-0.2458142
CSNK1E	0.9240132	PAK2	-0.3669175	RPS6KB1	1.93748838
CSNK1G1	-1.1191538	PAK3	-0.0793663	RPS6KB2	1.45729173
CSNK1G2	-2.1663529	PAK4	0.45317062	RPS6KC1	-0.3444728
CSNK1G3	-0.8949859	PAK6	-0.121212	RPS6KL1	-0.1403554
CSNK2A1	-1.8083921	PAK7	-0.7951723	RRM2B	-0.2050529
CSNK2A2	2.03843286	PALB2	-0.2280154	RYK	-0.3267681
CSNK2B	-2.0098955	PALB2	0.08893896	SBDS	-0.3360723
CYLD	-0.2676774	PANK1	1.45235725	SBK1	-1.139953
DAPK1	0.16171665	PANK2	-0.811242	SCYL1	0.82143399
DAPK2	0.7871394	PANK3	0.17023211	SCYL3	0.96124865
DAPK3	0.94039847	PANK4	0.10308847	SDHB	-0.0909775
DBF4	1.65601343	PAPSS1	0.93619198	SDHC	0.25380961
DCK	0.33725179	PAPSS2	0.95367933	SDHD	-0.8651272
DCLK1	0.81243224	PARP1	-0.8107376	SETMAR	-0.6706376
DCLK2	-0.548802	PARP2	-0.2326605	SGK1	-1.0422318
DCLK3	0.22829088	PASK	1.02872953	SGK2	-0.7797197
DCLRE1A	-0.9884664	PBK	-1.5324501	SGK223	1.56598331
DCLRE1B	0.58925422	PCK1	0.08999497	SGK3	1.07154401
DCLRE1C	0.46103521	PCK2	0.284445	SGK494	0.83233107
DDB1	-1.115107	PCNA	-0.9404029	SHFM1	-0.8954845
DDB2	-1.2721811	PDGFRA	-0.4667163	SHPK	-0.6471847
DDB2	2.19861791	PDGFRB	-0.1878766	SIK1	0.75101721
DDR1	-0.4051942	PDGFRL	1.10653355	SIK2	-0.1293431
DDR2	1.35337633	PDIK1L	0.15097311	SIK3	1.01133185
DGKA	-0.6646144	PDK1	-0.4249616	SKAP1	1.40027075
DGKB	0.26197001	PDK2	1.49728418	SLK	-1.1126582
DGKD	-0.0087585	PDK3	-0.1083295	SLX1A	-1.3215624
DGKG	0.38174567	PDK4	-1.7131285	SLX4	-0.9815001
DGKH	0.44539063	PDPK1	-0.5685572	SMAD4	0.83963268
DGKI	1.29348719	PDXK	-0.1433637	SMARCB1	-0.271087
DGKK	-0.0660374	PEAK1	0.52186222	SMG1	-0.6136075

DGKQ	-0.0878301	PER1	0.67449076	SMUG1	-1.0070453
DGUOK	0.01998022	PFKFB1	-1.5096137	SNRK	0.99716437
DLG1	0.25393131	PFKFB2	-0.9300965	SOCS1	-0.3435363
DLG2	-0.5461703	PFKFB3	1.41957492	SPEG	-1.5737419
DLG3	1.04790881	PFKFB4	-0.6539154	SPHK1	0.84740383
DLG4	-3.6571931	PFKL	-2.2609759	SPHK2	-1.5196128
DMC1	-1.0178632	PFKM	0.55634515	SPO11	0.51292911
DMPK	0.88395372	PFKP	-0.2655015	SRC	-0.5209873
DSTYK	2.15464225	PGK1	-1.362404	SRMS	-2.8998915
DTYMK	0.16888692	PGK2	0.41124964	SRP72	0.10342098
DUSP21	1.07199707	PHKA1	-0.0923375	SRPK1	-0.7543575
DUT	0.52374472	PHKA2	-0.4854359	SRPK2	-0.3760319
DYRK1A	-1.3400003	PHKB	-1.1261157	SRPK3	0.90466969
DYRK1B	0.58135616	PHKG1	0.35167885	STK10	0.75891049
DYRK2	-0.9138336	PHKG2	0.12932858	STK11	-1.7172641
DYRK3	1.78931464	PHOX2B	0.01824312	STK11	-1.2963848
DYRK4	-1.3759131	PI4K2A	0.27046279	STK16	0.01874368
EEF2K	-0.7292157	PI4K2B	0.93129736	STK17A	0.66762472
EFNA3	0.19536833	PI4KA	-0.2048616	STK17B	-2.1162229
EFNA4	0.19929188	PI4KB	-0.0379359	STK19	4.87E-05
EFNA5	0.38512791	PIK3C2A	-0.9932413	STK24	-1.3080113
EFNB3	-0.2996675	PIK3C2B	-1.1565166	STK25	1.18153501
EGFR	2.80964715	PIK3C2G	-1.3384578	STK26	-0.4377305
EIF2AK1	1.63019474	PIK3C3	-0.1876619	STK3	-0.3268349
EIF2AK2	-2.6496181	PIK3CA	0.53167172	STK31	0.49182643
EIF2AK3	0.21277616	PIK3CB	1.71037806	STK32A	-1.6199704
EIF2AK4	-1.0572023	PIK3CD	-1.4725909	STK32B	0.80895756
EME1	-1.1193639	PIK3CG	-0.1204121	STK32C	-1.302827
EME2	-2.7517255	PIK3R1	0.39544764	STK33	0.19858387
ENDOV	-0.0584755	PIK3R1	1.06149397	STK35	0.03982179
EP300	-1.4539183	PIK3R2	-1.6789422	STK36	-0.8398323
EPHA1	0.10413256	PIK3R3	0.65020755	STK38	-0.7594389
EPHA10	-0.4575403	PIK3R4	0.21469142	STK38L	-0.7400468
EPHA2	0.28010952	PIK3R5	0.399808	STK39	1.65021264
EPHA3	-0.9107055	PIKFYVE	-0.5480546	STK4	-1.9106641
EPHA4	0.89736541	PIM1	-0.4323763	STK40	-0.2509899
EPHA5	-0.5706993	PIM2	0.73913366	STKLD1	-0.4888016
EPHA6	-0.9340536	PIM3	1.90711285	STRADA	-0.7719982
EPHA7	-0.8940992	PINK1	1.03011538	STRADB	-0.0128516
EPHA8	0.9565139	PIP4K2A	-0.0807283	STYK1	0.15137077
EPHB1	-1.9813496	PIP4K2B	0.08487489	SUFU	-2.3121254
EPHB2	1.54767389	PIP4K2C	1.16586571	SYK	2.00209669
EPHB3	-0.0906898	PIP5K1A	1.89615267	TAB1	-1.0238607

EPHB4	-0.296779	PIP5K1B	0.3685974	TAF1	-1.4197128
EPHB6	-1.7644295	PIP5K1C	-1.4465204	TAF1L	0.38579305
ERBB2	1.91502786	PIP5KL1	-0.6207563	TAOK1	-1.0862889
ERBB3	0.0064828	PKDCC	0.8167198	TAOK2	-0.287755
ERBB4	0.5042515	PKIA	-0.5820881	TAOK3	-0.6588305
ERCC1	0.4599491	PKIB	-1.0835878	TBCK	0.72035932
ERCC2	0.11797971	PKLR	-0.8018744	TBK1	0.90437243
ERCC2	0.36856651	PKM	1.2507668	TDG	-0.0586246
ERCC3	-0.0503379	PKMYT1	-0.6251446	TDP1	1.55336314
ERCC3	0.69603884	PKN1	-1.2755416	TDP2	0.97203047
ERCC4	-1.1150249	PKN2	-0.3337682	TEC	1.1115753
ERCC4	-0.2835651	PKN3	-0.0908933	TEK	0.21289197
ERCC5	-0.7500533	PLK1	-0.7639298	TESK1	-0.4306226
ERCC5	0.60159021	PLK1	-0.3806727	TESK2	-0.3735788
ERCC6	-1.0565253	PLK1	0.58505173	TEX14	-0.2606861
ERCC8	-0.3223661	PLK2	-0.2334857	TGFBR1	-1.560595
ERN1	-1.7350835	PLK3	0.65796874	TGFBR2	-0.0358803
ERN2	0.00785202	PLK4	-0.5003097	TGFBR3	-2.0835855
ETNK1	0.00982329	PMS1	-2.2992903	THNSL1	-0.485866
ETNK2	-2.6413133	PMS1	1.22074624	TJP2	-0.0630873
EXO1	-0.7351304	PMS2	-0.5066492	TK2	-1.3640389
EXOSC10	-0.6719707	PMS2	0.01203919	TLK1	-0.503356
EXT1	-1.0861315	PMVK	-1.8247395	TLK2	-1.2588615
EXT2	1.27631569	PNCK	-0.7023535	TNIK	0.2238411
FAAP24	-1.0021893	PNKP	-2.0797656	TNK1	0.53455373
FAN1	-0.3384431	PNKP	0.43551465	TNK2	0.08311964
FANCA	-0.8815389	POLB	-0.1630522	TNKS	-0.4735161
FANCA	0.23244074	POLD1	-2.908846	TNKS2	4.54526341
FANCB	-0.7341038	POLE	-1.637734	TNNI3K	1.61254052
FANCC	-0.9370506	POLG	-0.2589288	TOPBP1	2.32169621
FANCC	-0.7626652	POLH	-0.4491008	TP53	-0.9758979
FANCD2	-0.8744255	POLI	-0.3879619	TP53	0.64379391
FANCD2	-0.3255982	POLK	-0.0948803	TP53BP1	0.68696209
FANCE	-1.5008822	POLL	1.25071708	TP53RK	-1.7528525
FANCE	-0.4317084	POLM	1.90320578	TPD52L3	-0.2529661
FANCF	0.17812251	POLN	1.14826993	TPK1	-1.4331867
FANCF	0.69503842	POLQ	-0.2324074	TREX1	0.13662241
FANCG	-0.41552	POMK	0.56886964	TREX2	0.20938989
FANCG	0.45426074	PRKAA1	0.28646813	TRIB1	-0.4371239
FANCI	-0.6776538	PRKAA2	0.38405578	TRIB2	0.48966956
FANCL	-0.609989	PRKAB1	-0.6856988	TRIB3	-0.0573887
FANCM	-1.0174574	PRKAB2	0.56016993	TRIM27	0.31936547
FAS	0.58824285	PRKACA	1.22045728	TRIO	-0.7265997

FASTK	-1.2332248	PRKACB	-0.0299962	TRPM6	-0.3003378
FBXW7	-1.1945166	PRKACG	-0.6851811	TRPM7	-0.1709275
FEN1	1.10932147	PRKAG1	-0.324593	TSC1	0.03299539
FER	-1.3995924	PRKAG2	0.26323904	TSC2	-1.0024844
FES	-0.5672935	PRKAG3	0.41328933	TSKS	1.48077641
FGFR1	-0.8502841	PRKAR1A	-0.2773039	TSSK1B	-0.7391901
FGFR2	0.84050215	PRKAR1A	1.71726412	TSSK2	-0.0871459
FGFR3	0.2148922	PRKAR1B	1.03969651	TSSK3	0.32825623
FGFR4	-1.1626378	PRKAR2A	-0.2592343	TSSK4	1.44507669
FGFRL1	1.80592823	PRKAR2B	0.5737086	TSSK6	0.45037894
FGR	-0.0411825	PRKCA	0.25900455	TTBK1	0.80441271
FH	0.00138397	PRKCB	0.38873901	TTBK2	2.64979124
FLCN	-0.0274149	PRKCD	-0.6164741	TTK	0.01745506
FLT1	0.39934563	PRKCE	-0.3927295	TWF1	1.27633408
FLT3	1.84632417	PRKCG	-1.2209371	TWF2	-0.7918855
FLT4	-0.8785371	PRKCH	0.25904132	TYK2	1.98718818
FN3K	0.7128391	PRKCI	1.01495079	TYRO3	-2.6778926
FN3KRP	-0.8711078	PRKCQ	-0.0620741	UBE2A	-0.8714809
FRK	0.16360788	PRKCSH	-0.6401872	UBE2B	-1.3135755
FUK	0.78775064	PRKCZ	1.39090358	UBE2N	-0.3684381
FXN	0.15868116	PRKD1	0.53421469	UBE2V2	-0.9626682
FYN	0.13110505	PRKD2	-1.1908586	UCK1	-1.0831424
GAK	-0.0296774	PRKD3	-1.2002306	UCK2	0.51217481
GALK1	-0.1623229	PRKDC	-0.3444212	UCKL1	-0.3847967
GALK2	0.98569201	PRKDC	0.63636511	UHMK1	-0.3008695
GCK	1.89980467	PRKG1	-1.6299145	ULK1	0.31090234
GEN1	0.00995853	PRKG2	-0.3939772	ULK2	-0.7338941
GK	0.20025599	PRKX	3.14188171	ULK3	1.08651024
GK2	-0.2447146	PRKY	0.2235331	ULK4	-1.5159907
GNE	1.74635262	PRPF4B	-0.2700985	UNG	-1.3557052
GOLGA5	0.05132874	PRPS1	-0.0035661	VHL	0.90089018
GPC3	-1.1220262	PRPS1L1	0.13355724	VRK1	-0.4657898
GRK1	0.32317254	PRPS2	-0.2626242	VRK2	0.88924959
GRK4	0.50466453	PSKH1	-0.5581037	VRK3	-1.1914663
GRK5	0.63906476	PSKH2	0.73417347	WAS	-0.9239317
GRK6	-1.7819449	PSTK	0.80688593	WEE1	0.15093079
GRK7	1.27046574	PTCH1	2.4240642	WNK1	1.77920284
GSG2	-0.1831377	PTEN	1.34054013	WNK2	-0.9373722
GSK3A	0.05497572	PTK2	0.42804184	WNK3	2.23168901
GSK3B	-0.2585202	PTK2B	1.19958871	WNK4	0.62618155
GTF2H1	-0.9846033	PTK6	-0.8377745	WRN	0.32936327
GTF2H1	-0.6625523	PTK7	-0.4605998	WRN	0.78350481
GTF2H2	-0.4486197	PXK	2.24266022	WT1	1.10750736

GTF2H3	-0.4405485	RAD1	-0.5561785	XAB2	-1.3360052
GTF2H4	0.2329726	RAD17	-2.1851162	XPA	-0.6313959
GTF2H5	0.26815001	RAD18	-1.4295962	XPA	0.41018116
GUCY2C	-0.2122613	RAD23A	-2.0459821	XPC	-0.6393036
GUCY2D	-0.2599929	RAD23B	-1.4583587	XPC	1.84787187
GUCY2EP	-0.8704094	RAD50	-1.659814	XRCC1	0.18568917
GUCY2F	-0.7395939	RAD51	-0.5723737	XRCC2	0.76791117
GUK1	0.17139837	RAD51B	1.04565189	XRCC3	1.68628014
H2AFX	0.28583541	RAD51C	-0.931525	XRCC4	0.97081162
HCK	-0.5910421	RAD51D	0.07891184	XRCC5	0.86995047
HELQ	-1.1082294	RAD52	0.13856288	XRCC6	0.05556921
HIPK1	-0.8920043	RAD54B	-1.1416004	XRCC6BP1	-0.0537942
HIPK2	-0.8138331	RAD54L	-0.6394855	XYLB	0.10683095
HIPK3	-0.8242159	RAD9A	0.44186201	YES1	-1.5157646
HIPK4	-0.2020183	RAF1	-0.1402325	ZAK	-1.6636376
HK1	0.6295173	RB1	-0.4337112	ZAP70	-1.3778234
HK2	0.18436184	RBBP8	-2.7724764	RPS6KA6	-0.2458142
HK3	0.50152453	RBKS	-0.8130377	RPS6KB1	1.93748838
HNF1A	-0.2351295	RDM1	0.74304738	RPS6KB2	1.45729173
HSPB8	-0.1513481	RECQL	0.29042558	RPS6KC1	-0.3444728
HUNK	-0.6094333	RECQL4	-1.8660055	RPS6KL1	-0.1403554
HUS1	-1.8208792	RECQL4	-1.1200425	RRM2B	-0.2050529
HUS1	1.66279788	RECQL5	-0.0180096	RYK	-0.3267681
ICK	1.32660802	RELA	0.98595977	SBDS	-0.3360723
IGF1R	-1.551815	RET	-0.204368	SBK1	-1.139953
IGF2R	0.17771598	REV1	-1.2325713	SCYL1	0.82143399
IKBKAP	2.10957788	REV3L	-0.7358218	SCYL3	0.96124865
IKBKB	-1.5130398	RFK	2.85551088	SDHB	-0.0909775
IKBKE	0.04737805	RIOK1	-1.6517769	SDHC	0.25380961
IKBKG	-0.3117809	RIOK2	0.89102862	SDHD	-0.8651272
IKZF1	1.07688926	RIOK3	-0.688001	SETMAR	-0.6706376
ILK	1.97455659	RIPK1	-0.6042294	SGK1	-1.0422318
INSR	-0.7272162	RIPK2	-0.2678359	SGK2	-0.7797197
INSRR	-1.6073	RIPK3	-1.1085508	SGK223	1.56598331
IP6K1	-0.0851492	RIPK4	-1.4473961	SGK3	1.07154401
IP6K2	-0.489817	RNASEL	0.2353424	SGK494	0.83233107
IP6K3	-2.3835137	ROCK1	0.01679727	SHFM1	-0.8954845
IPMK	0.45552773	ROCK2	-1.3898315	SHPK	-0.6471847
IPPK	-0.3227801	ROR1	0.519163	SIK1	0.75101721
IRAK1	0.61566788	ROR2	0.98788115	SIK2	-0.1293431
IRAK2	-1.1712097	ROS1	0.66056836	SIK3	1.01133185
IRAK3	-1.6643942	RPA1	-2.1175076	SKAP1	1.40027075
IRAK4	-0.0813481	RPA2	-2.6936586	SLK	-1.1126582

ITK	0.13813185	RPA3	-2.294134	SLX1A	-1.3215624
ITPK1	-0.8583903	RPA4	-0.6701026	SLX4	-0.9815001
ITPKA	-0.4882395	RPS6KA1	-0.3459327	SMAD4	0.83963268
ITPKB	0.40156418	RPS6KA2	-1.1960716	SMARCB1	-0.271087
ITPKC	2.04990756	RPS6KA3	-1.0243415	SMG1	-0.6136075
JAK1	0.18711457	RPS6KA4	-0.5009996	SMUG1	-1.0070453